SEISMIC SURFACE-WAVES AND ANISOTROPIC ALIGNMENTS IN THE OCEANIC UPPER-MANTLE

Sheila C Kirkwood

Thesis presented for the degree of Doctor of Philosophy of the University of Edinburgh in the Faculty of Science

1978

ACKNOWLEDGEMENTS

I thank my supervisor, Dr. Stuart Crampin, for suggesting the project, for his advice and assistance during the past three years, and for allowing me to use the anisotropic-surface-wave computer-modelling program, developed by himself and David Taylor, without which this work would have been impossible.

I am grateful to the Department of Geophysics of the University of Edinburgh, to the Institute of Geological Sciences and to the Edinburgh Regional Computing Centre for providing facilities for my research and to the various members of staff, particularly Charles Fyfe of I.G.S. and Malcolm Brown of E.R.C.C., who have provided assistance with computing.

My research work was financed by a Natural Environment Research Council studentship.

Finally, I should like to thank Mrs. L. Kirkwood who deciphered the script and typed this thesis.

ABSTRACT

Observations and theories of elastic anisotropy in the Earth's crust and upper mantle are reviewed and discussed.

Crampin and Taylor's (1971) procedure for computation of seismic surface-wave characteristics in a plane-layered anisotropic half-space is described and a modification to incorporate a surface water layer is developed.

Simplified models of anisotropic ocean-basin structure are examined, with particular reference to surface-wave particle-motion. Two types of anisotropic alignment are considered, one resulting from syntectonic recrystallisation of olivine in a horizontal-shear zone, the other from olivine glide-plane slip with horizontal or vertical slip-planes.

Alignment of the first type can cause slightly anomalous particle motion, of tilted-Rayleigh-type, in all surface-wave modes. The variation of anomaly amplitude with period in the fundamental mode can indicate the approximate depth to the anisotropic layer.

Alignment of the second type can cause highly anomalous particle-motion, of inclined-Rayleigh-type, in the third generalised mode, corresponding to the isotropic second-Rayleigh mode. The anomaly amplitude is rather insensitive to details of structure.

For either type of alignment, the sense of tilt, or

inclination, varies with direction of propagation, in a manner characteristic of the structural symmetry.

Some practical problems in observing surface-wave particle-motion in real ocean-basins are discussed. Several seismograms are presented showing tilted-Rayleigh-type particle-motion for modes corresponding to the isotropic fundamental-Rayleigh and Love modes. The azimuthal variation in sense of tilt is consistent with propagation in an anisotropic structure with a single, vertical symmetry-plane, parallel to the direction of lithospheric plate motion. Observations are consistent with theoretical models if aligned olivine b-axes are tilted down in the direction of plate-motion. Ave 'Lallemant and Carter's (1970) syntectonic recrystallisation model then suggests that the lithosphere is dragging the asthenosphere.

Preliminary results for the variation of anomaly amplitude with period suggest a high degree of alignment, stronger in the lithosphere than in the asthenosphere.

C O N T E N T S

C O N T E N T S (cont.)

1. INTRODUCTION AND REVIEW OF OBSERVATIONS AND THEORIES OF UPPER-MANTLE ANISOTROPY

1.1 Introduction

This study sets out to examine new evidence for the existence of large-scale, aligned anisotropy in the oceanic upper-mantle, to determine the symmetry of that alignment, and to examine the implications for theories of plate-tectonics. The method makes use of the anomalous surface-wave particle-motion associated with large scale anisotropy (Crampin 1975). Observations are compared with model predictions which are computed by a modified version of Crampin and Taylor's (1971) program for surface-wave propagation in plane-layered, anisotropic media. The modification, which allows for the effects of a surface water-layer, is described in Chapter 2. Some representative ocean-basin models are described in Chapter 3. Observations of surface-wave particle-motion and the relationship between observations and model predictions are examined in Chapters 4 and 5. The relevance of these results to plate-tectonic theories is discussed in Chapter 6.

There have been several previous studies of anisotropy in both continental and oceanic areas, and many explanations of its origin have been proposed. The remainder of this Chapter reviews the relevant observations and theories.

1.2 Surface-wave studies

Seismic surface-waves travel over the surface of the Earth, those with periods less than about 100 seconds having their energy concentrated in the crust and upper-mantle. Their phase-velocities and particle-motions depend on conditions at all depths to which they penetrate, in

the region in which they are travelling, with longer-period waves sampling a greater depth range. Group or phase-velocities, measured at any single seismic station, reflect the average conditions along the whole path which the waves have travelled. "Azimuthal-anisotropy" may show up as a regular variation of phase or group-velocity with azimuth of propagation, provided that allowance can be made for this path-averaging effect.

In an isotropic structure, two distinct types of surface-wave propagate, Rayleigh modes and Love modes. In an anisotropic structure the types are not distinct and all surface-waves belong to one family of "Generalized modes" (Crampin and Taylor 1971). These modes may show a close resemblance, in particle-motion and dispersion, to either isotropic type and in such cases may be described as "Rayleigh-type" or "Love-type". The correspondance between isotropic and anisotropic modes is described more fully in Crampin (1977a), for continental structure, and here, in Chapter 3, for oceanic structures.

Love-type modes, with predominantly-transverse particle-motion, are most sensitive to the velocities of horizontally-polarised shear-waves (β_{SH}) in the crust and upper-mantle. Rayleigh-type modes, with largely radial and vertical particle-motion are more sensitive to the velocities of longitunal and vertically-polarised shear waves (α and β_{SV} respectively) and are also sensitive to densities.

Several workers have found evidence for anisotropy in phase and group-velocities. McEvilly (1964) first reported that, for the central United States, Rayleigh and Love dispersions could not both be explained by the same model of crust and upper-mantle structure. Kanimuna (1966) found a similar discrepancy for Japan. In both studies β_{SH} seemed to be 6 - 8% higher than β_{SV} in the upper mantle. It was suggested (Thatcher

and Brune 1969, Boore 1969) that contamination of the fundamental Love mode by higher-mode energy could lead to erroneous estimates of Love-wave phase-velocity. There was a suggestion that this error should be random rather than systematic (Boore 1969), but enough doubt remained so that the apparent discrepancy was generally attributed to errors in phase-velocity estimates rather than to anisotropy in the upper mantle.

Knopoff (1972) noted that higher-mode interference could be minimised, and useful phase-velocity measurements made, by using very long travel paths. By using several long paths of different length and events of known focal mechanism, Forsyth (1975a, 1975b) was able to measure phase velocities for fundamental and first-higher Love modes, crossing the Nazca plate. He also measured fundamental-Rayleigh phase and group-velocities and found a maximum azimuthal-anisotropy of 2% at 70 seconds period for the Rayleigh-wave phase-velocity, with a velocity maximum perpendicular to the ridge crest. He could not resolve any azimuthal anisotropy for the Love-waves but he did find that β_{SH} is apparantly greater than β_{SV}, by about 0.15km/s, in the top 125km of the mantle.

Schlue and Knopoff (1976,1977) studied fundamental Love and Rayleigh phase-travel-times for paths crossing the Pacific basin. They did not resolve any azimuthal anisotropy but found structural anisotropy of about 3%, β_{SH} being greater than β_{SV}, in the upper mantle. They considered that their inversion showed that the anisotropy is confined to the low-velocity-zone.

All of the surface-wave studies above have used isotropic modelling to invert data from an apparantly anisotropic Earth. Crampin (1976) has pointed out that isotropic models are inappropriate and Kirkwood (1978) (reproduced here as Appendix 2) describes in some detail the

possible consequences for the interpretation of their results. The errors are probably much larger than those quoted so that, although the studies show that anisotropy is almost certainly present near the top of the upper mantle, the degree of anisotropy and its exact depth-range are not well determined. In particular, anisotropy may not be confined to the low-velocity-zone.

Crampin and King (1977) take a rather different approach. Crampin (1975) showed that the particle-motion of higher-mode surface-waves is particularly sensitive to the presence of anisotropy in the crust or upper-mantle. Crampin and King (1977) have observed coupled transverse and sagittal particle-motion for higher-mode waves for a number of paths across Eurasia. They interpret these as third-generalised mode (second-mode Rayleigh-type), with aligned anisotropy in the upper-mantle throughout N. Eurasia.

1.3 Refraction studies in oceanic regions

Hess (1964) first noted that P_n waves, which travel immediately beneath the moho, in the Pacific Ocean, showed a strong variation of velocity with azimuth of propagation. Other refraction studies in the Pacific (Raitt et al 1969, 1971, Morris et al 1969, Keen and Barrett 1971, and many others) confirmed Hess's findings. They found P_n velocity anisotropy of 3 - 8%, with the maximum velocity for propagation parallel to fracture zones and to the direction of spreading. Keen and Tramontini (1970) found a similar 8% P_n anisotropy in the Atlantic.

Refraction surveys sample only the crust and the topmost few kilometers of the upper-mantle so that the anisotropy seen by P_n waves may not be detectable by analysis of surface-waves phase-velocities, which would be affected only by a fairly thick anisotropic layer. However, an 8%

P-velocity anisotropy, such as that found for P_n, and a 3% SV-velocity anisotropy, such as might be expected if the P-anisotropy is due to aligned olivine, which extended 50 - 100 km down into the upper-mantle, would give a phase-velocity anisotropy for the fundamental Rayleigh-type mode of 1 - 3% (see Chapter 3). This would be compatible with the findings of Forsyth (1975b)

1.4 Generation of Anisotropy : proposed mechanisms

It is known that seismic anisotropy can be generated in several ways. A system of aligned cracks (Crampin 1978), or of thin, vertical layers with alternating high and low velocities (Aki 1968), will show both azimuthal-anisotropy and discrepancy between the velocity profiles 'seen' by Love and Rayleigh waves. Such systems are important for crustal anisotropy, but are unlikely to be important in the upper-mantle. A system of flat, penny-shaped cracks, or pockets of partial melt, was investigated by Garbin and Knopoff (1975) and used to explain the structural anisotropy found by Schlue and Knopoff (1977). Such a system would not explain the azimuthal-anisotropy observed by Forsyth (1975b) An anisotropic velocity distribution may also be induced directly by an anisotropic stress field in an otherwise isotropic medium (Backus 1965, Morris et al 1969). However, only a very small anisotropy, several orders of magnitude less than that observed, is likely to result from reasonable stress differences (Dahlen 1972). Upper-mantle anisotropy can be explained most easily in terms of preferred orientation of mineral grains, particularly olivine.

1.5 Anisotropy and deformation mechanisms in minerals

Almost all crystalline minerals are anisotropic to both light and sound waves. It is thought that the upper-mantle comprises mainly olivine (60 - 70%) with some ortho- and clinopyroxene (15 - 20% each) (eg. Ahrens

1972, Kennedy and Higgins 1972). The proportion of olivine will be greater where the mantle has been subjected to depletion by partial melting. Measurements have been made of the elastic constants for single crystals of these minerals, and of their pressure and temperature dependence (eg. Verma 1960, Kumazawa 1969, Kumazawa and Anderson 1969, Graham and Barsch 1969). These minerals show strong velocity-anisotropy of 15-25% for P-waves. For the orthorhombic minerals, maximum P-velocities occur for propagation along the crystallographic a-axis with minimum P-velocities along the b-axis. For the clinopyroxenes the P-velocity maximum is close to the c-axis (Kumazawa 1969). A number of studies have been made of seismic velocities in metamorphic rocks which contain aligned olivine or pyroxene crystals, and the expected anisotropy has been found (eg. Birch 1960, 1961, Kern and Fakhimi 1975, Meissner and Fakhimi 1977).

It is known that preferred orientation of minerals can arise during deformation. Deformation may take place by slip on particular crystallographic planes or by dynamic (syntectonic) recrystallisation. Raleigh (1968) observed that, for temperatures between 400°C and 800°C the dominant deformation mechanism in olivine was slip in the [100] direction on all {o k ℓ} planes. Ortho- and clinopyroxenes were found to deform by slip in the [001] direction on (100) planes. (Raleigh 1967, Raleigh and Talbot 1967). In a more complex study, Carter and Ave 'Lallemant (1970) found three different modes of glide-plane deformation in experimentally-deformed olivine, each occuring for different temperature, pressure and strain-rate regimes. For any given pressure, the dominant slip system was (010) [100] at high temperatures, {o k ℓ} [100] at intermediate temperatures and {110} [001] at low temperatures. Their results are summarised in Figure 1.1. They found also (Ave 'Lallemant and Carter 1970), that recrystallisation

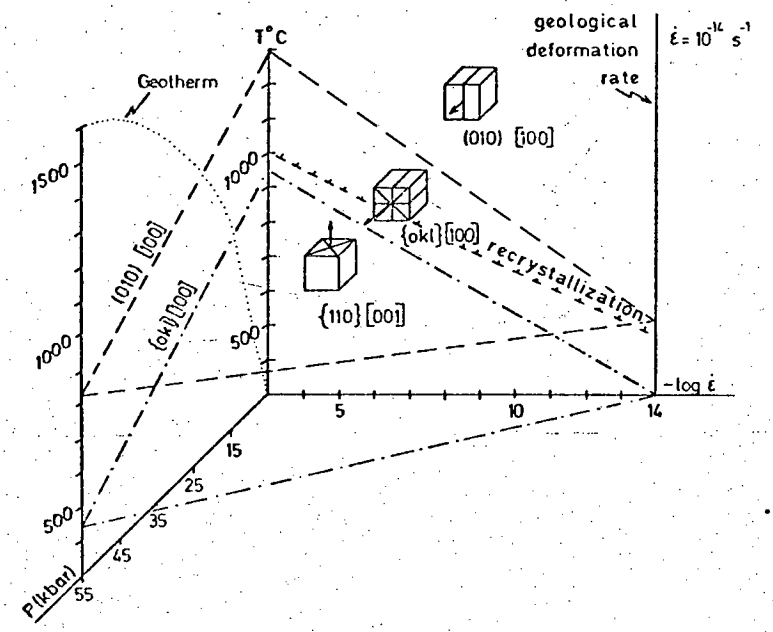

Figure 1.1 Laboratory experiments on the deformation of olivine at various pressures, P , and temperatures, T , as a function of the deformation rate, $\dot{\varepsilon}$. (after Carter and Ave 'Lallemant 1970).

of the olivine became increasingly important at higher temperatures. Olivine recrystallised under stress to form strain-free grains with b-axes aligned parallel to the direction of maximum compressive stress, the grains being slightly flattened to form foliation planes perpendicular to the b-axes. There was no preferred stress direction in the foliation plane and so, no alignment of a- or c-axes. On the basis of field observations and thermodynamic arguments, however, the authors suggest that olivine a-axes would align parallel to a minimum compressive stress. Although measurements were made for strain rates only in the interval 10^{-3} to $10^{-8} s^{-1}$, the authors extrapolate their findings to a 'representative geological strain-rate' of $10^{-14} s^{-1}$ and conclude that recrystallisation of olivine is the dominant mechanism of deformation in the upper mantle, above $500^{o}C$. Preferred orientation then occurs as the olivine b and a-axes align with the maximum and minimum compressive stresses, respectively (Figure 1.2), at 45^{o} to shear planes.

Other authors (eg. Nicolas and Poirier 1976) disagree and consider that alignment takes place by glide-plane slip, the glide-plane aligning along shear planes with the dominant slip direction parallel to the flow-lines.

1.6 Crystalline Alignment in the upper-mantle:theories

Hess (1964) proposed a model where olivine in the uppermost mantle is aligned by shear at transform faults. He supposed that the olivine glide-plane (010) should align in a vertical plane parallel to the transform fault, with a-and c-axes aligned randomly in that plane. This would result in an 18% - 20% P_n anisotropy, if the olivine were completely aligned, with maximum velocities parallel to the transform fault.

Francis (1969) considered that the temperature and pressure at the

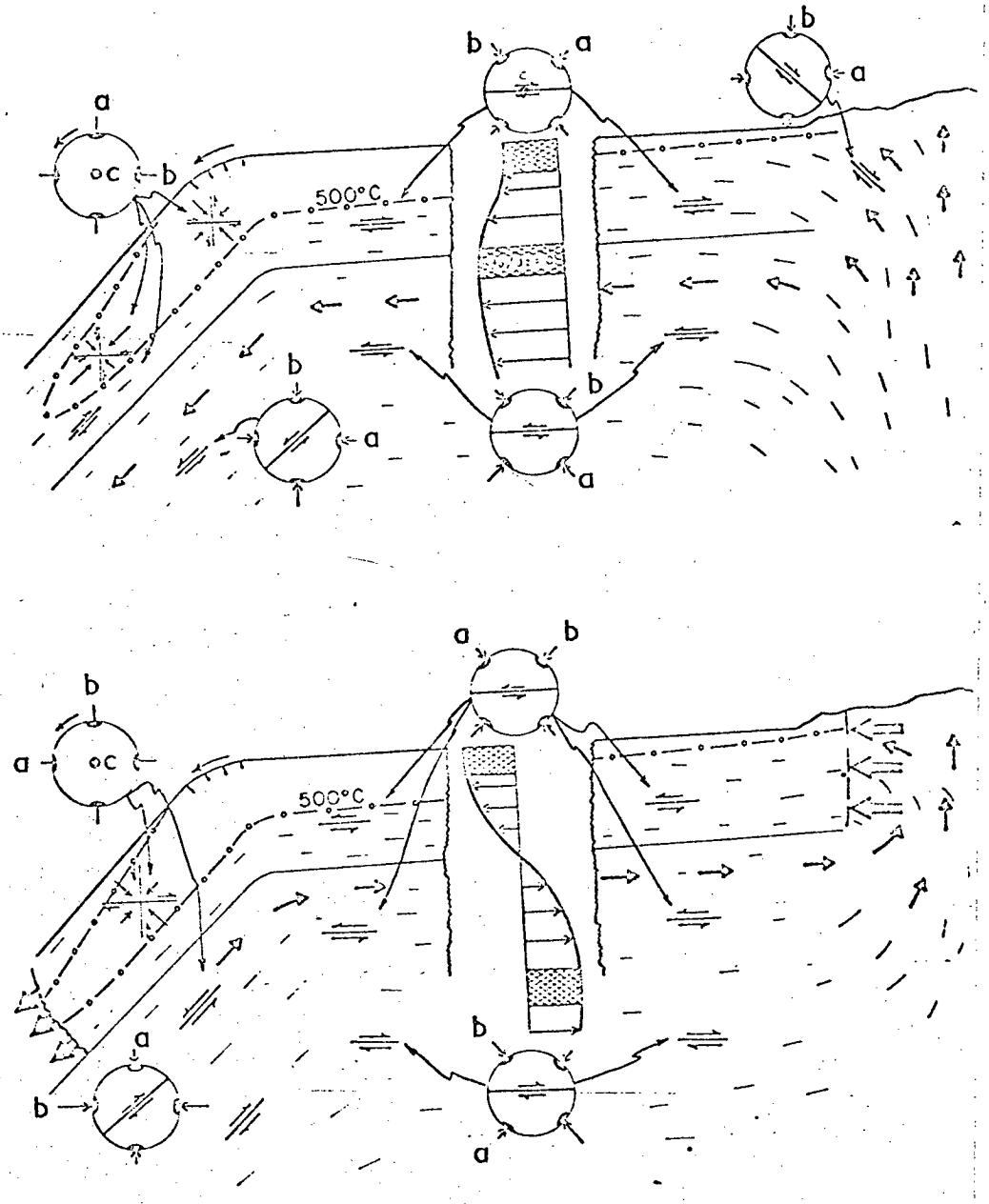

Figure 1.2 Schematic illustrations of "flow-fields", planes of maximum shearing stress, principal stress directions and alignment of olivine crystallographic axes by syntectonic recrystallisation (after Ave 'Lallemant and Carter 1970).

crust/mantle boundary (about 200°C, 2kb) are too low to permit glide-plane creep. He therefore proposed a model in which alignment takes place deeper in the mantle. Upwelling mantle material must change its direction of flow, from vertical to horizontal, beneath the ocean ridge and this would result in large shear-stresses. The olivine a-axes would align along flow lines with slip on all $\{o\ k\ \ell\}$ planes, the a-axis being carried into a horizontal orientation, parallel to the direction of spreading (Figure 1.3) . Thus, Francis' (1969) model also gives P_n anisotropy of up to 20%, with the maximum velocity parallel to the transform faults.

Ave 'Lallemant and Carter's (1970) model of alignment by recrystallisation (Figure 1.2) has a- and b- axes at 45° to the horizontal, with c-axes parallel to the mid-ocean-ridge crest. This can give P_n anisotropy of up to 5% (using Kumazawa and Anderson (1969) to estimate the elastic constants of olivine), with maximum velocities parallel to the direction of spreading, provided that the alignment produced above 500°C is 'frozen in' as the lithosphere cools.

1.7 Field observations of mantle rocks

It is not possible to sample upper-mantle rocks directly but there are several places on the earth's surface where upper-mantle material seems to have risen, relatively unaltered, through the crust. Kimberlite pipes, for example, contain fragments of peridotite which have equiliberated at depths of 100-200 km beneath continental-shield areas (for example see Green and Guegen 1974). Peridotite fragments have been found in alkali basalts, the basalts being similar to those erupted at mid-ocean ridges and in rift-valleys. These peridotites were formed at depths of 50-120 km, probably beneath an oceanic area (Basu 1977). Large intrusive bodies of peridotite are commonly found in Alpine belts, again thought to have risen directly from the upper-mantle (eg. Cristensen

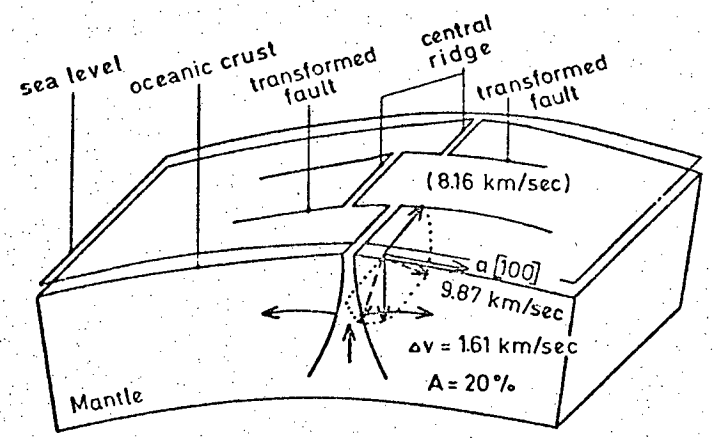

Figure 1.3 Orientation of olivine axis in relation to ridge axis following alignment by glide-plane slip in the upper-mantle (after Francis 1969).

1971, Peselnick et al 1974).

Evidence for glide-plane slip, in the form of kink-bands, and for extensive recrystallisation, especially of olivine, is common in these rocks. A pattern of little deformation with no crystalline alignment, grading into strong glide-plane deformation and strong alignment, with eventual complete recrystallisation and weak alignment, is frequently found (eg. Basu 1977, Boullier and Nicolas 1975, Mercier and Nicolas 1975). Nicolas and his co-authors maintain that there is evidence only for deformation by glide-plane slip, with foliation-planes corresponding to slip-planes. They find strong alignment of olivine b-axes perpendicular to the foliation-plane and alignment of a-axes in that plane. In one area (Peselnick et al 1974), they observed that the foliation-plane corresponded to a structural plane showing evidence of extension along it, so that alignment was by slip on the (010) plane, now the foliation plane, in the [100] direction.

Ave 'Lallemant and Carter (1970), however, claim that many naturally deformed peridotites show similar fabric and texture to those induced by syntectonic recrystallisation in their laboratory experiments. The correlation of recovery-recrystallisation with random crystal-alignment, mentioned above, may arise when the stress causing the initial deformation is removed before recrystallisation is complete.

All of these fragments of upper-mantle have somehow been introduced into the crust and do not have the same history as the rocks now forming the upper mantle. The fragments may have been injected following diapiric upwelling in the upper-mantle, so that the deformation mechanisms seen are likely to be a response to the stresses, temperatures and pressures associated with that upwelling, rather than with steady, lateral flow in the upper-mantle. (Green and Guegen 1974, Basu 1977). Thus the

controversy over whether the observed deformations took place by glide-plane slip, by syntectonic recrystallisation, or by a combination of both, is not necessarily directly relevant to arguments on the mechanism of upper-mantle flow and crystal alignment in the lithosphere and asthenosphere. Either mechanism could generate large scale alignment.

1.8 Potential for study of anisotropic alignments using surface-wave particle-motion

Each of the two mechanisms discussed above would result in crystalline alignment with a characteristic symmetry (Figure 3.2), each symmetry pattern having a characteristic effect on surface-wave particle-motion. It should be possible, therefore, to determine the main mechanism of alignment from analysis of surface waves. The details of the alignment depend on details of the stress and flow pattern in the upper-mantle, which in turn depend on the mechanism of ocean-floor spreading. The details which can be resolved using surface-wave particle-motion data can help discriminate between alternative theories concerning that mechanism.

2. THEORY OF NORMAL-MODE SURFACE-WAVE PROPAGATION IN A PLANE-LAYERED, ANISOTROPIC HALF-SPACE WITH A SURFACE WATER LAYER.

2.1 Introduction

The mathematical treatment of elastic-wave propagation in a plane-layered, anisotropic half-space has been developed by Crampin(1970) and a procedure for the computation of dispersion and particle-motion characteristics of normal-mode surface-waves has been described by Crampin and Taylor (1971). A description of that procedure follows, in section 2.2. Crampin and Taylor consider only solid layers, so a modification to their method, which allows oceanic structures to be modelled, is described in section 2.3.

2.2 Matrix formulation for normal-mode surface-wave propagation

Let x_1, x_2, x_3, = standard cartesian coordinates, with x_3 increasing downwards,

u_1, u_2, u_3, = components of displacement corresponding to the directions x_1, x_2, x_3,

p_{jk} = the j^{th} component of force on unit area perpendicular to the x_k axis, that is, the jk^{th} element of the stress tensor,

s_{mn} = $\frac{1}{2}\left(\frac{\partial u_m}{\partial x_n}+\frac{\partial u_n}{\partial x_m}\right)$, the mn^{th} element of the strain tensor,

ω = angular frequency,

t = time,

ρ = density

δ_{jk} = 1 for j=k, = 0 for j≠k equations (2.1)

Summation over the values 1,2,3 is understood with respect to all vector and tensor suffices which appear twice in any given term.

Within a homogeneous, elastic, anisotropic layer, stress is a linear function of strain:

$$p_{jk} = C_{jkmn}\, s_{mn} \qquad j,k,m,n = 1,2,3 \tag{2.2}$$

The 81 elements of C_{jkmn} are reduced to 21 independant elastic constants by the symmetry relations:

$$C_{jkmn} = C_{kjmn} = C_{mnjk} \tag{2.3}$$

The wave-equation is derived by setting the internal stress, per unit volume, equal to density x acceleration:

$$\frac{\partial p_{jk}}{\partial x_k} = \rho \frac{d^2 u_j}{dt^2}, \qquad j=1,2,3 \tag{2.4}$$

The periodic solution has the form:

$$u_j = a_j \exp\left[\, i\omega(t - q_k x_k)\right], \qquad j=1,2,3 \tag{2.5}$$

For normal-mode surface-waves, propagating in the x_1 direction, only those waves with no component of propagation vector in the x_2 direction need be considered. For such waves, $q_2 = 0$ and $q_1 = \frac{1}{c}$. where c is the phase velocity in the x_1 direction. Substitution of (2.5), (2.2) and (2.1) into (2.4) gives three simultaneous equations in a_j :

$$\rho a_j = C_{jkmn}\, a_m\, q_k\, q_n, \qquad j=1,2,3$$

which may be written as :

$$(-\rho\delta_{jm} + C_{jkmn}\, q_k\, q_n)\, a_j = 0, \qquad j=1,2,3 \tag{2.6}$$

The condition for non-trivial solutions for a_j is :

$$\det(F) = 0, \tag{2.7}$$

where elements of F are :

$$F_{jm} = -\rho\delta_{jm} + C_{jkmn}\, q_k\, q_n \tag{2.8}$$

For given values of c, q_1 and q_2 are known and equation (2.8) can be expanded to a 6^{th} order polynomial in q_3 which, in appropriate conditions (Crampin 1970), has six roots, $q_3(n)$, n =1,2,3,4,5,6, which form complex conjugate pairs. Substitution of each value for $q_3(n)$, in turn, into (2.6), gives the relative amplitudes of $a_1(n)$, $a_2(n)$, $a_3(n)$ for each value of n. Each component of displacement is a linear combination of the displacements for each root:

$$u_j = \sum_{n=1}^{6} f(n)a_j(n)\, \exp\ i\omega(t-\tfrac{x}{c}1-q_3(n)x_3)\ , \quad j=1,2,3 \tag{2.9}$$

From (2.2) and (2.1) it follows that the stress components may be written as :

$$P_{jk} = -i\omega\sum_{n=1}^{6} f(n)a_m(n)\Big[\tfrac{1}{c}C_{jkm1} + q_3(n)C_{jkm3}\Big] \times \exp\Big[-i\omega q_3(n)x_3\Big]\exp\Big[\,i\omega(t-\tfrac{x}{c}1)\Big], \quad j = 1,2,3 \tag{2.10}$$

In matrix notation, the expressions for both displacement and stress may be written :

$$(u_1, u_2, u_3, P_{13}, P_{23}, P_{33}) = ER(x_3)(f(1),f(2),f(3),f(4),f(5),f(6)) \tag{2.11}$$

where, if e_{mn} and r_{mn} are the elements of E and R , respectively :

$$e_{jn} = a_j(n) \text{ for } j = 1,2,3$$

$$e_{jn} = \sum_{m=1}^{3} a_m(n) \left[\frac{i}{c} C_{s(j)3m1} + C_{s(j)3m3}\, q_3(n) \right]$$

for $j = 4,5,6$ with $s(j) = j-3$

and $r_{jn}(x_3) = \delta_{jn} \exp(-i\omega q_3(n) x_3) \exp\left[i\omega(t - \frac{x_1}{c}) \right]$

so that matrix E is independant of x_3.

The propagation of normal-mode surface-waves is controlled by the boundary conditions at interfaces between layers. The conditions are that u_1, u_2, u_3, p_{13}, p_{23}, p_{33} are continuous across each interface. Consider a layered structure with (n-1) plane, horizontal layers overlying an infinite half-space. The layers are numbered 1 to n, starting at the free surface. E_t, R_t and $f(n)_t$ refer to a layer numbered t, thickness d.

$$(u_1, u_2, u_3, p_{13}, p_{23}, p_{33}) \text{ at depth Z in layer t} = E_t\, R(Z)_t\, (f(1)\cdots\cdots f(6))_t \qquad (2.12)$$

$$(u_1, u_2, u_3, p_{13}, p_{23}, p_{33}) \text{ at depth Z+d in layer t} = E_t\, R(Z+d)_t\, (f(1)\cdots f(6))_t \qquad (2.13)$$

but $R(Z+d) = R(d)R(Z)$

and $R^{-1}(Z+d) = R^{-1}(Z)R^{-1}(d)$

combining (3.12) and 3.13) gives

$$(u_1, u_2, u_3, p_{13}, p_{23}, p_{33}) \text{ at top of layer t} \qquad (2.14)$$
$$= E_t\, R(d) E_t^{-1}\, (u_1, u_2, u_3, p_{13}, p_{23}, p_{33}) \text{ at base of layer t}$$

but the boundary conditions require u_j, p_{j3} for $j = 1,2,3$, at the base of layer t, are the same as at the top of layer t + 1, so :

(2.15)

$(u_1, u_2, u_3, p_{13}, p_{23}, p_{33})$ at top of layer t =

$$A_t(u_1, u_2, u_3, p_{13}, p_{23}, p_{33})$$
at top of layer t + 1

where $A_t = E_t\, R(d)_t E_t^{-1}$

by repeated application of (2.15)

$(u_1, u_2, u_3, p_{13}, p_{23}, p_{33})$ at free surface = (2.16)

$$A_1 A_2 .. A_{n-1} E_n R_n(Z_n)(f(1).... f(6))_n$$

or $(u_1, u_2, u_3, p_{13}, p_{23}, p_{33})_{at\ x_3=0} = G\ (f(1)..... f(6))_n$

(2.17)

For propagation of surface-waves there can be no stresses across the free surface and no sources at infinity. The $(f(1), f(2),.... f(6))_n$ are the relative excitations of the six roots, $q_3(r)$, r = 1,6 in the semi-infinite half-space. These roots, $q_3(r)$, are a function of the elastic constants of the half-space and of the phase-velocity and do not depend on the presence of other layers. If q is real, there is no decay of the wave with depth and an upward-travelling wave would imply a source at infinity. It is reasonable to expect that any real root, +q, will be matched by one, -q, corresponding to upward and downward-travelling waves, with the same wave-number. If q is complex, the roots form complex-conjugate pairs. A root with negative imaginary part would imply an increase in amplitude with depth. So the excitation functions f(r) for half of the roots must be zero.

(2.16) and (2.17) then give :

$$(u_1, u_2, u_3, 0,0,0) = G\,(f(1), f(2), f(3),0,0,0)_n \qquad (2.18)$$

For a non-trivial solution

$$\det (H) = 0 \qquad (2.19)$$

where $h_{mn} = g_{m+3,n}$ $\quad m,n = 1,2,3$

h_{mn} and g_{mn} being the elements of H and G, respectively.

The h_{mn} are functions of the thicknesses and elastic constants of the layers, the phase-velocity, c, and the angular frequency, ω, of the waves. Once these are adjusted to give det (H) = 0 then f(1), f(2), f(3), in the semi-infinite half space, can be found from

$$H \begin{pmatrix} f(1) \\ f(2) \\ f(3) \end{pmatrix} = \underline{0} \qquad (2.20)$$

and u_1, u_2, u_3 can be found using (2.18).

The u_j are, in general, complex and represent the relative amplitudes and phases of the three components of particle-motion at the free surface. To locate one point on a normal-mode dispersion-curve, for a specified, layered structure, the procedure described in Crampin and Taylor (1971) computes solutions as follows:

1. Take a value for c
2. Calculate F (eqn. 2.7) and solve for $q_3(n)$, $a_j(n)$ for each layer
3. Take a value for ω
4. Form matrices E, E^{-1}, R (eqn. 2.11) for each layer
5. Combine to form G (eqn. 2.16)
6. Find det(H) (eqn. 2.19)

7. If det(H) $\neq$ 0 increment c or ω and go to 2 or 4, respectively
8. Calculate f(1), f(2), f(3), u_1, u_2, u_3 for successful values of c,ω

It is obviously more efficient to fix c and search for ω (step 7), and if the program is used in this way, then a set of dispersion-curves for the fundamental and 3 higher-modes, with about 10 points per curve, can be calculated in about 15 minutes of ICL 4/75 c.p.u. time.

Crampin and Taylor (1971) treat only solid layers. A modification for oceanic models is now described.

2.3 Modification for a surface liquid layer

In general, each normal-mode surface-wave in an anisotropic structure has displacements in all three orthogonal directions. However, in directions parallel to planes of structural symmetry, two independant types of mode propagate: Rayleigh-type modes with only vertical and radial displacements and Love-type modes with only transverse horizontal displacements. For such modes the 6 x 6 E-matrices of equations (2.11) are singular, so computations must be made using 4 x 4 and 2 x 2 submatrices. A Love-type mode will not be affected by a surface water layer, so only Rayleigh and generalised-type modes need be considered.

It is convenient to modify the above procedure after step 5, changing the boundary conditions at the top of the solid layers.

For a liquid layer :

$$C_{jkmn} = \delta_{jk}\,\delta_{mn}\,\lambda \tag{2.21}$$

where λ is Lame's constant for the liquid

using $q_1 = \frac{1}{c}$ and $q_2 = 0$ and applying (2.8)

gives

$$F = \begin{pmatrix} \frac{\lambda}{c^2} - \rho & 0 & \frac{\lambda q_3}{c} \\ 0 & -\rho & 0 \\ \frac{\lambda q_3}{c} & 0 & \lambda q_3^2 - \rho \end{pmatrix} \tag{2.22}$$

equation (2.7) gives

$$\left(\frac{\lambda}{c^2} - \rho\right)(-\rho)\left(\lambda q_3^2 - \rho\right) + \frac{\lambda q_3}{c}\left(\frac{\rho \lambda q_3}{c}\right) = 0$$

leading to $q_3^2 = \frac{\rho}{\lambda} - \frac{1}{c^2}$

$$q_3 = \pm \frac{1}{\lambda^{\frac{1}{2}}}\left(\rho - \frac{\lambda}{c^2}\right)^{\frac{1}{2}} \tag{2.23}$$

from equation (2.6)

$$\rho a_1 = C_{1111} a_1 q_1^2 + C_{1133} a_3 q_1 q_3$$

substituting for q_1 and q_3 gives

$$a_1\left(\rho - \frac{\lambda_2}{c}\right) = \pm \frac{\lambda^{\frac{1}{2}}}{c}\left(\rho - \frac{\lambda_2}{c}\right)^{\frac{1}{2}} a_3$$

so $$\frac{a_1}{a_3} = \pm \left(\frac{\lambda}{\rho c^2 - \lambda}\right)^{\frac{1}{2}}$$

setting $a_1(1) = a_1(2) = 1$

$a_3(1) = +qc$

$a_3(2) = -qc$

where $$q = \left|\left(\frac{\rho c^2 - \lambda}{\lambda c^2}\right)^{\frac{1}{2}}\right| \tag{2.24}$$

Usisng (2.9) and 2.10) for displacement and stress components in the water layer :

$$u_3 = \left[f(1)qc \exp(-i\omega qx_3) - f(2)qc \exp(+i\omega qx_3) \right] \exp i\omega (t - \frac{x}{c}1)$$

$$p_{33} = -i\omega \left[f(1) \frac{\lambda}{c} + \lambda q^2 c \exp(-i\omega qx_3) + f(2) \frac{\lambda}{c} + \lambda q^2 c \exp(+i\omega qx_3) \right] \exp i\omega (t - \frac{x}{c}1) \quad (2.25)$$

Using the value of q in (2.24), equations (2.25) can be written:

$$\begin{pmatrix} u_3 \\ p_{33} \end{pmatrix} = \begin{pmatrix} qc & -qc \\ -i\omega\rho c & -i\omega\rho c \end{pmatrix} \begin{pmatrix} \exp(-i\omega qx_3) & 0 \\ 0 & \exp(+i\omega qx_3) \end{pmatrix} \begin{pmatrix} f(1) \\ f(2) \end{pmatrix} \exp i\omega (t - \frac{x}{c}1) \quad (2.26)$$

from which it follows that :

$$\begin{pmatrix} u_3 \\ p_{33} \end{pmatrix}_{x_3=d} = \begin{pmatrix} qc & -qc \\ -i\omega\rho c & -i\omega\rho c \end{pmatrix} \begin{pmatrix} \exp -i\omega qd & 0 \\ 0 & \exp +i\omega qd \end{pmatrix} \begin{pmatrix} -i\omega\rho c & qc \\ +i\omega\rho c & qc \end{pmatrix} \begin{pmatrix} u_{33} \\ p_{33} \end{pmatrix}_{x_3=0} \frac{1}{(-i\omega)2qc^2\rho} \quad (2.27)$$

where d is the depth of the liquid layer.

The stress across the free surface of the liquid is zero, so equation (2.27) gives :

$$(u_3)_{x_3=d} = \tfrac{1}{2}(e^{-i\omega qd} + e^{+i\omega qd})(u_3)_{x_3=0} = (\cos \omega qd)(u_3)_{x_3} = 0$$

$$(p_{33})_{x_3=d} = \frac{-i\omega\rho}{2q}(e^{-i\omega qd} - e^{+i\omega qd})(u_3)_{x_3} = 0$$

$$= \frac{\omega\rho}{q} (\sin \omega qd) \ (u_3)_{x_3} = 0 \quad (2.28)$$

For propagation of a generalised surface-wave mode, the 6 x 6 matrix G (equation 2.18) is formed as if there were no surface liquid layer.

This gives :

$$(u_1, u_2, u_3, p_{13}, p_{23}, p_{33})_{\text{at base of liquid layer}} = G(f(1), f(2), f(3), 0, 0, 0) \qquad (2.29)$$

The boundary conditions at the solid / liquid interface are that $p_{13} = p_{23} = 0$ and u_3 and p_{33} are continuous. Using

$$(u_3)_{x_3=d} = A(u_3)_{x_3=d} \quad \text{where} \quad A = \cos \omega q d$$

$$(p_{33})_{x_3=d} = B(u_3)_{x_3=d} \quad \text{where} \quad B = \frac{\rho \omega}{q} \sin \omega q d \qquad (2.30)$$

matrix G can be replaced by G', with

$$g'_{m6} = Bg_{m3} - Ag_{m6} \ , \ m = 1, 2, \ldots 6$$

$$\text{and } g'_{mn} = g_{mn} \quad \text{for } n \neq 6 \ , \ m = 1, 2, \ldots 6 \qquad (2.31)$$

where g'_{mn} and g_{mn} are the elements of G' and G , respectively.

Then $(u_1, u_2, u_3, 0, 0, 0) = G' (f(1), f(2), f(3), 0, 0, 0)$

which is of the same form as equation (2.19), where H is derived from G' rather than G. The u_1, u_2, and u_3 then refer to displacements at the top of the solid layers.

For propagation of Rayleigh-type waves, G is a 4 x 4 matrix with

$$(u_1, u_3, p_{13}, p_{33}) = G (f(1), f(2), 0, 0)$$

so G is replaced by G' with

$$g'_{m4} = Bg_{m2} - Ag_{m4} \ , \ m = 1, 2, 3, 4$$

$$\text{and } g'_{mn} = g_{mn} \quad \text{for } n \neq 4 \ , \ m = 1, 2, 3, 4 \qquad (2.32)$$

2.4 Comparison of computed dispersions: anisotropic and isotropic techniques

Dispersion calculated using the anisotropic modelling program, modified in this way, can be checked for consistancy with isotropic modelling. It is possible to generate an anisotropic layer which is transversely isotropic, being symmetric about, for example, the a-axis which is aligned horizontally. Body waves travelling in a plane perpendicular to this axis will all travel with one of 3 velocities, say α , β_{SV} and β_{SH}, depending on their polarisations, and independant of their direction of travel within that plane. Surface-waves travelling parallel to this plane have either pure Rayleigh or pure Love-type motion and their equations of motion are identical to those for isotropic models with the velocities α and β_{SV} or β_{SH} , respectively, in the appropriate layer. So, as the direction of propagation approaches 90^{o} away from the axis of symmetry, the dispersion, calculated by the anisotropic modelling program, should approach that calculated by an isotropic modelling program for the appropriate models. Such a comparison is shown in Figure 2.1. The isotropic curves are computed by a program based on Dorman (1959 and 1962) for the plane-layer models shown in Table 2.1, which are intended to represent oceanic crust and upper-mantle. The anisotropic data are for a model with the low-velocity-zone in the isotropic models replaced by an anisotropic layer, with the elastic constants shown in Table 2.2 and for propagation in a direction 89.9^{o} away from the symmetry axis. As Figure 2.1 shows , the anisotropic modelling technique gives excellent agreement with the isotropic method.

TABLE 2.1

description	thickness km	α km/s	β km/s		ρ $kg/m^3 \times 10^{-3}$
water	4.5	1.50	0.00		1.0
sediment	0.5	2.02	0.25		1.9
crust	6.0	6.60	3.80		2.9
lithosphere	60.0	8.10	4.40		3.3
low-velocity zone	60.0	7.172	4.105	for Rayleigh waves	3.4
			4.236	for Love waves	
upper mantle		8.25	4.55		3.5

Table 2.1 Isotropic model used to generate the dispersion curves in Figure 2.1.

TABLE 2.2

LOWVTOL

Density = 3400 kg/m^3

j k m n	C_{jkmn}(kb)
1 1 1 1	2252
2 2 2 2	1749
3 3 3 3	1749
1 1 2 2	508
2 2 3 3	603
3 3 1 1	508
1 2 1 2	610
2 3 2 3	573
1 3 1 3	610

Table 2.2 Elastic constants, C_{jkmn} of the material forming the low velocity zone in the model used to calculate the anisotropic dispersion data shown in Figure 2.1

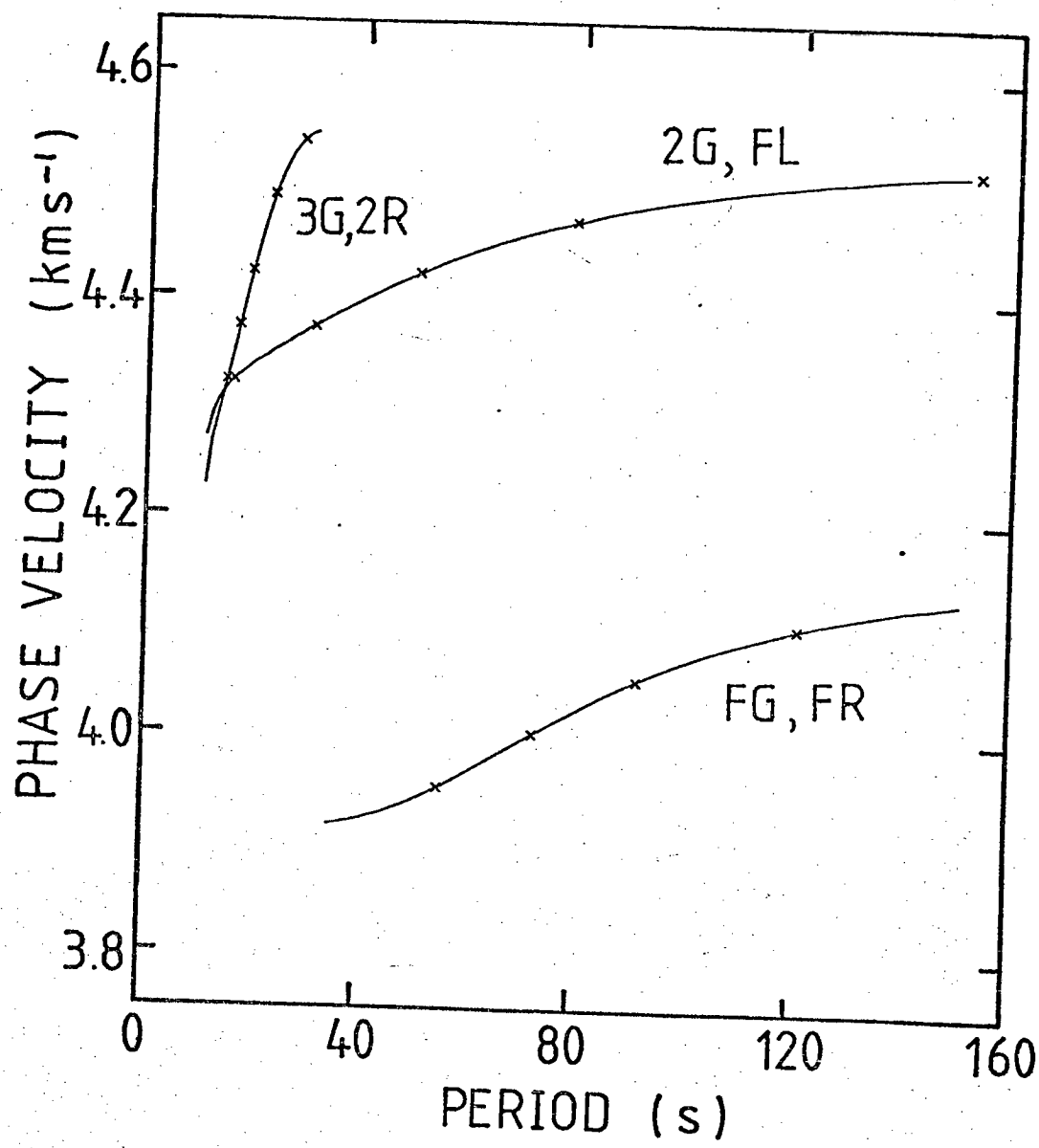

Figure 2.1 Comparison of phase-velocity dispersions for the first three surface-wave modes, calculated by isotropic and anisotropic modelling programs (see text). Solid lines are for the isotropic model, crosses for the anisotropic model and are plotted by computer.

3. MODELS OF OCEAN BASIN STRUCTURE AND SURFACE-WAVE CHARACTERISTICS

3.1. Introduction

The method described in Chapter 2 has been used to calculate the characteristics of normal-mode surface-wave propagation in several models of ocean-basin structure, described in detail in Appendix 1. This study does not aim to model any particular ocean-basin but tries to assess the likely effect, on surface-wave particle-motion, of large-scale,aligned anisotropy in the upper-mantle. Simple six-layer models are used, with an anisotropic layer, or layers, forming part, or all, of the top 120km of the "upper-mantle".

3.2. The basic model

All models are variations on a basic,isotropic model, S-ISOT, which represents a simplified,stable ocean-basin, some thousands of kilometers away from a mid-ocean ridge. The six structural layers, and their elastic constants, are shown in Table 3.1.

Information about the structure of real ocean-basins comes from several sources. In general, P-wave velocities are best estimated by refraction studies, S-wave velocities by surface-wave studies and densities by direct sampling (sediments and upper-crust), by correlation of seismic and gravity profiles (crust), or by considerations of heat-flow, topography and isostasy (uppermost upper-mantle). There have been many refraction studies of the crust and the top of the upper-mantle,giving P-velocities similar to those used for S-ISOT (eg. Houtz and Ewing 1963, Bishop and Lewis 1973, Hussong et al 1972). (Oceanic layer 2 is not represented in the simplified model used here.

	layer name	thickness km	α km/s	β km/s	ρ g/cm^3
Crust :	water	4.5	1.50	0.00	1.0
	sediment	0.5	2.02	0.25	1.9
	layer 3	6.0	6.60	3.80	2.9
Lithosphere :	layer 4	60.0	8.10	4.40	3.3
Low-velocity-zone :	layer 5	60.0	7.48	4.10	3.4
Upper-mantle :	layer 5	HS	8.25	4.55	3.5

Table 3.1 Structure of isotropic ocean-basin model S-ISOT.

This will affect dispersion at short periods, but surface-waves at these periods are rather insensitive to conditions in the upper-mantle and so are not important in the present study). There have been a few refraction studies of the deeper layers, and almost all have found zones of low P-velocity beneath oceanic and tectonically active regions. (eg. Green and Hales 1968, Hales et al 1970). The estimates of velocity in such zones vary from 7.0 km/s to 7.8 km/s and for the region below it, from 8.1 km/s to 8.6 km/s. Values within these ranges are used in S-ISOT.

Shear-velocities in oceanic sediments lie in the range 0.1 to 0.4 km/s (Sykes and Oliver, 1964b) . Such low shear-velocities can have a pronounced effect on particle-motion. Sykes and Oliver (1964a) showed that certain higher-modes propagate which have large amplitudes in the sediment layer, although most of their energy travels in the crust and upper-mantle. The horizontal component of particle-motion is effectively amplified, and may have its phase reversed, relative to the vertical component, by the sediment layer. It is therefore important that a realistic sediment layer be incorporated in a model used to study particle-motion. The thickness of sediment chosen, 0.5 km, is typical of the areas near the continental margins, and hence near recording stations, in the Atlantic, Western Pacific and Indian oceans (Lisitsyn 1974).

Shear-velocities in the crust and upper mantle, and the thicknesses of the layers in the upper mantle, are similar to those found in the various surface-wave studies (eg. Kovach and Press 1961, Forsyth 1975b, Schlue and Knopoff 1976).

Sediment densities have been measured directly and are reported in Nafe and Drake (1963). Crustal densities have been estimated by Talwani et al (1965), by correlation of seismic and gravity data, for part of the North Atlantic. Densities in the lithosphere and asthenosphere are those used by Sclater and Francheteau (1970) in relating heat-flow to topography for the North Pacific. The density of the deeper mantle is that found by Press (1970) for the depth range 100 - 200 km, the only range in which he found that density estimates were well-constrained by the seismic and moment-of-inertia data.

3.3. Anisotropic upper-mantle layers

Two studies, Forsyth 1975 and Schlue and Knopoff 1976, have found shear-wave anisotropy of 2-6% in the top 130 km of the oceanic upper mantle. As outlined in Chapter 1, it is thought that this may be due to a preferred orientation of olivine in the upper-mantle. The elastic constants of single crystals of olivine, and the P-wave velocities in an olivine-rich peridotite have been measured for temperatures up to 800^{o}K, and pressures up to 10kb (Graham and Barsch 1969, Meissner and Fakhimi 1977, Peselnick et al 1974). It has been found that the degree of anisotropy does not vary significantly within the temperature and pressure range of the experiments. The pure olivine samples showed P-wave anisotropy of about 25% and average S-wave anisotropy of 10-18%, depending on the particular sample. The peridotite showed a P-wave anisotropy of about 5%.

Pressures and temperatures in the lower lithosphere and asthenosphere are probably higher than those used in the experimental work, although there is some controversy over temperatures. Sclater and

Francheteau (1970), for example, consider that temperatures must rise rapidly in the upper mantle, to reach 1300°K near the base of the lithosphere. Tozer (1972), on the other hand, believes that temperatures are controlled by large-scale convection and may be much less than 1300°K, down to several hundred kilometers. However, pressures within the lithosphere and asthenosphere, being below 20kb, are well below those which might cause phase-changes in the olivine, so that Graham and Barsch's (1969) results can reasonably be extrapolated to the higher temperatures, if they exist, and pressures, in the top 200 km of the upper-mantle.

The anisotropy observed in surface-wave studies and in the peridotite samples may, therefore, be modelled by assuming a composition of 20-50% aligned olivine, 50-80% isotropic material.

Forsyth (1975b) found that the maximum phase-velocity anisotropy occurred for Rayleigh-waves with periods near 70 seconds and showed that, if this was due to shear-wave anisotropy, the anisotropy is probably more pronounced in the low-velocity-zone than in the lithosphere. So, the initial model used here for anisotropy in the low-velocity-zone has a layer with 50% aligned olivine (TTOL5050 in Table A1.4). Anisotropy in the lithosphere is modelled with 20% aligned olivine (XTOL2080 in Table A1.4). Different proportions are used in the later models.

Anisotropic materials are based on the elastic constants for olivine determined by Verma (1960), which are not significantly different from those reported by other authors. They are listed in Table A1.4 (Appendix 1) and the associated body-wave velocities are illustrated

by Figure A1.2. The isotropic materials mixed with the olivine are chosen so that the average seismic velocities are close to those for the basic,isotropic model, S-ISOT.

It might seem more realistic to extrapolate Graham and Barsch's (1969) measurements on olivine to appropriate temperatures and pressures and then combine with a proportion of isotropic material. The necessary isotropic materials would then be more realistic but, as the degree of anisotropy is not expected to change significantly within the appropriate range of temperature or pressure, the elastic constants of the mixture would not differ greatly from those formed as above. In view of the considerable uncertainty in estimating appropriate temperatures, and the non-detailed nature of models used in this study, such extrapolations are not considered worthwhile.

The olivine is modified to a transversely isotropic form (TOLIVINE in Table A1.4) which is symmetrical about the crystallographic a-axis. Such alignment, with the a-axis and (010) or (001) plane horizontal, is a likely consequence of deformation by glide-plane slip in the upper-mantle (Carter and Ave 'Lallemant 1970). Alignment by syntectonic recrystallisation may also be important and may even predominate (Ave 'Lallemant and Carter 1970). This should be modelled by olivine with preferred orientation of all three crystallographic axes, with a- and b-axes inclined at 45^{o} to the vertical and with c-axis horizontal. However the velocity variations in orthorhombic olivine are very similar to those in the transversely isotropic olivine (Figure A1.2) so that, as a first approximation, the same materials as above (XTOL2080 and TTOL5050) are used,tilted into an appropriate orientation.

3.4. Structural symmetry and characteristic surface-wave particle motion

Models with olivine aligned by glide-plane slip have two vertical planes of symmetry, parallel to the olivine a- and c- axes. The names of such models here include the suffix 010. Where olivine is aligned by syntectonic recrystallisation, the structure has only one plane of symmetry, perpendicular to the c- axis. Models of this type are indicated by the suffix 110.

The character of surface-wave particle-motion is determined by the symmetry of the structure (Crampin 1975). The characteristic particle-motions of the two types of structural symmetry are illustrated in Figures 3.1 and 3.2. Waves travelling parallel to any of the vertical symmetry planes have pure Rayleigh or pure Love-type particle-motion. Waves travelling in other directions have, in any structure with two planes of symmetry (010 models), inclined-Rayleigh-type particle motion, ie. elliptical, in a vertical plane inclined to the direction of propagation, at some angle between zero and ninety degrees. Such particle-motion shows vertical and radial components coupled to a transverse component, with vertical component $\pm\frac{\pi}{2}$ out of phase with the other two. When a structure has only one vertical plane of symmetry (110 models), the surface-wave particle-motion, for propagation away from a plane of symmetry, is a combination of inclined- and tilted-Rayleigh-type, ie. elliptical, in a plane which is inclined to the direction of propagation and tilted away from the vertical. In this case radial, transverse and vertical components of particle motion are again coupled but the relative phases are different from those in simple, inclined-Rayleigh motion. For

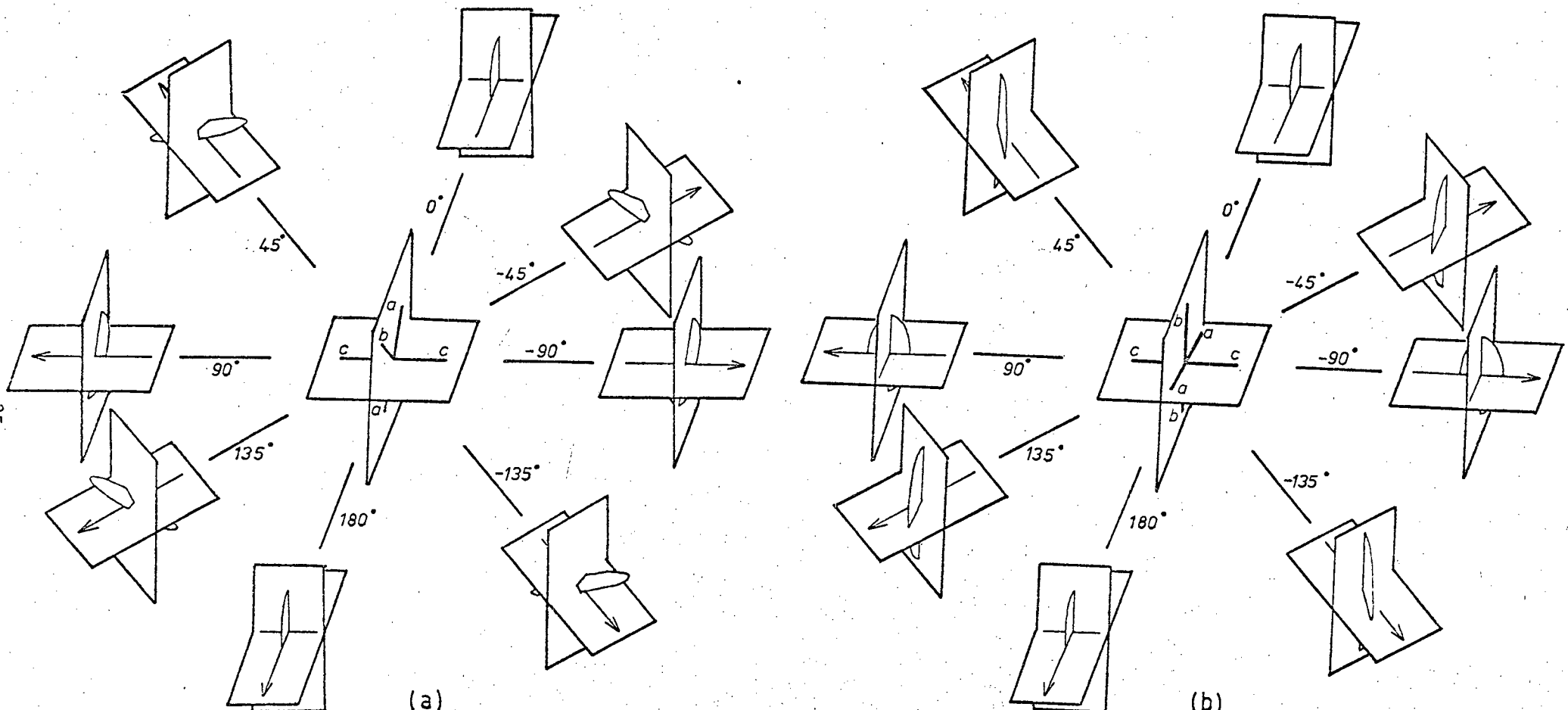

Figure 3.1 Characteristic particle-motion for surface-waves in models with (a) one vertical plane of structural symmetry or (b) two vertical planes of symmetry. The orientations of olivine crystallographic axes in (a) 110-models and (b) 010-models (see text) are indicated at the centers of the diagrams. Angles indicate the convention used for azimuth of wave-propagation. Note that pure Rayleigh- or pure Love-type particte motion occurs for propagation parallel to symmetry planes, i.e. at 0° in (a) and at 0° and 90° in (b).

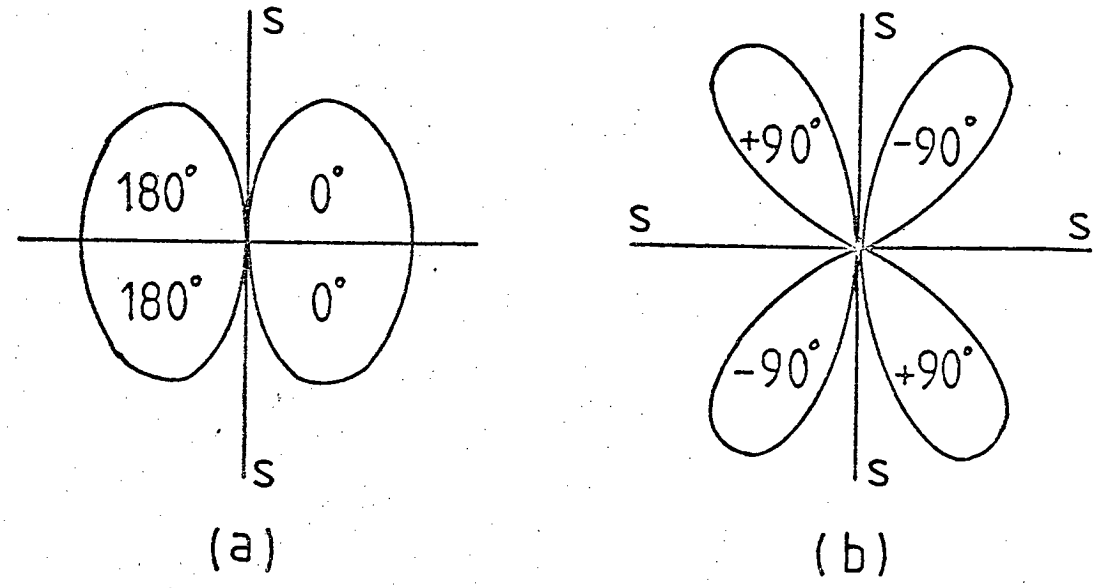

Figure 3.2 Characteristic azimuthal variation in relative phases of transverse and vertical components of surface-wave particle motion and amount of (a) anomalous tilt for 110-models and (b) anomalous inclination for 010-models (see text). Lines SS indicate the directions of planes of structural symmetry

propagation at right angles to the plane of symmetry, the radial motion is $\pm\frac{\pi}{2}$ out of phase with the other two components. In other directions the phase relations depend on the mode, the period, and the model.

The details of particle-motion will vary from model to model so several models must be considered in an examination of possible effects in real surface-waves. The dispersion and particle-motion for several different models, and the structures of the various models examined, are described in detail in Appendix 1. Those details are summarised in Figures 3.3 to 3.15.

3.5 Model Phase-velocities, particle-motion and the correspondance between isotropic and anisotropic modes

The dispersions of the first four generalised modes, FG, 2G, 3G, and 4G for two anisotropic models, S3T and S1X are plotted in Figures 3.4 and 3.5. Model S3T has an anisotropic low-velocity-zone, S1X an anisotropic lithosphere. Data are for four directions of propagation, at 30^{o} intervals away from a plane of symmetry (see Appendix 1 for details). The dispersion of the first two Rayleigh and Love modes for the isotropic model S-ISOT are plotted in Figure 3.3, for comparison. On the basis of their dispersion, FG and 3G correspond to isotropic fundamental and first-higher Rayleigh modes, 2G and 4G correspond to fundamental and first-higher Love modes. The anisotropic low-velocity-zone in S3T has a greater degree of anisotropy than the lithosphere in S1X and this is reflected in the degree of surface-wave phase-velocity anisotropy. It is worth

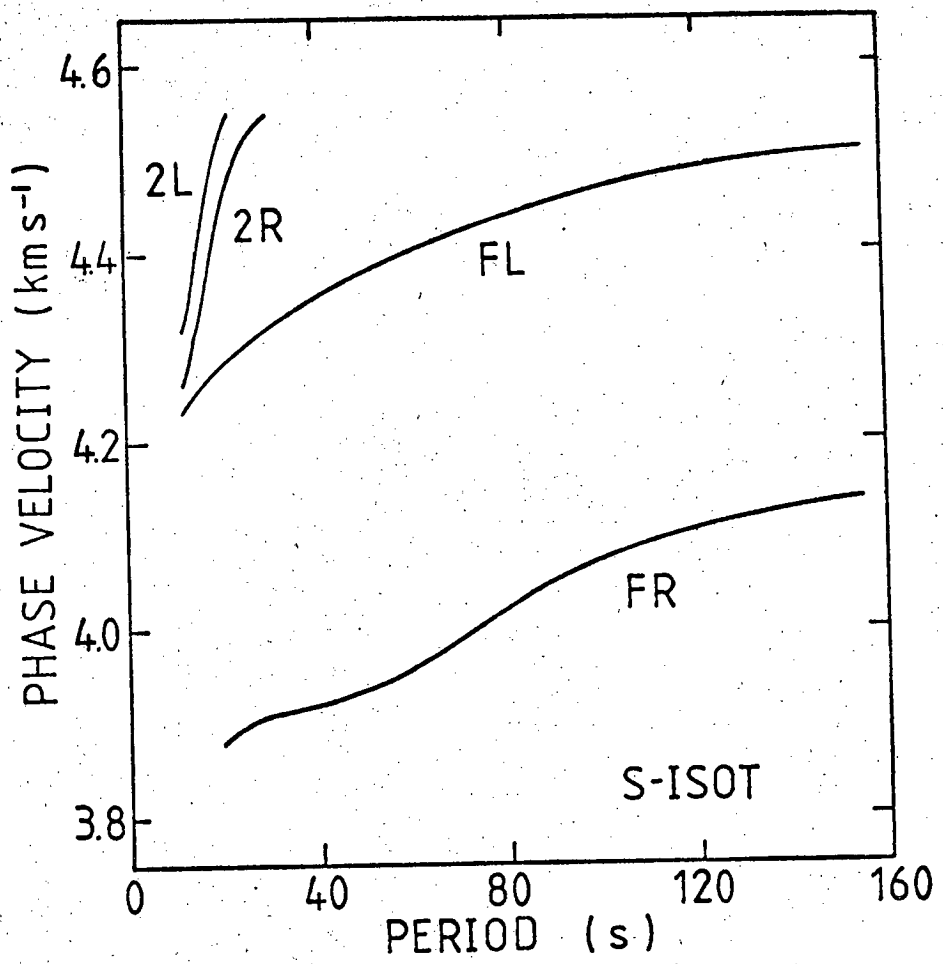

Figure 3.3

Phase-velocity dispersion of fundamental and first-higher Rayleigh and Love modes in isotropic model S-ISOT.

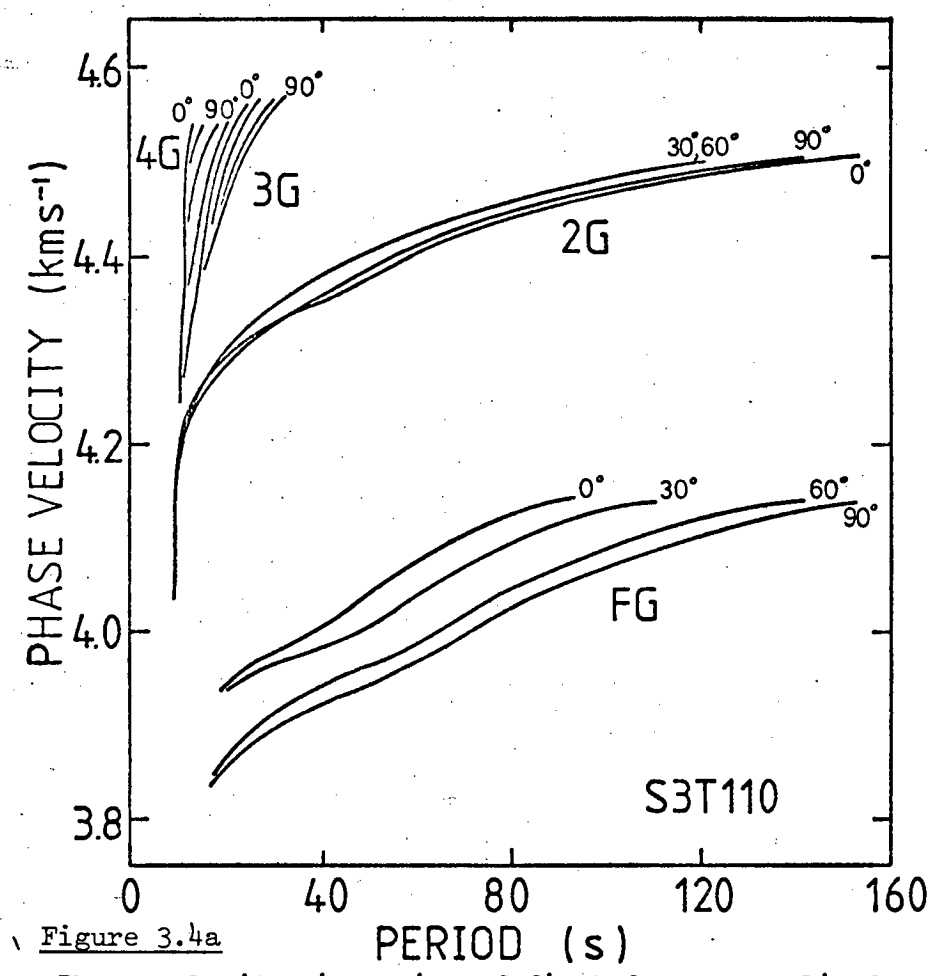

Figure 3.4a

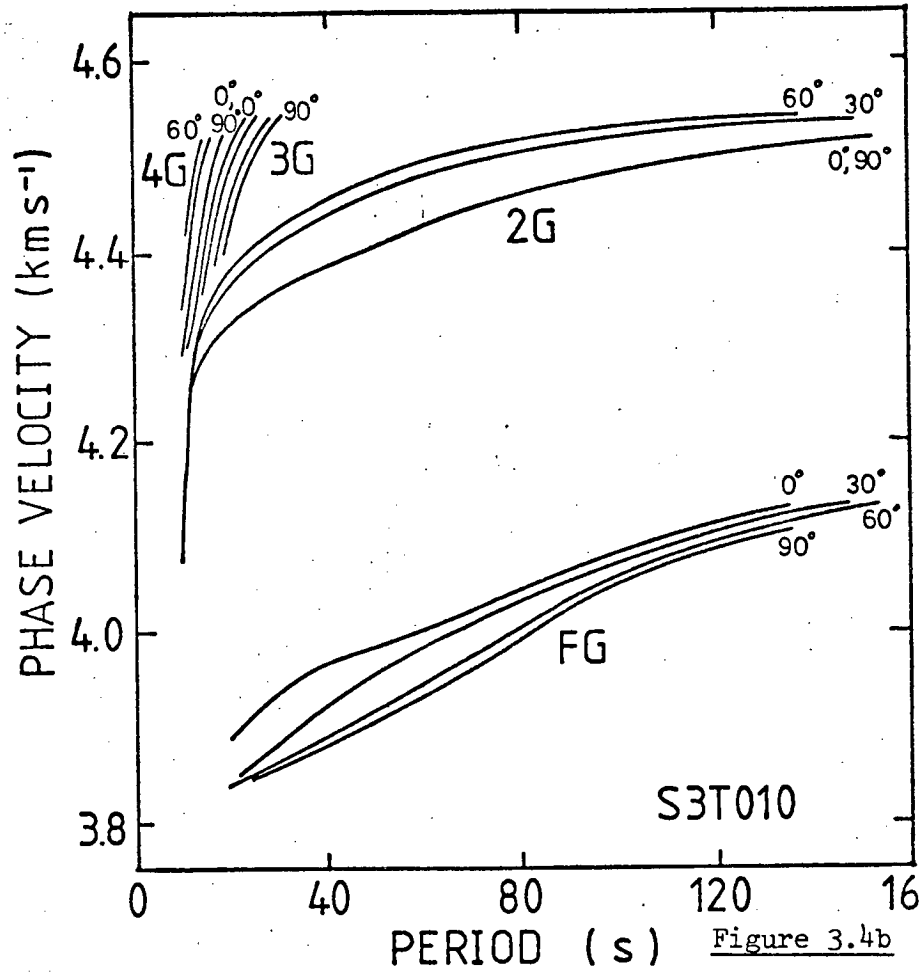

Figure 3.4b

Phase-velocity dispersion of first four generalised surface-wave modes, for four different azimuths of propagation for model S3T, which has an anisotropic low-velocity-zone.

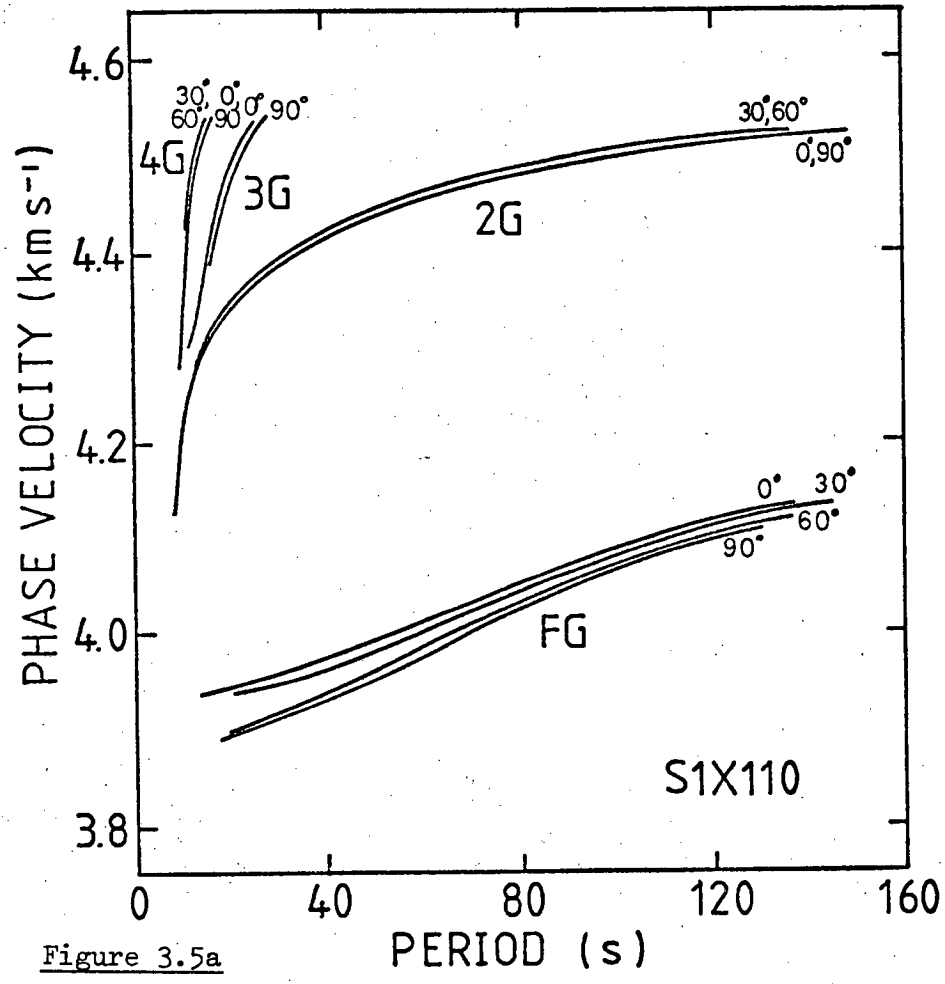

Figure 3.5a

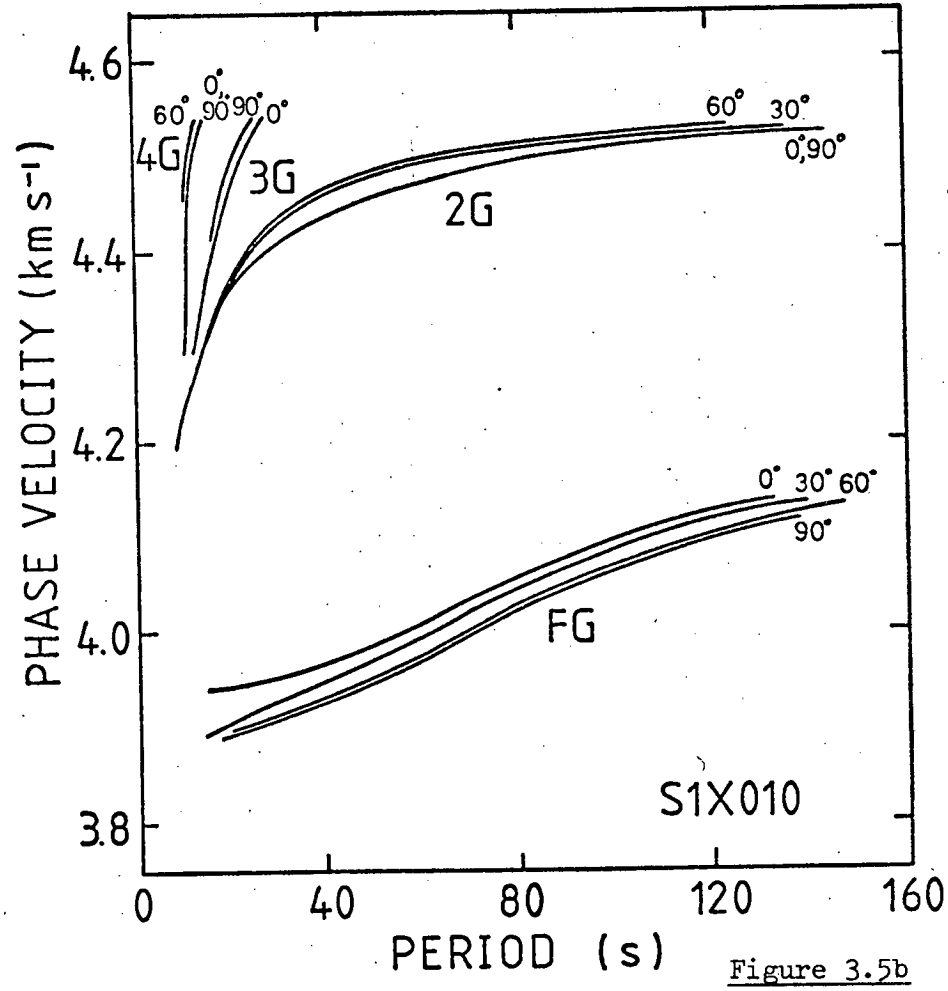

Figure 3.5b

Phase-velocity dispersion of first four generalised surface-wave modes, for four different azimuths of propagation for model S1X, which has an anisotropic lithosphere.

noting that the minimum and maximum phase-velocities occur at 90° intervals for modes corresponding to isotropic Rayleigh modes, and at approximately 45° intervals for modes corresponding to isotropic Love modes. The degree of phase-velocity anisotropy is generally rather greater for FG than for 2G, but is similar for both types of model, 110 and 010.

The particle-motion for surface-waves in these two models are illustrated by Figures 3.6 and 3.7. The symmetry planes lie in the directions 0°, for 110-models, and 0° and 90°, for 010-models. The particle motion in FG and 3G is generally similar to that in isotropic Rayleigh waves, that in 2G and 4G is closer to that for isotropic Love waves. (Mode 3G in S3T110 is exceptional in that it seems closer to a Love-mode, Figure 3.6a)

3.6 Particle-motion anomalies

3.6(a) General description

Particle-motion diagrams for all the models are shown in Figures 3.6 - 3.15

The most striking anomalies, ie. departures from pure Rayleigh-type or pure Love-type particle-motion, are in mode 3G. Inclined-Rayleigh-type motion occurs in the 010-models with inclinations of up to 60°, and particle-motion completely intermediate between Love- and Rayleigh- type occurs in the 110-models. In these 110-models, there are also fairly large anomalies in FG and 2G, and smaller effects in 4G. There are no anomalies in modes FG and 2G in any model of 010-type, except at the shortest periods.

In general the amplitudes of anomalies do not vary much with direction of propagation except very close to a symmetry direction where they fall rapidly to zero. This can be seen in the individual particle-motion diagrams, and is illustrated in more detail in Figure 3.16.

3.6(b) Effects of location of anisotropic layers

Models with anisotropy in the lithosphere include the letter X in their name, T indicates anisotropy in the low-velocity-zone. The variations of anonomaly amplitudes with period are summarised in Figure 3.17, which shows that, in 2G and 3G, anomalies tend to increase with decreasing period, down to about 15s. In FG, for models with anisotropy in the low-velocity-zone, anomalies have a maximum at intermediate periods and become smaller at short periods. Models with an anisotropic lithosphere show FG anomalies increasing at short periods.

The location of the anisotropy also has an effect on the maximum amplitude of any anomaly. For example, the anomalies generated in FG and 2G in S1X are slightly larger than those in S3T (Figures 3.7 and 3.6), although the latter has a greater degree of intrinsic anisotropy, so that the particle-motion in these modes is rather more sensitive to anisotropy in the lithosphere. Conversely, comparison of S3X and S1T (Figures 3.9 and 3.8), where the former includes a greater degree of anisotropy, shows that anomalies in 3G are affected more by anisotropy in the low-velocity zone. This is particularly marked for 010-models.

3.6(c) Changes in degree of anisotropy

Models S3T and S3X have similar structures to S1T and S1X respectively, but incorporate a greater degree of olivine alignment. Comparison of the particle-motion diagrams (Figures 3.6 with 3.8 and 3.7 with 3.9) shows that an increase in the degree of anisotropy results in a large increase in the anomalies in FG and 2G in the 110-models, but little change in the 3G anomalies for either 110-or 010-models.

3.6(d) Changes in the thickness of an anisotropic layer

Figures 3.10, 3.11 and 3.12 show results for models A3T, A1X and C1X which have only a thin (10km) anisotropic layer, situated at the top of the low-velocity-zone, the top of the lithosphere or the base of the low-velocity-zone, respectively. There are virtually no anomalies visible in any mode, except for 3G in model A3T.

So, although a rather thick layer is necessary to generate significant anomalies in FG and 2G, a rather thin layer can generate large anomalies in 3G.

If the anisotropy extends throughout both the lithosphere and the low-velocity-zone (model S3XT, Figure 3.13), there are large anomalies in FG, 2G and 3G. Those in 2G are rather larger than the sum of those produced by an anisotropic lithosphere and low-velocity-zone in isolation. Those in 3G are similar to those found for an anisotropic low-velocity-zone, additional evidence

that 3G is particularly sensitive to anisotropy in that zone.

The anomalies in FG and 2G in this model, S3XT, are larger than in any other model examined. However, the particle-motion is still close enough to Rayleigh or Love-type, respectively, especially at long periods, that anomalies would not be noticed on seismograms, unless a specific search were made.

3.6(e) Pure olivine vs. transversely isotropic olivine

Olivine aligned by syntectonic recrystallisation is not likely to be transversely isotropic, so two models with fully anisotropic olivine have been generated, S6T and S4X, with similar structure and degree of anisotropy to S3T and S1X. Details are in Appendix 1, particle-motion is illustrated by Figures 3.14 and 3.15. The particle-motion is very similar to that in S3T and S1X, the only significant difference being an increase in the anomalous vertical component of 2G, at short periods, in model S6T110. This might be expected as the pure olivine has a larger velocity variation in any vertical plane than the transversely isotropic olivine, apparently giving a greater tilting effect on the plane of particle-motion.

3.7 Effects of the Earth's sphericity

No method has yet been developed which would allow modelling of surface-waves in a spherical, gravitating, anisotropic Earth. In the isotropic case, the effects of sphericity can be modelled by imposing an extra velocity-gradient on a plane-layered structure (eg. Biswas and Knopoff, 1970), resulting in increased phase-velocities, especially at long periods, and slight changes in particle-motion. These effects for model S-ISOT are illustrated in Figure 3.18, and are quite small.

It is reasonable to expect similar effects in the anisotropic case, so that the amplitude of particle-motion anomalies might be changed by a few per cent. However, the character of particle-motion, whether inclined-Rayleigh or tilted-Rayleigh type, depends simply on the presence of two or one vertical, structural-symmetry planes, and will not be affected by sphericity.

Figures 3.6-3.15 Plots of particle-motion in each of the first four generalised surface-wave modes for models of anisotropic ocean basin structure. Particle-motion plots are in pairs, the upper plot being a horizontal cross-section, the lower plot a vertical section, parallel to the direction of wave-propagation. Vertical and horizontal sections are drawn to the same scale (see below).

The exact composition of each model is detailed in Appendix I

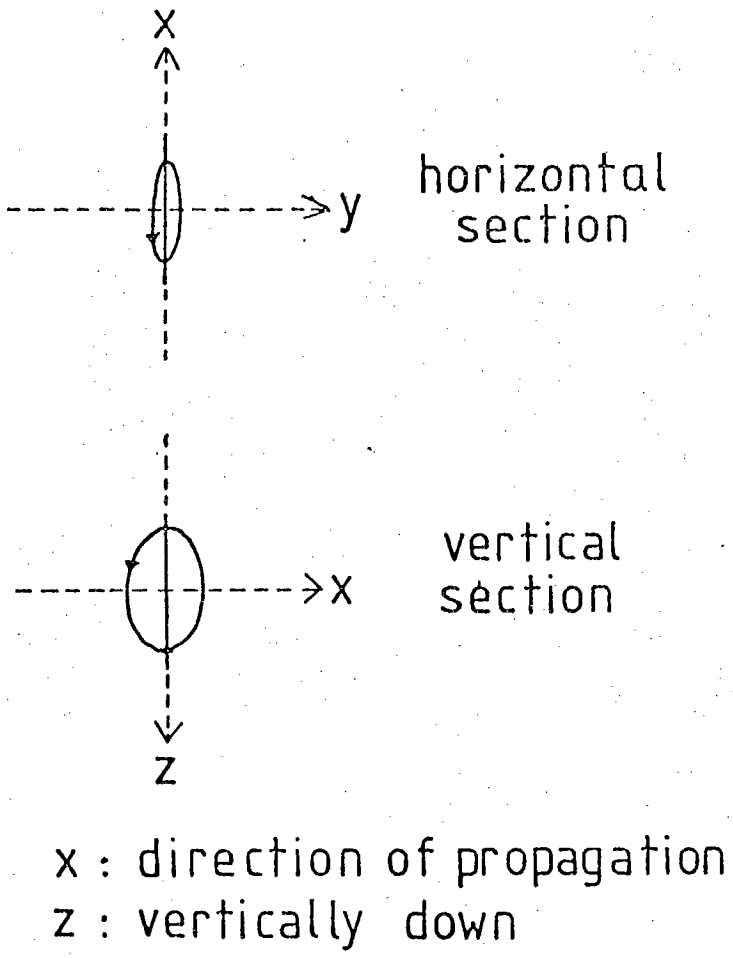

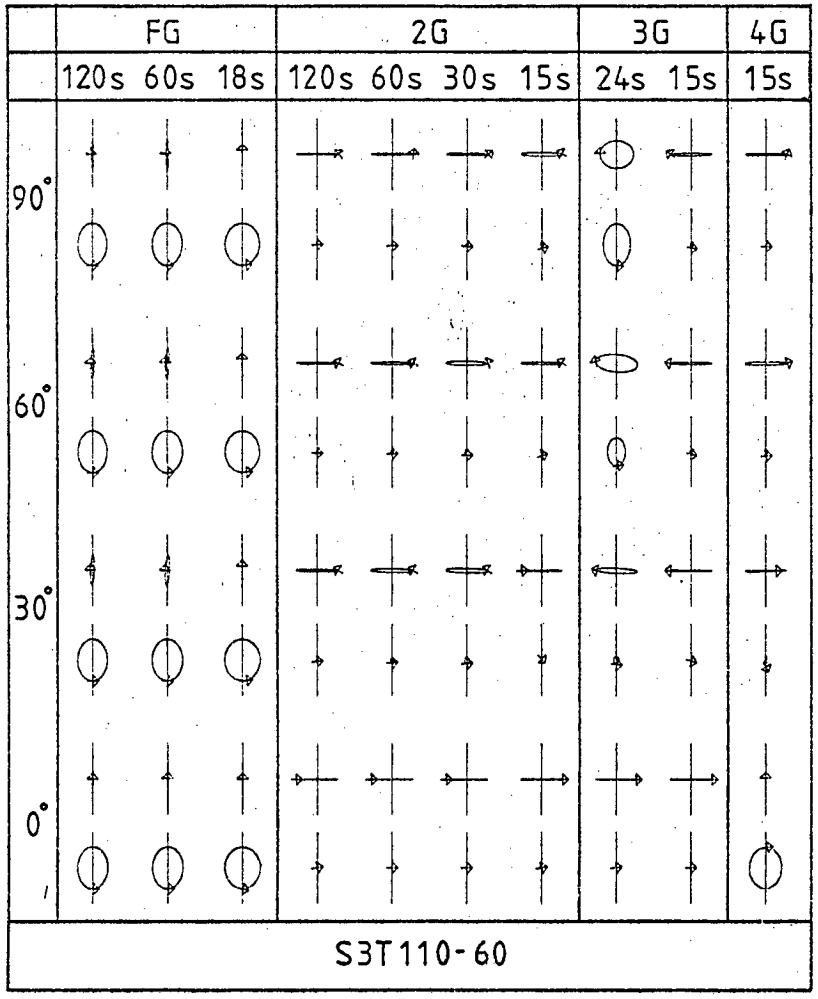

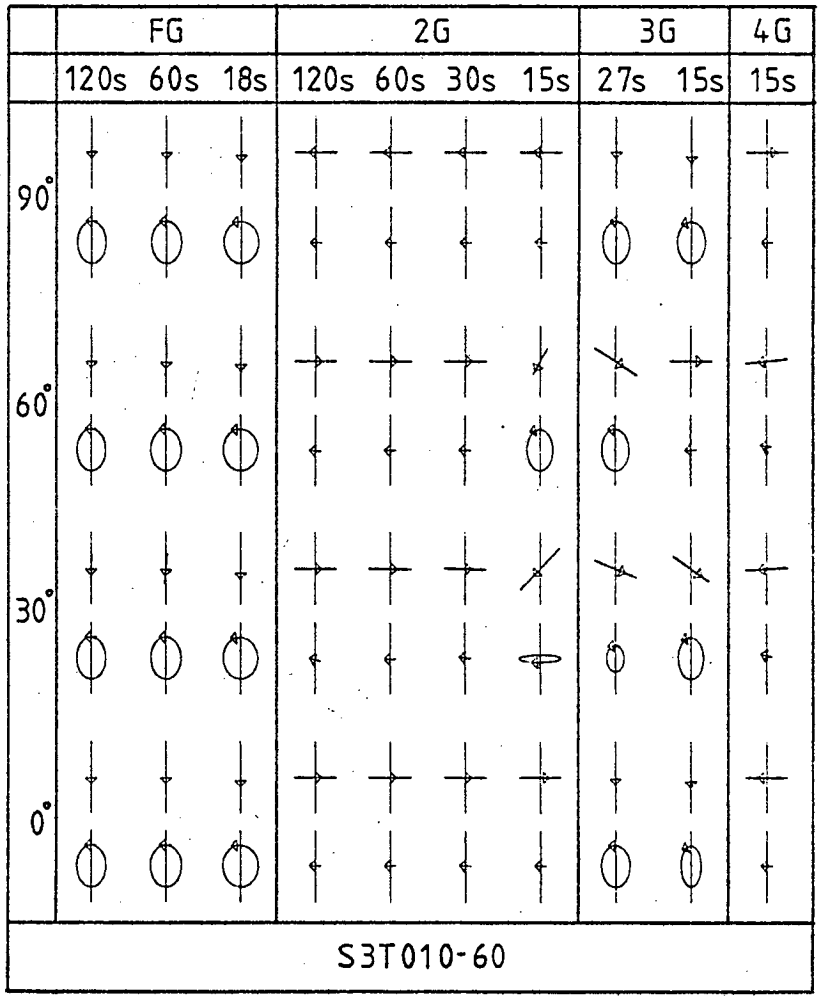

Figure 3.6a Model S3T has an anisotropic low-velocity zone Figure 3.6b

see explanation on p.46

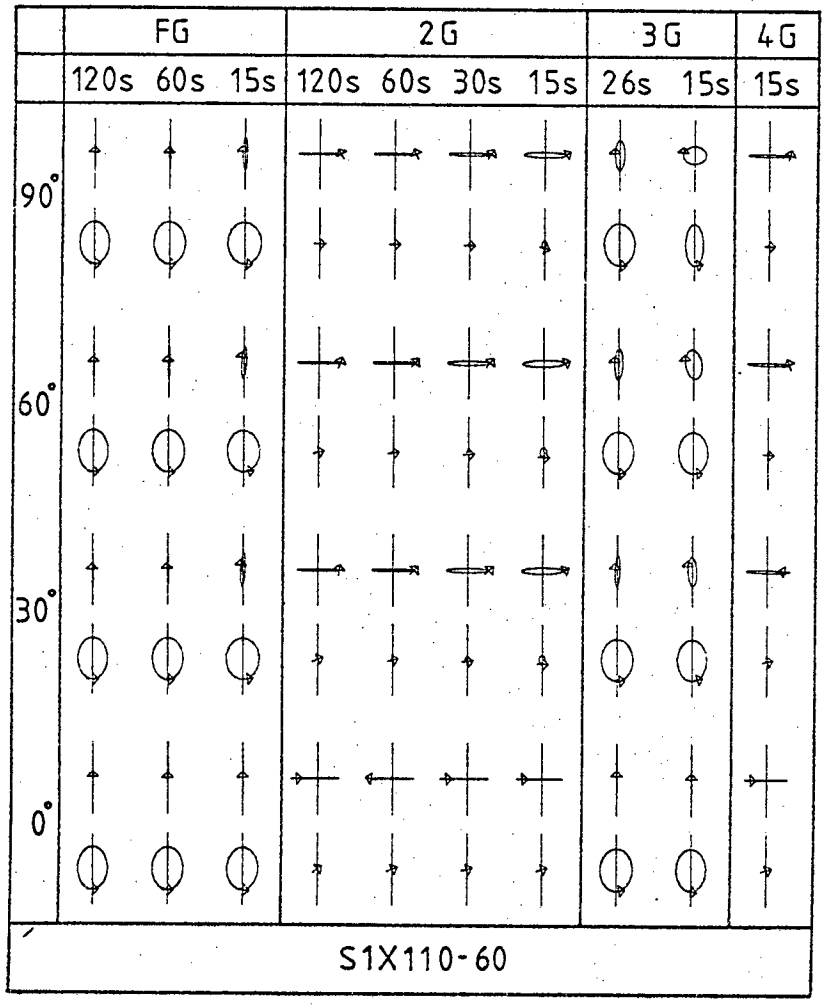

Figure 3.7a Model S1X has an anisotropic lithosphere

see explanation on p.46

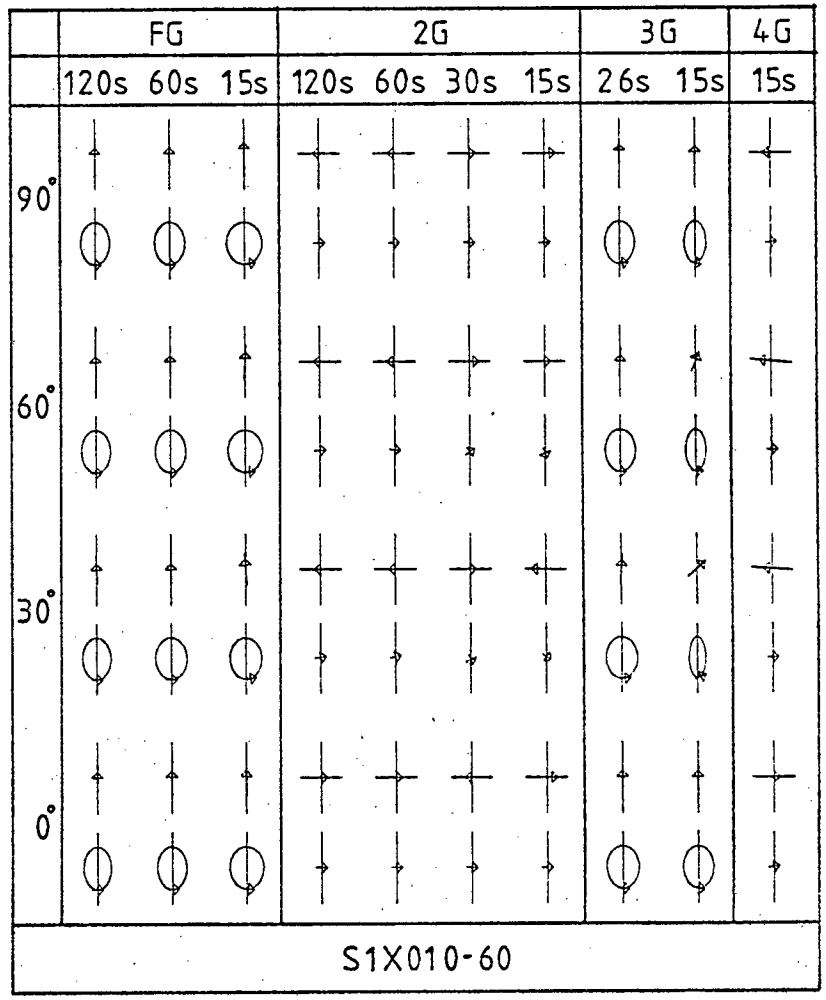

Figure 3.7b

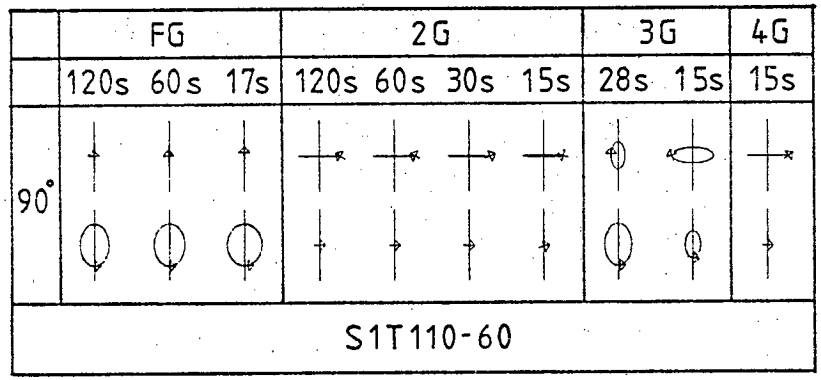

Figure 3.8a Model S1T has a slightly anisotropic low-velocity-zone

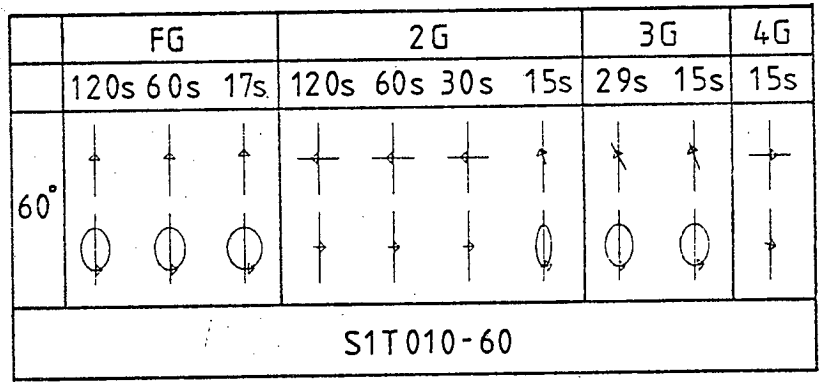

Figure 3.8b

see explanation on p.46

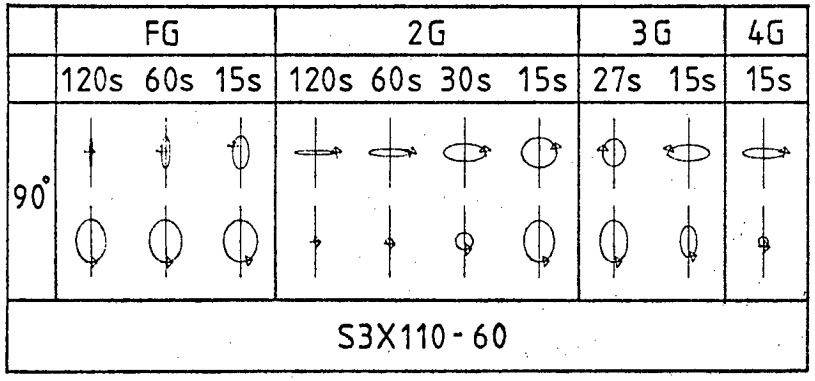

Figure 3.9a Model S3X has a highly anisotropic lithosphere

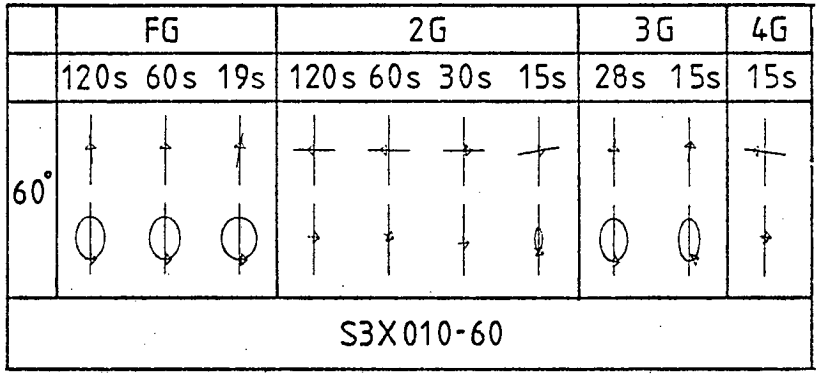

Figure 3.9b

see explanation on p.46

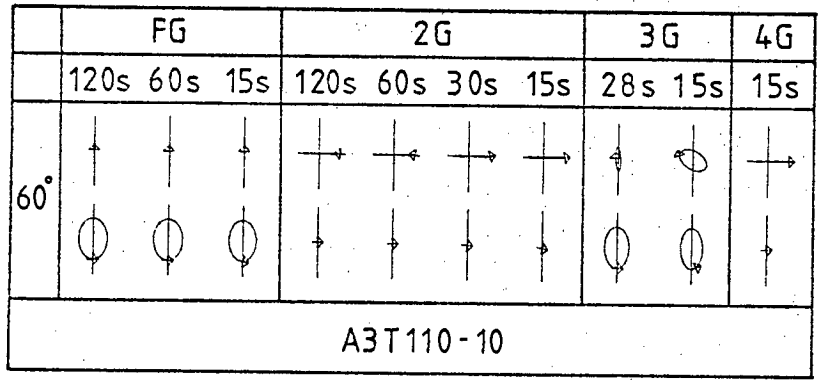

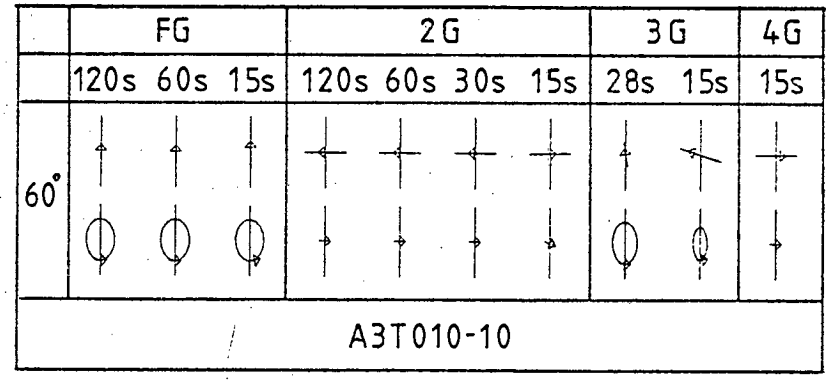

Figure 3.10a Model A3T has a 10km anisotropic layer ta the top of the low-velocity-zone Figure 3.10b

see explanation on p.46

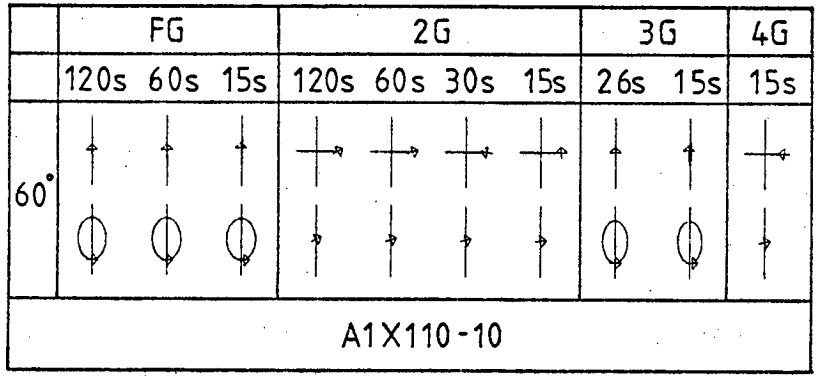

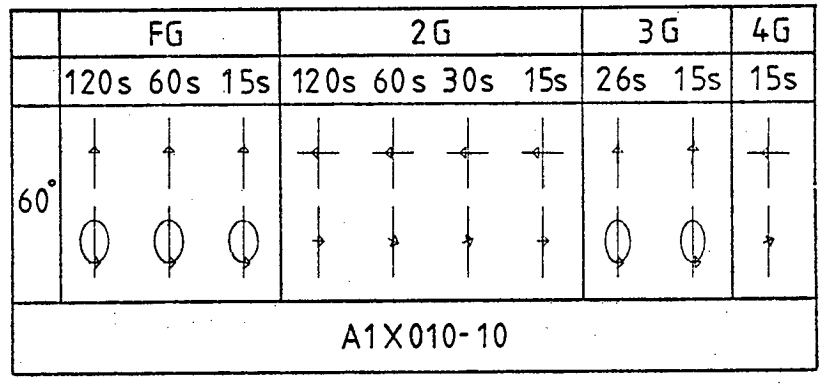

Figure 3.11a Model A1X has a 10km anisotropic layer at the top of the lithosphere Figure 3.11b

see explanation on p.46

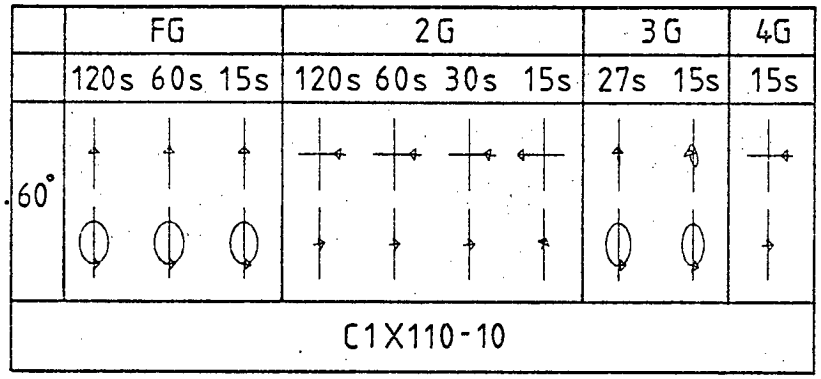

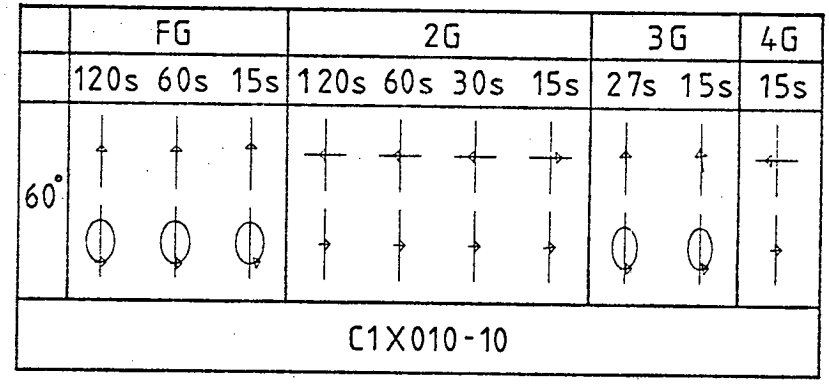

Figure 3.12a Model C1X has a 10km anisotropic layer at the base of the lithosphere Figure 3.12b

see explanation on p.46

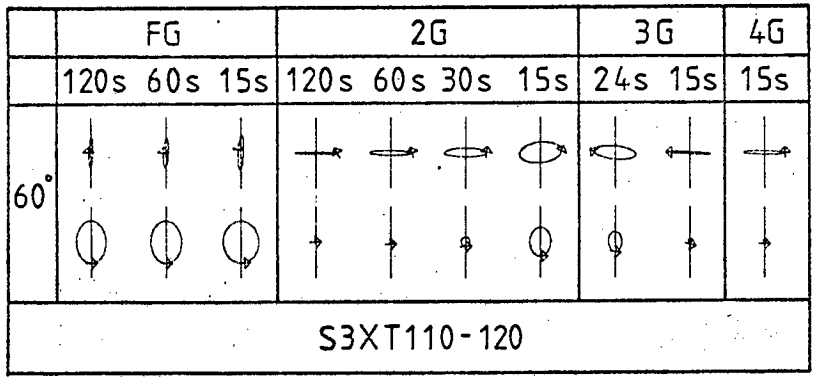

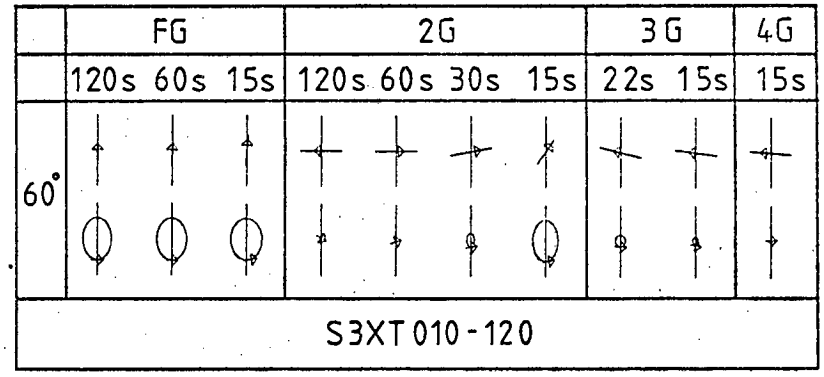

Figure 3.13a Model S3XT has both lithosphere and low-velocity-zone anisotropic Figure 3.13b

see explanation on p.46

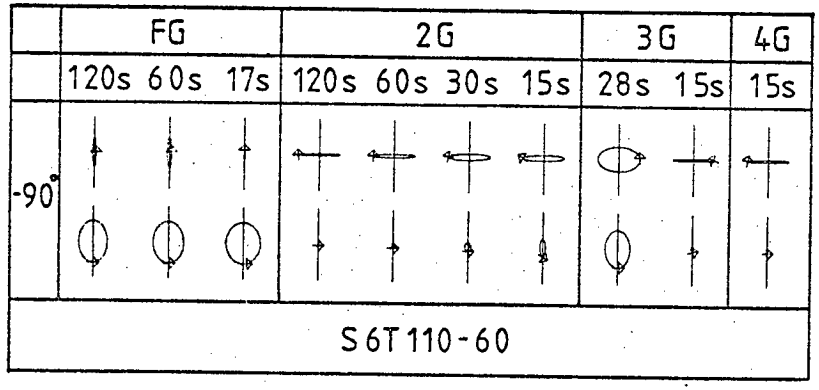

Figure 3.14 · Model S6T has an anisotropic low-velocity zone, incorporating orthorhombic olivine
see explanation on p.46

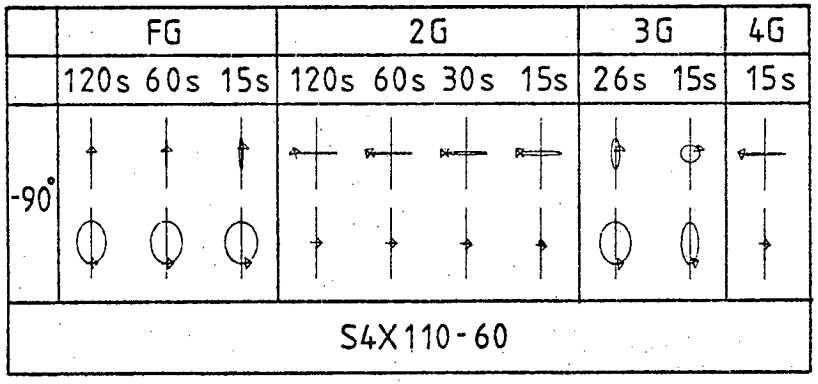

Figure 3.15 Model S4X has an anisotropic lithosphere, incorporating orthorhombic olivine
see explanation on p.46

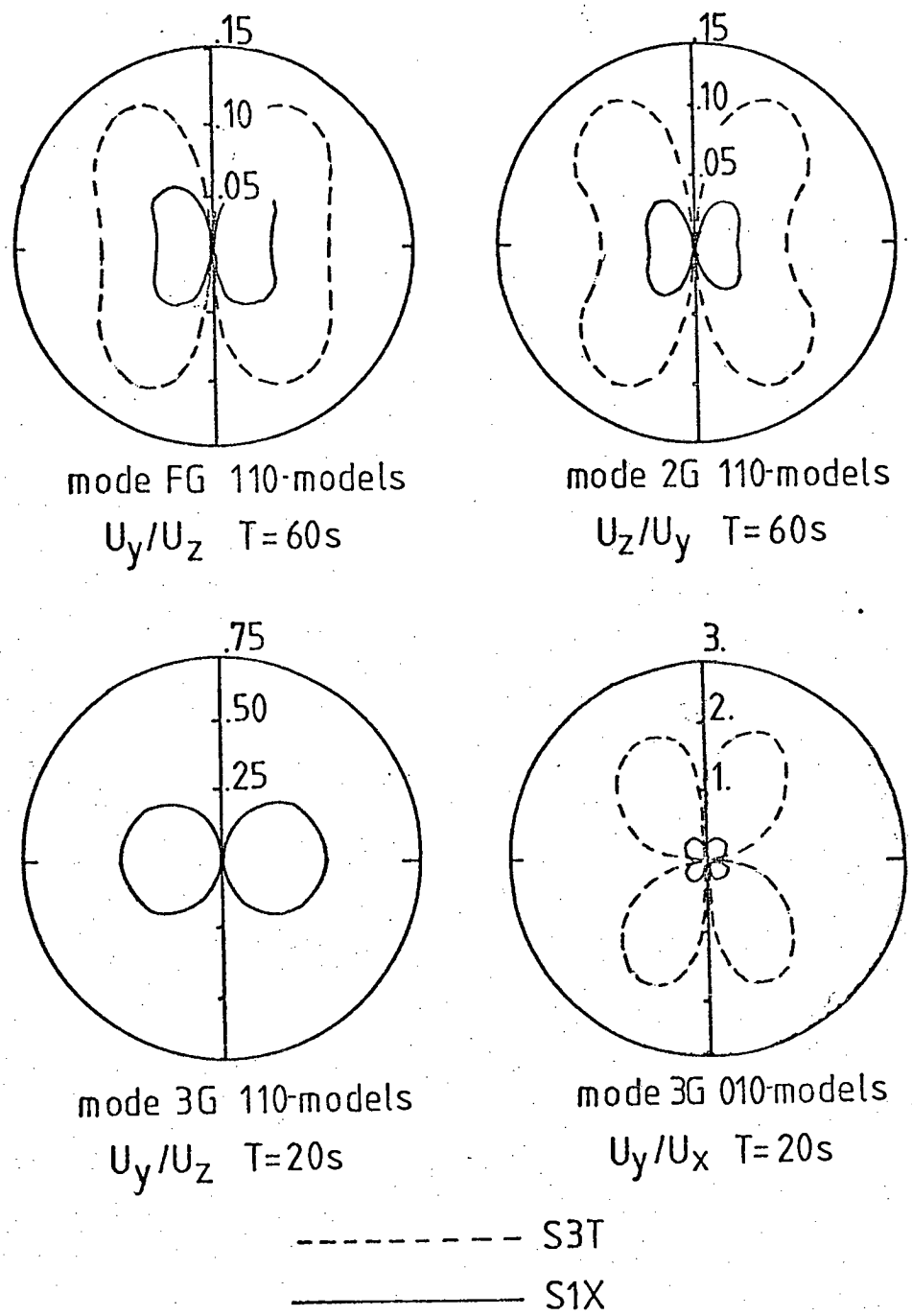

Figure 3.16 Theoretical azimuthal variation of the amplitude of particle-motion anomalies, models S3T and S1X.

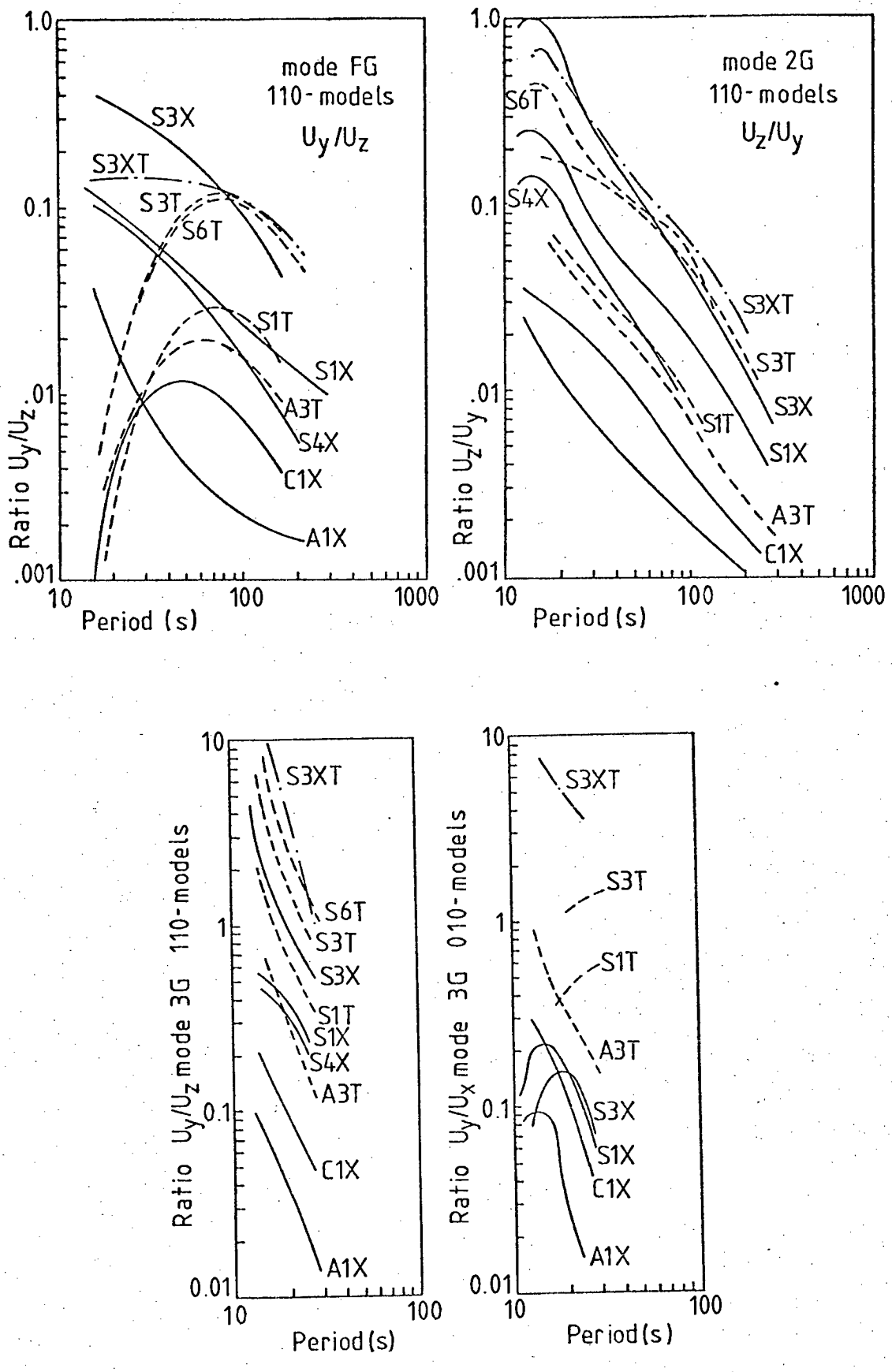

Figure 3.17 Variation with wave period of the maximum amplitude of particle-motion anomalies, for several models.

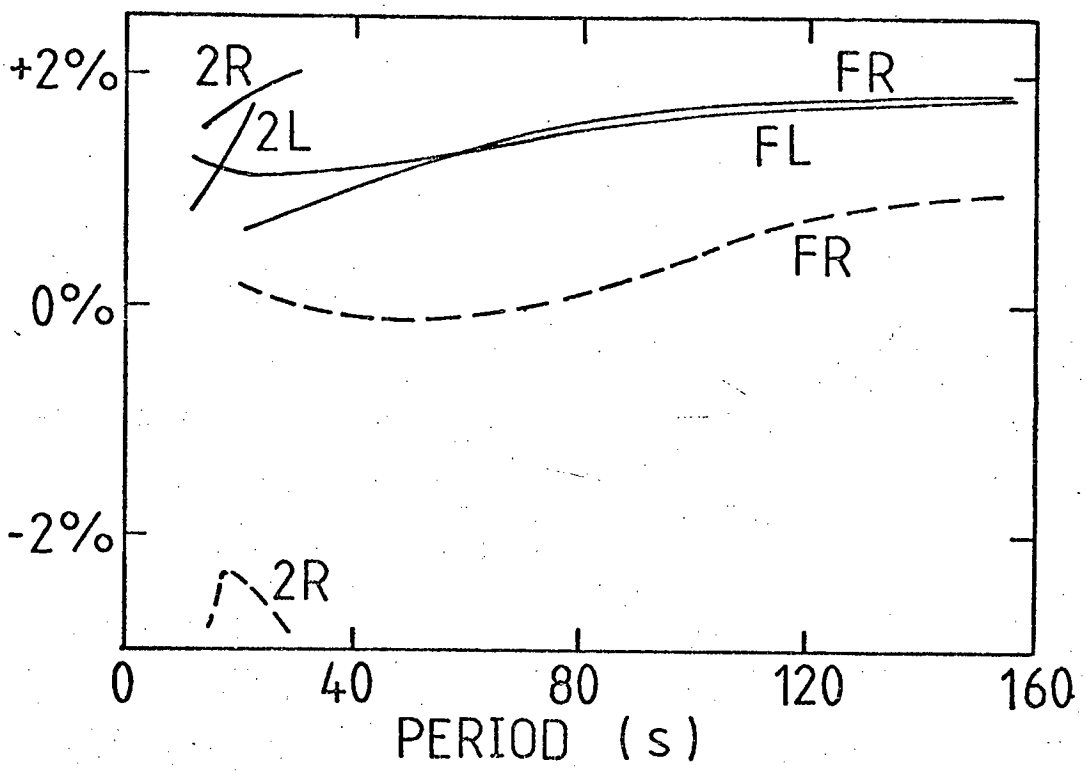

Figure 3.18 Changes in phase-velocity (solid lines) and in ellipticity of Rayleigh- wave particle-motion (dotted lines), when allowance is made for Earth-curvature in model S-ISOT.

3.8 General Conclusions

Large particle-motion anomalies are likely to occur in the third generalised surface-wave mode, 3G, which corresponds approximately to the isotropic second-Rayleigh mode, in the presence of almost any reasonable amount and alignment of anisotropic material in the top 120km of the oceanic upper-mantle, only a very thin anisotropic layer being required if located in the low-velocity zone. Similar anomalies are found for surface-waves propagating in models of continental structure, which can also be generated by rather thin (10km or less) anisotropic layers in the upper-mantle (Crampin and King 1977).

When olivine has been aligned by glide-plane slip on horizontal planes (010- models), even a rather large thickness of anisotropic material does not cause any significant anomalies in the other surface-wave modes, FG, 2G and 4G. If, however, the olivine is aligned, as by syntectonic recrystallisation in a zone of horizontal shearing, with a- and b-axes inclined to the horizontal (110-models) then quite large particle-motion anomalies occur in all modes, provided that a fairly thick (a few tens of kilometers), anisotropic zone is present.

If olivine alignment in the real Earth has occurred in glide-plane slip, then the 010-models are appropriate and observations of particle-motion for the 3G mode should show inclined-Rayleigh-type motion, with a variation in inclination, with azimuth of propagation, such as that indicated in Figure 3.2b. For several reasons it will be difficult to observe such particle-motion on seismograms. Any error

in assigning a direction of travel to the wave, or any error in calibration of horizontal seismograms, will cause pure Rayleigh-type motion to appear as inclined-Rayleigh-type. More important is the fact that the group-velocity of the 3G mode is very close to those of 2G, 4G and higher modes, so that several, interfering wave-trains will be recorded on the seismogram. Only events in which 3G is preferentially excited will be useful. If observations can be made, then the relative phases of the radial and transverse components of particle motion, as shown by the + and - signs in Figure 3.2b, will provide a good method for locating the planes of symmetry of the underlying structure. However, since these 3G anomalies vary rather irregularly with the depth, thickness, or degree of anisotropy present, little information about these parameters is likely to be resolvable from the observations.

If olivine alignment in the real earth is similar to that in the 110-models, then anomalous particle-motion should be fairly easily observed in <u>any</u> mode. Anomalies in 2G should be easiest to observe as, over a range of periods for which anomalies should occur, for very long travel paths, this mode will arrive after the higher surface-wave modes and before the fundamental mode. For paths longer than about 7000km, it also arrives after most of the body-wave phases. Vertical and transverse components will show coupling on the seismogram. Such coupling cannot result from direction of travel or calibration errors so that accuracy in measuring these parameters is much less important than for observation of the inclined Rayleigh-type motion characteristic of the 010-models. The pattern of relative phases of vertical and transverse components, as shown in Figure 3.2a, will, again, indicate the plane of symmetry of the underlying structure.

In all the 110-models used here, the particle-motion ellipse in mode 2G is tilted towards the direction of olivine a-axes, in the manner illustrated by Figure 3.1a, so that a pattern of relative phases as shown in Figure 3.2a also indicates the direction of alignment of the a-axes within the plane of structural symmetry. This in turn indicates the sense of shear, for alignment by syntectonic recrystallisation, in the anisotropic zone (Figure 1.2) The period for which the amplitude of particle-motion anomalies is greatest, especially in FG, depends on the depth to the anisotropic layer, so some information about this parameter should be resolvable (Figure 3.17)

If, as is likely, both glide-plane slip and syntectonic recrystallisation produce alignment of olivine in the upper-mantle, each mechanism predominating in a different depth range, then anomalies due to the latter alignment will be much more obvious. Even quite large amounts of olivine aligned by glide-plane slip may be present, although the particle-motion appears to indicate only the alternative alignment.

4. RECORDING AND MEASURING PARTICLE-MOTION ANOMALIES

4.1 Introduction

There are five major problems in observing the particle-motion of oceanic surface-waves:

1. Several oceanic higher-modes, including 2G, have rather similar group-velocity dispersions. To allow observation of particle-motion in a particular mode, at a particular frequency, that mode must either travel at a different group-velocity, or be preferrentially excited, compared with the other modes, at similar frequencies.
2. Recording stations are sited on land, either on islands or on the edge of a continent, and so cannot record the true particle-motion of an oceanic wave. Records from long-period ocean-bottom seismographs would be useful, provided three orthogonal components were recorded, and the orientations of the instruments accurately known. However, such records are not yet generally available.
3. Certain particle-motion anomalies can only be observed if the direction of the wave's phase-velocity is known (Figure 3.1b). As the earth is not spherically symmetric, a wave will not travel exactly along the great-circle path from epicenter to recording station and it's direction of travel cannot be accurately measured, unless a large array is available.
4. Inhomogeneities in the structure close to a recording station can distort particle-motion, sometimes in a highly symmetric fashion, imitating the effects of large-scale, anisotropic alignments.

5. Few recording instruments are sufficiently accurately calibrated to allow precise measurements of the relative amphitudes and and phases of the components of particle-motion.

Each of these problems must be considered in some detail before useful observations can be collected.

4.2 Surface-wave group-velocities

As explained in Chapter 3, anisotropy in the oceanic upper-mantle may be indicated by anomalous particle-motion in modes FG and 2G, for one type of anisotropic alignment, or in mode 3G, for the second type. It is necessary to observe such a mode over a range of periods without interference from other modes. If the various surface-wave modes excited by an event travel at different velocities, in the period range of interest, they may be separated on a seismogram by filtering.

The group-velocities of the first four modes, for model S-ISOT, are shown in Figure 4.1. Group-velocities depend on the structure of the model, but, for periods above 20 seconds, similar results are found for most models of ocean-basin structure. (eg. Saito and Takeuchi 1966, Thatcher and Brune 1969).

At periods below 15 seconds, the group-velocities of the higher-modes, and the fundamental Love-mode, are all rather close and the dispersion may change markedly between similar models (eg. Sykes and Oliver 1964a).

Approximate group velocities may be calculated for anisotropic models by differentiating the phase-velocity dispersion (Crampin and Taylor

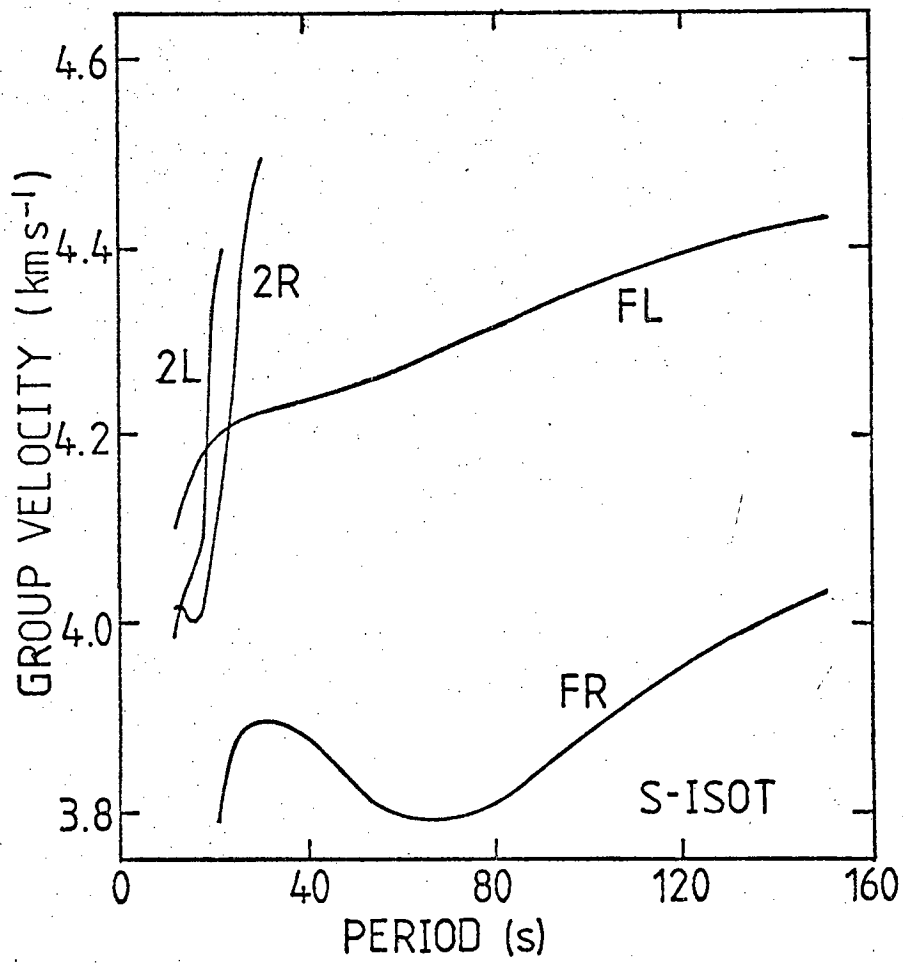

Figure 4.1 Group-velocities for fundamental and first-higher Rayleigh and Love modes in isotropic ocean-basin model S-ISOT.

1971). This will give similar results to S-ISOT, for periods down to about 20 seconds, as isotropic and anisotropic phase-velocity dispersions are similar (Figures 3.3 - 3.5). At shorter periods particularly below 15 seconds, the anisotropic modes may exchange characteristics, from Love-type to Rayleigh-type, or vice-versa, with corresponding sharp changes in gradient in the phase-velocity dispersion. As a result, there may be marked maxima and minima in group-velocity, at periods which vary from one direction to another in the same model, and between models.

It is, therefore, impossible to predict group-velocities at periods less than 20 seconds accurately, without detailed knowledge of the structure, and of any anisotropy present.

The group-velocity curves in Figure 4.1 show that, for suitably long travel paths, the fundamental Rayleigh-mode, or FG in the anisotropic case, for periods above 20 seconds, will arrive after all the other modes. The fundamental Love-mode, or 2G, will arrive after the higher modes at periods above 30 seconds. When the second-Rayleigh mode, or 3G, as appropriate, is not present, as is likely for many events (see next section), 2G may be isolated down to 20 seconds. At shorter periods there may be group-velocity differences between modes sufficient to isolate each mode on a seismogram. It will, however, be impossible to identify a mode by its group-velocity alone. The second Rayleigh and Love modes, or 3G and 4G, and any higher modes, cannot be separated, even at periods above 15 seconds, as their group-velocities are too close together. (There are no computations for the higher modes shown here, but Kovach and Anderson (1964) for example , report group-velocity computations for several

higher modes. In the period range 10 - 30 seconds many of these have velocities between 4 and 4.5 km/s.)

4.3 Relative excitations of surface-wave modes

Excitation of surface-waves depends on focal depth, focal mechanism, direction of propagation (for most focal mechanisms) and on the structure in which an event occurs. Methods are available for computation of the relative excitation of different modes in isotropic structures (eg. Saito 1967) and Forsyth (1975a), for example, gives results for fundamental and second Love-modes, for a surface-focus and an oceanic structure (Figure 4.2).

Relative excitation in the anisotropic case can be roughly estimated from the particle-displacement/depth variations, for the different modes, provided that focal mechanism and direction of propagation are favourable. These variations, for the oceanic models used in this study, are illustrated by Figure 4.3. A particular mode at a particular period is most likely to be excited by an event which occurs at a depth corresponding to a particle-displacement maximum, and will not be excited by an event at the same depth as a node.

In order to observe particle-motion anomalies in mode 3G, it is necessary that this mode be preferentially excited relative to 2G, 4G and other higher-modes. This mode is most likely to occur for events at 80 - 150 km depth, which are also likely to excite 2G and 4G at similar periods. Modes 2G and 4G have predominantly transverse particle-motion and so might be eliminated by suitable choice of focal mechanism. However, many higher Rayleigh-modes, corresponding to the odd numbered generalised modes, also have large

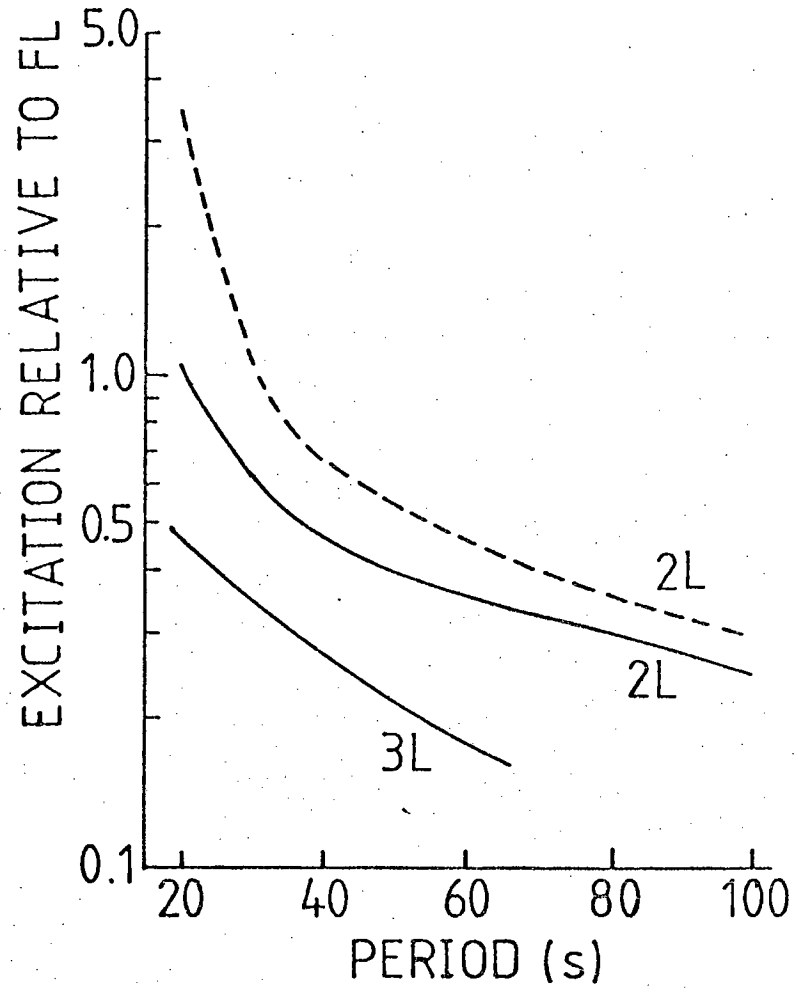

Figure 4.2 Theoretical excitation of higher-mode Love-waves, relative to the fundamental Love mode. Solid lines are for a shallow earthquake in the 0-10 M.y. zone, dashed line is for a shallow event in the 10-50 M.y. zone (from Forsyth 1975a).

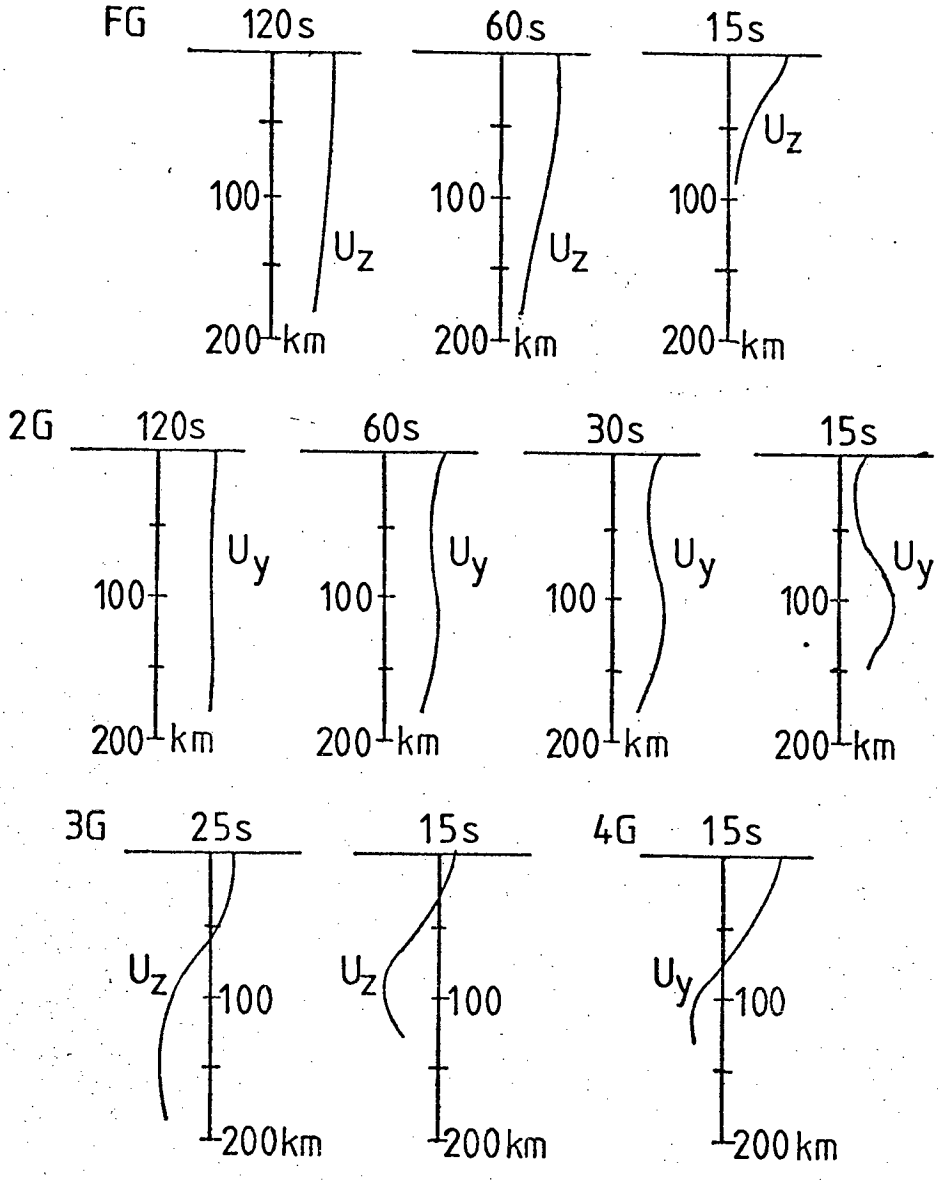

Figure 4.3 Particle-motion displacement amplitude as a function of depth and period, for the first four generalised surface-wave modes in anisotropic ocean-basin model S1X010-60-30°. Other anisotropic models are similar.

displacements in the low-velocity-zone (Kovach and Anderson 1964) and so several modes are likely to be excited. So, although it may be possible to find higher Rayleigh-type modes for a few earthquakes, it will be very difficult to determine which mode is present, 3G, 5G or higher .

In order to observe particle-motion anomalies in 2G down to periods of 15 seconds or less, it would be useful if all higher-modes could be excluded. Since the higher Rayleigh-modes, similar to mode 3G, have large displacements in the low-velocity zone, and only small displacements above 50 km depth, they should have less relative excitation in shallow earthquakes. However, such events are likely to excite 4G in preference to 2G, at the short periods under consideration (Figure 4.2).

There is a node for 4G, and for all higher Love-modes, (Stephens and Isaacs 1977), corresponding to even numbered generalised modes, at the top of the low-velocity zone, so an event near 70 km depth should excite only 2G, and odd numbered generalised modes. Group-velocities may allow isolation of the separate modes and any predominantly transverse arrival is then likely to be mode 2G.

4.4. Distortion of particle-motion by changes in structure

Slight, localised, changes in structure, such as those associated with the presence of an oceanic island in the middle of a stable ocean basin, will have little effect on the characteristics of a passing surface-wave, whose wavelength is likely to be comparable with, or larger than, the size of the anomalous region. However, particle-motion within the anomalous region may be rather different

from that expected on the ocean floor. A large deviation is likely when particle-motion is a rapidly varying function of depth within the crust, as the existence of an island implies an increase in crustal thickness to at least twice that common beneath the deep-ocean. Fortunately, for all the modes of interest in this study, FG, 2G, 3G and 4G, there is only a slow variation of particle-motion through the crust (with the exception of mode 3G at periods less than 12 secs), and so particle-motion is likely to be reliably recorded at ocean island sites.

The change in structure in passing from an oceanic to a continental region will have a much larger effect. At the boundary, a wave may be transmitted, reflected or converted to other modes, depending on the period, the mode, and the detailed structures at the boundary. Several attempts have been made to model surface-wave propagation across both passive and active margins (eg. McGarr 1969a, Kane and Spence 1963, Mal and Knopoff 1965, Gregerson and Alsop 1976) and it seems likely that considerable mode-conversion must take place. Only those modes whose energy-depth distributions are similar in both continental and oceanic structures (ie. FG and 2G at long periods) will cross the margin relatively undisturbed. If anisotropy is confined to the oceanic region, some conversion must take place even for these modes. For example, a transverse component associated with the Rayleigh-type mode FG would be converted to a Love-mode in the continental structure. The oceanic modes 3G and 4G have large amounts of energy travelling in the low-velocity zone, and modes FG and 2G at short periods are concentrated in the crust and upper-lithosphere. Continental and oceanic areas have very different crustal and upper-mantle structures, so considerable reflection and mode-conversion

are likely to take place at the continental margin. It may be possible to estimate the oceanic particle-motion from recordings made close to the margin, provided a large proportion of the energy is transmitted rather than reflected at the structural boundary, as the sum of the newly generated modes should then show the same particle-motion as the original wave. It is probable that only the longer periods of FG and 2G will be transmitted with sufficient energy (McGarr 1969a).

4.5 Lateral refraction of surface waves

Studies of refraction of surface-waves have been reported by several authors including Evernden (1953 and 1954), McGarr (1969b) and Capon (1970). The fullest investigation is Capon's, which used the Large Aperture Seismic Array in Montana (LASA) to measure the direction of approach of Rayleigh wave energy for 26 events, each at several periods and at different time intervals along the wave train. Capon was looking for arrivals which had been reflected or refracted at continental edges and many of his paths crossed or passed close to regions of complex structure. In the present study, only waves which have travelled mainly in a single ocean basin will be useful so only 6 of Capon's paths, shown in Figure 4.4, are relevant. His findings, for the energy arriving first along these paths, are summarised in Table 4.1. To eliminate any effect due to the location of LASA, a study has been made of fundamental Rayleigh and Love arrivals at the Alaskan Long Period Array (ALPA). Direction of approach has been determined by beam-energy analysis using a procedure developed by A.L.Levshin and J.Fyen (private communication) at NORSAR.

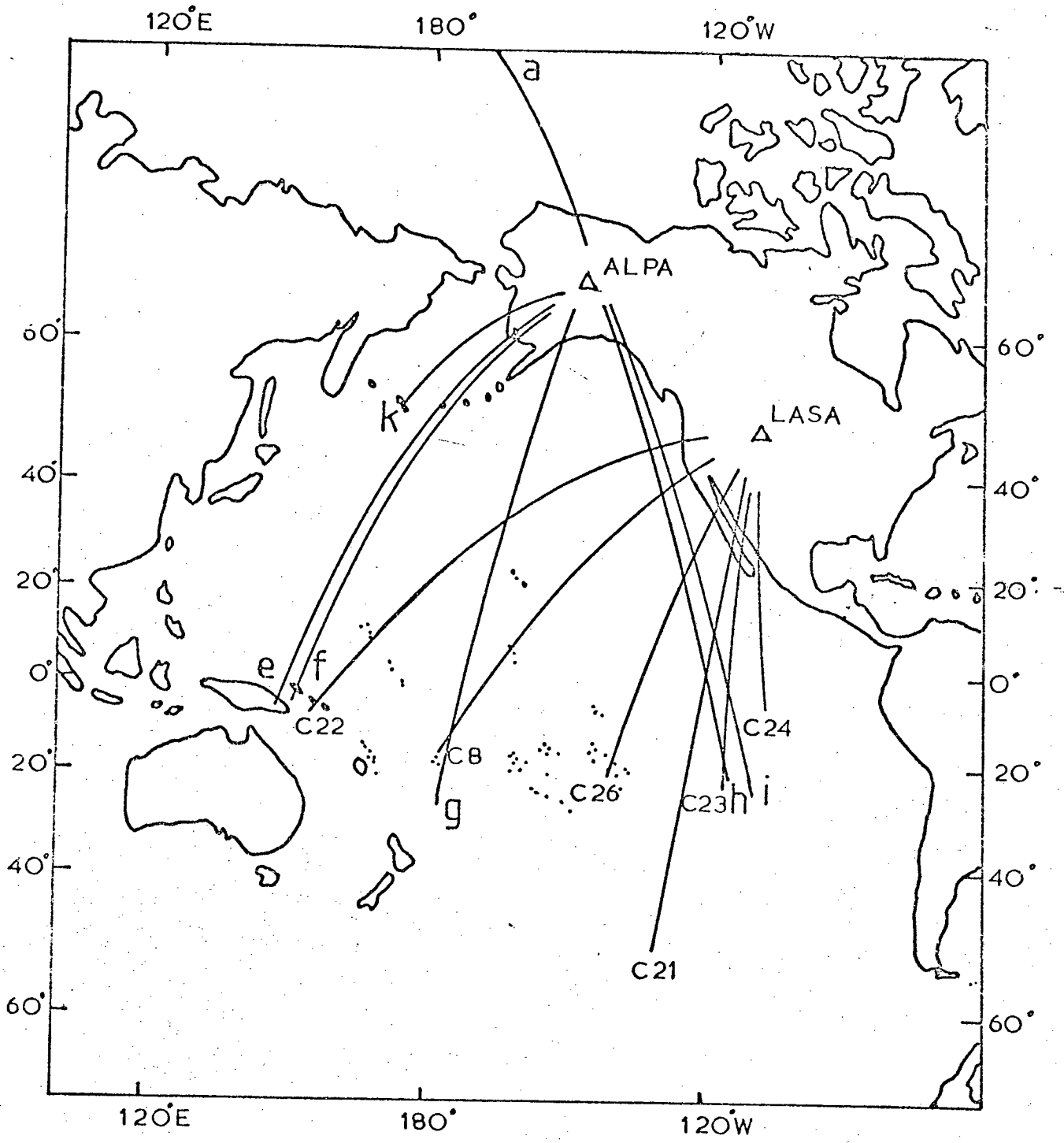

Figure 4.4 Travel-paths of surface-waves examined for lateral refraction effects. C8-C24 are from Capon (1970), a-h from the present study.

Event	all periods	Azimuthal deviations (degrees) 40secs	33secs	25secs	20secs
C8		0	0	0	-5
C21		0	-5	-7	
C22		0	0	3	3
C23		0	0	-29	
C24		0	0		13
C26		0	0	0	6
a	4				
e	0				
f	0				
g	0				
h	10				
i	6				
k	0				

Table 4.1 Direction of approach of first arrival of Rayleigh-wave energy, relative to great-circle path from epicenter. C8-C26 are arrivals at LASA, measured by Capon(1970). a-k are the present study, measured at ALPA (see text).

The paths used are shown in Figure 4.4 and the plots of beam-energy against azimuth and arrival time are shown in Figure 4.5. These results are also summarised in Table 4.1, which shows that, in most cases, the energy arriving at the start of a wave train approaches along the great-circle path from the epicentre. However, in three cases, C21,C23 and (h),quite large deviations are found and smaller deviations can be seen for paths(a),(i)and C22. The records for (h) (Figure 4.6) show radial and vertical motion with the Love-wave arrival and transverse motion with the Rayleigh-wave arrival, consistant with the suggestion that both Love and Rayleigh waves have been similarly refracted. The same effect can be seen for event (i) on Figure 4.7.

That refraction is observed at both LASA and ALPA for signals from events in the same area suggests that refraction takes place near the source, within the ocean basin.

McGarr (1969b), proposed similar, horizontal refraction of Rayleigh-waves, in the Pacific basin, to account for large variations in the recorded amplitude of signals between closely spaced stations in North America. None of the long-period arrays is sufficiently close to an ocean-basin to be useful for observation of oceanic particle-motion, so single stations in more suitable sites must be used. In view of the array results described above, the direction of propagation of energy arriving at the start of a surface-wave train can only be taken as the great-circle azimuth plus or minus 10-15^{o}. So, small anomalies of the inclined-Rayleigh type (Figure 3.1b) will not be observable.

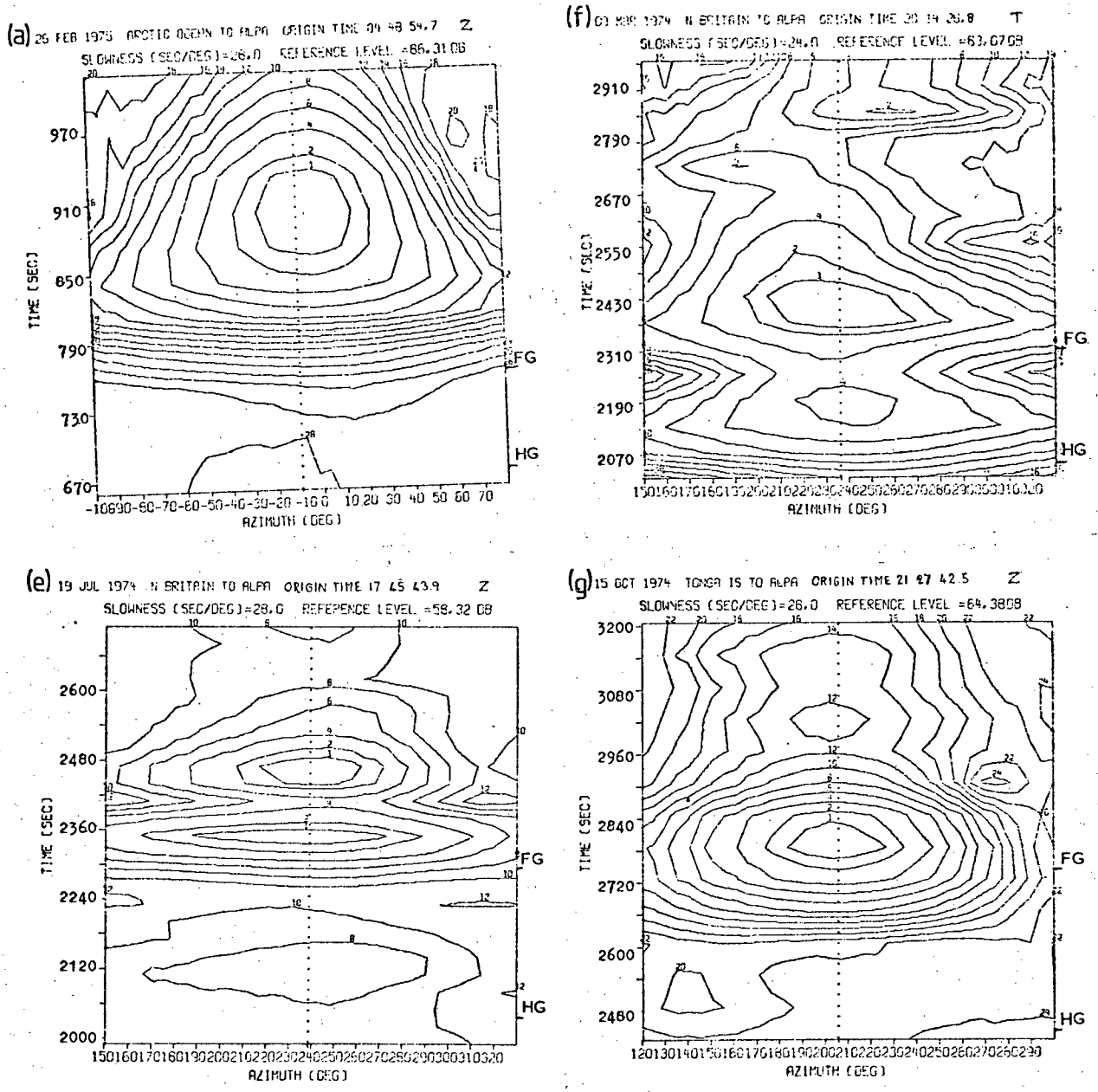

Figure 4.5 Array beam-energy as a function of approach azimuth and time (measured from origin time) for surface-wave arrivals at ALPA. Contours are beam-energy in decibels down from maximum. The dotted lines mark the azimuth of the great-circle path from the epicenter to ALPA. FG and HG mark the expected arrival times corresponding to group velocities of 4.0km/s and 4.5km/s.

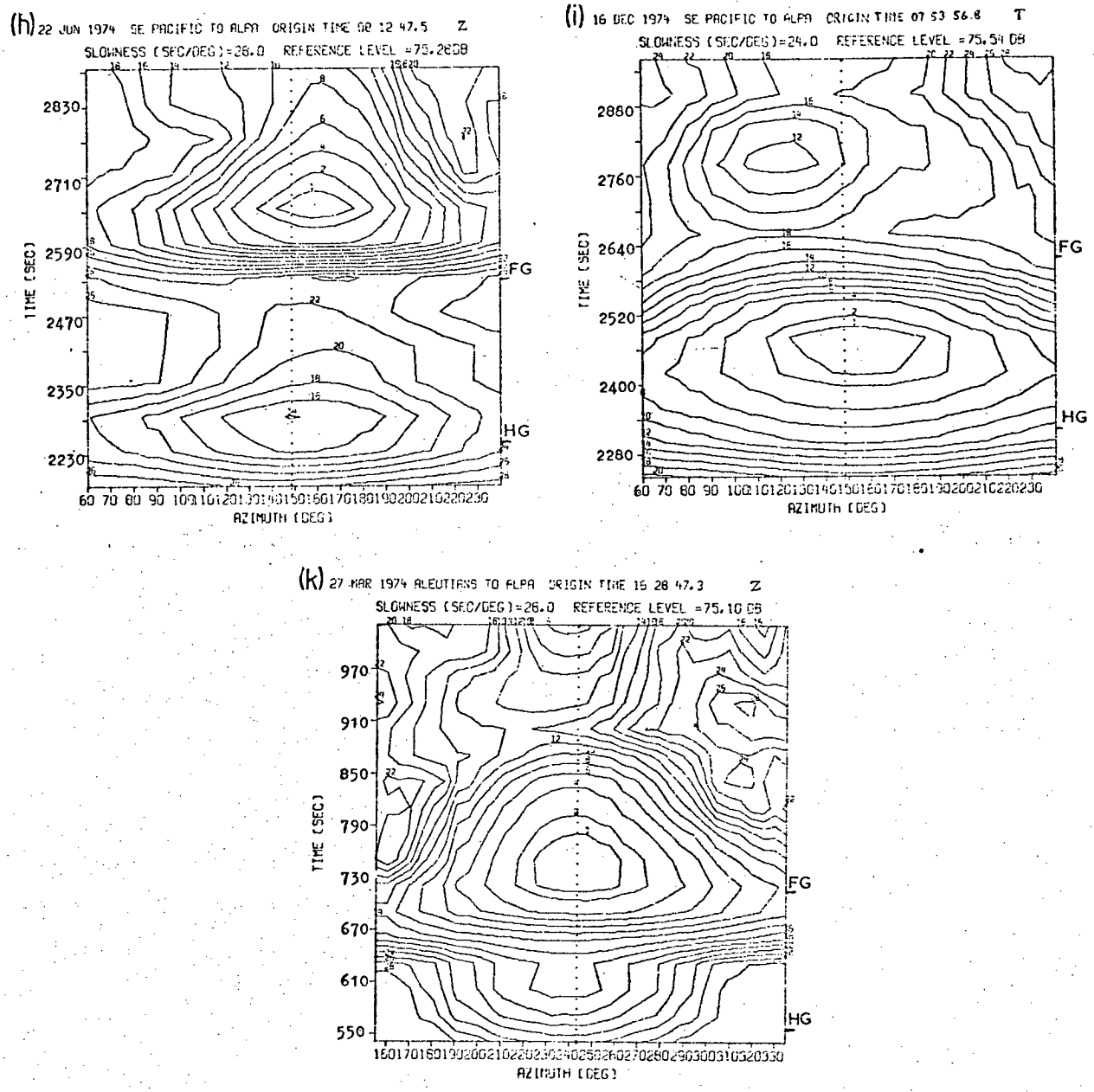

Figure 4.5 (cont)

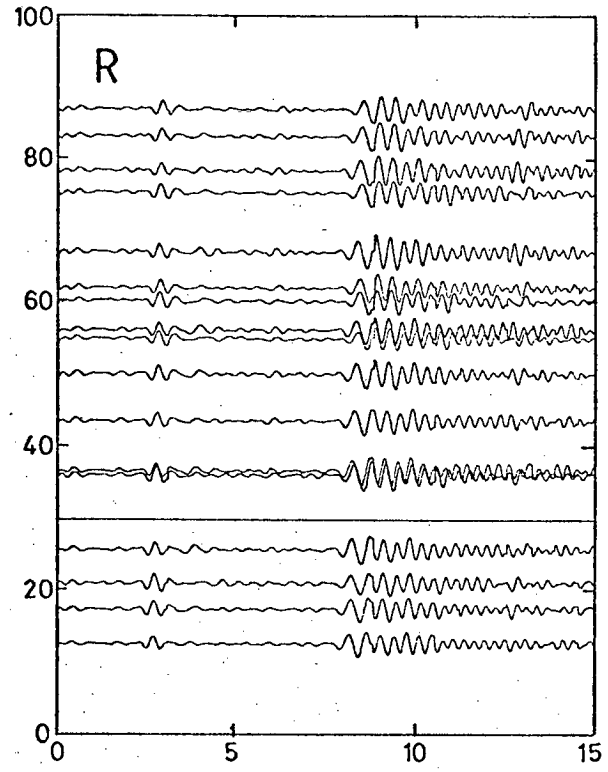

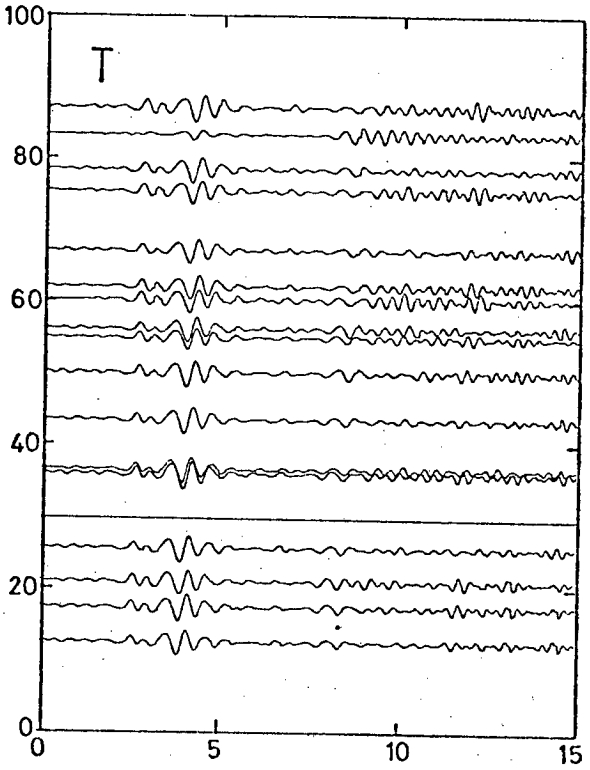

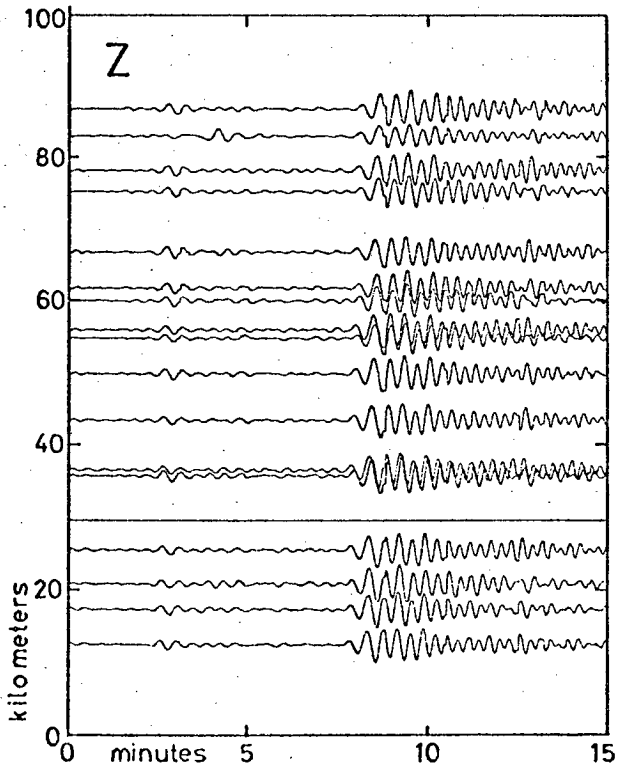

Figure 4.6

Surface-waves recorded at ALPA from event (h), Figure 4.5. Records start at 08.48.00h

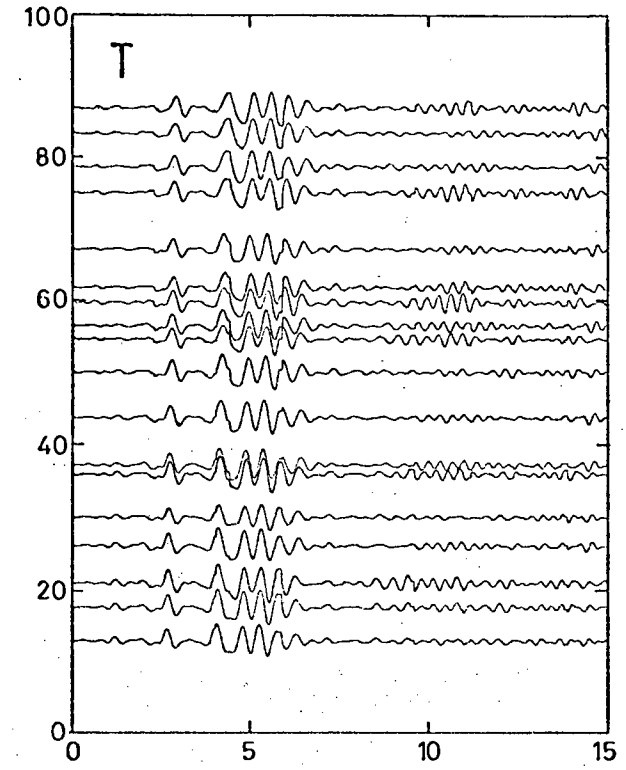

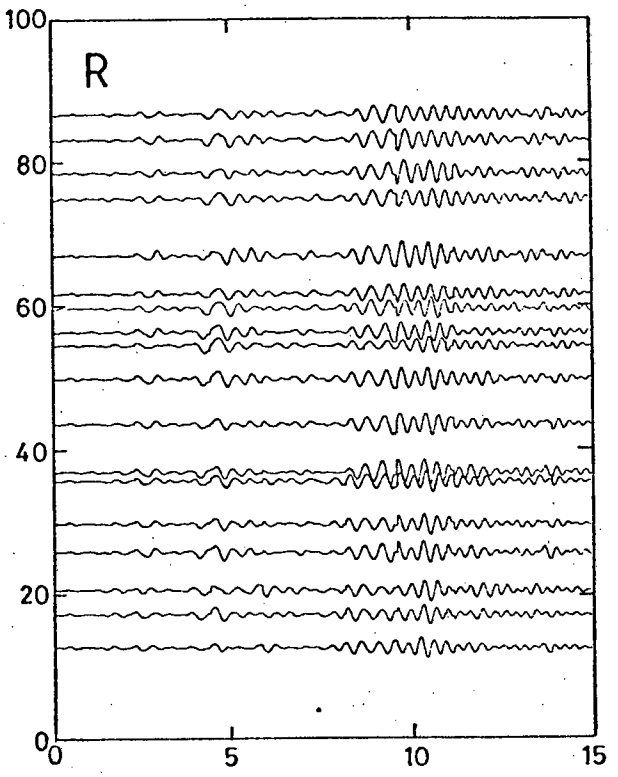

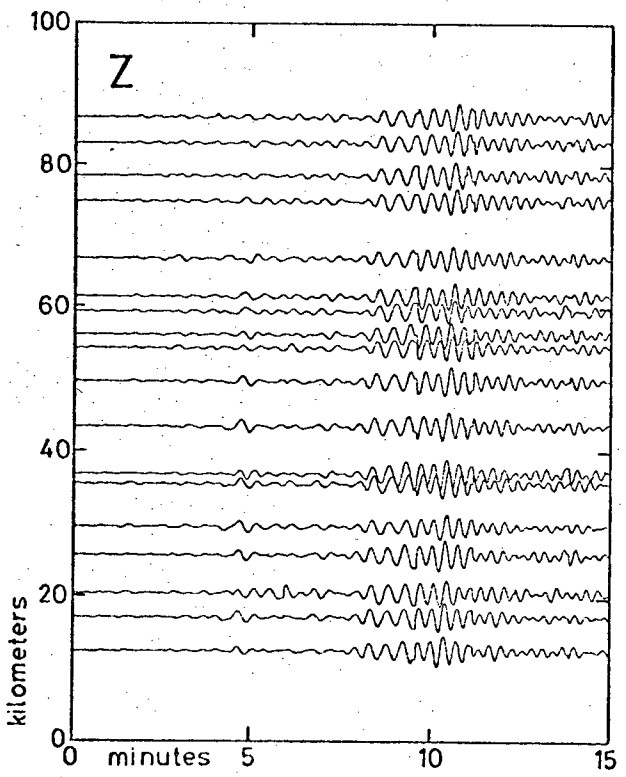

Figure 4.7

Surface-waves recorded at ALPA from event (i), figure 4.5. Records start at 08.30.00h

4.6 Distortion of particle-motion by local inhomogeneities near a recording station

Inhomogeneities in the rock immediately surrounding a seismic vault may cause the strains associated with incoming seismic waves to produce a local tilting effect, introducing spurious components of particle-motion (Rodgers 1968, King 1971). It is unlikely that this could produce a highly symmetric pattern of anomalous particle-motion, and certainly different stations should show rather different anomalies. This, however, can introduce a large error in any single observation of the magnitude of a particle-motion anomaly.

One particular local condition would produce a symmetrical pattern of anomalies, similar to that produced by anisotropy, and that is a dipping layer beneath the station. Langston (1977), for example, has demonstrated that a dipping moho will generate, from an incoming vertically-polarised shear-wave, reflected waves of both horizontally-polarised-shear and longitudonal type, and vice-versa. From this it follows that an incoming pure Love-type wave, for example, could generate transverse, radial and vertical components of particle-motion at the recording station. No anomalous components would be generated by waves travelling parallel to the dip of the inclined layer, so that the pattern of particle-motion might resemble that for propagation in an anisotropic structure with one vertical plane of symmetry (Figure 3.1a)

So, only when similar anomalies can be observed at several recording stations, each situated in an area of different structure, will it be possible to say that they are caused by anisotropic alignments along

the wave paths. Anomalies, even if arranged in a symmetrical pattern, which occur at only one station, or at several stations in similar locations, must be explained in terms of the special situations of those stations.

4.7 Recording instruments and response characteristics

Three types of seismograph are used in this study, WWSSN, HGLP and SRO. There are 115 stations in the World Wide Standard Seismograph Network, offering a wide coverage of suitable oceanic areas. The three-component set of long-period instruments is usually located in a vault, with recordings made photographically on paper chart. Low magnitude signals will be lost in the unavoidable noise, mainly due to surface weather. Only a limited recording range is available, so that fairly low magnification must be used if large, local signals are to be contained. So, only large-magnitude, distant events are recorded with sufficient amplitude for particle-motion studies. The High Gain Long Period stations, of which 10 were operational by 1976, located as shown in Figure 4.8, are basically improved versions of the WWSSN long-period stations. The system is described in detail by Savino et al. (1972). The sensors are sealed in airtight tanks and located in mines or tunnels, to minimise noise due to air-pressure changes. Careful shaping of the seismograph response, to coincide with a minimum in background noise at periods near 30s, allows lower amplitude signals to be seen and recording on digital tape allows a much greater range of amplitudes to be recorded, so that magnifications around fifty times those on WWSSN stations are available (see Figure 4.9a). This greatly increases the number of distant events which can be studied.

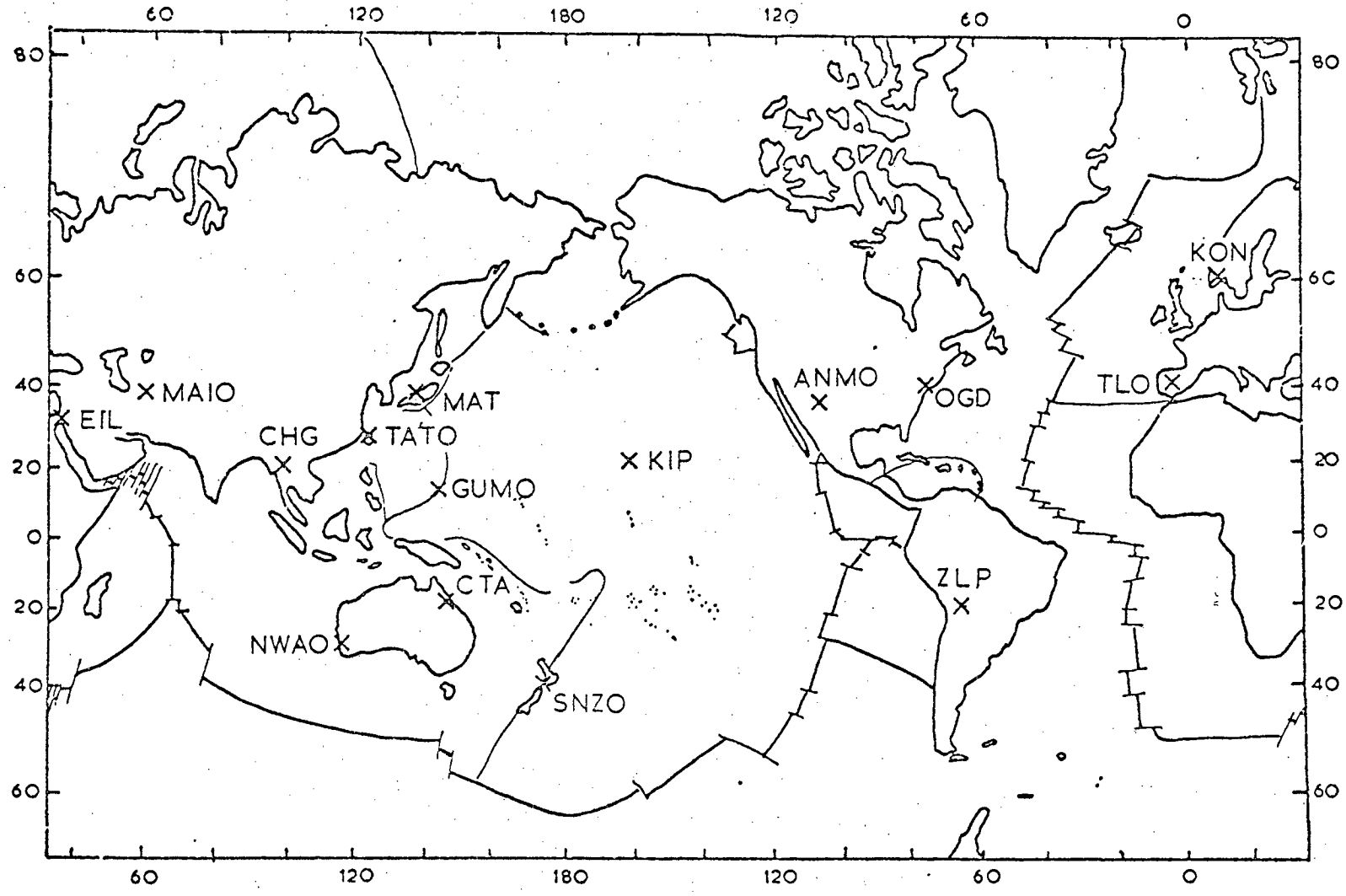

Figure 4.8 Locations of Seismic Research Observatories (four letter codes ending in '0') and High Gain Long Period stations (three letter codes)

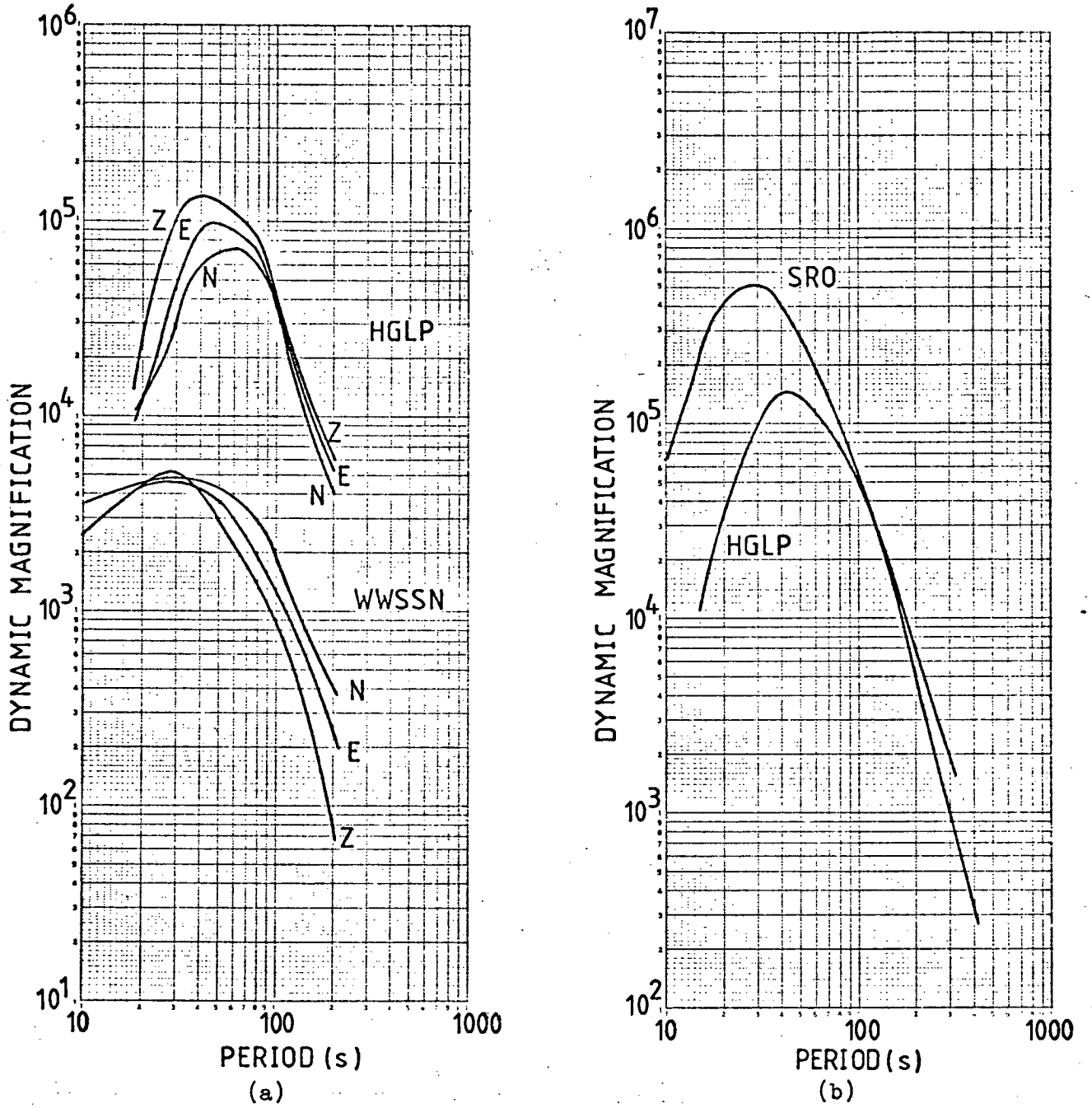

Figure 4.9 Typical response characteristics for long-period seismometers.
(a) WWSSN and HGLP(pre-1976) magnifications at Charters Towers(CTA) from Savino et al.(1972)
(b) SRO and standardised HGLP(post-1976) magnifications. These are the same for all instruments.

The Seismic Research Observatories, locations shown on Figure 4.8, are a more recent development. Instrumentation and installation are described by Peterson et al (1975). Broadband seismometers are used, the output being filtered to produce short and long-period records on both paper chart and digital magnetic-tape. The seismometers are located in boreholes, at depths of about 100m, to reduce weather noise. These SRO stations operate with magnifications about four times those of the HGLP stations.

The three seismograms produced at any one station show the vertical, north-south and east-west components of ground-motion, respectively, each modified by the response function of the appropriate recording instrument. Typical response functions are shown in Figure 4.9. In a study of particle-motion anomalies only the relative amplitudes and phases of the three components of ground-motion, at the same period, need be measured. So, no correction need be made for the variation of response with period, provided that each instrument in a three-component set shows the same variation. However, very few stations have such well matched instruments. Of those used in this study, only the SRO stations, the HGLP stations since early 1976, and KIP (HGLP) before then, have the same response curves for each of their three seismometers (Figure 4.9b). At other stations, discrepancies of up to 50% in amplitude response and 10^{o} in phase response are common (Figure 4.9a).

In this study, while searching simply to determine the character of particle-motion anomalies, these discrepancies can be ignored. The phase-discrepancies are small compared to the phase-differences required to discriminate between inclined-Rayleigh and tilted-Rayleigh-

type anomalies, which are around 90° (Figure 3.1). The discrepancies in amplitude response between horizontal components are generally less than 25%, and much less for periods less than 35 seconds. Any spurious inclination for Rayleigh-wave motion introduced by this response discrepancy would be less than 8°, less than the uncertainty in determining the direction of propagation (Figure 4.10). Any large inclination, similar to those expected in mode 3G in the presence of anisotropy, could not be generated by the discrepancies in response curves.

Generally, discrepancies in amplitude response will introduce an error in measuring the relative amplitudes of components of particle-motion. This is important only when the variation of anomaly amplitude with period is being studied, perhaps to determine the depth to the anisotropic layer, or the exact location of symmetry planes. For such studies HGLP (post 1976) or SRO records will be most useful. WWSSN records are unlikely to be useful as their responses cannot be sufficiently accurately determined from their calibration pulses, due to slight mis-alignments of the recording mechanisms (James and Linde 1971, Mitchell and Landisman 1969).

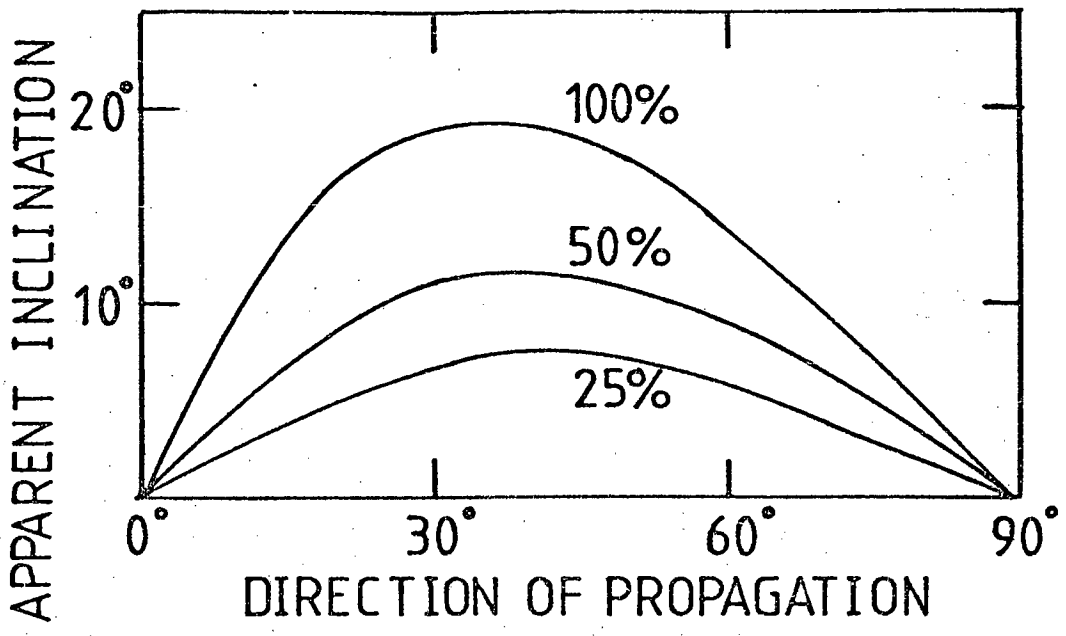

Figure 4.10 Apparent inclination of Rayleigh particle-motion when incoming wave shows no inclination but the two horizontal seismometers used to record the signal have different magnifications. Curves are for discrepancies in magnification between the two instruments of 25%, 50% and 100%.

5. OBSERVATIONS OF PARTICLE-MOTION IN OCEANIC SURFACE-WAVES

5.1 Sources of data

The Pacific Ocean was chosen for study as it offers a good azimuthal range of purely-oceanic, long travel-paths to several recording stations. Initially, WWSSN records were examined, these being readily available in microfilm form at the Institute of Geological Sciences in Edinburgh. Several records of surface-waves from events along the East Pacific Rise, recorded at WWSSN stations on the west coast of South America are included in this study. These show, mainly, the fundamental Rayleigh-type mode (FG) although, in a few cases, the first Love-type mode (2G) carries enough short period energy to be clearly visible on top of FG. In these records the mode 2G can be separated by filtering. Generally, however, the path lengths for most events recorded at WWSSN stations are too short to allow separation of the higher-modes (including 2G) from the many body wave phases (see travel-time curves in Figure 5.1).

A second problem with the WWSSN records is the skewness introduced by slight mis-alignment in the recording system (James and Linde 1971), illustrated in Figure 5.2. This skewness, generally of the order of $\frac{1}{2}^{o}$ can be estimated if a large amplitude, monotonic signal is present on a record, and is found to vary from instrument to instrument, and from day to day. Because of the ever-present noise the skewness cannot be measured to better than about 20%, even under the most favourable conditions, and so corrections cannot be accurately made. Any small uncorrected skew can lead to large errors in the relative phase of N-S, E-W and vertical components which, in turn, will lead to spurious radial or transverse components, which are formed by

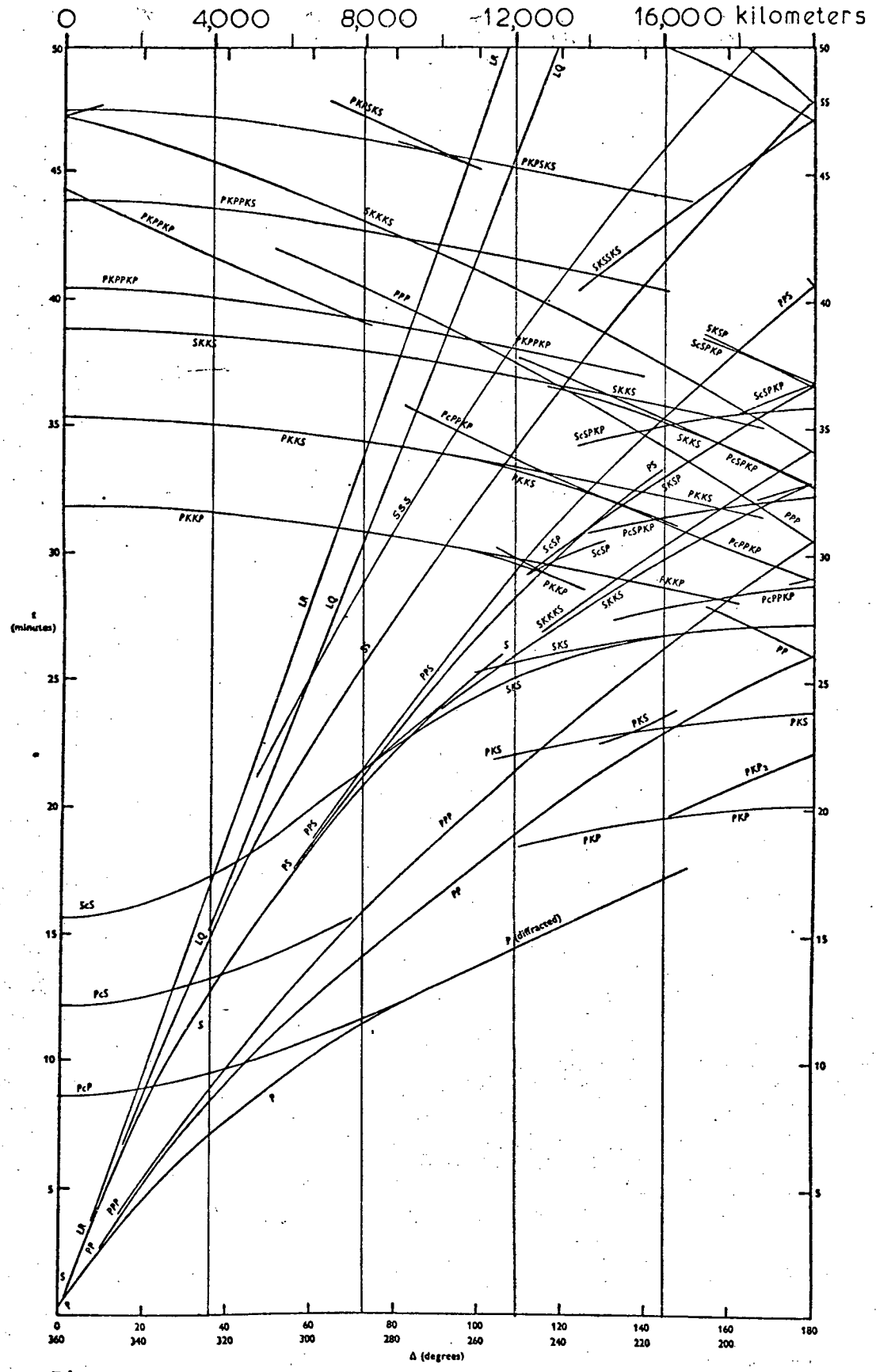

Figure 5.1 Travel-times of surface waves and the main body-wave phases from a surface-focus earthquake. The curves LQ and LR correspond to group velocities of 4.4km/s and 4.0km/s. (from Jeffreys 1970).

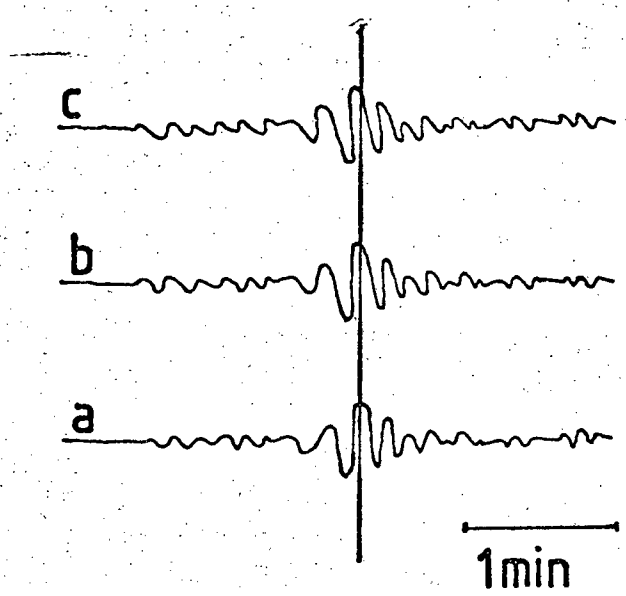

Figure 5.2 Seismogram trace digitised using (c) zero-deflection line as base line, (b) after correction for spiralling of zero-deflection trace around recording drum and (a) after correction for mis-alignment of galvanometer deflection with drum axis.
Vertical scale reduced to exaggerate skewness.

rotating the horizontal seismograms. Since small anomalous components, and relative phases, are very important in this study of particle-motion, WWSSN records must be supplemented with more accurate data.

Data from HGLP and SRO seismometers is recorded directly in digital form, and so avoids the skewness problems described above. The increased magnification available at these stations also allows more distant earthquakes to be recorded. The greater accuracy provided by direct recording, rather than manual digitisation of a photographic record, also allows smaller-amplitude, shorter-period signals to be separated by filtering. One disadvantage is that data from these stations are not so easily accessible.

Tapes containing both HGLP and SRO data are available only for selected days, since 1975, and these have to be ordered from Teledyne-Geotech, in Alexandria, Virginia. For this study, three of the most active of the days offered, which appeared to have the most suitably spaced events, in space and time, were selected, with the aid of U.S.C.G.S. P.D.E. listings. These provided useful recordings for 13 travel-paths. In addition, recordings for 12 specific events from pre-1975 HGLP tapes were obtained, providing records for another 12 travel-paths.

Many of the possible station-event pairs available on these tapes were not used. In some cases the data could not be recovered from the tape, in others one component was missing. Where a complete record was obtained, it is included in this study only if there is a clear maximum on the vertical and/or horizontal components, corresponding to the expected arrival times of the fundamental or higher surface-wave modes. All the stations, events and travel-paths

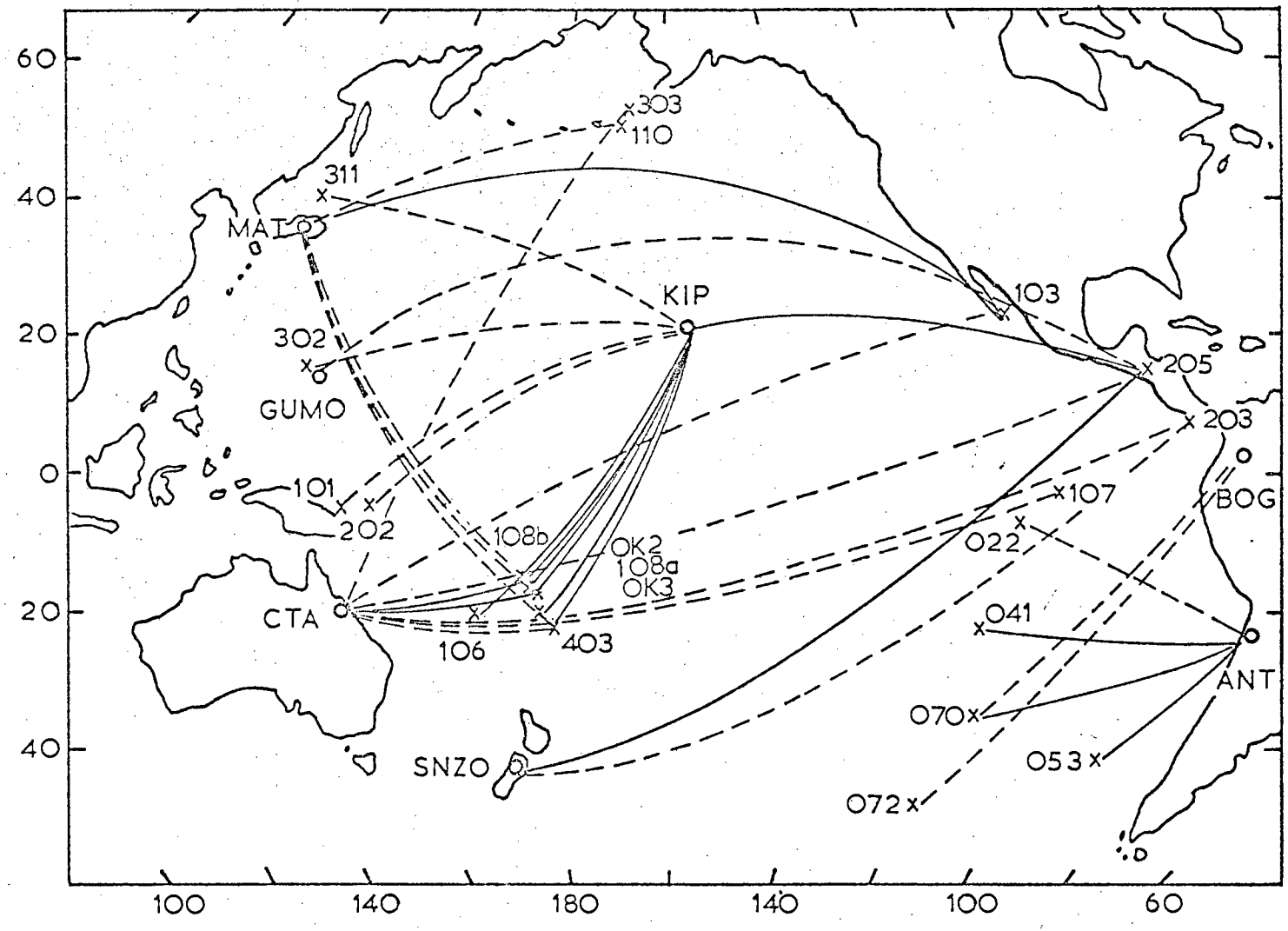

Figure 5.3 Map showing travel paths of surface-waves used in this particle-motion study. Solid lines correspond to the seismograms shown in Figures 5.6a-5.6n.

Station code	type of instrument	location	latitude	longitude
ANT	WWSSN	Antofagasta,Chile	23 41'56"S	70 24'54"W
BOG	WWSSN	Bogota,Colombia	4 37'23"N	74 3'54"W
CTA	HGLP	Charters Towers,Australia	20 5'18"S	146 15'16"E
GUMO	SRO	Guam,Marianas Islands	13 35'16"N	144 51'59"E
KIP	WWSSN	Kipapa,Hawaii	21 25'24"N	158 0'54"W
KIP	HGLP	Kipapa,Hawaii	21 25'24"N	158 0'54"W
MAT	HGLP	Matsushiro,Japan	36 32'30"N	138 12'23"E
SNZO	SRO	South Karori,New Zealand	41 18'37"S	174 42'17"E

Table 5.1 Locations of recording stations.

code	location	latitude	longitude	depth(km)	m_b	date	time
OK2	Tonga Islands Region	-15.98	-179.40	70	5.7	12 Aug 1974	02 52 42
OK3	Tonga Islands Region	-18.82	-179.50	55	5.4	13 Aug 1974	12 52 47
022	Northern Easter Islands Cordilliera	-6.15	-107.30	33	4.7	6 Sep 1964	21 5 47
041	Easter Islands Region	-22.13	-113.80	180	5.7	6 Nov 1965	9 22 4
053	West Chile Rise	-41.44	-85.50	33	5.6	6 Jan 1965	9 19 1
072	Easter Islands Cordilliera	-49.40	-116.20	33	4.8	20 Sep 1964	4 33 30
070	Easter Islands Cordilliera	-35.41	-106.00	33	4.9	31 Aug 1964	2 14 20
101	Solomon Islands	-6.88	150.03	38	6.3	18 Jan 1973	9 28 14
103	Southern California	25.84	-109.93	17	5.4	25 Mar 1973	22 42 01
106	New Hebrides	-21.93	173.71	33	5.0	23 Mar 1974	20 25 52
107	Galapagos Islands Region	-4.37	-102.11	33	6.1	10 May 1974	8 12 5
108a	Tonga Islands Region	-16.06	-179.38	29	5.3	13 Aug 1974	5 53 7
108b	Tonga Islands Region	-15.52	-179.11	33	4.9	13 Aug 1974	7 20 17
110	Aleutians	52.41	-168.28	41	5.7	24 Aug 1974	10 41 11
202	Solomon Islands	-6.26	154.72	50	5.5	13 Mar 1976	5 22 44
203	Off Coast of Central America	3.99	-85.81	76	5.0	13 Mar 1976	10 31 46
205	Guatemala	14.77	-90.61	70	5.4	13 Mar 1976	16 30 42
302	Marianas Islands	13.77	144.69	116	5.5	28 Mar 1976	1 42 37
303	Fox Islands,Aleutian Islands	52.70	-167.15	36	5.2	28 Mar 1976	6 55 15
311	Hokkaido,Japan Region	41.73	142.81	53	5.1	28 Mar 1976	22 20 8
403	Tonga Islands	-21.93	-175.03	54	5.5	4 May 1976	8 30 7

Table 5.2 Locations and origin times of earthquakes (from USCGS PDE listings).

Path	Length (km)	Back azimuth	Path	Length (km)	Back azimuth
ANT022	4396	290	KIPOK2	4746	211
ANT041	4430	263	KIPOK3	5024	209
ANT053	2416	212	KIP101	6472	247
ANT070	3660	241	KIP106	5690	214
			KIP108a	4752	211
BOGO70	5543	214	KIP108b	4687	211
BOGO72	7230	209	KIP202	5993	245
			KIP205	7071	84
CTA103	12288	69	KIP302	6105	272
CTA107	12081	102	KIP311	5922	307
CTA108a	3656	89	KIP403	5135	202
CTA108b	3697	88			
CTA203	14108	100	MAT103	10092	57
CTA205	13930	86	MAT108a	7325	135
CTA303	9228	26	MAT108b	7295	134
CTA403	10373	112	MAT110	4489	50
			MAT403	8118	135
GUM205	13110	65			
			SNZ203	11092	93
			SNZ205	11423	82

Table 5.3 Paths for which surface-waves were observed.

included in the study are tabulated in Tables 5.1 - 5.3, and are shown on the map in Figure 5.3.

Ideally, travel paths should be longer than 8000km, so that surface-waves are not contaminated by body-wave arrivals (Figure 5.1). However, few good records were found for very long paths. The shorter period surface-waves, in particular, are generally recorded only for shorter paths, so several of these are included in the study. The multiple-S body-phases will generally interfere with the higher-mode surface-waves, including 2G, only at the longer periods. The lengths of the paths used (Table 5.3) and the dispersion of the surface-waves (Figure 4.1), are such that for periods below about 20 seconds the mode 2G, at least, should arrive after any large-amplitude body-wave.

5.2 Treatment of data

WWSSN microfilm records are printed and digitised at one second time intervals. Before further analysis, corrections are made for skewness if there is a large enough signal for measurement. Appropriate sections of HGLP data are selected from the day-tapes and each component adjusted according to the 30 second digital sensitivity setting, taken from the station log for pre-1976 data, or from the standardised settings listed in the system description provided by Teledyne-Geotech, for later records. SRO instruments all record with the same digital sensitivity so no corrections are needed.

The records are now plotted (Figure 5.6). N - S and E - W components are rotated to give components transverse to and radially along the

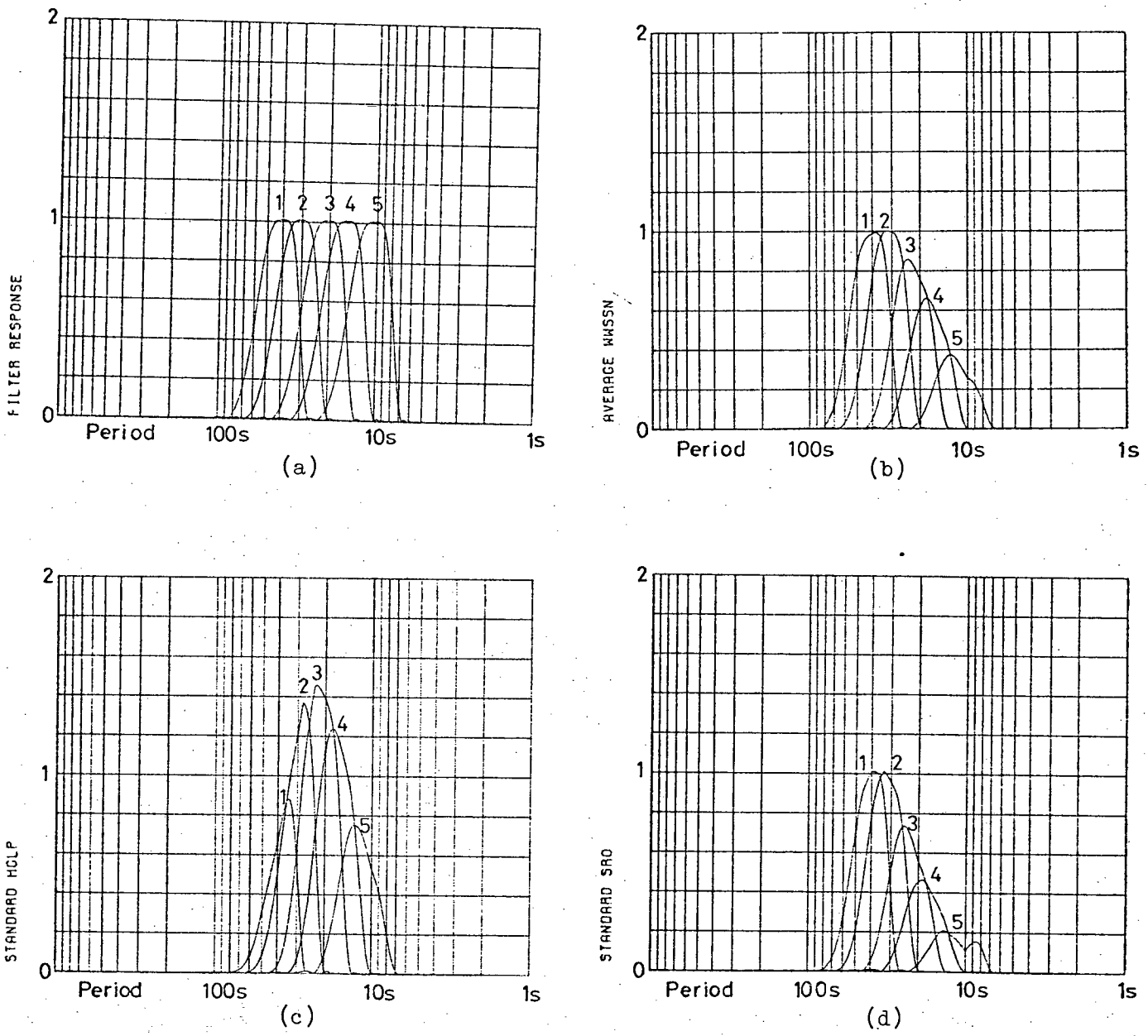

Figure 5.4 Amplitude response of bandpass filters (1) 32-64seconds, (2) 24-48seconds, (3) 16-32seconds, (4) 12-24seconds, (5) 8-16seconds. (a) filter response alone, (b),(c) and (d) the effect of combining filter and instrument responses for typical WWSSN, post-1976 HGLP and SRO seismometers.

presumed direction of travel, the great-circle azimuth from the event, at the recording station. Vertical, radial and transverse components, labelled Z , R and T, are then filtered, by each of five, overlapping bandpass-filters in turn. The filtering allows the characteristics of particle-motion at several periods to be examined. The filter responses, and the effect of these responses combined with individual instrument responses are shown in Figure 5.4. The filters are convolution-type and a filter half-width equal to twice the long-period limit of the filter is used, giving steep-sided response-bands. Particle-motion is plotted for each one-minute-section of record, for each filter-band, each plot comprising a horizontal section and the vertical section along the direction of travel. (see Figure 5.5) A selection of the records used are shown in Figure 5.6a - 5.6n.

5.3 Surface-wave modes recorded

Most records show Rayleigh-type arrivals corresponding to a group-velocity of 4.0 km/s or less, and Love-type arrivals at group-velocities near 4.5 km/s. These correspond to the modes FG (Rayleigh-type), 2G and higher, even-numbered, generalised modes (Love-type). Most of the records reproduced here (Figures 5.6a - 5.6m) are those for which surface-wave arrivals are visible in all filter-bands. On many other records studied the signals are lost in noise, for periods below about 20 seconds, as in Figure 5.6n.

Figures 5.6a-5.6n

Multiply-filtered seismograms and particle-motion plots for selected surface-wave travel paths in the Pacific Ocean.

Particle-motion plots are in pairs, as shown below, each pair corresponding to a one-minute time interval of a filtered trace. Each member of the pair is drawn to the same scale.

Seismograms are in alphabetical order according to station name and numerical order of event number

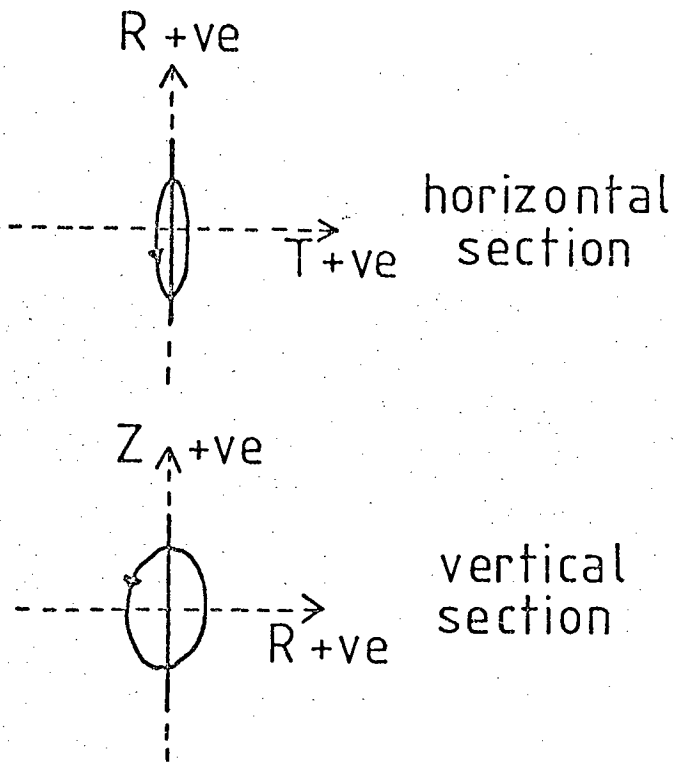

R +ve: direction of propagation
Z +ve: vertically up

Figure 5.5 Key to particle-motion plots.

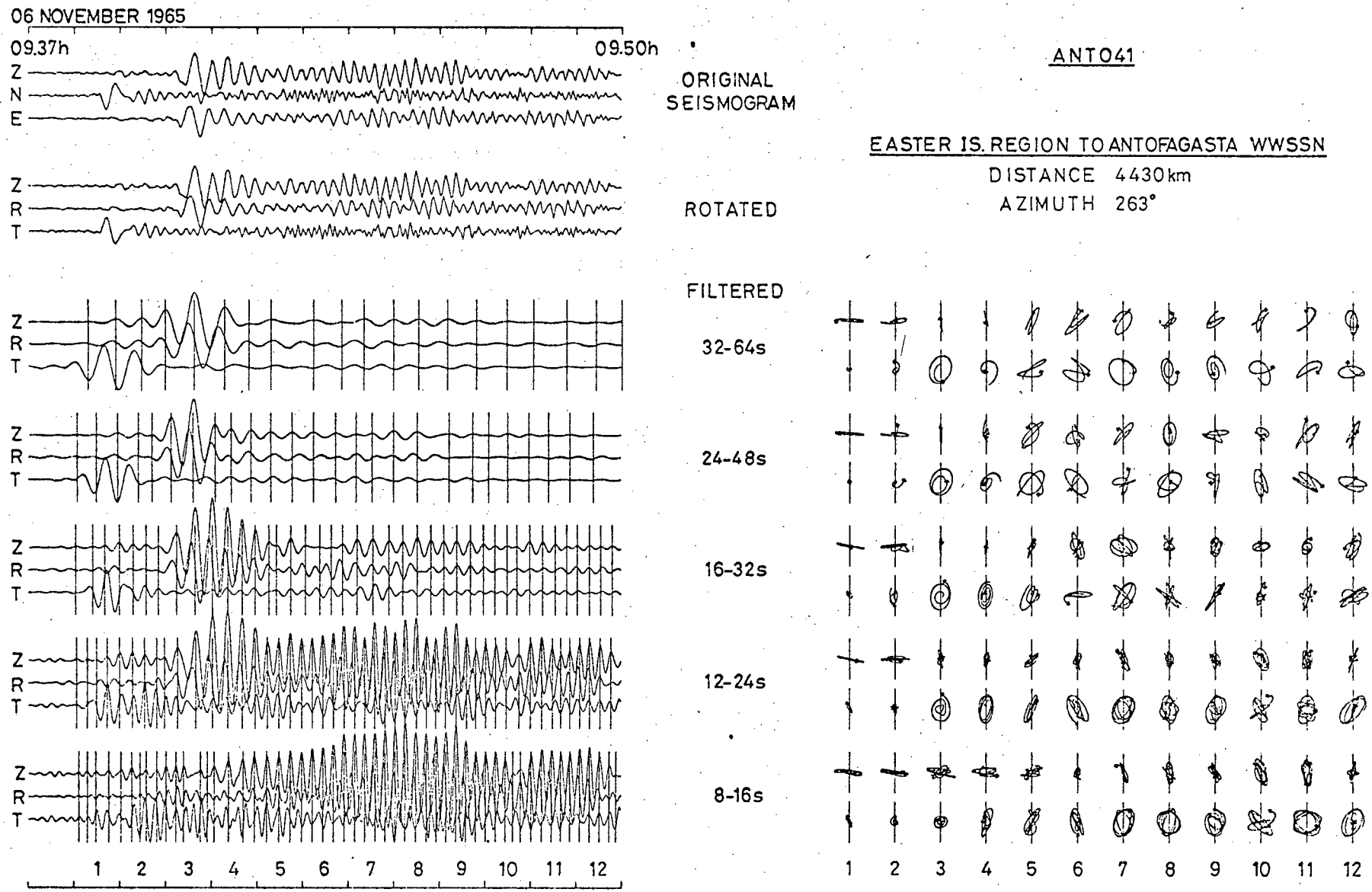

Figure 5.6a see key on p.94

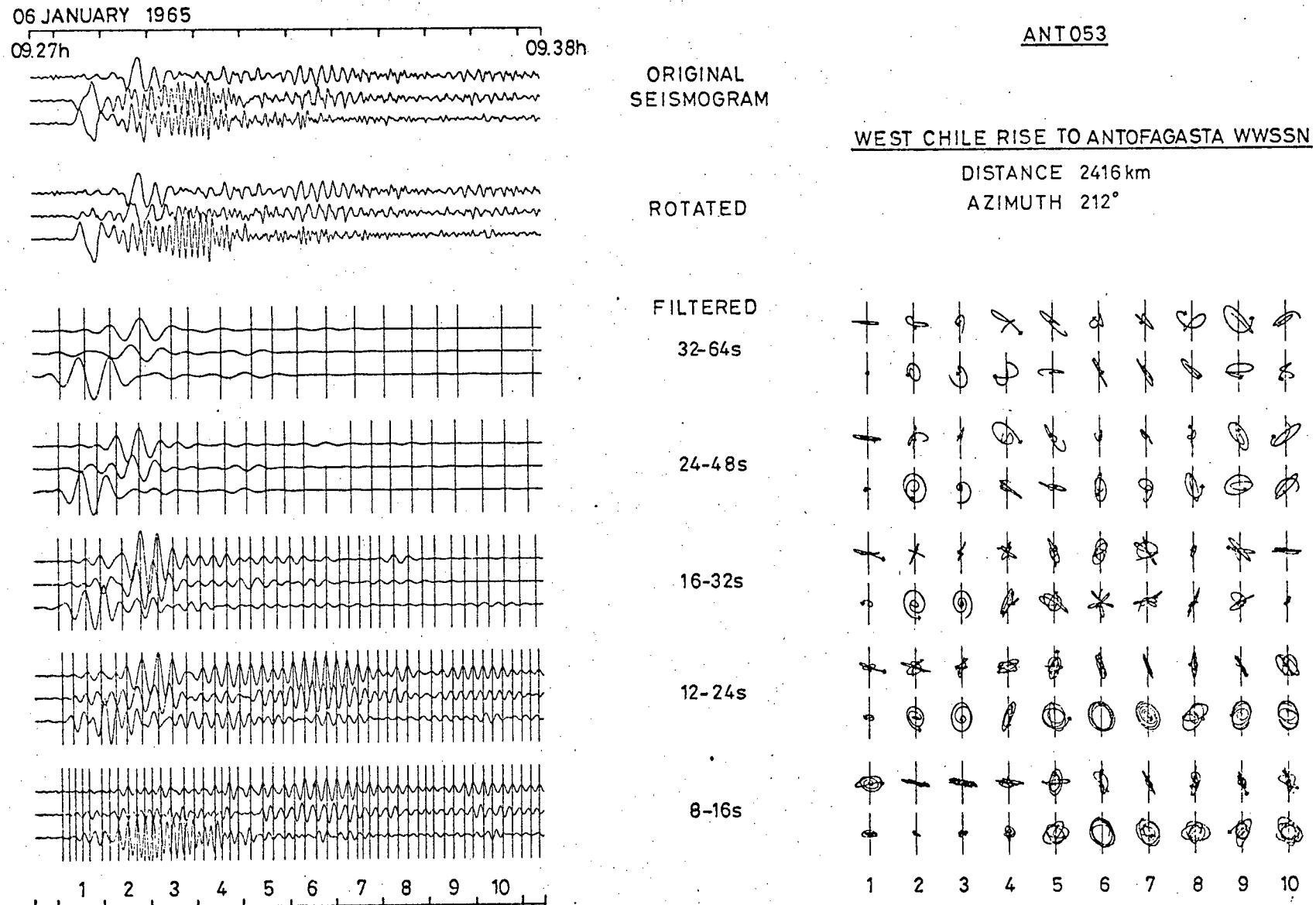

Figure 5.6b see key on p.94

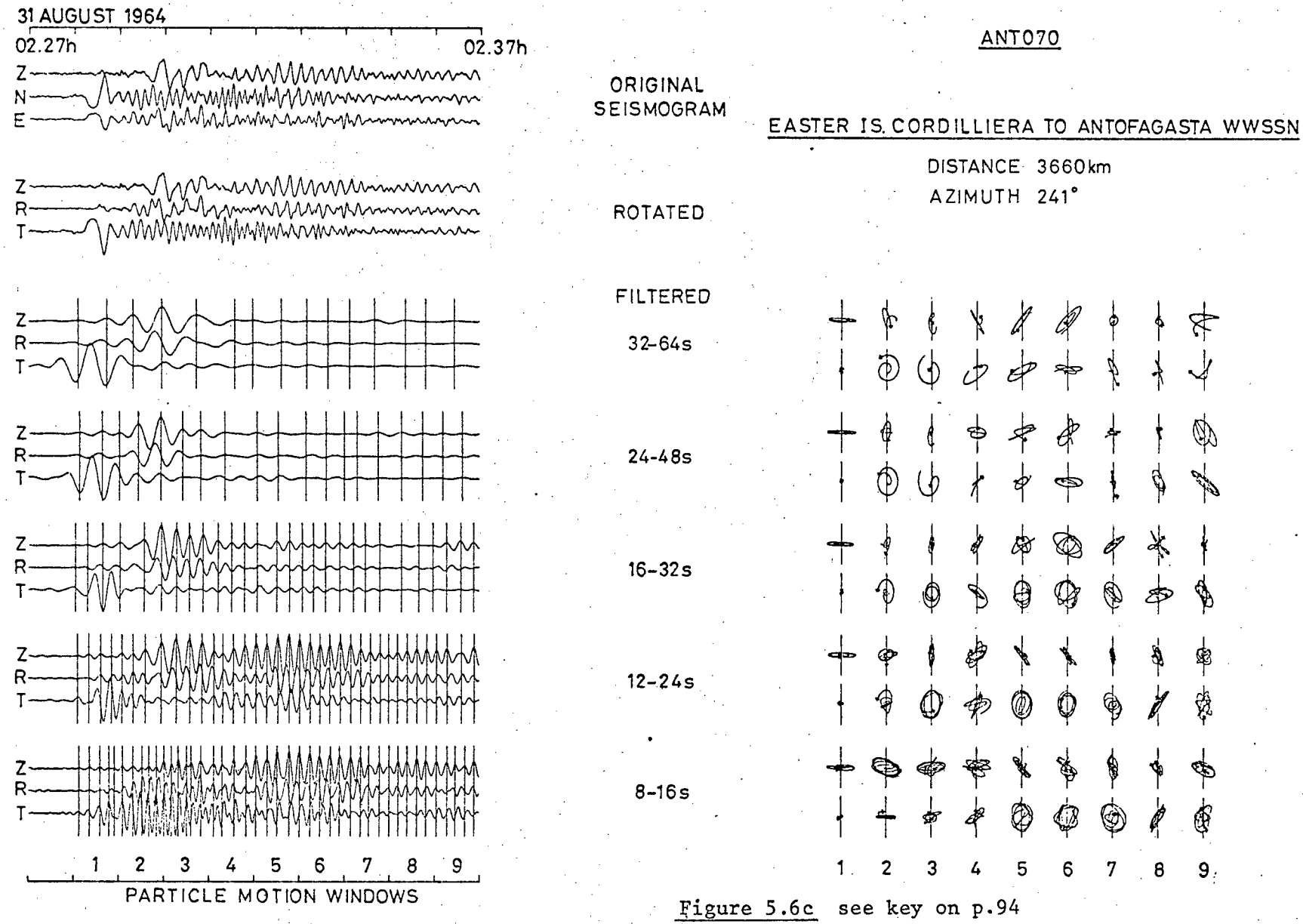

Figure 5.6c see key on p.94

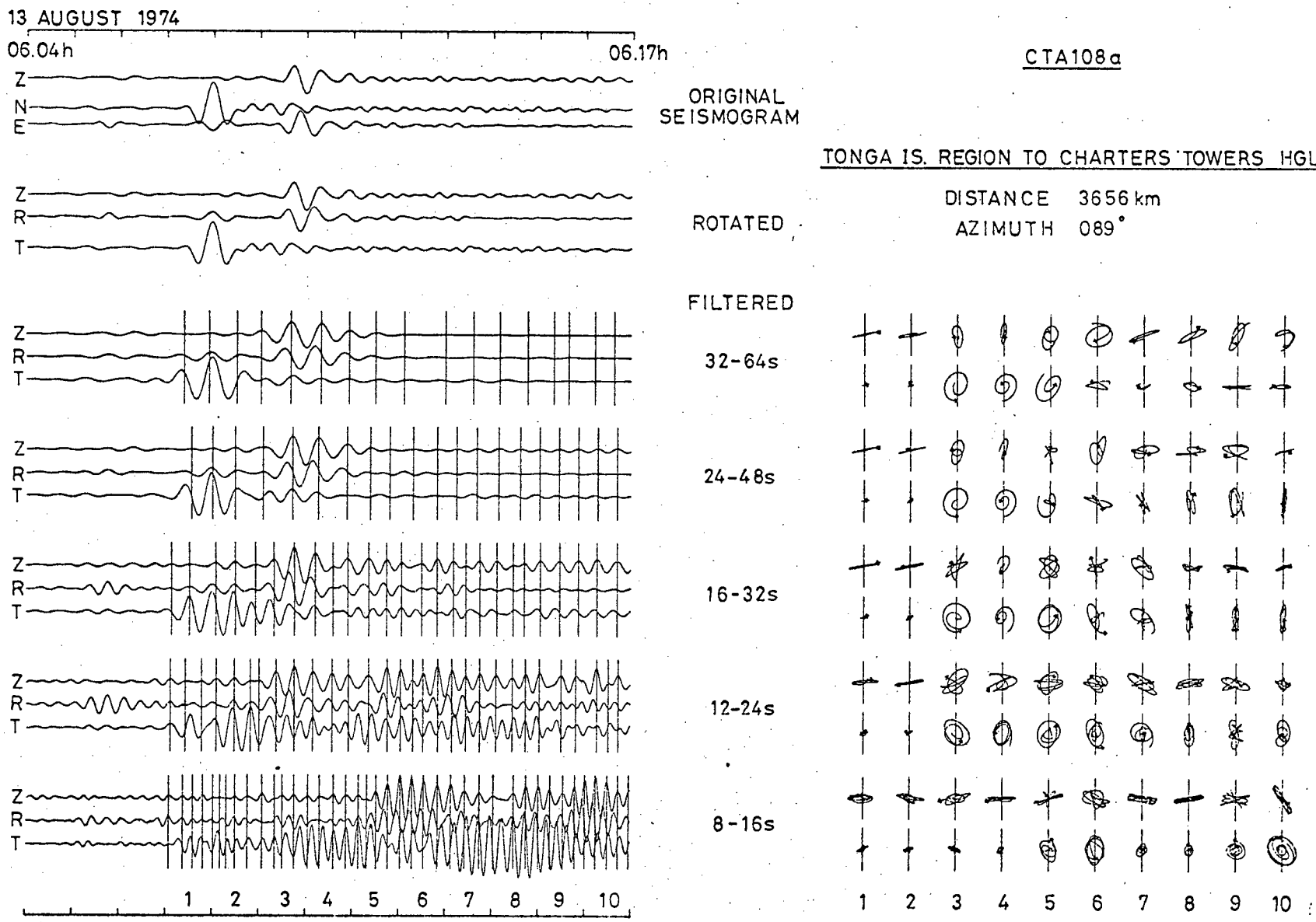

Figure 5.6d see key on p.94

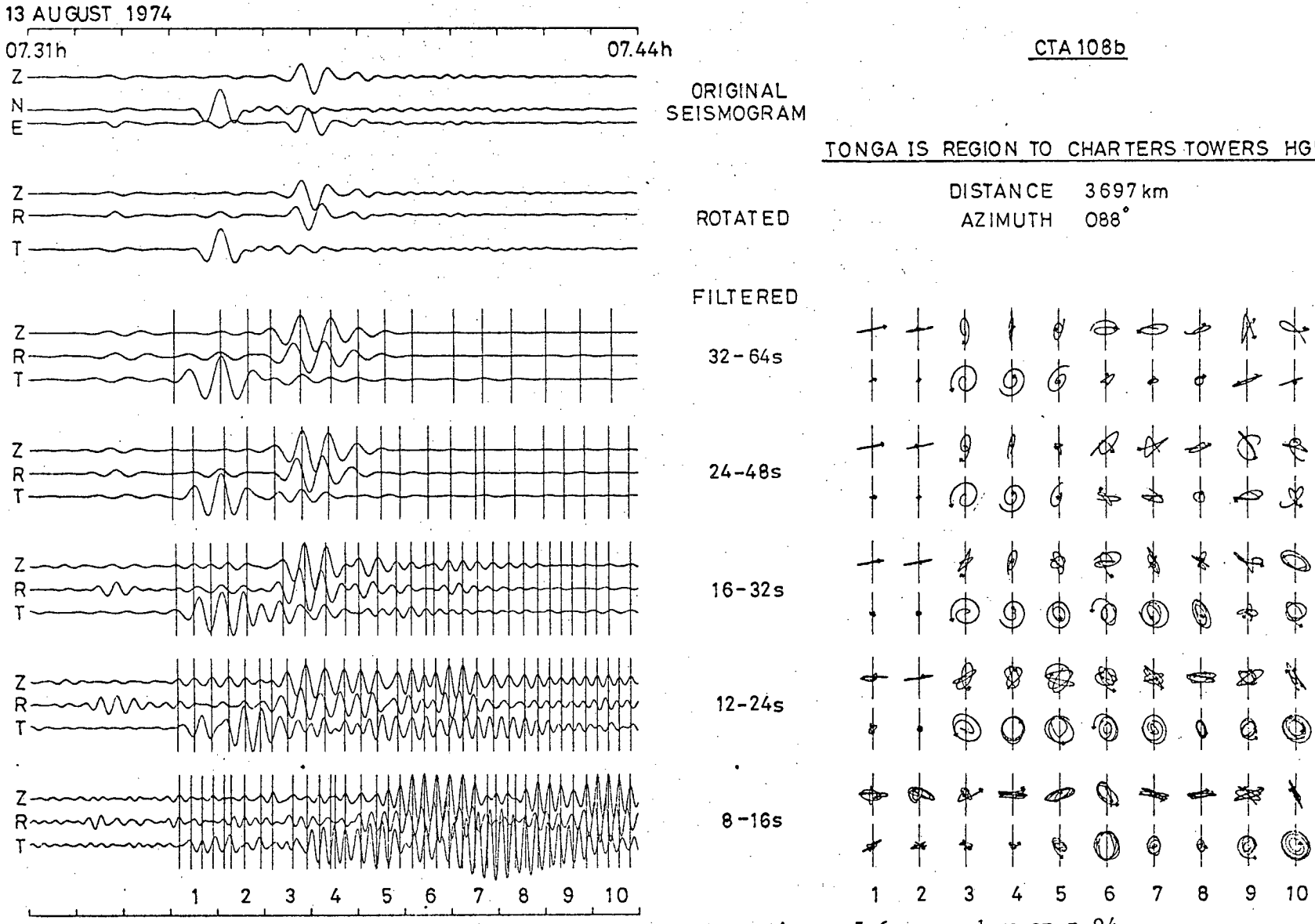

Figure 5.6e see key on p.94

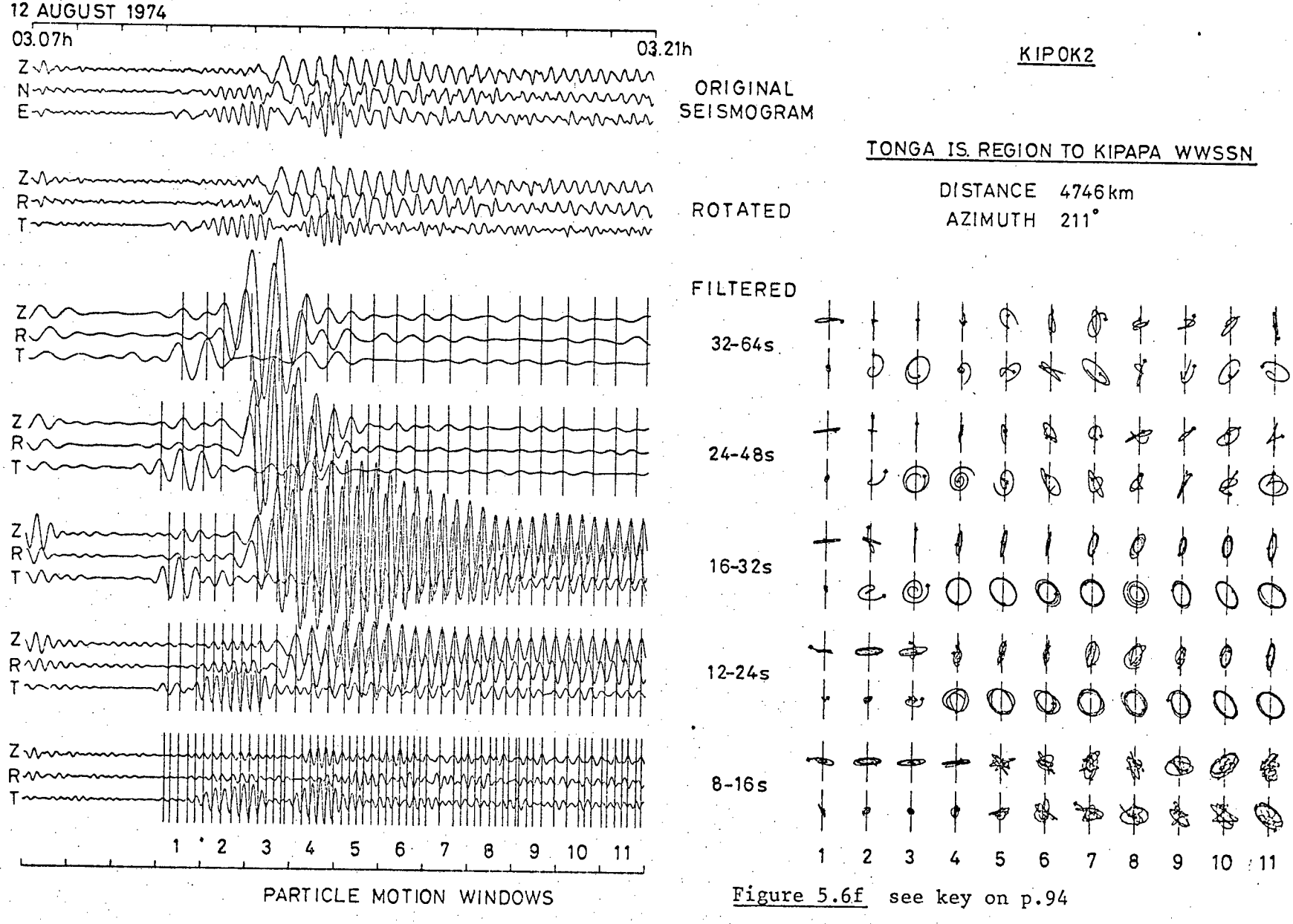

Figure 5.6f see key on p.94

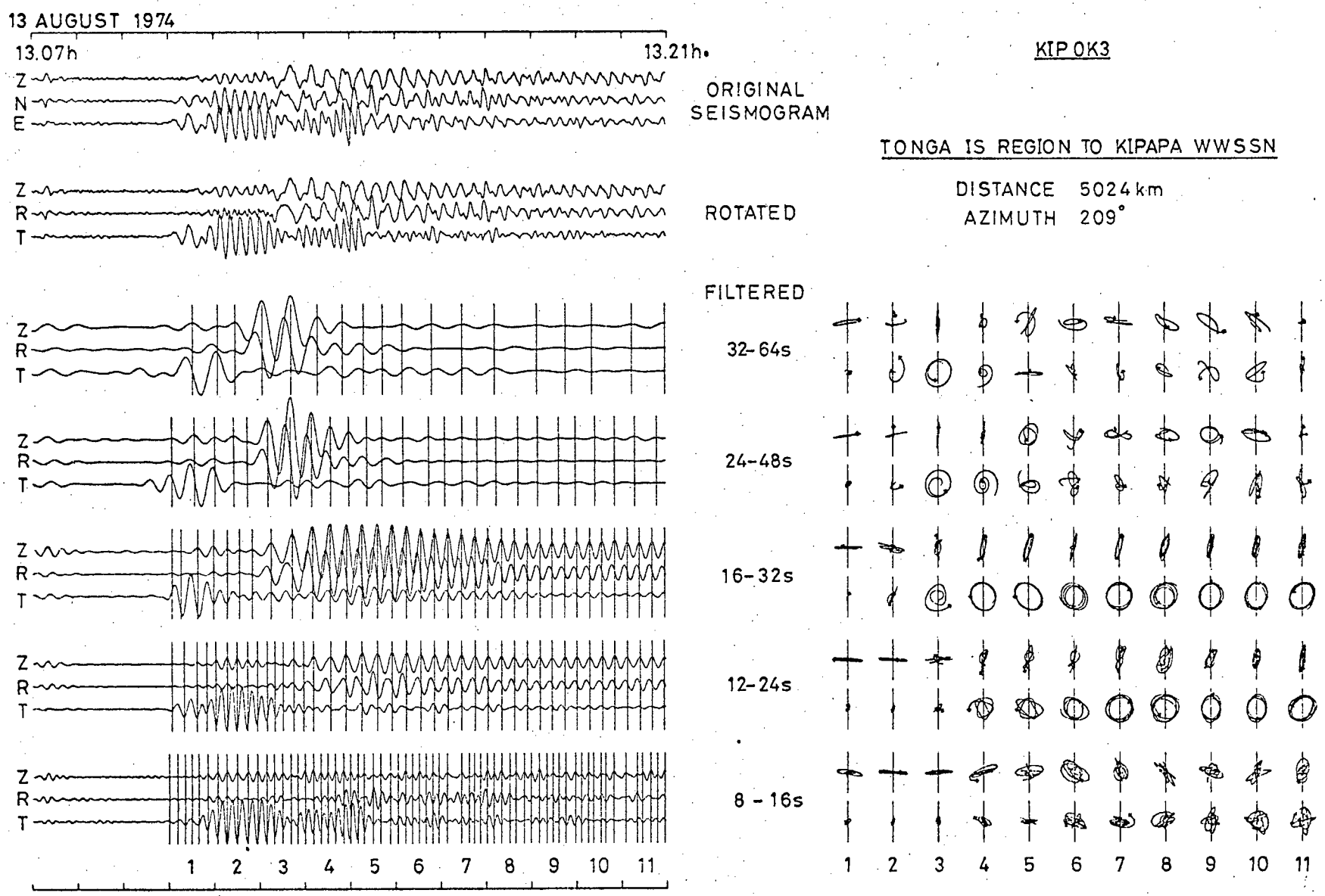

Figure 5.6g see key on p.94

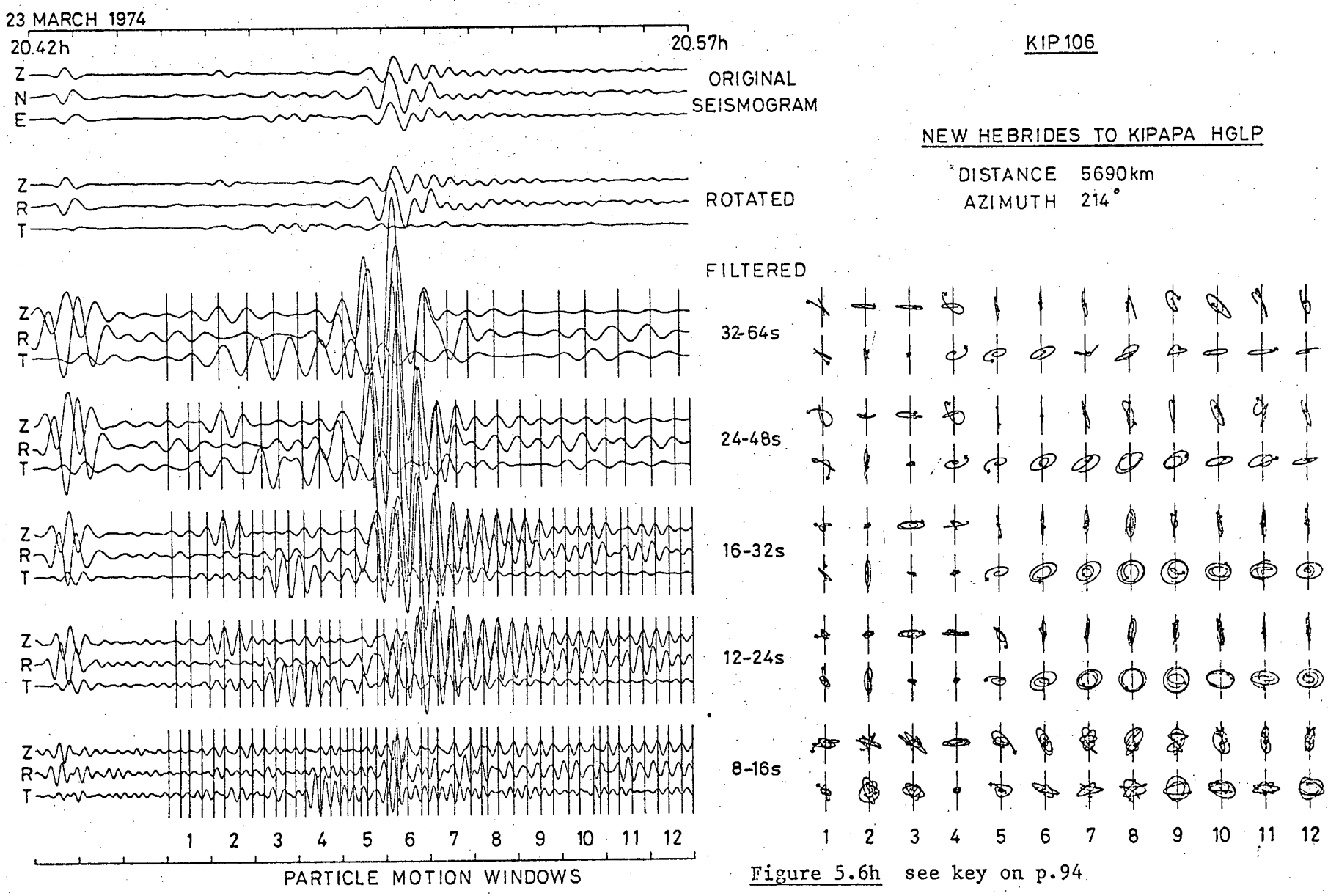

Figure 5.6h see key on p.94

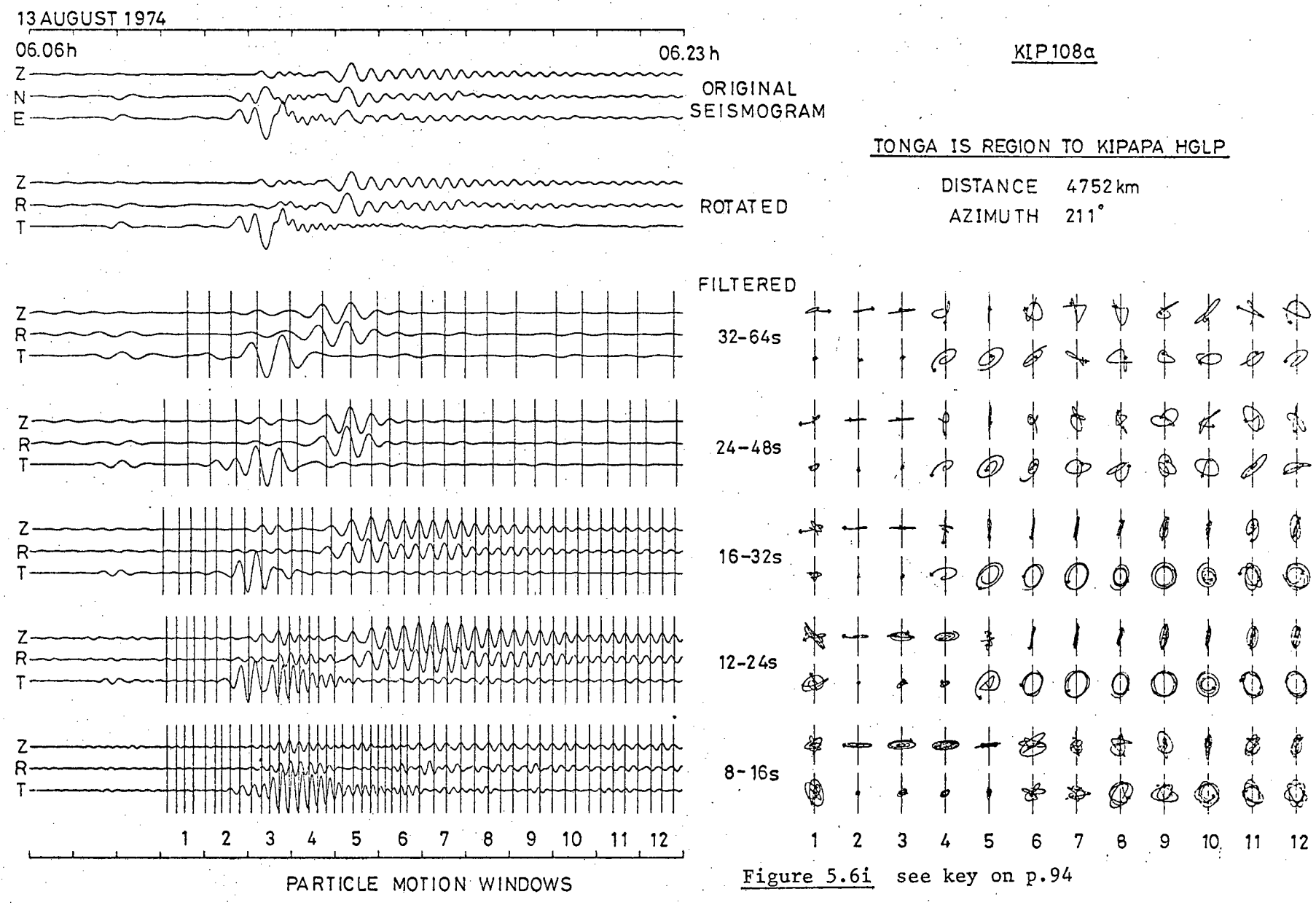

Figure 5.6i see key on p.94

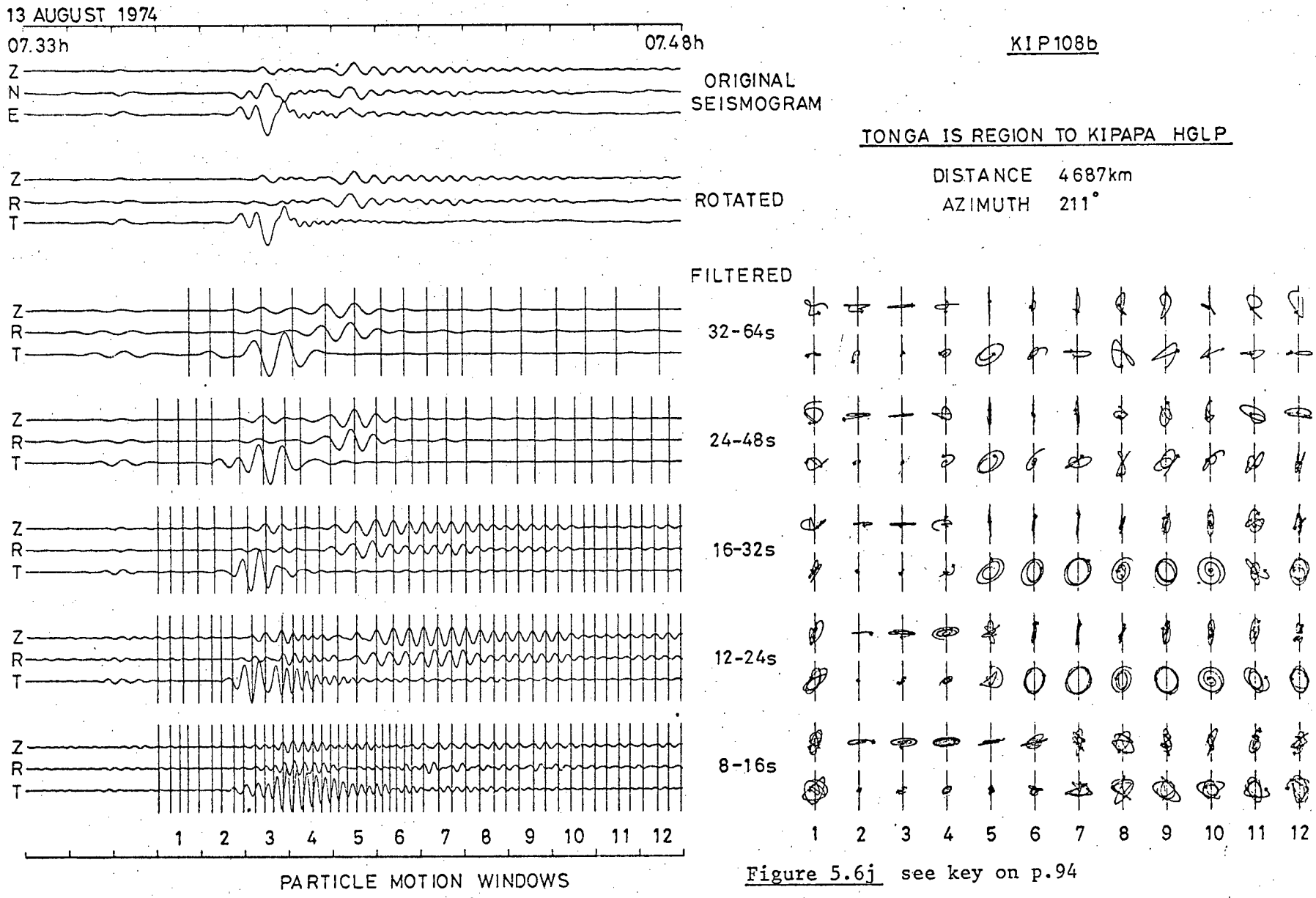

Figure 5.6j see key on p.94

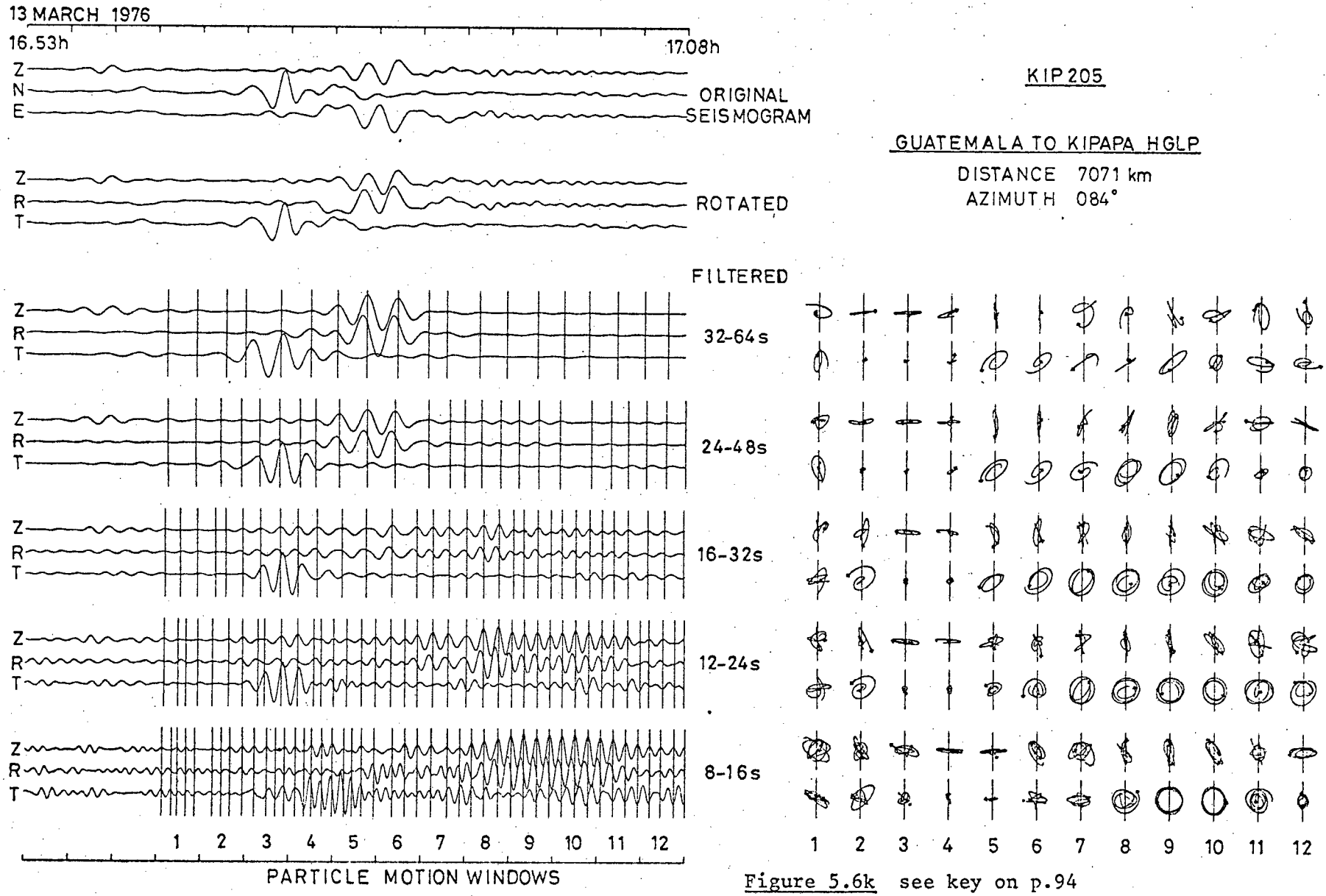

Figure 5.6k see key on p.94

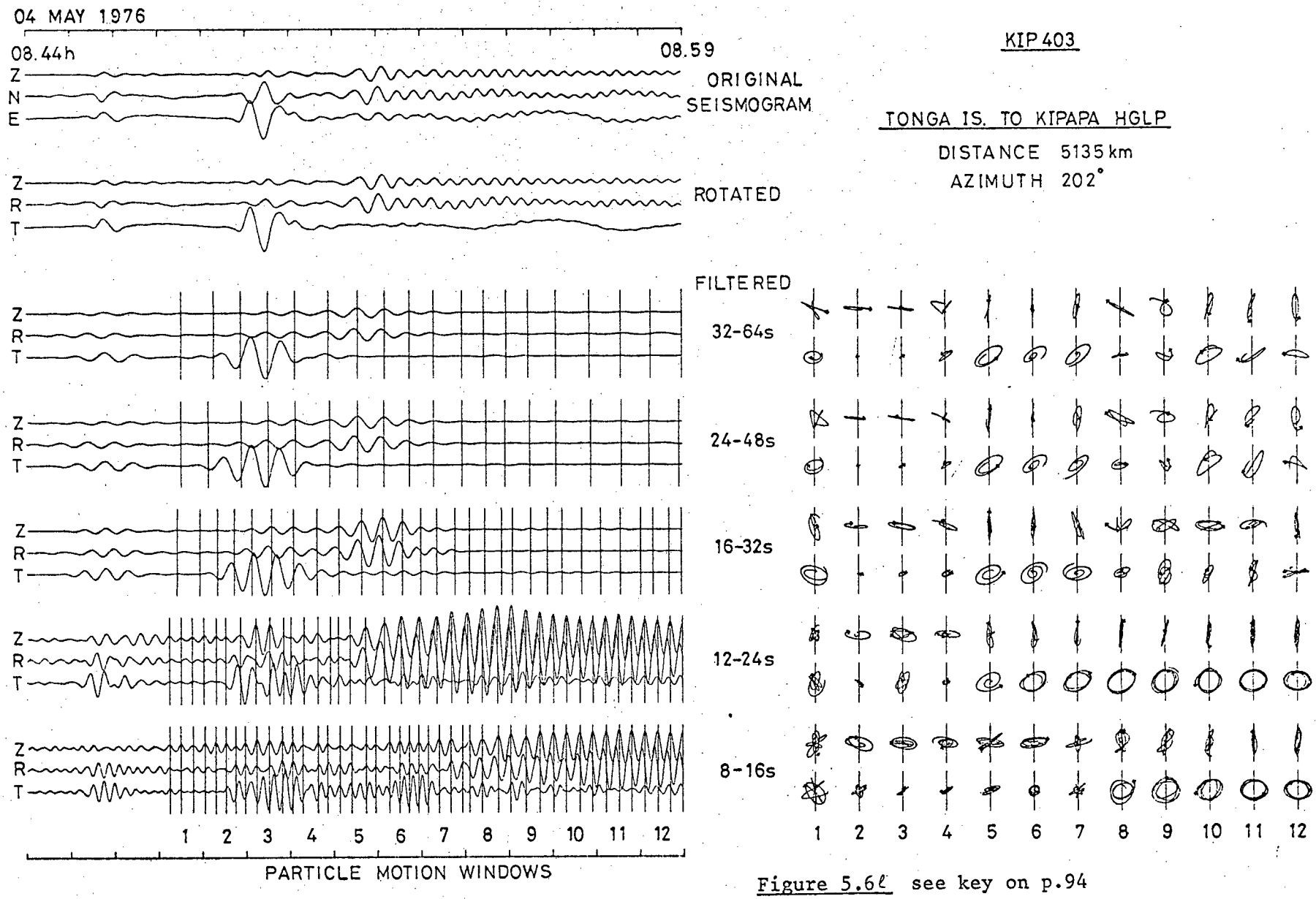

Figure 5.6ℓ see key on p.94

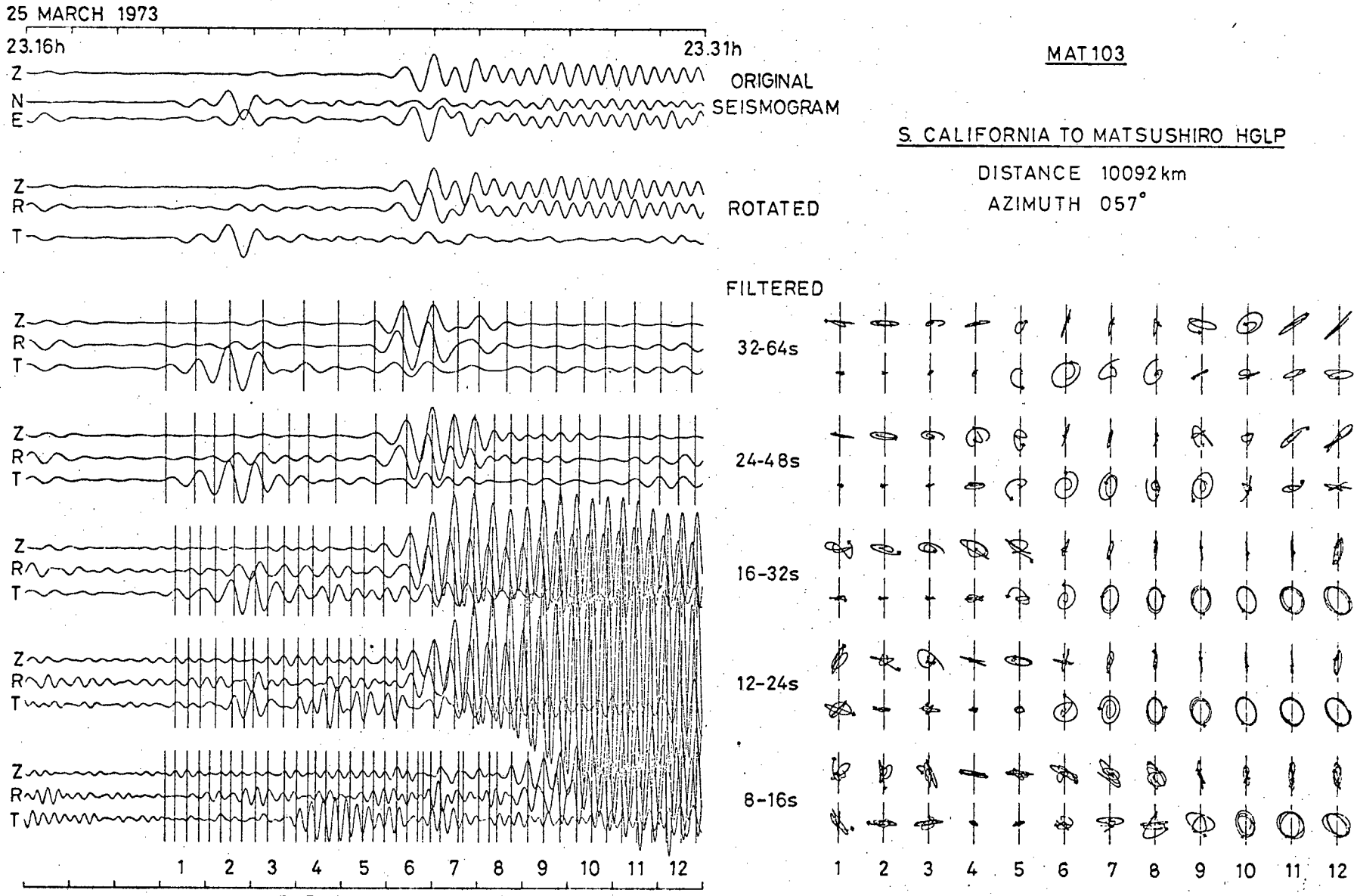

Figure 5.6m see key on p.94

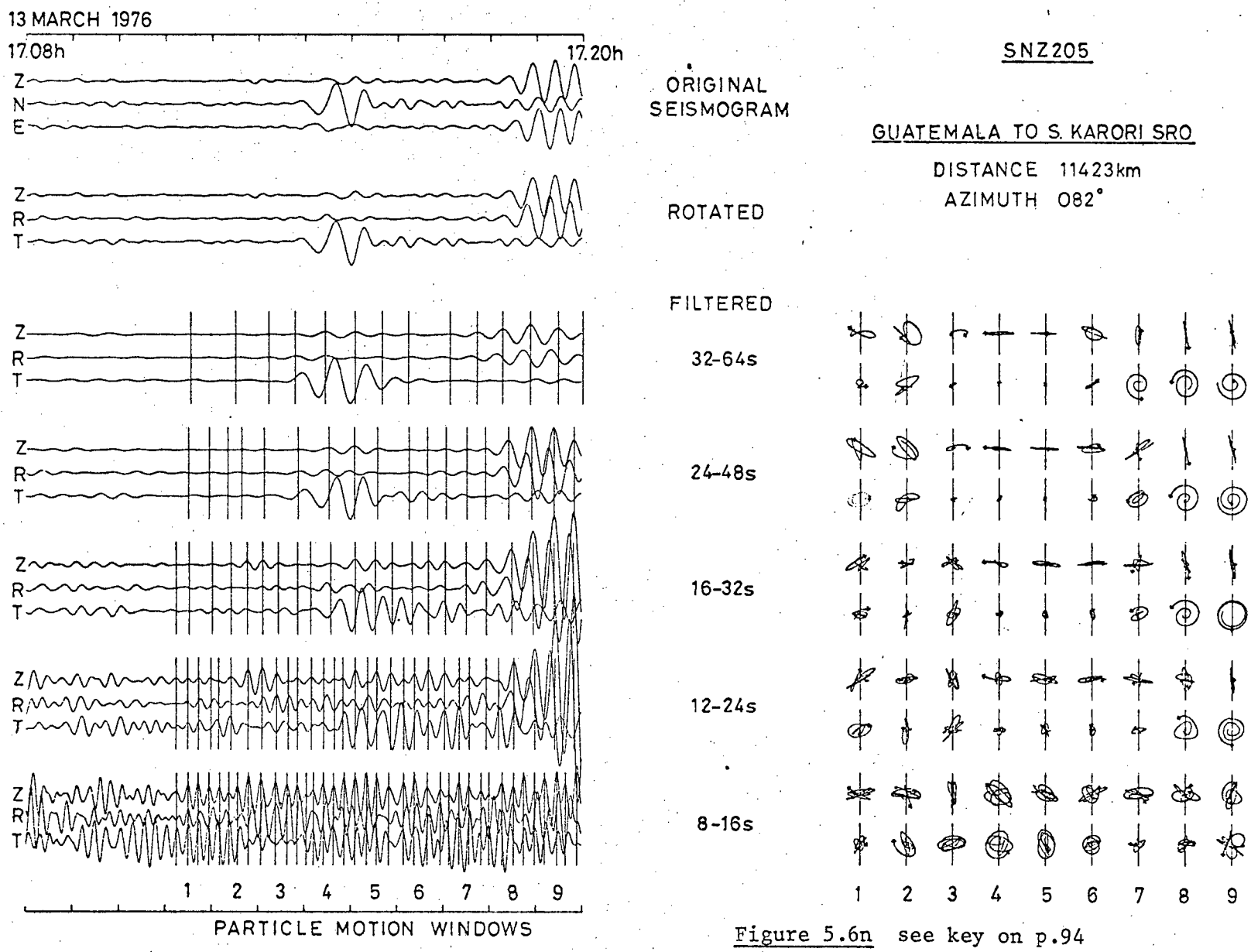

Figure 5.6n see key on p.94

5.3(a) Fundamental Rayleigh-type mode

Rayleigh-type wave trains with regular dispersion and slowly decaying amplitude occur only at the island station, Kipapa (HGLP and WWSSN), (Figures 5.6f - 5.6ℓ). At other stations, especially at shorter periods (below 24 seconds) the wave trains show rapid beating, indicating either multipathing of the fundamental mode, or interference with other modes, which are likely to be generated at the continent/ocean boundary.

5.3(b) Love-type modes

Body-wave arrivals are apparant on all the records for paths of less than 6000km, arriving more or less simultaneously with the start of the Love-type wave-train, corresponding to the SS-phase. (Figures 5.6a -j,ℓ).
The surface-waves show dispersion, appearing later in each filtered section, as the period decreases, while the body-wave arrives at the same time, whatever the period.

The surface-wave train may include more than one Love-type mode. Most of the events considered, for which depth determinations are available, occurred in the depth range 20-80km. The quoted depths are subject to uncertainties of $\pm$ 20 km or more, so it is not possible to determine which events occurred close to the displacement-amplitude node for higher Love-type modes, which is near 70km depth. In general then, both 2G and higher modes are expected, but some events may show only 2G.

The difference in arrival times between 2G and the higher modes is, for periods above 20 seconds, between one and three minutes, depending on the particular path length. The modes will overlap where the path is short and the length of the wave train is comparable to this time difference, but may appear separate for the very long travel paths. On many records for short paths, the wave-train shows variations in amplitude, or beats, suggesting the presence of two or more interfering Love-type modes. (eg. ANT041, ANT053, CTA108a, CTA108b, KIP403, Figures 5.6a,b,d,e,ℓ). There is some suggestion of a 2G arrival, after the main Love-type arrival, on the records for long paths, MAT103 and SNZ205. (Figures 5.6m,n).

5.3(c) Higher Rayleigh-type modes

Records for ten events occurring below 80km depth were examined, but only two, clear surface-wave records were found, KIP302 and ANT041 (Figure 5.6a). These are the only records on which higher Rayleigh-type modes might be expected. However, there are large Love-type arrivals on both records, and only small vertical and radial components at the appropriate arrival time, so no higher Rayleigh-type modes can be isolated.

5.4 Surface-wave particle-motion anomalies : observations

The most obvious anomalies on the seismograms occur in the Love-type modes. Wherever there is an evenly dispersed wave-train on the transverse component, this is coupled to a small, vertical component. This is apparent at all periods, but is clearest at short periods, particularly on the Kipapa records KIPOK2, KIPOK3, KIP108a and

KIP108b, (Figures 5.6f,g,i,j), where the vertical and transverse components are nearly 180° out of phase, over nine or ten cycles. The relative phase of vertical and transverse components appears to change with period, probably due to interference with the SS-arrival and between different modes at the longer periods. On one record, where there is no simultaneous body-wave arrival and only one Love-type mode appears to be present, KIP205 (Figure 5.6k), the vertical and transverse components are in phase at all periods.

The particle-motion plots highlight other anomalous features. Both Love-type and fundamental-Rayleigh-type waves have particle-motion which is elliptical rather than linear, in horizontal section. This, again, is clearest on the records from Kipapa.

Particle-motion is, clearly, tilted-Rayleigh-type in all the surface-wave modes recorded. There is no evidence of any significant inclined-Rayleigh-type anomaly, but these might be expected only in higher Rayleigh-type modes, which are not clearly shown on any of the seismograms.

5.5 Anisotropy or noise ?

Similar particle-motion anomalies are recorded on different types of instrument (WWSSN, HGLP and SRO), installed in different sites and in very different tectonic settings. Antofagasta, for example,is situated above an active subduction zone, Kipapa is on a mid-ocean island and Charters Towers on a stable continental shield. It seems unlikely that the anomalies are generated near the recording station, and much more probable that they are genuine effects of the structure along the waves' paths.

Anomalies such as those visible in the Love-type modes might arise from a chance coincidence of the group-velocities of Love and higher-Rayleigh modes. To explain the features of constant phase-difference at all periods (KIP205) and over paths of different lengths (KIPOK2, KIP106, KIP403) would require an exact coincidence over a range of periods and through slightly different structures, which is highly unlikely. Also, the higher Rayleigh-modes should not be significantly excited by the shallow events used. The anomalies in the fundamental Rayleigh-type mode could not arise in this way, there being no Love-type mode with appropriate dispersion, nor could they result from lateral refraction.

The presence of large-scale anisotropic alignments in the Pacific upper-mantle has been demonstrated by other studies (Forsyth 1975b, Schlue and Knopoff 1977) so that it is quite reasonable to propose that this is responsible for the observed anomalies, provided those anomalies show a symmetrical pattern which is consistant with the proposed alignments.

5.6 Patterns in particle-motion anomalies: predictions

The tilted-Rayleigh-type particle-motion observed on the seismogram is characteristic of propagation in a structure with only one vertical plane of symmetry. The consequent pattern of anomalies is illustrated by Figures 3.1a and 3.2a. If several waves of the same mode arrive at a central point along different directions, then the direction of the structural symmetry plane divides them into two groups. The particle-motion ellipse for those arriving on one side of the symmetry plane is tilted down to the right (looking along the direction of travel). For waves arriving on the other side, the tilt is down to the left. This is shown on the seismograms (Figure 5.6) as a phase difference between vertical and transverse components of 0^{o} (tilt down to left) or 180^{o} (tilt down to right).

5.7 Patterns at a single station: observations

The best azimuthal range of travel-paths in a single region is provided by the arrivals at Kipapa. The sense of tilt for the Love-type modes can be determined by the vertical-transverse phase-difference at short periods, where the modes are isolated from the SS-arrivals. Where there are two or more modes interfering to cause beats in the wave train, then the modes are in phase when there is a maximum in beat-amplitude. The model studies in Chapter 3 show that the Love-type higher modes 2G and 4G show the same phase-difference between vertical and transverse components. So, if transverse components of two modes are in phase, so are the vertical components. The characteristic phase-difference for the Love-type modes can therefore/

therefore be measured where there is clear beating, or a clear single mode.

The sense of tilt for the fundamental Rayleigh-type mode might also be estimated from the phase-differences on the seismogram. However, as there is likely to be a spurious transverse component generated by the large radial component, if the direction of travel is slightly different from that assumed, it is better to determine the sense of tilt for mode FG from the particle-motion diagrams.

The simplest check on consistancy with the expected pattern is provided by KIP205 and KIPOK2, (Figures 5.6k, 5.6a). These record waves which have arrived from approximately opposite directions, and so should show tilts of opposite sense. For KIPOK2, the particle-motion ellipse in the Love-type mode at 12 seconds, tilts down to the right, in the Rayleigh-type mode FG, at about 20 seconds, it tilts to the left. For KIP205, mode 2G (apparantly the only higher-mode present), the tilt is to the left. For FG there is a significant transverse component only at rather short periods, where the tilt is down to the right. So these anomalies are consistant with the predicted pattern.

(Note that, since these waves are travelling approximately north-east (KIPOK2) and west (KIP205), the particle-motion ellipse in both cases is tilted down to the south or south-east in mode 2G, and to the north or north-east in mode FG).

The other arrivals at Kipapa are along azimuths close to KIPOK2, and show the same phase-differences as that record. A greater azimuthal range of travel paths is needed to determine the direction of the

structural symmetry plane, or to check for consistency with some assumed direction.

5.8 Patterns at several stations: a consistent model

The data from all the recording stations may be combined if it is assumed that the vertical structural symmetry plane coincides with the direction in which the oceanic lithosphere is moving, relative to the rest of the upper-mantle. Estimates of the direction of movement for each of the major tectonic plates have been made by Morgan (1971), as shown in Figure 5.7. It is possible that the anisotropic alignment in a region is controlled by the direction of plate-motion at the time when that region of the lithosphere formed (Crampin 1977b) and this may be different from the present direction of movement. The Pacific lithosphere near Hawaii, for example, was formed when the plate was moving in a slightly more westerly direction, but the difference is small (about 13^{o}), especially when considered in relation to the uncertainties in determining motion relative to the underlying mantle.

Direction of wave travel relative to the direction of plate movement near the recording station have been determined for each path using Table 5.4, which is derived from Figure 5.7.

The sense of tilt for the tilted-Rayleigh-type particle-motion can be determined from the seismograms. The program which plots the seismograms and particle-motion diagrams routinely determines the maximum amplitude of each component, in each one minute interval, and this information can be used to calculate the degree of tilt.

therefore be measured where there is clear beating, or a clear single mode.

The sense of tilt for the fundamental Rayleigh-type mode might also be estimated from the phase difference on the seismograms. However, as there is likely to be a spurious transverse component generated by the large radial component, if the direction of travel is slightly different from that assumed, it is better to determine the sense of tilt for mode FG from the particle-motion diagrams.

The simplest check on consistency with the expected pattern is provided by KIP205 and KIPOK2,(Figures 5.6k,5.6f). These record waves for travel-paths 120^{o}apart so it is likely that the structural-symmetry plane lies between them. For a given mode, the particle-motions for the two paths should then show tilts of opposite sense. For KIPOK2, the particle-motion ellipse in the Love-type mode, at 12 seconds period, tilts down to the right. For KIP205, mode 2G (apparantly the only Love-type mode present) the tilt is to the left. For KIPOK2, the particle-motion ellipse in the Rayleigh-type mode,FG, at 20 seconds period, tilts to the left. For KIP205, mode FG,the tilt is down to the right. So these anomalies are consistent with the expected pattern.

(Note that, since these waves are travelling approximately north-east (KIPOK2) and west (KIP205), the particle-motion ellipse for both paths is tilted down to the south or south-east in mode 2G, and to the north or north-west in mode FG).

The other arrivals at Kipapa are along azimuths close to KIPOK2,and show the same particle-motion tilts as that record. A greater azimuthal range of travel paths is needed to determine the direction of the

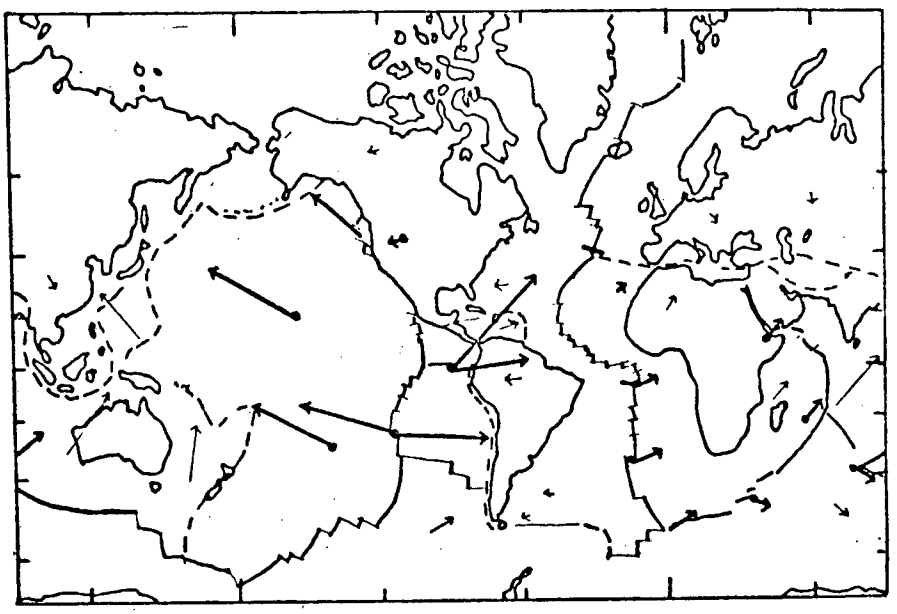

Figure 5.7 Direction and speed of lithospheric plate-motion relative to the undelying mantle. Bold arrows are for 'hot spots'. (from Morgan 1971)

Station	Direction of plate-motion
ANT	093°
BOG	083°
CTA	007°
GUMO	280°
KIP	300°
MAT	276°
SNZO	299°

Table 5.4 Direction of lithospheric-plate movement relative to the underlying mantle near seismic stations. (derived from Figure 5.7)

Figures 5.8 and 5.9 show the effect of plotting the measured tilts against direction of wave travel, for the fundamental Rayleigh-type mode (Figure 5.8) and for the Love-type modes (Figure 5.9). The anomalies are measured where they are most clearly shown, near 15 seconds period in Love-type modes and near 20 seconds period in FG. The degree of tilt, effectively the relative amplitudes of vertical and radial components, is used only to indicate the significance of each data point. An even variation of anomaly amplitude, or degree of tilt, with azimuth would be expected in an idealised model (Figure 3.16). Because of differences in structure near each site, slight variations in period between wave trains measured and the possibility of interference between 2G and other Love-type modes, it is not likely that any simple pattern in anomaly-amplitude would be apparant in the observational data.

The plots in Figures 5.8 and 5.9 do each show a pattern in tilt-sense which is consistent with the proposed structural symmetry, with very few inconsistent observations. In mode FG, the tilt is down towards the direction of plate-movement, in the Love-type modes the tilt is down in the opposite direction. This pattern of opposite tilts for FG and 2G (or 4G) is found in all the model structures of 110-type considered in Chapter 3, with the olivine a-axis tilted down in the same direction as the Love-type particle-motion, that is, away from the direction of plate-motion.

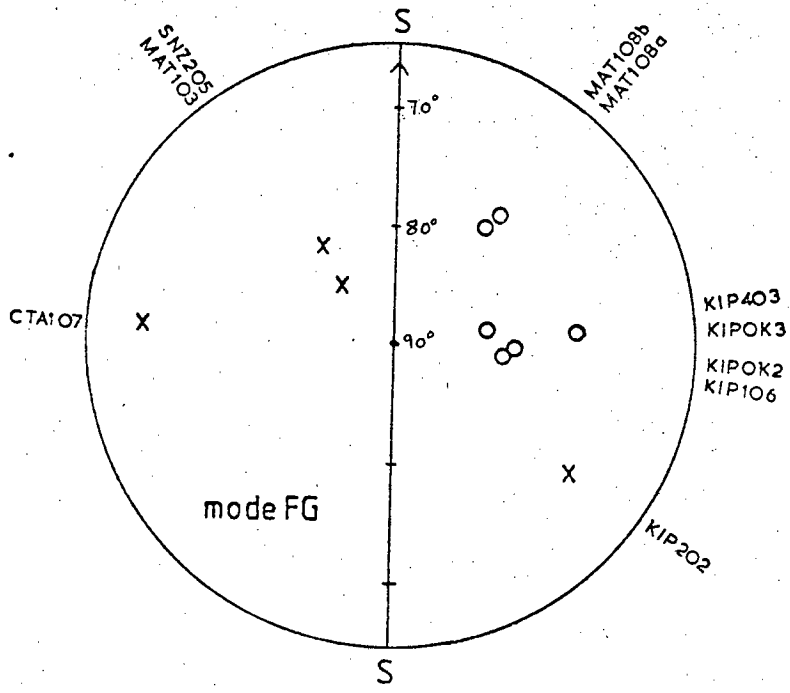

o tilt down to left

x tilt down to right

Figure 5.8 Sense and degree of tilt for particle-motion in mode FG plotted against direction of wave travel, relative to the direction of plate-motion, SS.

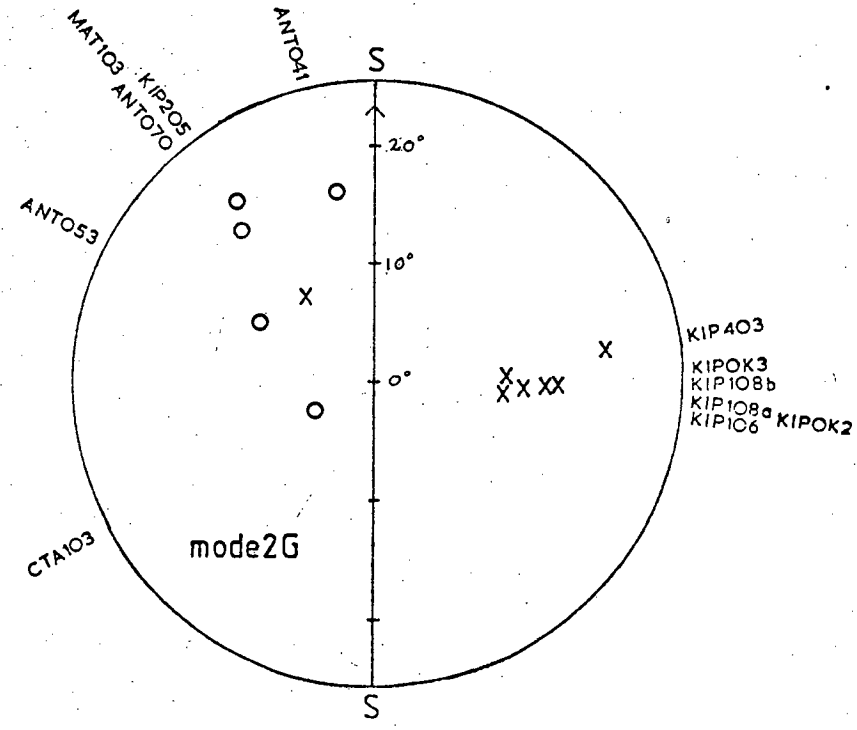

o tilt down to left

x tilt down to right

Figure 5.9 Sense and degree of tilt for particle-motion in mode 2G plotted against direction of wave travel, relative to the direction of plate-motion, SS.

5.9 Implications of observed patterns

The observed particle-motion anomalies, and the symmetrical pattern into which they fit, can be explained by anisotropic alignment in the upper-mantle, only if the alignment is such as to produce only one vertical plane of structural symmetry. In particular, alignment of olivine by glide-plane slip in a zone of horizontal shearing, could not account for the observations, as this would produce two vertical planes of symmetry (the 010-models in Chapter 3), with characteristically different patterns of particle-motion (Figures 3.1b, 3.2b).

If aligned olivine is responsible for the observed effects, then one of the three crystallographic axes must show preferred alignment in a direction which is neither vertical nor horizontal. If the syntectonic-recrystallisation mechanism proposed by Ave 'Lallemant and Carter (1970) is responsible for the olivine alignment, then the olivine b-axes should be aligned parallel to the maximum compressive-stress, and the a-axes parallel to the minimum. (Figure 1.2). The models studied in Chapter 3 are consistent with the observations only if the olivine b-axes are tilted down towards the direction of plate-movement. This corresponds to Figure 1.2b. In other words, the particle-motion data suggests that the lithosphere is dragging the asthenosphere and not vice-versa.

5.10 Amplitude of particle-motion anomalies : some preliminary results

Two amplitude measurements are useful: the ratios of Z/T for mode 2G, and the horizontal-section ellipticity for mode FG. These ratios are rather insensitive to small variations in assumptions about direction of propagation, and are expected to show a variation with period that may be useful in discriminating between possible model structures. (see Figure 3.17)

Only a few of the records used in this study are suitable for such measurements, these being the records from KIP (HGLP) for dates since 1976. The recording sensitivity settings and instrument responses are not sufficiently well documented prior to that date and at other stations the range of periods for which particle-motion can be determined is too small. With such a small number of records no azimuthal variation of anomaly magnitude can be resolved. However, the models on Chapter 3 indicate that this variation may indeed be small, for all directions of propagation more than a few degrees away from the trace of the structural symmetry plane.

The maximum amplitudes of Z,R and T components, for each 60 second time interval, are routinely listed by the program which plots the seismograms. Using this data in conjunction with the plots it is possible to select appropriate Z/T ratios for the Love-type modes at each period. Similarly, horizontal-section ellipticity can be found for mode FG from the maximum R and T amplitudes so long as any inclination is very small. (In fact the ratio T/Z, which is virtually the same as T/R, is used to allow direct comparison with the model results in Figure 3.17). The corresponding periods can be measured on the seismogram.

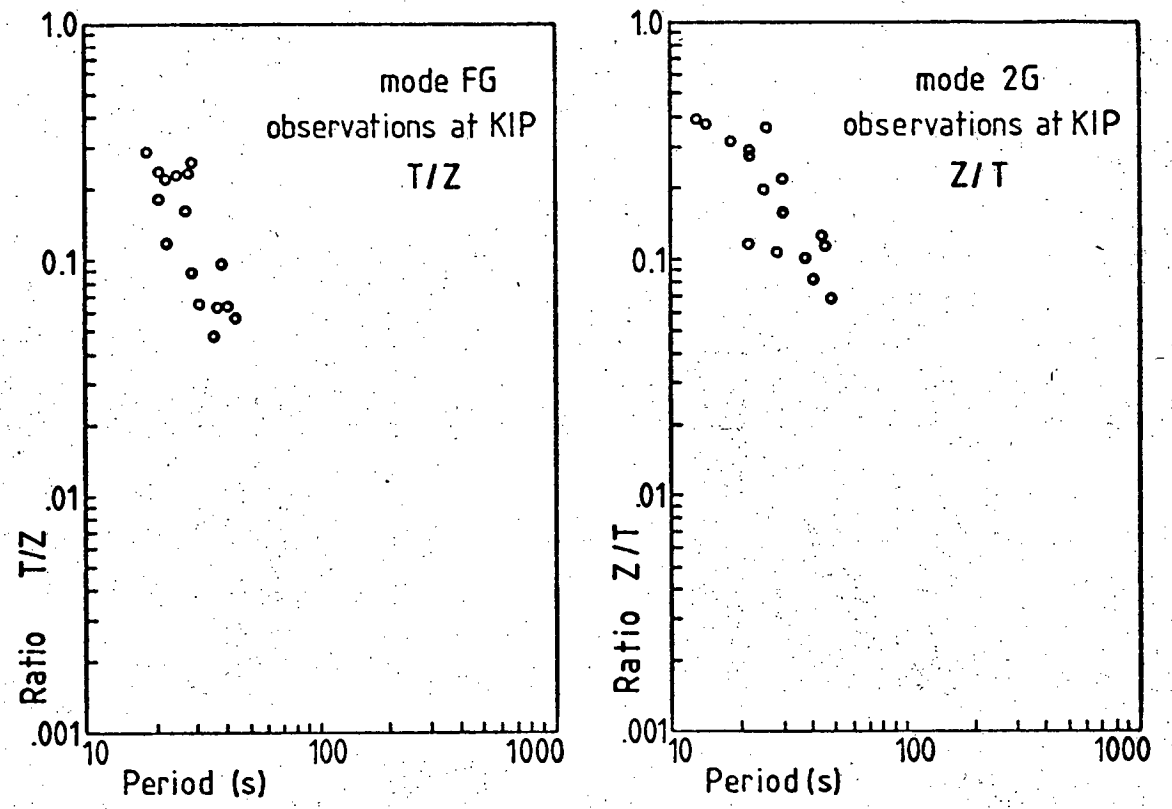

Figure 5.10 Degree of tilt of particle-motion ellipse away from vertical (FG)and horizontal (2G), as a function of wave period. Data is for the paths KIP202, KIP205, KIP302, KIP311, KIP403.

The measured ratio of Z/T for the Love-type modes will usually refer to two or more interfering modes, usually 2G and 4G, and will lie between the values appropriate for each mode in isolation, being closest to that for the dominant mode. According to the models in Chapter 3, the ratio of Z/T should be about twice as large for mode 2G as for mode 4G, so measurements of the ratio of Z/T may be up to 100% lower than the true value for 2G.

The results are shown in Figure 5.10 and, even with allowance for the uncertainty for mode 2G, demonstrate that both FG and 2G show an increase in anomaly magnitude with decreasing period. The Figures 5.6a - 5.6n provide qualitative confirmation of this.

As the model curves in Figure 3.17 show, the increase in FG anomaly magnitude suggests that the anisotropic alignment is stronger in the lithosphere than in the asthenosphere, but, in view of the very small number of records used, and the small number of models studied, this result can provide no definite proof. The level of anomaly amplitude in both FG and 2G suggests a fairly strong alignment (nearer 50% than 20%) even if a 60km thick zone is evenly anisotropic.

6. CONCLUSIONS

6.1 Results of surface-wave particle-motion study

a) Theoretical models

The study of surface-wave characteristics in anisotropic models of ocean-basin structure predicted that particle-motion anomalies might provide a powerful method for determining the geometry of aligned anisotropy in the oceanic upper-mantle, and might also yield information about the location and degree of alignment in any anisotropic layer. Anomalies could be expected in the third-generalised surface-wave mode, corresponding to the isotropic second-Rayleigh-mode, in the presence of almost any reasonable anisotropic layer. Anomalies would occur in the fundamental, second and fourth generalised modes, corresponding to the isotropic fundamental Rayleigh, and first and second Love-modes, in the presence of fairly thick anisotropic layers, with certain symmetries.

b) Observations, symmetry and possible geometry of anisotropic alignments

Using relatively few observations it has been possible to derive considerable information about anisotropy in the upper-mantle beneath the Pacific Ocean. The observation of predominantly tilted-Rayleigh-type particle-motion indicates control by a structure with a single vertical symmetry plane. Such symmetry cannot result from alignment of anisotropic elements, such as flat cracks or pockets of partial melt (Garbin and Knopoff, 1975) or mineral crystallographic axes, along purely horizontal or vertical directions. There must be alignment of some anisotropic element in a direction between

horizontal and vertical.

Results obtained from measurement of the amplitude of particle-motion anomalies suggest that there may be a high degree of alignment, particularly in the lithosphere. However, more observations and further modelling will be required to confirm and refine this hypothesis.

c) Generation of anisotropy, shear-zones and the driving-mechanisms of plate-tectonics

Anisotropic elements may align along slip-planes in shear-zones. To produce the correct geometry of alignment these slip-planes must be tilted significantly away from the horizontal or vertical. It is difficult to imagine how the predominantly horizontal movements associated with plate-tectonics could cause such tilted slip-planes.

A more plausible explanation is offered by Ave 'Lallemant and Carter's (1970) theory of alignment of olivine by syntectonic recrystallisation, where horizontal shearing results in alignment of olivine a and b- axes at 45° to the horizontal (Figure 1.2) The observed particle-motion anomalies are consistent with models incorporating such olivine alignment, where the single vertical structural symmetry plane in the anisotropic model coincides with the direction of lithospheric-plate movement over the mantle below, and the olivine b-axes are tilted down in the direction of plate motion

According to Ave'Lallemant and Carter (1970) such alignment should be generated in the upper-mantle at temperatures above $500^{\circ}C$, where

the lithosphere is moving faster than the asthenosphere (Figure 1.2). Alignment might be generated in young, hot lithosphere, close to the mid-ocean ridge, and be 'frozen in' as it cools and thickens, moving away from the ridge. Alternatively, alignment might be generated in the hotter asthenosphere, throughout the ocean-basin. In either case, the moving oceanic lithosphere must drag the asthenosphere beneath it at some stage in its evolution.

6.2 Comparison with other studies of anisotropy in the oceanic upper-mantle

The model of oceanic upper-mantle anisotropy suggested by the particle-motion data, with fairly strong alignment of crystalline olivine by syntectonic recrystallisation, probably 'frozen in' to the oceanic lithosphere, is not necessarily a complete one. Layers with alignment of higher symmetry may be present which would not affect particle-motion in the surface-wave modes observed.

The proposed alignment of olivine by syntectonic recrystallisation is inadequate to account for the P_n anisotropy of 8%, found by refraction studies, at the top of the lithosphere, as it predicts less than 3% P_n anisotropy, although with the right sense (ie. maximum P-velocity parallel to the direction of plate-motion). Some other alignment must occur at the very top of the lithosphere, perhaps slip-plane alignment of olivine or a system of parallel cracks.

The results of surface-wave dispersion studies can be qualitatively explained by the syntectonic recrystallisation model. Taking

S1X110 (Figure 3.5a) as a suitable model, but perhaps with stronger olivine alignment, the theoretical phase-velocities for the fundamental Rayleigh-type mode, FG, are greatest for propagation parallel to the direction of plate motion (0^{o}), which agrees with the observations of Forsyth (1975b) for the Nazca plate. The azimuthal anisotropy is only 1%, half that found by Forsyth, but stronger olivine alignment would give a suitable increase. Comparison of the FG and 2G dispersions for S1X110 (Figure 3.5a) with those for the fundamental Rayleigh and Love-modes in the isotropic model S-ISOT (Figure 3.3) indicates that an isotropic model very similar to S-ISOT could model the anisotropic FG dispersion, but shear-velocities higher than those in S-ISOT would be required to model the anisotropic 2G mode. This corresponds to the structural anisotropy found by Forsyth (1975b) and Schlue and Knopoff (1977).

The model of anisotropy derived, rather simply, from observations of surface-wave particle-motion is therefore consistent with models based on the much more sophisticated analysis of surface-wave phase-velocities, and in fact tells more about the geometry and hence the possible causes, of oceanic upper-mantle anisotropy.

REFERENCES

Aki, K., 1968. Seismological evidences for the existence of soft, thin layers in the upper mantle under Japan, J. geophys. Res., 73, 585-594.

Ahrens, T.J., 1972. The state of mantle minerals, Tectnophys. 13, 189-220.

Ave 'Lallemant, H.G., & Carter, N.L., 1970. Syntectonic recrystallization of olivine and modes of flow in the upper mantle, Geol. Soc.Am.Bull, 81, 2203-2220.

Backus, G.E., 1965. Possible forms of seismic anisotropy of the upper mantle under oceans, J. geopys. Res., 70, 3429-3439.

Basu, A.R., 1977. Textures, microstructures and deformation of ultramafic xenoliths from San Quentin, Baja, California, Tectonophys. 43, 213-246.

Birch, F., 1960, 1961. The velocity of compressional waves in rocks to 10 kilobars, Part I and Part II. J. geophys. Res. vol.65, 1083-1102, vol.66, 2199-2224.

Bishop, T.N., & Lewis, B.T.R., 1973. Seismic refraction results from the E. Pacific Rise near 14°N, 104°W, Trans. A.G.U., 54,377.

Biswas, N.N., & Knopoff, L. 1970. An exact Earth flattening correction for Love -waves, Bull. seism. Soc.Am., 60, 1123-1127.

Boore, D.M., 1969. Effect of higher mode contamination on measured Love wave phase velocities, J. geophys. Res., 74, 6612-6616.

Boullier, A.M. & Nicolas, A., 1975. Classification of textures and fabrics of peridotites from S. African Kimberlites, In: L.H. Ahrens, Ed., Physics and Chemistry of the Earth,Pergamon Press, Oxford. 9, 97-105.

Capon, J., 1970. Analysis of Rayleigh wave multi-path propagation at LASA, Bull. seism. Soc.Am., 60, 1701-1731.

Carter, N.L. & Ave 'Lallemant, H.G., 1970. High temperature flow of dunite and peridotite, Geol.Soc.Am.Bull.,81,2181-2202.

Crampin, S., 1970. The dispersion of surface waves in multilayered anisotropic media, Geophys.J.R. astr.Soc., 21, 387-402.

Crampin S., 1975. Distinctive particle motion of surface waves as a diagnostic of anisotropic layering, Geophys.J.R. astr.Soc. 40,177-186.

Crampin S., 1976. A comment on "The early structural evolution and anisotropy of the oceanic upper mantle", Geophys.J.R. astr.Soc., 46,193-197.

Crampin S., 1977a. A review of the effects of anisotropic layering on the propagation of seismic waves, Geophys.J.R.astr.Soc. 49,9-27.

Crampin, S., 1977b. Paleoanisotropy in the Upper Mantle, Nature, 270, 162-163.

Crampin, S., 1978. Seismic wave propagation through a cracked solid: polarization as a possible dilatancy diagnostic, Geophys. J.R.astr.Soc., 53, 467-496.

Crampin, S. & King, D.W., 1977. Evidence for anisotropy in the upper mantle beneath Eurasia from the polarization of higher mode surface waves, Geophys.J.R.astr.Soc.,49,59-85.

Crampin, S. & Taylor, D.B., 1971. The propagation of surface waves in anisotropic media, Geophys.J.R.astr.Soc.,25,71-87.

Cristensen, N.I., 1971, Fabric, seismic anisotropy and tectonic history of the Twin Sister dunite, Washington, Bull, geol. Soc.Am.,82,1681-1694.

Dahlen, F.A., 1972. Elastic velocity anisotropy in the presence of an anisotropic initial stress, Bull. seism.Soc.Am.,61, 1183-1194.

Dorman, J., 1959. Numerical solutions for Love wave dispersion on a half space with double surface layer, Geophys.24, 12-29

Dorman, J., 1962. Period equation for waves of Rayleigh type on a layered, liquid-solid half-space, Bull. seism.Soc.Am., 52,389-397.

Evernden, J.F., 1953. Direction of approach of Rayleigh waves and related problems, Part I, Bull.seism.Soc.Am.,43, 225-274.

Evernden, J.F., 1954. Direction of approach of Rayleigh.waves and related problems, Part II, Bull.seism.Soc.Am.,44, 159-184.

Forsyth, D.W. 1975a. A new method for the analysis of multi-mode surface wave dispersion: application to Love wave propagation in the E. Pacific, Bull.seism.Soc.Am.,65, 323-342.

Forsyth, D.W. 1975b. The early structural evolution and anisotropy of the oceanic upper mantle, Geophys. J.R.astr.Soc.,43, 103-162.

Francis, T., 1969. Generation of seismic anisotropy in the upper mantle along the mid-oceanic ridges, Nature, 221,162-165.

Garbin H.D., & Knopoff L., 1975. Elastic moduli of a medium with liquid filled cracks, Q. appl.Math. 33,301-303

Graham, E.K. and Barsch, G.R., 1969. Elastic constants of single-crystal fosterite as a function of temperature and pressure, J.geophys. Res.,74, 5949-5960.

Green, H.W., & Gueguen, Y., 1974. Origin of kimberlite pipes by diapiric upwelling in the upper mantle, Nature, 249,617-620.

Green,R.W.E., & Hales,A.L., 1968. The travel times of P waves to 30° in the Central United States and upper mantle structure, Bull seism.Soc.Am., 58,267-289.

Gregerson,S & Alsop, L.E., 1976. Mode conversion of Love waves at a continental margin, Bull. seism.Soc.Am. 66 ,1855-1872

Hales A.L., Helsley, C.E., & Nation, J.B.,1970. P travel times for an oceanic path, J.geophys.Res., 75,7362-7381.

Hess, H., 1964. Seismic anisotropy of the uppermost mantle under oceans, Nature, 203,629-631.

Houtz R.E. and Ewing J.I., 1963. Detailed sedimentary velocities from seismic refraction profiles in the Western North Atlantic, J.geophys.Res.,68, 5233-5258

Hussong, D.M., Johnson S.H., Woolard, G.P., & Compbell J.F., 1972. Crustal structure of the Nazca plate; 1972 prelim.report (abs) Trans.Am.geophys.Un.,53,415.

James D.E. & Linde A.T., 1971. A source of major error in the digital analysis of World Wide Standard Station seismograms, Bull. seism. Soc.Am., 61 , 723-728.

Jeffreys, H., 1970. 'The Earth', fifth edition, Cambridge University Press.

Kane, J., and Spence, J., 1963. Rayleigh-wave transmission on elastic wedges, Geophys., 28,715-723.

Kanimuna, K., 1966. The crust and upper mantle structure in Japan,1, phase velocities of Love and Rayleigh waves, Bull.earthq.Res.Inst., 44, 481-494

Keen, C.E. & Barrett, D.L., 1971. A measurement of seismic anisotropy in the north-east Pacific, Can.J.earth.Sci., 8, 1056-1064.

Keen, C.E. and Tramontini, C., 1970. A seismic refraction survey on the mid-Atlantic ridge, Geophys.J.R.astr.Soc., 20, 473-491.

Kennedy, G.C. & Higgins, G.H., 1972. Melting temperatures in the Earth's mantle, Tectonophys. 13, 221-232.

Kern, H. and Fakhimi, M., 1975. Effect of fabric anisotropy on compressional-wave propagation in various metamorphic rocks for the range 20-700°C at 2 kbars, Tectonophys.,28,227-244.

King, G.C.P., 1971. The siting of strainmeters for teleseismic and tidal studies, Bull.R.Soc.N.Zealand, 9, 818-829.

Kirkwood, S.C., 1978. The significance of isotropic inversion of anisotropic surface-wave dispersion, Geophys.J.R.astr.Soc. 55, in press.

Knopoff, L., 1972. Observation and inversion of surface wave dispersion, Tectonophys.,13,497-519.

Kovach, R.L. & Anderson D.L., 1964. Higher mode surface waves and their bearing on the structure of the Earth's mantle, Bull. seism.Soc.Am. 54, 164-174.

Kovach, R.L. & Press, F., 1961. Rayleigh wave dispersion and crustal structure in the eastern Pacific and Indian oceans. Geophys. J.R.astr.Soc., 4, 202-216.

Kumazawa, M., 1969. The elastic constants of single-crystal orthopyroxene, J. geophys.Res., 74, 5973-5980.

Kumazawa, M. and Anderson, O.L., 1969. Elastic moduli, pressure derivatives, and temperature derivatives of single-crystal olivine and single-crystal fosterite, J.geophys. Res., 74, 5961-5972.

Langston, C.A., 1977. The effect of planar dipping structure on source and receiver responses for constant ray parameter. Bull. seism.Soc.Am., 67, 1029-1050.

Lisitsyn, A.P., 1974. Thickness of the sedimentary layer on the ocean floor, Dolkady, 217, 820-823.

Mal, A.K. & Knopoff, L., 1965. Transmission of Rayleigh waves past a step change in elevation, Bull.seism.Soc.Am., 55, 319-334.

McEvilly, T.V., 1964. Central U.S. crust - upper mantle structure from Love and Rayleigh wave phase velocity inversion. Bull. seism.Soc.Am.,54, 1997-2016.

McGarr, A., 1969a. Amplitude variations of Rayleigh waves - propagation across a continental margin, Bull.seism.Soc.Am., 59, 1281-1305.

McGarr, A., 1969b. Amplitude variations of Rayleigh waves - horizontal refraction, Bull.seism.Soc.Am., 59, 1307-1334.

Meissner R. & Fakhimi, M., 1977. Seismic anisotropy as measured under high-pressure, high-temperature conditions, Geophys. J.R.astr.Soc., 49, 133-144.

Mercier, J.C. & Nicholas, A., 1975. Textures and fabrics of upper-mantle peridotites as illustrated by xenoliths from basalts, J. Petrol., 16, 454-487.

Mitchell, B.J. & Landisman, M., 1969. Electromagnetic seismograph constants by least squares inversion, Bull,seism.Soc.Am., 59, 1335-1348.

Morgan, J.W., 1971. Convection plumes in the lower mantle, Nature, 230, 42-43.

Morris, G.B., Raitt, R.W. & Shor, G.G., 1969. Velocity anisotropy and delay time maps of the mantle near Hawaii, J.geophys. Res., 74, 4300-4316.

Nafe C.E., & Drake C.L., 1963. Physical properties of marine sediments, The Sea, ed. M.N. Hill, 3, 794-815.

Nicolas A., & Poirier, J.P., 1976. Crystalline plasticity and solid state flow in metamorphic rocks, ed. Bott, Selected topics in geological sciences, John Wiley, London.

Peselnick L., Nicholas, A., & Stevenson P.R., 1974. Velocity anisotropy in a mantle peridotite from the Ivrea zone: application to upper mantle anisotropy, J.geophys.Res. 79, 1175-1182.

Petersen, J., Butler, H.M., Holcomb, L.G., & Hutt, C.R., 1976. The seismic research observatory project, Bull.seism.Soc.Am., 66, 2049-2068.

Press, F., 1970. Earth models consistent with geophysical data, Phys.Earth Planet Inter., 3, 3-22.

Raitt, R.W., Shor, G.G., Francis, T.J.G., & Morris, G.B., 1969. Anisotropy of the Pacific upper mantle, J.geophys.Res., 74, 3095-3109.

Raitt, R.W., Shor, G.G., Morris, G.B., & Kirk, H.K., 1971. Mantle anisotropy in the Pacific Ocean, Tectonophys. 12, 173-186.

Raleigh, C.B., 1967. Plastic deformation of upper-mantle silicate minerals, Geophys.J.R.astr.soc., 14, 45-46.

Raleigh, C.B., 1968. Mechanisms of plastic deformation of olivine, J. geophys. Res., 73, 5391-5406.

Raleigh, C.B., & Talbot, J.L., 1967. Mechanical twinning in naturally and experimentally deformed diopside, Am.J.Sci., 265, 151-165.

Rodgers, P.W., 1968. The response of the horizontal pendulum seismometer to Rayleigh and Love waves, tilt and free oscillations of the Earth, Bull.seism.Soc.Am., 58, 1384-1406.

Saito, M., 1967. Excitation of free oscillations and surface-waves by a point source in a vertically heterogeneous Earth, J.geophys. Res., 72, 3689-3700.

Saito, M. & Takeuchi, H., 1966. Surface waves across the Pacific, Bull. seism.Soc.Am., 56 , 1067-1091.

Savino, J.M., Murphy, A.J., Ry n, J.M.W., Tatham, R., Sykes, L.R., Choy, G.L., & McCanny, K., 1972. Results from the High-Gain Long-Period Seismograph experiment, Geophys. J.R.astr.Soc. 31, 179-203.

Schlue, J.W., & Knopoff, L., 1976. Shear wave anisotropy in the upper mantle of the Pacific Basin, Geophys.Res.Lett., 3 , 359.

Schlue, J.W., & Knopoff, L., 1977. Shear wave polarization anisotropy in the Pacific Basin, Geophys.J.Roy.astr.Soc., 49, 145-165.

Sclater J.G. and Francheteau, J., 1970. The implications of terrestrial heat flow observations on current tectonic and geochemical models of the crust and upper-mantle of the Earth, Geophys.J.R.astr.Soc., 20, 509-542.

Smith, M.L. & Dahlen, F.A., 1973. The azimuthal dependence of Love and Rayleigh wave propagation in a slightly anisotropic medium, J. geophys.Res., 78, 3321-3333.

Stephens, C., & Isaacs, B.L., 1977. Towards an understanding of Sn: normal modes of Love waves in an oceanic structure, Bull.seism.Soc.Am., 67, 69-78.

Sykes, L.R., & Oliver, J., 1964a. The propagation of short-period seismic surface waves across oceanic areas: part I - theoretical study, Bull.seism.Soc.Am., 54, 1349-1372.

Sykes, L.R., & Oliver, J., 1964b. The propagation of short-period seismic surface waves across oceanic areas: part II - analysis of seismograms, Bull.seism.Soc.Am., 54, 1373-1415.

Talwani, M., LePichon, X., & Ewing, M., 1965. Crustal structure of the mid-ocean ridges, J.geophys.Res., 70, 341-351.

Thatcher, W., & Brune, J.N., 1969. Higher-mode interference and observed anomalous apparent Love wave phase velocities, J.geophys.Res.,74, 6603-6611.

Tozer, D.C., 1972. The present thermal state of the terrestial planets, Phys.Earth Planet Inter., 6, 182-197.

Verma, R.K., 1960. Elasticity of some high-density crystals, J.geophys.Res., 65, 757-766.

APPENDIX I

Models of ocean-basin structure incorporating anisotropic layers

Details of models and characteristics of normal-mode surface-wave propagation.

Key to model names: full names have form ABChkl - xy-pq

ABC — model structure as shown in Tables A1.1 - A1.4

hkl — indicates orientation of olivine-axis in the anisotropic layer (See Figure A1.1)

xy — indicates thickness of anisotropic layer in kilometers

pq — indicates direction of propagation relative to vertical plane containing olivine a-axis (See Figure A1.1)

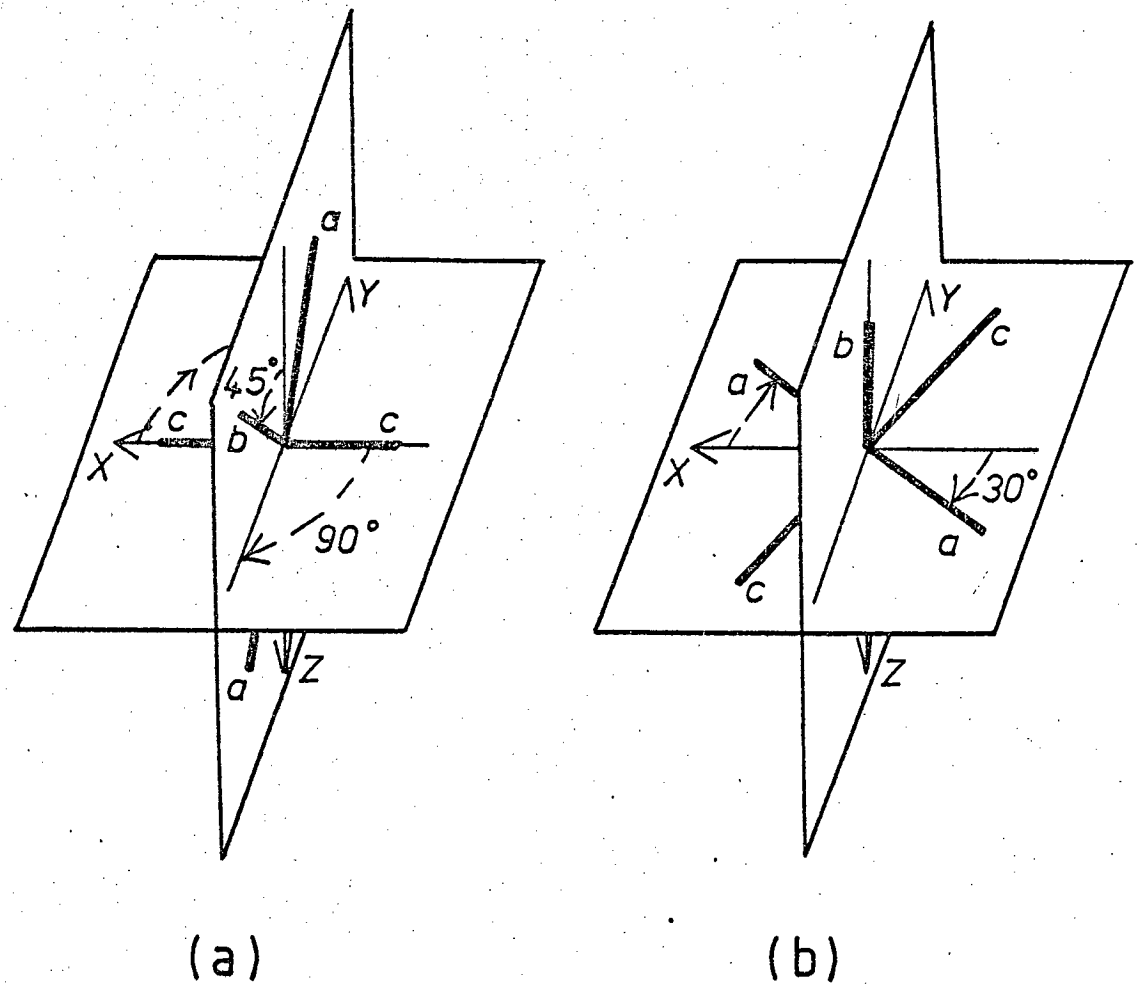

Figure A1.1 Relative orientation of crystallographic a,b, and c axes and particle-motion X,Y, and Z axes for models with (a) 110-cut olivine , azimuth of propagation 90°
(b) 010-cut olivine , azimuth of propagation 30°

TABLE A1.1 SUMMARY OF MODEL STRUCTURES

Model	Location	Anisotropic layer thickness (km)	% Aligned olivine
S-ISOT	-	-	-
S1X	all of lithosphere	60	20
S3X	all of lithosphere	60	50
S4X	all of lithosphere	60	20
A1X	top of lithosphere	10	20
C1X	top of low-velocity zone	10	20
S1T	all of low-velocity zone	60	20
S3T	all of low-velocity zone	60	50
S6T	all of low-velocity zone	60	50
A3T	base of lithosphere	10	50
S3XT	all of lithosphere plus low-velocity zone	120	20,50

TABLE A1.2 COMPOSITION OF MODEL S-ISOT

Model S-ISOT

		thickness (km)	α km/s	β km/s	ρ $kg/m^3 \times 10^{-3}$
	water	4.5	1.50	0.00	1.0
crust:	sediment	0.5	2.02	0.25	1.9
	layer 3	6.0	6.60	3.80	2.9
lithosphere:	layer 4	60.0	8.10	4.40	3.3
low-velocity-zone :	layer LV	60.0	7.48	4.10	3.4
upper mantle:	layer 5	0.00	8.25	4.55	3.5

TABLE A1.3 STRUCTURE OF ANISOTROPIC MODELS

	thickness (km)	layer name
Model A1X	4.5	Water
	6.0	layer 3
	10.0	XTOL2080
	50.0	layer 4
	60.0	layer LV
		layer 5
Model A3T	4.5	water
	6.0	layer 3
	60.0	layer 4
	10.0	TTOL5050
	50.0	layer LV
		layer 5
Model C1X	4.5	water
	6.0	layer 3
	50.0	layer 4
	10.0	XTOL2080
	60.0	layer LV
		layer 5
Model S1X	4.5	water
	0.5	sediment
	6.0	layer 3
	60.0	XTOL2080
	60.0	layer LV
		layer 5
Model S1T	4.5	water
	0.5	sediment
	6.0	layer 3
	60.0	layer 4
	60.0	TTOL2080
		layer 5
Model S3X	4.5	water
	0.5	sediment
	6.0	layer 3
	60.0	XTOL5050
	60.0	layer LV
		layer 5
Model S3XT	4.5	water
	0.5	sediment
	6.0	layer 3
	60.0	XTOL2080
	60.0	TTOL5050
		layer 5

TABLE A1.3 (cont)

	thickness	layer name
Model S3T	4.5	water
	0.5	sediment
	6.0	layer 3
	60.0	layer 4
	60.0	TTOL5050
		layer 5
Model S4X	4.5	water
	0.5	sediment
	6.0	layer 3
	60.0	XAOL2080
	60.0	layer LV
		layer 5
Model S6T	4.5	water
	0.5	sediment
	6.0	layer 3
	60.0	layer 4
	60.0	XAOL5050
		layer 5

TABLE A1.4 ELASTIC CONSTANTS OF ANISOTROPIC LAYERS

AOLIVINE:
Olivine elastic constants
from Verma 1960
Density = 3324 kg/m^3

j k m n	C_{jkmn} (kb)
1 1 1 1	3240
2 2 2 2	1980
3 3 3 3	2490
1 1 2 2	590
2 2 3 3	780
3 3 1 1	790
1 2 1 2	793
2 3 2 3	667
1 3 1 3	810

XTOL5050:
50% TOLIVINE
50% α = 7.34km/s, β = 4.69 km/s
Density = 3324 kg/m^3

j k m n	C_{jkmn} (kb)
1 1 1 1	2465
2 2 2 2	1962
3 3 3 3	1962
1 1 2 2	710
2 2 3 3	755
3 3 1 1	710
1 2 1 2	766
2 3 2 3	604
1 3 1 3	766

TOLIVINE:
Transversely isotropic olivine,
symmetrical about a-axis
Density = 3324 kg/m^3

j k m n	C_{jkmn} (kb)
1 1 1 1	3240
2 2 2 2	2235
3 3 3 3	2235
1 1 2 2	690
2 2 3 3	780
3 3 1 1	690
1 2 1 2	801.5
2 3 2 3	727.5
1 3 1 3	801.5

TTOL2080:
20% TOLIVINE
80% α = 7.10km/s, β = 3.91 km/s
Density = 3324 kg/m^3

j k m n	C_{jkmn} (kb)
1 1 1 1	1989
2 2 2 2	1788
3 3 3 3	1788
1 1 2 2	680
2 2 3 3	698
3 3 1 1	680
1 2 1 2	559
2 3 2 3	545
1 3 1 3	559

XTOL2080:
20% TOLIVINE
80% α = 7.78 km/s, β = 4.54 km/s
Density = 3324 kg/m^3

j k m n	C_{jkmn} (kb)
1 1 1 1	2254.87
2 2 2 2	2052.37
3 3 3 3	2052.37
1 1 2 2	665.26
2 2 3 3	710.26
3 3 1 1	665.26
1 2 1 2	708.05
2 3 2 3	671.05
1 3 1 3	708.05

XAOL2080:
20% AOLIVINE
80% α =7.78 km/s, β = 4.54 km/s
Density = 3324 kg/m^3

j k m n	C_{jkmn} (kb)
1 1 1 1	2255
2 2 2 2	2003
3 3 3 3	2105
1 1 2 2	630
2 2 3 3	668
3 3 1 1	670
1 2 1 2	707
2 3 2 3	681
1 3 1 3	710

TABLE A1.4 (cont)

TTOL5050:
50% TOLIVINE
50% α= 5.65 km/s, β=3.27 km/s
Density = 3324 kg/m^3

j k m n	C_{jkmn} (kb)
1 1 1 1	2151.75
2 2 2 2	1649.25
3 3 3 3	1649.25
1 1 2 2	522.25
2 2 3 3	567.25
3 3 1 1	522.25
1 2 1 2	578
2 3 2 3	541
1 3 1 3	578

TAOL5050
50% AOLIVINE
50% α= 5.65 km/s, β= 3.27 km/s
Density = 3324 kg/m^3

j k m n	C_{jkmn} (kb)
1 1 1 1	2151.75
2 2 2 2	1520
3 3 3 3	1775
1 1 2 2	470
2 2 3 3	565
3 3 1 1	570
1 2 1 2	574
2 3 2 3	511
1 3 1 3	582

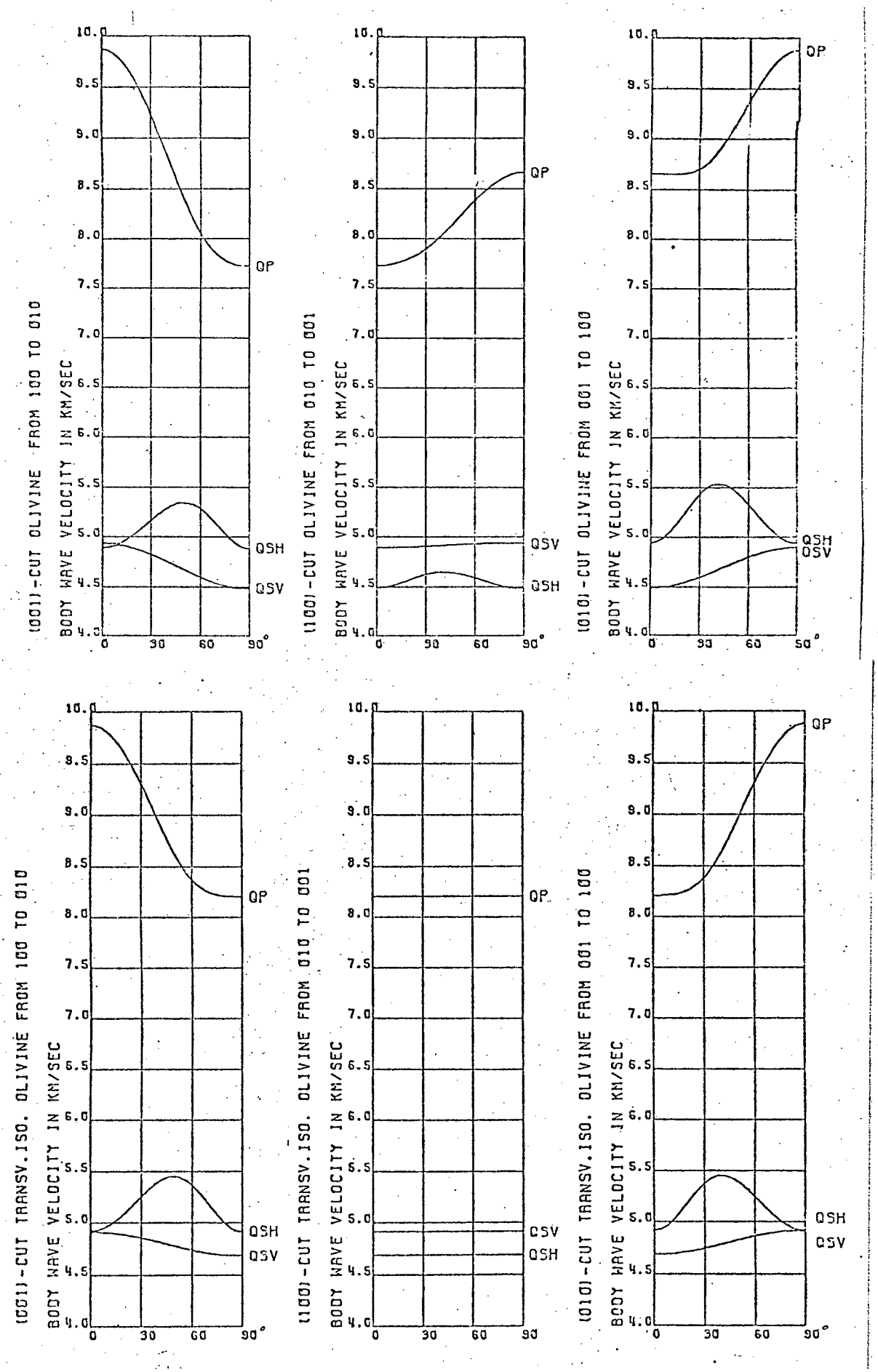

Figure A1.2 Body-wave velocities in AOLIVINE (top) and TOLIVINE. (see Table A1.4)

Table A1.5 Dispersion and particle-motion data for ocean-basin models.

Models are arranged in alphabetical order.

Data comprise period, phase-velocity (PHVEL), relative amplitudes and phases of the three components of particle-motion at the top of the solid layers (U,PHI), angle between directions of group and phase-velocities (GPANG), and XYANG which is $\tan^{-1}$ UY/UX

S-ISOT FR FL 2R 2L

PERIOD	PHVEL	GPVEL	UX/UZ
20.00	3.87335	3.75396	0.549345
30.00	3.91032	3.84699	0.661437
40.00	3.91792	3.87941	0.704463
50.00	3.93540	3.82511	0.702566
60.00	3.96229	3.79202	0.694495
70.00	3.99297	3.78831	0.686612
80.00	4.02271	3.80862	0.681006
90.00	4.04895	3.84253	0.677972
100.00	4.07095	3.88113	0.677065
110.00	4.08890	3.91897	0.677639
120.00	4.10339	3.95341	0.679301
130.00	4.11505	3.98353	0.681488
140.00	4.12446	4.00945	0.683957
150.00	4.13209	4.03140	0.686516
160.00	4.13833	4.04994	0.689026
170.00	4.14347	4.06558	0.691429
180.00	4.14774	4.07879	0.693672
190.00	4.15132	4.08996	0.695734
200.00	4.15434	4.09947	0.697606
210.00	4.15691	4.10753	0.699289
000000000000000	0000000000000	0000000000000	0000000000000
12.00	4.22711	4.10116	
14.00	4.24614	4.13235	
16.00	4.26093	4.15655	
18.00	4.27275	4.17649	
20.00	4.28263	4.19282	
22.00	4.29128	4.20635	
24.00	4.29913	4.21949	
26.00	4.30644	4.21606	
28.00	4.31338	4.22051	
30.00	4.32004	4.22402	
40.00	4.35076	4.23867	
50.00	4.37813	4.25328	
60.00	4.40216	4.27210	
70.00	4.42283	4.29345	
80.00	4.44034	4.31563	
90.00	4.45504	4.33734	
100.00	4.46733	4.35777	
110.00	4.47762	4.37650	
120.00	4.48625	4.39339	
130.00	4.49352	4.40846	
140.00	4.49967	4.42183	
150.00	4.50489	4.43366	
160.00	4.50937	4.44411	
170.00	4.51321	4.45334	
180.00	4.51654	4.46152	
190.00	4.51943	4.46876	
200.00	4.52195	4.47521	
000000000000000	0000000000000	0000000000000	0000000000000
12.00	4.26071	4.01673	-0.313775
14.00	4.30462	4.01680	0.081137
16.00	4.35084	4.09317	0.279102
18.00	4.39814	4.21732	0.374953
20.00	4.44213	4.36783	0.435503
22.00	4.47902	4.14615	0.473673
24.00	4.50732	4.23566	0.493353
26.00	4.52743	4.32427	0.514796
28.00	4.54036	4.40655	0.526776
30.00	4.54700	4.49104	0.534149
000000000000000	0000000000000	0000000000000	0000000000000
12.00	4.31991	3.98661	
14.00	4.37581	4.03305	
16.00	4.42732	4.05670	
18.00	4.47667	4.06590	
20.00	4.52012	4.34590	
22.00	4.54736	4.39791	
000000000000000	0000000000000	0000000000000	0000000000000
000000000000000	0000000000000	0000000000000	0000000000000

A1X110-10-59.9 FG 2G 3G 4G

PERIOD	PHVEL	XYANG	GPANG	UX	PHIX	UY	PHIY	UZ	PHIZ
158.546	4.140	0.180	0 -0.018	0.681	0.	0.002	-26.	1.000	90.
108.570	4.090	0.211	0 -0.026	0.669	-0.	0.002	-13.	1.000	90.
84.782	4.040	0.212	0 -0.034	0.671	0.	0.002	2.	1.000	90.
67.464	3.990	0.218	0 -0.042	0.683	-0.	0.003	25.	1.000	90.
49.182	3.940	0.326	0 -0.057	0.708	0.	0.004	64.	1.000	90.
15.462	3.840	2.853	0 -0.317	0.696	-0.	0.037	106.	1.000	90.
342.906	4.540	89.925	0 -0.002	0.001	0.	1.000	-90.	0.000	176.
115.050	4.490	89.772	0 -0.017	0.004	0.	1.000	-90.	0.002	164.
72.221	4.440	89.630	0 -0.030	0.006	-0.	1.000	-89.	0.002	152.
47.876	4.390	89.487	0 -0.041	0.010	0.	1.000	-89.	0.004	139.
30.160	4.340	89.098	0 -0.043	0.016	0.	1.000	-89.	0.007	122.
12.674	4.240	88.493	0 -0.006	0.026	0.	1.000	-85.	0.027	103.
27.347	4.540	1.359	0 -0.001	0.598	-0.	0.014	93.	1.000	90.
22.621	4.490	2.799	0 -0.003	0.612	0.	0.030	95.	1.000	90.
19.836	4.441	4.008	0 -0.004	0.616	0.	0.043	96.	1.000	90.
17.558	4.390	5.192	0 -0.004	0.610	0.	0.055	98.	1.000	90.
15.451	4.340	6.665	0 -0.003	0.580	-0.	0.068	100.	1.000	90.
10.835	4.240	8.740	0 -0.006	1.000	0.	0.118	100.	0.469	90.
19.203	4.540	88.308	0 -0.055	0.021	0.	1.000	-83.	0.009	116.
16.231	4.490	88.313	0 -0.101	0.024	0.	1.000	-82.	0.013	109.
13.506	4.440	88.566	0 -0.124	0.025	-0.	1.000	-81.	0.017	106.
10.759	4.390	76.483	0 -0.080	0.354	0.	1.000	88.	0.209	39.
10.428	4.340	20.834	0 -0.194	1.000	0.	0.381	94.	0.733	90.
9.642	4.240	11.054	0 -0.173	1.000	0.	0.195	101.	0.948	90.

A1X010-10-59.9 FG 2G 3G 4G

PERIOD	PHVEL	XYANG	GPANG	UX	PHIX	UY	PHIY	UZ	PHIZ
158.277	4.140	0.674	0 -0.066	0.680	0.	0.003	0.	1.000	90.
108.436	4.090	0.855	0 -0.087	0.669	-0.	0.010	0.	1.000	90.
84.685	4.040	0.925	0 -0.105	0.671	-0.	0.011	0.	1.000	90.
67.331	3.990	0.944	0 -0.119	0.682	-0.	0.011	0.	1.000	90.
49.202	3.940	0.902	0 -0.130	0.705	-0.	0.011	-0.	1.000	90.
15.850	3.840	1.019	0 -0.256	0.694	-0.	0.012	180.	1.000	90.
336.021	4.540	89.999	0 -0.012	0.000	0.	1.000	-0.	0.002	-90.
110.371	4.490	89.997	0 -0.081	0.000	0.	1.000	-0.	0.002	-90.
68.064	4.440	89.990	0 -0.140	0.000	0.	1.000	-0.	0.011	-90.
44.195	4.390	89.980	0 -0.179	0.000	-0.	1.000	0.	0.015	-90.
27.580	4.340	89.930	0 -0.166	0.000	0.	1.000	-0.	0.021	-90.
12.586	4.240	89.222	0 -0.016	0.014	0.	1.000	-0.	0.013	-90.
27.356	4.540	0.977	0 -0.001	0.593	-0.	0.001	180.	1.000	90.
22.635	4.490	0.968	0 -0.003	0.605	-0.	0.010	-180.	1.000	90.
19.823	4.440	1.974	0 -0.005	0.606	0.	0.021	180.	1.000	90.
17.576	4.390	3.212	0 -0.006	0.601	-0.	0.034	-180.	1.000	90.
15.468	4.340	5.192	0 -0.006	0.570	0.	0.052	180.	1.000	90.
10.846	4.240	4.608	0 -0.003	1.000	-0.	0.081	-0.	0.465	90.
18.105	4.540	89.677	0 -0.254	0.006	0.	1.000	-0.	0.021	-90.
14.929	4.490	89.540	0 -0.427	0.008	0.	1.000	-0.	0.020	-90.
11.855	4.440	88.708	0 -0.455	0.023	0.	1.000	-0.	0.013	-90.
10.716	4.390	12.852	0 -0.157	1.000	-0.	0.228	-0.	0.592	90.
10.456	4.340	3.012	0 -0.223	1.000	0.	0.053	-0.	0.724	90.
9.716	4.240	1.527	0 -0.141	1.000	0.	0.027	180.	0.943	90.

A3T110-10-59.9 FG 2G 3G 4G

PERIOD	PHVEL	XYANG		GPANG	UX	PHIX	UY	PHIY	UZ	PHIZ
157.677	4.140	0.755	0	-0.057	0.686	0.	0.009	103.	1.000	90.
106.776	4.090	1.291	0	-0.117	0.675	-0.	0.015	103.	1.000	90.
82.756	4.040	1.570	0	-0.174	0.677	-0.	0.019	104.	1.000	90.
64.970	3.990	1.671	0	-0.229	0.689	-0.	0.020	104.	1.000	90.
44.607	3.940	1.493	0	-0.270	0.713	0.	0.019	105.	1.000	90.
18.779	3.890	0.232	0	-0.068	0.707	-0.	0.003	105.	1.000	90.
16.115	3.840	0.082	0	-0.027	0.680	-0.	0.001	106.	1.000	90.
14.655	3.790	0.035	0	-0.013	0.655	0.	0.000	106.	1.000	90.
14.093	3.740	0.017	0	-0.007	0.631	-0.	0.000	107.	1.000	90.
13.583	3.690	0.009	0	-0.004	0.610	-0.	0.000	108.	1.000	90.
13.215	3.640	0.005	0	-0.002	0.590	-0.	0.000	108.	1.000	90.
12.928	3.590	0.003	0	-0.001	0.571	-0.	0.000	109.	1.000	90.
12.697	3.540	0.001	0	-0.001	0.555	-0.	0.000	109.	1.000	90.
12.503	3.490	0.001	0	-0.000	0.539	0.	0.000	109.	1.000	90.
0000000000000000000000000000000000000000000000000000000000000000000000000000000000000000000000000000										
359.533	4.540	89.869	0	-0.006	0.002	-0.	1.000	-88.	0.001	83.
120.851	4.490	89.664	0	-0.041	0.007	-0.	1.000	-87.	0.005	90.
75.915	4.440	89.394	0	-0.075	0.011	0.	1.000	-87.	0.012	90.
51.235	4.390	89.171	0	-0.102	0.014	0.	1.000	-88.	0.019	90.
32.959	4.340	88.793	0	-0.127	0.021	-0.	1.000	-91.	0.030	90.
12.627	4.240	88.037	0	-0.071	0.034	-0.	1.000	-103.	0.116	90.
0000000000000000000000000000000000000000000000000000000000000000000000000000000000000000000000000000										
27.659	4.540	11.736	0	-0.008	0.535	0.	0.122	75.	1.000	90.
22.489	4.490	19.714	0	-0.073	0.592	0.	0.212	68.	1.000	90.
19.551	4.440	27.162	0	-0.164	0.589	0.	0.302	65.	1.000	90.
17.233	4.390	36.504	0	-0.273	0.575	0.	0.426	65.	1.000	90.
15.004	4.340	51.182	0	-0.391	0.526	0.	0.656	65.	1.000	90.
10.243	4.240	15.586	0	-0.463	1.000	-0.	0.279	-113.	0.806	90.
0000000000000000000000000000000000000000000000000000000000000000000000000000000000000000000000000000										
20.305	4.540	89.459	0	0.037	0.009	0.	1.000	-81.	0.016	92.
17.670	4.490	89.480	0	0.046	0.009	-0.	1.000	-97.	0.016	91.
15.422	4.440	89.622	0	0.035	0.007	-0.	1.000	-104.	0.013	91.
13.097	4.390	89.871	0	0.021	0.002	-0.	1.000	-104.	0.006	91.
9.552	4.240	16.092	0	-0.405	0.996	0.	0.287	63.	1.000	90.
0000000000000000000000000000000000000000000000000000000000000000000000000000000000000000000000000000										
0000000000000000000000000000000000000000000000000000000000000000000000000000000000000000000000000000										

A3T010-10-59.9 FG 2G 3G 4G

PERIOD	PHVEL	XYANG		GPANG	UX	PHIX	UY	PHIY	UZ	PHIZ
160.402	4.140	0.157	0	-0.029	0.685	0.	0.002	0.	1.000	90.
109.229	4.090	0.269	0	-0.041	0.672	-0.	0.003	180.	1.000	90.
85.243	4.040	0.598	0	-0.073	0.674	-0.	0.007	180.	1.000	90.
67.861	3.990	0.833	0	-0.120	0.684	-0.	0.010	180.	1.000	90.
49.928	3.940	0.925	0	-0.177	0.706	-0.	0.011	-180.	1.000	90.
16.149	3.840	0.054	0	-0.022	0.681	-0.	0.001	180.	1.000	90.
0000000000000000000000000000000000000000000000000000000000000000000000000000000000000000000000000000										
331.504	4.540	89.999	0	-0.037	0.000	0.	1.000	-0.	0.004	-90.
109.180	4.490	89.936	0	-0.239	0.001	0.	1.000	-0.	0.006	-90.
67.492	4.440	89.830	0	-0.402	0.003	0.	1.000	-0.	0.003	-90.
43.664	4.390	89.732	0	-0.524	0.005	-0.	1.000	0.	0.002	90.
14.993	4.290	88.552	0	-0.550	0.025	-0.	1.000	-180.	0.047	90.
0000000000000000000000000000000000000000000000000000000000000000000000000000000000000000000000000000										
27.942	4.540	9.050	0	-0.061	0.586	-0.	0.093	0.	1.000	90.
22.711	4.490	14.361	0	-0.138	0.594	0.	0.152	0.	1.000	90.
19.902	4.440	18.639	0	-0.172	0.593	0.	0.200	0.	1.000	90.
17.668	4.390	24.197	0	-0.201	0.582	-0.	0.262	0.	1.000	90.
13.331	4.290	71.518	0	-0.393	0.334	-0.	1.000	-0.	0.383	90.
0000000000000000000000000000000000000000000000000000000000000000000000000000000000000000000000000000										
20.579	4.540	89.932	0	0.011	0.001	-0.	1.000	-0.	0.002	90.
17.819	4.490	89.908	0	0.011	0.002	-0.	1.000	-180.	0.003	90.
15.539	4.440	89.914	0	0.006	0.001	-0.	1.000	-180.	0.003	90.
13.178	4.390	89.993	0	0.004	0.000	-0.	1.000	-180.	0.000	90.
10.248	4.290	0.826	0	-0.087	1.000	-0.	0.015	-0.	0.814	90.
0000000000000000000000000000000000000000000000000000000000000000000000000000000000000000000000000000										
0000000000000000000000000000000000000000000000000000000000000000000000000000000000000000000000000000										

C1X110-10-59.9 FG 2G 3G 4G

PERIOD	PHVEL	XYANG		GPANG	UX	PHIX	UY	PHIY	UZ	PHIZ
158.325	4.140	0.312	0	-0.017	0.686	-0.	0.004	94.	1.000	90.
106.977	4.090	0.598	0	-0.035	0.677	-0.	0.007	101.	1.000	90.
82.353	4.040	0.790	0	-0.057	0.680	-0.	0.009	103.	1.000	90.
63.823	3.990	0.919	0	-0.085	0.694	0.	0.011	105.	1.000	90.
32.595	3.940	0.840	0	-0.127	0.726	-0.	0.011	107.	1.000	90.
18.359	3.890	0.214	0	-0.050	0.704	-0.	0.003	108.	1.000	90.
16.022	3.840	0.095	0	-0.025	0.678	0.	0.001	109.	1.000	90.
14.624	3.790	0.048	0	-0.014	0.654	0.	0.001	110.	1.000	90.
14.006	3.740	0.026	0	-0.009	0.631	0.	0.000	111.	1.000	90.
13.582	3.690	0.015	0	-0.005	0.609	0.	0.000	111.	1.000	90.
13.213	3.640	0.009	0	-0.004	0.590	0.	0.000	112.	1.000	90.
12.927	3.590	0.005	0	-0.002	0.571	0.	0.000	112.	1.000	90.
12.696	3.540	0.003	0	-0.002	0.554	-0.	0.000	112.	1.000	90.
12.513	3.490	0.002	0	-0.001	0.539	-0.	0.000	113.	1.000	90.
0000000000000000000000000000000000000000000000000000000000000000000000000000000000000000000000000000										
349.060	4.540	89.926	0	-0.002	0.001	0.	1.000	-89.	0.000	141.
115.861	4.490	89.774	0	-0.016	0.004	-0.	1.000	-87.	0.003	106.
72.585	4.440	89.648	0	-0.029	0.006	-0.	1.000	-86.	0.006	98.
48.207	4.390	89.499	0	-0.039	0.009	-0.	1.000	-87.	0.011	94.
30.170	4.340	89.219	0	-0.046	0.014	0.	1.000	-90.	0.019	91.
11.948	4.240	89.325	0	-0.020	0.003	-0.	1.000	76.	0.038	-90.
0000000000000000000000000000000000000000000000000000000000000000000000000000000000000000000000000000										
27.298	4.540	4.423	0	-0.005	0.529	0.	0.046	76.	1.000	90.
22.159	4.490	7.255	0	-0.022	0.593	0.	0.075	67.	1.000	90.
19.362	4.440	9.956	0	-0.043	0.589	0.	0.103	62.	1.000	90.
17.085	4.390	13.779	0	-0.069	0.573	-0.	0.140	59.	1.000	90.
14.897	4.340	21.522	0	-0.095	0.523	0.	0.206	58.	1.000	90.
10.314	4.240	5.492	0	-0.112	1.000	-0.	0.096	-125.	0.777	90.
0000000000000000000000000000000000000000000000000000000000000000000000000000000000000000000000000000										
20.352	4.540	89.699	0	0.009	0.005	-0.	1.000	-69.	0.008	91.
17.449	4.490	89.760	0	0.014	0.004	0.	1.000	-77.	0.007	91.
15.395	4.440	89.840	0	0.010	0.003	-0.	1.000	-79.	0.005	91.
13.041	4.390	89.938	0	0.004	0.001	0.	1.000	-74.	0.003	91.
10.398	4.340	88.099	0	-0.002	0.033	-0.	1.000	-71.	0.025	90.
9.655	4.240	2.215	0	-0.061	1.000	-0.	0.039	44.	0.980	90.
0000000000000000000000000000000000000000000000000000000000000000000000000000000000000000000000000000										
0000000000000000000000000000000000000000000000000000000000000000000000000000000000000000000000000000										

C1X010-10-59.9 FG 2G 3G 4G

PERIOD	PHVEL	XYANG		GPANG	UX	PHIX	UY	PHIY	UZ	PHIZ
159.098	4.140	0.100	0	-0.013	0.685	0.	0.001	[illegible]	1.000	90.
107.828	4.090	0.132	0	-0.025	0.675	-0.	0.002	180.	1.000	90.
83.351	4.040	0.340	0	-0.043	0.678	-0.	0.004	180.	1.000	90.
65.013	3.990	0.506	0	-0.075	0.691	0.	0.006	180.	1.000	90.
41.903	3.940	0.598	0	-0.129	0.719	-0.	0.007	180.	1.000	90.
16.855	3.840	0.067	0	-0.030	0.679	-0.	0.001	180.	1.000	90.
0000000000000000000000000000000000000000000000000000000000000000000000000000000000000000000000000000										
336.167	4.540	89.999	0	-0.012	0.000	0.	1.000	-0.	0.182	-90.
110.776	4.490	89.969	0	-0.078	0.001	0.	1.000	-0.	0.004	-90.
62.604	4.440	89.914	0	-0.133	0.001	0.	1.000	-0.	0.003	-90.
44.653	4.390	89.868	0	-0.175	0.002	-0.	1.000	0.	0.003	-90.
16.312	4.290	89.725	0	-0.158	0.005	-0.	1.000	-180.	0.009	90.
0000000000000000000000000000000000000000000000000000000000000000000000000000000000000000000000000000										
27.428	4.540	2.430	0	-0.026	0.529	0.	0.025	0.	1.000	90.
22.284	4.490	4.429	0	-0.064	0.593	0.	0.047	0.	1.000	90.
19.498	4.440	6.642	0	-0.083	0.590	-0.	0.069	0.	1.000	90.
17.246	4.390	9.471	0	-0.097	0.576	-0.	0.096	-0.	1.000	90.
12.824	4.290	38.701	0	-0.115	0.327	0.	0.262	-0.	1.000	90.
0000000000000000000000000000000000000000000000000000000000000000000000000000000000000000000000000000										
20.346	4.540	89.774	0	-0.005	0.004	0.	1.000	-0.	0.006	90.
17.657	4.490	89.835	0	-0.002	0.003	0.	1.000	-0.	0.005	90.
15.392	4.440	89.878	0	-0.005	0.002	-0.	1.000	-0.	0.004	90.
13.011	4.390	89.942	0	-0.013	0.001	0.	1.000	-0.	0.003	90.
10.231	4.290	0.978	0	-0.029	1.000	0.	0.017	180.	0.820	90.
0000000000000000000000000000000000000000000000000000000000000000000000000000000000000000000000000000										
0000000000000000000000000000000000000000000000000000000000000000000000000000000000000000000000000000										

S1X110-60--0.1 FG 2G 3G 4G

PERIOD	PHVEL	XYANG		GPANG	UX	PHIX	UY	PHIY	UZ	PHIZ
150.059	4.140	0.007	0	0.001	0.690	-0.	0.000	-129.	1.000	91.
101.356	4.090	0.009	0	0.001	0.701	0.	0.000	-108.	1.000	91.
72.945	4.040	0.013	0	0.002	0.734	-0.	0.000	-93.	1.000	91.
14.875	3.940	0.038	0	0.006	0.747	-0.	0.000	-66.	1.000	92.
0000000000000000000000000000000000000000000000000000000000000000000000000000000000000000										
284.160	4.540	89.995	0	-0.000	0.000	-0.	1.000	90.	0.000	166.
89.472	4.490	89.993	0	-0.001	0.000	0.	1.000	91.	0.000	136.
51.695	4.440	89.988	0	-0.002	0.000	-0.	1.000	91.	0.000	117.
31.237	4.390	89.976	0	-0.002	0.000	-0.	1.000	88.	0.000	104.
20.403	4.340	89.956	0	-0.002	0.001	-0.	1.000	86.	0.001	98.
15.055	4.290	89.961	0	-0.001	0.001	0.	1.000	87.	0.001	98.
11.436	4.240	89.924	0	-0.000	0.001	0.	1.000	-102.	0.000	-92.
9.204	4.140	.134	0	0.010	1.000	-0.	0.002	-69.	0.090	91.
8.951	4.090	0.179	0	0.010	1.000	-0.	0.003	-68.	0.071	91.
0000000000000000000000000000000000000000000000000000000000000000000000000000000000000000										
26.196	4.540	0.034	0	0.000	0.746	0.	0.000	-76.	1.000	92.
21.655	4.490	0.053	0	0.000	0.796	0.	0.001	-79.	1.000	91.
18.254	4.440	0.081	0	0.000	0.739	0.	0.001	-83.	1.000	91.
15.944	4.390	0.059	0	0.001	0.708	0.	0.001	-90.	1.000	91.
13.731	4.340	0.093	0	0.001	0.254	0.	0.000	151.	1.000	92.
11.514	4.290	0.133	0	0.001	1.000	0.	0.002	-72.	0.074	-89.
9.665	4.240	0.129	0	0.009	1.000	-0.	0.002	-71.	0.116	91.
8.290	4.140	89.996	0	-0.009	0.002	0.	1.000	111.	0.000	92.
8.797	4.090	89.942	0	-0.012	0.003	0.	1.000	112.	0.000	92.
0000000000000000000000000000000000000000000000000000000000000000000000000000000000000000										
17.649	4.540	89.931	0	-0.003	0.000	-0.	1.000	108.	0.000	101.
14.329	4.490	89.937	0	-0.004	0.000	0.	1.000	113.	0.000	105.
12.256	4.440	89.907	0	-0.003	0.000	-0.	1.000	-92.	0.000	-102.
10.721	4.390	1.534	0	-0.371	1.000	-0.	0.027	103.	0.038	91.
10.407	4.340	0.355	0	0.022	1.000	0.	0.006	-75.	0.105	91.
10.163	4.290	0.173	0	0.012	1.000	0.	0.003	-73.	0.115	91.
7.120	4.240	0.033	0	0.007	1.000	-0.	0.001	-68.	0.273	-90.
7.114	4.190	0.054	0	0.000	1.000	-0.	0.001	-78.	0.241	-90.
6.477	4.140	0.037	0	0.006	1.000	0.	0.001	-66.	0.474	-90.
6.164	4.090	0.035	0	0.005	1.000	-0.	0.001	-64.	0.632	-90.
0000000000000000000000000000000000000000000000000000000000000000000000000000000000000000										
0000000000000000000000000000000000000000000000000000000000000000000000000000000000000000										

S1X010-60--0.1 FG 2G 3G 4G

PERIOD	PHVEL	XYANG		GPANG	UX	PHIX	UY	PHIY	UZ	PHIZ
134.707	4.140	0.020	0	0.002	0.657	-0.	0.000	-180.	1.000	90.
97.059	4.090	0.016	0	0.002	0.669	0.	0.000	180.	1.000	90.
73.007	4.040	0.011	0	0.003	0.698	-0.	0.000	-180.	1.000	90.
15.748	3.940	0.023	0	0.006	0.812	-0.	0.000	-0.	1.000	90.
0000000000000000000000000000000000000000000000000000000000000000000000000000000000000000										
247.439	4.540	90.000	0	-0.001	0.000	0.	1.000	180.	0.000	-90.
74.841	4.490	89.999	0	-0.004	0.000	0.	1.000	180.	0.000	-90.
41.404	4.440	89.999	0	-0.006	0.000	-0.	1.000	-180.	0.000	-90.
25.947	4.390	89.999	0	-0.005	0.000	0.	1.000	-0.	0.000	90.
18.739	4.340	89.999	0	-0.003	0.000	-0.	1.000	0.	0.000	90.
14.487	4.290	89.991	0	-0.002	0.000	-0.	1.000	-180.	0.000	-90.
11.214	4.240	89.997	0	-0.001	0.000	-0.	1.000	0.	0.000	90.
9.487	4.140	0.045	0	0.000	1.000	0.	0.001	0.	0.106	90.
9.174	4.090	0.053	0	0.007	1.000	0.	0.001	-0.	0.088	90.
8.921	4.040	0.070	0	0.007	1.000	-0.	0.001	-0.	0.069	90.
14.835	3.890	0.026	0	0.006	0.726	0.	0.000	-0.	1.000	90.
0000000000000000000000000000000000000000000000000000000000000000000000000000000000000000										
25.752	4.540	0.032	0	0.000	0.764	0.	0.000	-0.	1.000	90.
20.746	4.490	0.075	0	0.001	0.795	0.	0.001	0.	1.000	90.
18.067	4.440	0.109	0	0.001	0.791	0.	0.002	-0.	1.000	90.
15.910	4.390	0.159	0	0.001	0.721	0.	0.002	-0.	1.000	90.
13.868	4.340	0.462	0	0.001	0.359	0.	0.003	-0.	1.000	90.
11.771	4.290	0.085	0	0.001	1.000	-0.	0.001	180.	0.187	-90.
10.236	4.240	0.033	0	0.004	1.000	-0.	0.001	-0.	0.114	90.
8.854	4.140	89.962	0	-0.011	0.001	0.	1.000	180.	0.000	90.
8.759	4.090	89.953	0	-0.011	0.001	0.	1.000	180.	0.000	90.
8.684	4.040	89.935	0	-0.011	0.001	0.	1.000	180.	0.000	90.
8.485	3.890	0.178	0	0.002	1.000	0.	0.003	-180.	0.023	90.
0000000000000000000000000000000000000000000000000000000000000000000000000000000000000000										
14.953	4.540	89.989	0	-0.009	0.000	0.	1.000	180.	0.000	-90.
12.561	4.490	89.990	0	-0.012	0.000	-0.	1.000	-180.	0.000	-90.
10.922	4.390	0.078	0	0.006	1.000	0.	0.001	-0.	0.066	90.
10.686	4.340	0.055	0	0.006	1.000	-0.	0.001	-0.	0.091	90.
10.395	4.290	0.051	0	0.005	1.000	0.	0.001	0.	0.109	90.
9.497	4.240	0.254	0	0.001	1.000	-0.	0.004	0.	0.105	90.
7.186	4.190	0.020	0	0.000	1.000	0.	0.000	144.	0.225	-90.
0000000000000000000000000000000000000000000000000000000000000000000000000000000000000000										
0000000000000000000000000000000000000000000000000000000000000000000000000000000000000000										

S1X110-60-29.9 FG 2G 3G 4G

PERIOD	PHVEL	XYANG		GPANG	UX	PHIX	UY	PHIY	UZ	PHIZ
150.519	4.140	1.296	0	-0.142	0.692	-0.	0.016	53.	1.000	91.
104.671	4.090	2.[illegible]	0	-0.225	0.699	0.	0.025	75.	1.000	91.
77.103	4.040	2.911	0	-0.354	0.726	-0.	0.036	88.	1.000	91.
15.309	3.990	5.[illegible]17	0	-1.305	0.790	-0.	0.120	113.	1.000	91.
000000000000000000000000000000000000000000000000000000000000000000000000000000										
272.[illegible]	4.540	89.477	0	0.019	0.009	0.	1.000	-90.	0.006	163.
84.794	4.490	89.[illegible]39	0	0.127	0.030	0.	1.000	-89.	0.021	130.
47.939	4.440	89.[illegible]52	0	0.218	0.055	0.	1.000	-90.	0.044	112.
30.761	4.390	89.[illegible]39	0	0.257	0.106	0.	1.000	-94.	0.099	101.
19.555	4.340	89.[illegible]12	0	0.186	0.185	-0.	1.000	-93.	0.190	97.
14.143	4.290	89.[illegible]28	0	0.075	0.156	-0.	1.000	-98.	0.215	98.
11.[illegible]	4.240	89.[illegible]11	0	0.013	0.388	0.	1.000	77.	0.019	-92.
9.417	4.140	1[illegible].155	0	-1.345	1.000	-0.	0.347	110.	0.102	90.
9.11[illegible]	4.090	21.[illegible]30	0	-1.311	1.000	0.	0.386	111.	0.064	90.
000000000000000000000000000000000000000000000000000000000000000000000000000000										
26.223	4.540	.993	0	-0.025	0.754	0.	0.119	100.	1.000	91.
21.172	4.490	13.336	0	-0.071	0.732	-0.	0.185	95.	1.000	91.
18.265	4.440	15.416	0	-0.101	0.777	0.	0.214	90.	1.000	91.
16.[illegible]66	4.390	16.[illegible]05	0	-0.125	0.704	0.	0.210	81.	1.000	91.
13.[illegible]80	4.340	25.[illegible]95	0	-0.142	0.310	-0.	0.148	30.	1.000	92.
11.[illegible]58	4.290	24.[illegible]82	0	-0.147	1.000	-0.	0.418	116.	0.126	-90.
10.139	4.240	24.[illegible]67	0	-1.094	1.000	-0.	0.365	109.	0.116	90.
8.644	4.140	74.378	0	0.695	0.280	0.	1.000	-69.	0.016	92.
8.744	4.090	71.461	0	0.659	0.335	0.	1.000	-69.	0.017	92.
000000000000000000000000000000000000000000000000000000000000000000000000000000										
16.126	4.540	89.[illegible]41	0	0.403	0.073	0.	1.000	-74.	0.065	100.
13.503	4.490	8[illegible].360	0	0.523	0.034	0.	1.000	-63.	0.056	110.
11.[illegible]	4.440	82.778	0	0.351	0.127	0.	1.000	95.	0.032	-94.
11.109	4.390	5[illegible].529	0	-0.515	0.661	0.	1.000	101.	0.024	90.
10.744	4.340	3[illegible].999	0	-1.167	1.000	0.	0.700	104.	0.084	90.
10.416	4.290	25.179	0	-1.154	1.000	0.	0.470	106.	0.107	90.
9.38[illegible]	4.240	3[illegible].53[illegible]	0	-0.084	1.000	0.	0.590	104.	0.105	90.
7.150	4.190	[illegible].835	0	-0.045	1.000	-0.	0.173	109.	0.232	-90.
6.643	4.140	7.925	0	-1.196	1.000	0.	0.159	113.	0.405	-90.
6.323	4.090	7.[illegible]39	0	-1.136	1.000	-0.	0.137	114.	0.546	-90.
000[illegible]										
000[illegible]										

S1X010-60-29.9 FG 2G 3G 4G

PERIOD	PHVEL	XYANG		GPANG	UX	PHIX	UY	PHIY	UZ	PHIZ
146.430	4.140	3.739	0	-0.395	0.671	-0.	0.044	0.	1.000	90.
102.952	4.090	3.039	0	-0.443	0.678	-0.	0.037	0.	1.000	90.
78.342	4.040	2.117	0	-0.526	0.700	-0.	0.026	0.	1.000	90.
52.692	3.990	0.631	0	-0.728	0.753	-0.	0.008	0.	1.000	90.
15.273	3.890	5.052	0	-1.324	0.769	-0.	0.068	0.	1.000	90.
000000000000000000000000000000000000000000000000000000000000000000000000000000										
196.804	4.540	89.933	0	0.115	0.001	0.	1.000	-0.	0.036	-90.
57.761	4.490	89.[illegible]54	0	0.509	0.006	0.	1.000	-0.	0.067	-90.
32.970	4.440	89.[illegible]84	0	0.681	0.002	-0.	1.000	-180.	0.079	90.
23.027	4.390	88.780	0	0.504	0.021	0.	1.000	-180.	0.098	90.
17.767	4.340	88.221	0	0.306	0.031	-0.	1.000	-180.	0.108	90.
14.098	4.290	88.897	0	0.174	0.012	0.	1.000	-0.	0.073	-90.
11.027	4.240	82.469	0	0.100	0.132	-0.	1.000	0.	0.003	90.
9.984	4.140	4.777	0	-0.984	1.000	-0.	0.034	-180.	0.116	90.
9.630	4.090	5.162	0	-0.968	1.000	-0.	0.090	180.	0.111	90.
9.292	4.040	5.776	0	-0.944	1.000	-0.	0.131	180.	0.096	90.
9.007	3.990	6.825	0	-0.914	1.000	-0.	0.120	180.	0.076	90.
8.630	3.890	12.900	0	-0.813	1.000	-0.	0.229	180.	0.041	90.
000000000000000000000000000000000000000000000000000000000000000000000000000000										
26.182	4.540	5.036	0	-0.091	0.745	-0.	0.073	180.	1.000	90.
21.119	4.490	12.318	0	-0.234	0.771	-0.	0.168	180.	1.000	90.
18.396	4.440	17.177	0	-0.286	0.766	0.	0.237	-180.	1.000	90.
16.194	4.390	23.600	0	-0.283	0.704	-0.	0.306	180.	1.000	90.
14.101	4.340	47.565	0	-0.244	0.396	0.	0.433	-180.	1.000	90.
11.949	4.290	15.150	0	-0.194	1.000	-0.	0.271	-0.	0.287	-90.
10.406	4.240	5.099	0	-0.748	1.000	0.	0.089	180.	0.107	90.
8.760	4.140	86.044	0	-0.996	0.069	-0.	1.000	0.	0.003	90.
8.692	4.090	85.512	0	-0.950	0.078	0.	1.000	-0.	0.003	90.
8.631	4.040	84.762	0	-0.913	0.092	-0.	1.000	0.	0.003	90.
8.579	3.990	83.609	0	-0.890	0.112	-0.	1.000	0.	0.003	90.
8.495	3.890	77.409	0	-0.947	0.223	-0.	1.000	0.	0.005	90.
000000000000000000000000000000000000000000000000000000000000000000000000000000										
12.706	4.540	86.386	0	1.030	0.063	-0.	1.000	0.	0.024	-90.
11.424	4.490	7.516	0	-0.843	1.000	0.	0.132	0.	0.030	-90.
11.225	4.440	5.545	0	-1.079	1.000	0.	0.097	-180.	0.616	90.
11.031	4.390	6.202	0	-1.140	1.000	0.	0.110	-180.	0.049	90.
10.815	4.340	6.426	0	-1.135	1.000	0.	0.113	-180.	0.077	90.
10.546	4.290	6.849	0	-0.927	1.000	-0.	0.120	-180.	0.100	90.
9.530	4.240	24.196	0	-0.132	1.000	0.	0.449	-180.	0.113	90.
7.253	4.190	2.911	0	-0.070	1.000	0.	0.051	-180.	0.208	-90.
7.105	4.140	3.186	0	-0.951	1.000	-0.	0.056	180.	0.250	-90.
6.851	4.090	3.401	0	-0.932	1.000	0.	0.059	-180.	0.329	-90.
6.537	4.040	3.599	0	-0.903	1.000	0.	0.063	-180.	0.448	-90.
6.190	3.990	3.766	0	-0.879	1.000	0.	0.066	-180.	0.617	-90.
5.542	3.890	4.012	0	-0.808	0.873	0.	0.061	180.	1.000	-90.
000000000000000000000000000000000000000000000000000000000000000000000000000000										
000000000000000000000000000000000000000000000000000000000000000000000000000000										

S1X110-60-59.9 FG 2G 3G 4G

PERIOD	PHVEL	XYANG		GPANG	UX	PHIX	UY	PHIY	UZ	PHIZ
165.640	4.140	0.710	0	-0.093	0.693	-0.	0.009	63.	1.000	90.
109.879	4.090	1.029	0	-0.161	0.696	-0.	0.020	86.	1.000	90.
82.547	4.040	3.527	0	-0.253	0.714	0.	0.032	95.	1.000	90.
59.546	3.990	3.745	0	-0.440	0.755	-0.	0.049	100.	1.000	90.
15.233	3.890	0.532	0	-1.100	0.772	-0.	0.129	108.	1.000	90.
0000000000000000000000000000000000000000000000000000000000000000000000000000000000000000000000000000										
272.851	4.540	69.426	0	-0.019	0.010	-0.	1.000	-90.	0.004	149.
84.672	4.490	84.154	0	-0.122	0.032	0.	1.000	-90.	0.019	113.
47.787	4.440	89.791	0	-0.202	0.058	-0.	1.000	-91.	0.044	102.
28.575	4.390	89.836	0	-0.224	0.105	-0.	1.000	-94.	0.095	97.
19.487	4.340	70.003	0	-0.151	0.173	0.	1.000	-99.	0.182	94.
14.813	4.290	81.701	0	-0.061	0.164	0.	1.000	-101.	0.232	95.
11.419	4.240	64.816	0	-0.023	0.572	-0.	1.000	77.	0.030	-91.
9.731	4.140	14.131	0	-0.930	1.000	0.	0.239	106.	0.113	90.
9.377	4.090	10.520	0	-0.917	1.000	-0.	0.297	106.	0.100	90.
9.17	4.040	14.763	0	-0.884	1.000	-0.	0.332	107.	0.081	90.
0000000000000000000000000000000000000000000000000000000000000000000000000000000000000000000000000000										
26.5	4.540	14.078	0	-0.810	0.736	0.	0.193	93.	1.000	91.
21.350	4.490	21.240	0	-0.851	0.764	0.	0.297	88.	1.000	91.
18.569	4.440	25.155	0	-0.885	0.761	0.	0.357	84.	1.000	90.
16.3	4.390	29.726	0	-0.122	0.701	0.	0.400	78.	1.000	90.
14.159	4.340	47.813	0	-0.155	0.397	0.	0.426	64.	1.000	91.
11.956	4.290	10.523	0	-0.171	1.000	-0.	0.297	152.	0.284	-90.
10.447	4.240	14.293	0	-0.096	1.000	0.	0.305	109.	0.104	90.
8.83	4.140	77.520	0	-0.276	0.221	0.	1.000	-74.	0.012	91.
8.735	4.090	76.944	0	-0.283	0.249	0.	1.000	-73.	0.012	91.
8.65	4.040	75.971	0	-0.316	0.296	0.	1.000	-73.	0.012	91.
0000000000000000000000000000000000000000000000000000000000000000000000000000000000000000000000000000										
15.918	4.540	85.729	0	-0.269	0.075	-0.	1.000	-79.	0.066	95.
13.325	4.490	86.211	0	-0.327	0.029	0.	1.000	-71.	0.059	102.
11.832	4.440	74.248	0	-0.247	0.190	0.	1.000	97.	0.041	-92.
11.241	4.690	49.377	0	-0.351	0.856	-0.	1.000	100.	0.007	90.
10.545	4.740	31.907	0	-0.585	1.000	0.	0.601	102.	0.060	90.
10.445	4.790	22.934	0	-0.541	1.000	-0.	0.420	103.	0.092	90.
9.545	4.240	31.763	0	-0.098	1.000	-0.	0.610	87.	0.114	90.
7.257	4.190	7.053	0	-0.057	1.000	0.	0.141	109.	0.206	-90.
6.159	4.140	7.061	0	-0.474	1.000	0.	0.140	107.	0.313	-90.
6.30	4.090	7.121	0	-0.942	1.000	0.	0.141	108.	0.423	-90.
6.259	4.040	7.081	0	-0.904	1.000	0.	0.141	108.	0.579	-90.
0000000000000000000000000000000000000000000000000000000000000000000000000000000000000000000000000000										
0000000000000000000000000000000000000000000000000000000000000000000000000000000000000000000000000000										

S1X010-60-59.9 FG 2G 3G 4G

PERIOD	PHVEL	XYANG		GPANG	UX	PHIX	UY	PHIY	UZ	PHIZ
166.566	4.140	1.779	0	-0.207	0.690	-0.	0.021	0.	1.000	90.
111.803	4.090	1.384	0	-0.251	0.689	0.	0.017	0.	1.000	90.
85.703	4.040	0.735	0	-0.320	0.703	-0.	0.010	0.	1.000	90.
65.542	3.990	0.072	0	-0.442	0.731	-0.	0.001	0.	1.000	90.
16.390	3.890	3.395	0	-1.085	0.834	-0.	0.057	-180.	1.000	90.
0000000000000000000000000000000000000000000000000000000000000000000000000000000000000000000000000000										
195.699	4.540	39.057	0	-0.114	0.001	0.	1.000	-0.	0.021	-90.
56.367	4.490	89.793	0	-0.572	0.004	0.	1.000	-0.	0.042	-90.
32.116	4.440	89.730	0	-0.613	0.005	-0.	1.000	-180.	0.055	90.
22.625	4.390	88.487	0	-0.420	0.026	-0.	1.000	-180.	0.080	90.
17.563	4.340	87.009	0	-0.234	0.051	-0.	1.000	-180.	0.115	90.
13.997	4.290	89.494	0	-0.122	0.009	0.	1.000	180.	0.118	90.
10.976	4.240	40.672	0	-0.067	1.000	-0.	0.859	0.	0.047	90.
9.084	4.140	4.777	0	-0.934	1.000	-0.	0.084	-180.	0.116	90.
9.630	4.090	5.162	0	-0.968	1.000	-0.	0.090	180.	0.111	90.
9.292	4.040	5.775	0	-0.944	1.000	-0.	0.101	180.	0.096	90.
9.087	3.990	6.025	0	-0.914	1.000	-0.	0.120	180.	0.076	90.
8.630	3.890	12.903	0	-0.813	1.000	-0.	0.229	180.	0.041	90.
0000000000000000000000000000000000000000000000000000000000000000000000000000000000000000000000000000										
26.914	4.540	3.524	0	-0.068	0.715	0.	0.044	180.	1.000	90.
21.741	4.490	7.087	0	-0.181	0.744	0.	0.092	180.	1.000	90.
18.953	4.440	9.435	0	-0.237	0.745	0.	0.124	180.	1.000	90.
16.703	4.390	12.074	0	-0.261	0.701	-0.	0.150	180.	1.000	90.
14.564	4.340	21.181	0	-0.257	0.484	0.	0.188	180.	1.000	90.
12.350	4.290	9.943	0	-0.231	1.000	0.	0.175	-0.	0.664	-90.
10.687	4.240	4.509	0	-0.563	1.000	-0.	0.079	-180.	0.085	90.
8.766	4.140	86.044	0	-0.996	0.069	-0.	1.000	0.	0.003	90.
8.692	4.090	85.512	0	-0.950	0.078	0.	1.000	-0.	0.003	90.
8.631	4.040	84.702	0	-0.913	0.092	-0.	1.000	0.	0.003	90.
8.579	3.990	83.609	0	-0.890	0.112	-0.	1.000	0.	0.003	90.
8.495	3.890	77.409	0	-0.947	0.223	-0.	1.000	0.	0.005	90.
0000000000000000000000000000000000000000000000000000000000000000000000000000000000000000000000000000										
12.427	4.540	84.535	0	-0.715	0.096	-0.	1.000	-0.	0.044	-90.
11.584	4.490	3.172	0	-0.741	1.000	0.	0.055	-0.	0.079	-90.
11.361	4.440	4.212	0	-0.939	1.000	0.	0.074	-180.	0.022	-90.
11.198	4.390	4.861	0	-0.964	1.000	0.	0.085	-180.	0.018	90.
11.001	4.340	4.941	0	-0.917	1.000	0.	0.086	-180.	0.051	90.
10.756	4.290	5.159	0	-0.890	1.000	0.	0.090	-180.	0.081	90.
9.779	4.240	12.242	0	-0.144	1.000	-0.	0.217	-180.	0.120	90.
7.402	4.190	2.194	0	-0.082	1.000	0.	0.038	180.	0.170	-90.
7.105	4.140	3.136	0	-0.951	1.000	-0.	0.056	180.	0.250	-90.
6.851	4.090	3.401	0	-0.932	1.000	0.	0.059	-180.	0.329	-90.
6.537	4.040	3.529	0	-0.908	1.000	0.	0.063	-180.	0.448	-90.
6.190	3.990	3.760	0	-0.879	1.000	0.	0.066	-180.	0.617	-90.
5.542	3.890	4.812	0	-0.808	0.873	0.	0.061	180.	1.000	-90.
0000000000000000000000000000000000000000000000000000000000000000000000000000000000000000000000000000										
0000000000000000000000000000000000000000000000000000000000000000000000000000000000000000000000000000										

S1X110-60-89.9 FG 2G 3G 4G

PERIOD	PHVEL	XYANG		GPANG	UX	PHIX	UY	PHIY	UZ	PHIZ
169.087	4.140	0.159	0	-0.000	0.693	-0.	0.002	90.	1.000	90.
112.07[illegible]	4.09[illegible]	0.[illegible]	0	-0.001	0.694	-0.	0.012	90.	1.000	90.
85.14[illegible]	4.04[illegible]	1.[illegible]	0	-0.001	0.709	-0.	0.022	90.	1.000	90.
68.72[illegible]	3.99[illegible]	2.[illegible]	0	-0.001	0.742	0.	0.035	90.	1.000	90.
15.00[illegible]	3.89[illegible]	7.[illegible]	0	-0.004	0.864	-0.	0.112	90.	1.000	90.
0000[illegible]										
234.12[illegible]	4.540	89.552	0	-0.000	0.008	0.	1.000	-90.	0.001	90.
89.28[illegible]	4.490	89.773	0	-0.001	0.025	0.	1.000	-90.	0.013	90.
51.35[illegible]	4.440	89.531	0	-0.002	0.043	-0.	1.000	-90.	0.031	90.
36.75[illegible]	4.39[illegible]	89.[illegible]	0	-0.002	0.075	0.	1.000	-90.	0.066	90.
20.16[illegible]	4.34[illegible]	89.[illegible]	0	-0.001	0.129	0.	1.000	-90.	0.129	90.
14.99[illegible]	4.29[illegible]	89.[illegible]	0	-0.001	0.131	0.	1.000	-90.	0.177	90.
11.46[illegible]	4.24[illegible]	89.[illegible]	0	-0.000	0.488	-0.	1.000	90.	0.033	-90.
9.56[illegible]	4.19[illegible]	13.13[illegible]	0	-0.003	1.000	-0.	0.233	90.	0.115	90.
9.50[illegible]	4.09[illegible]	13.17[illegible]	0	-0.003	1.000	-0.	0.234	90.	0.106	90.
9.17[illegible]	4.04[illegible]	14.29[illegible]	0	-0.003	1.000	-0.	0.255	90.	0.088	90.
8.01[illegible]	3.99[illegible]	18.96[illegible]	0	-0.003	1.000	0.	0.305	90.	0.068	90.
6.50[illegible]	3.89[illegible]	35.44[illegible]	0	-0.002	1.000	0.	0.712	90.	0.037	90.
0000[illegible]										
20.16[illegible]	4.540	17.074	0	-0.000	0.730	0.	0.224	90.	1.000	90.
21.427	4.490	24.719	0	-0.000	0.757	0.	0.349	90.	1.000	90.
18.65[illegible]	4.440	29.414	0	-0.000	0.755	0.	0.426	90.	1.000	90.
16.42[illegible]	4.390	34.962	0	-0.000	0.701	-0.	0.490	90.	1.000	90.
14.29[illegible]	4.340	52.316	0	-0.001	0.434	-0.	0.555	90.	1.000	90.
12.18[illegible]	4.29[illegible]	3.612	0	-0.001	1.000	-0.	0.151	-91.	0.415	-90.
10.56[illegible]	4.240	12.389	0	-0.002	1.000	0.	0.220	90.	0.095	90.
8.651	4.140	89.178	0	-0.003	0.173	0.	1.000	-90.	0.010	90.
8.751	4.090	79.144	0	-0.003	0.192	-0.	1.000	-90.	0.009	90.
8.672	4.040	77.373	0	-0.003	0.224	0.	1.000	-90.	0.009	90.
8.617	3.990	74.262	0	-0.003	0.282	0.	1.000	-90.	0.010	90.
8.49[illegible]	3.89[illegible]	55.091	0	-0.004	0.693	0.	1.000	-90.	0.017	90.
000[illegible]										
16.54[illegible]	4.540	89.411	0	-0.002	0.063	0.	1.000	-90.	0.051	90.
13.91[illegible]	4.490	87.746	0	-0.003	0.039	0.	1.000	-90.	0.049	90.
12.60[illegible]	4.44[illegible]	84.74[illegible]	0	-0.003	0.092	0.	1.000	90.	0.039	-90.
11.29[illegible]	4.39[illegible]	51.637	0	-0.001	0.797	0.	1.000	90.	0.004	-90.
11.[illegible]	4.34[illegible]	21.695	0	-0.002	1.000	0.	0.547	90.	0.051	90.
10.71[illegible]	4.29[illegible]	2.[illegible]	0	-0.002	1.000	0.	0.369	90.	0.085	90.
9.63[illegible]	4.24[illegible]	34.729	0	-0.000	1.000	-0.	0.683	90.	0.117	90.
7.31[illegible]	4.19[illegible]	0.[illegible]	0	-0.000	1.000	0.	0.106	90.	0.191	-90.
7.66[illegible]	4.14[illegible]	0.[illegible]	0	-0.004	1.000	0.	0.115	90.	0.280	-90.
6.71[illegible]	4.09[illegible]	0.[illegible]	0	-0.004	1.000	-0.	0.117	90.	0.376	-90.
6.34[illegible]	4.04[illegible]	0.[illegible]	0	-0.003	1.000	0.	0.118	90.	0.517	-90.
6.03[illegible]	3.99[illegible]	0.[illegible]	0	-0.003	1.000	0.	0.118	90.	0.711	-90.
5.423	3.89[illegible]	0.[illegible]	0	-0.003	0.766	0.	0.090	90.	1.000	-90.
000[illegible]										
000[illegible]										

S1X010-60-89.9 FG 2G 3G 4G

PERIOD	PHVEL	XYANG		GPANG	UX	PHIX	UY	PHIY	UZ	PHIZ
173.637	4.140	0.003	0	-0.000	0.695	-0.	0.000	0.	1.000	90.
114.715	4.090	0.002	0	-0.001	0.692	-0.	0.000	0.	1.000	90.
88.064	4.040	0.000	0	-0.001	0.703	-0.	0.000	180.	1.000	90.
60.588	3.990	0.002	0	-0.001	0.726	-0.	0.000	180.	1.000	90.
17.148	3.890	0.015	0	-0.004	0.854	-0.	0.000	180.	1.000	90.
000000000										
247.436	4.540	90.000	0	-0.001	0.000	0.	1.000	-0.	0.000	-90.
74.832	4.490	90.000	0	-0.005	0.000	0.	1.000	-0.	0.000	-90.
41.359	4.440	90.000	0	-0.007	0.000	-0.	1.000	0.	0.000	-90.
25.046	4.390	89.998	0	-0.006	0.000	0.	1.000	180.	0.000	90.
18.634	4.340	89.994	0	-0.004	0.000	-0.	1.000	-180.	0.000	90.
14.404	4.290	89.997	0	-0.002	0.000	-0.	1.000	-180.	0.000	90.
11.156	4.240	89.857	0	-0.001	0.003	-0.	1.000	0.	0.000	90.
10.115	4.140	0.020	0	-0.004	1.000	0.	0.000	180.	0.114	90.
9.762	4.090	0.021	0	-0.004	1.000	0.	0.000	180.	0.114	90.
9.410	4.040	0.023	0	-0.003	1.000	0.	0.000	180.	0.102	90.
9.099	3.990	0.026	0	-0.003	1.000	-0.	0.000	180.	0.083	90.
8.673	3.890	0.045	0	-0.003	1.000	-0.	0.001	180.	0.045	90.
0000000000										
27.188	4.540	0.012	0	-0.000	0.703	0.	0.000	180.	1.000	90.
21.989	4.490	0.023	0	-0.001	0.733	0.	0.000	180.	1.000	90.
19.191	4.440	0.028	0	-0.001	0.735	-0.	0.000	180.	1.000	90.
16.940	4.390	0.033	0	-0.001	0.700	0.	0.000	180.	1.000	90.
14.806	4.340	0.045	0	-0.001	0.519	0.	0.000	180.	1.000	90.
12.585	4.290	0.014	0	-0.001	0.928	-0.	0.000	-0.	1.000	-90.
10.826	4.240	0.024	0	-0.002	1.000	-0.	0.000	-180.	0.070	90.
8.831	4.140	89.935	0	-0.010	0.000	-0.	1.000	0.	0.000	90.
8.741	4.090	89.983	0	-0.010	0.000	0.	1.000	-0.	0.000	90.
8.660	4.040	89.981	0	-0.009	0.000	0.	1.000	-0.	0.000	90.
8.610	3.990	89.977	0	-0.009	0.000	0.	1.000	-0.	0.000	90.
8.518	3.890	89.956	0	-0.008	0.001	0.	1.000	-0.	0.000	90.
000000000										
14.764	4.540	89.996	0	-0.011	0.000	0.	1.000	-0.	0.000	-90.
12.389	4.490	89.997	0	-0.014	0.000	-0.	1.000	0.	0.000	90.
11.448	4.440	0.075	0	-0.003	1.000	0.	0.001	180.	0.041	-90.
11.266	4.390	0.038	0	-0.003	1.000	0.	0.001	-180.	0.003	90.
11.073	4.340	0.029	0	-0.003	1.000	0.	0.001	180.	0.039	90.
10.035	4.290	0.026	0	-0.002	1.000	0.	0.000	180.	0.072	90.
9.915	4.240	0.044	0	-0.001	1.000	-0.	0.001	180.	0.122	90.
7.488	4.190	0.008	0	-0.000	1.000	-0.	0.000	-179.	0.150	-90.
000000000										
000000000										

SIT110-60 89.9 FG 2G 3G 4G

PERIOD	PHVEL	XYANG		GPANG	UX	PHIX	UY	PHIY	UZ	PHIZ
164.163	4.140	1.144	0	-0.001	0.692	0.	0.014	90.	1.000	90.
112.491	4.090	2.077	0	-0.001	0.683	-0.	0.025	90.	1.000	90.
88.604	4.040	2.479	0	-0.002	0.688	0.	0.030	90.	1.000	90.
71.691	3.990	2.513	0	-0.002	0.703	-0.	0.031	90.	1.000	90.
55.712	3.940	2.183	0	-0.002	0.732	0.	0.028	90.	1.000	90.
17.431	3.840	0.088	0	-0.000	0.831	0.	0.001	90.	1.000	90.
376.173	4.540	89.842	0	-0.000	0.003	0.	1.000	-90.	0.000	89.
127.190	4.490	89.517	0	-0.001	0.008	0.	1.000	-90.	0.006	90.
81.480	4.440	89.252	0	-0.001	0.013	-0.	1.000	-90.	0.014	90.
56.173	4.390	89.010	0	-0.002	0.017	0.	1.000	-90.	0.022	90.
37.445	4.340	88.737	0	-0.002	0.022	-0.	1.000	-90.	0.030	90.
15.138	4.240	87.385	0	-0.002	0.046	0.	1.000	-90.	0.083	90.
28.251	4.540	27.358	0	-0.003	0.652	0.	0.338	90.	1.000	90.
22.987	4.490	38.140	0	-0.002	0.662	0.	0.556	90.	1.000	90.
20.152	4.440	46.829	0	-0.003	0.692	-0.	0.737	90.	1.000	90.
17.917	4.390	56.293	0	-0.004	0.667	0.	1.000	90.	0.985	90.
15.917	4.340	69.142	0	-0.005	0.381	0.	1.000	90.	0.644	90.
11.266	4.240	37.238	0	-0.006	1.000	0.	0.760	-90.	0.011	-90.
21.028	4.540	88.352	0	-0.001	0.029	-0.	1.000	-90.	0.043	90.
18.475	4.490	88.401	0	-0.002	0.028	0.	1.000	-90.	0.042	90.
16.456	4.440	88.779	0	-0.002	0.021	0.	1.000	-90.	0.035	90.
14.532	4.390	89.459	0	-0.002	0.009	0.	1.000	-90.	0.024	90.
12.665	4.340	89.375	0	-0.002	0.011	-0.	1.000	90.	0.013	-90.
10.494	4.240	63.930	0	-0.007	0.489	0.	1.000	90.	0.051	90.

SIT010-60-59.9 FG 2G 3G 4G

PERIOD	PHVEL	XYANG		GPANG	UX	PHIX	UY	PHIY	UZ	PHIZ
166.744	4.140	0.005	0	-0.065	0.690	-0.	0.000	0.	1.000	90.
115.262	4.090	0.015	0	-0.111	0.680	-0.	0.010	180.	1.000	90.
91.391	4.040	1.326	0	-0.173	0.684	0.	0.016	180.	1.000	90.
74.628	3.990	1.572	0	-0.250	0.698	-0.	0.019	180.	1.000	90.
59.245	3.940	1.562	0	-0.306	0.724	-0.	0.020	-180.	1.000	90.
17.429	3.840	0.072	0	-0.024	0.932	-0.	0.001	180.	1.000	90.
300.288	4.540	89.999	0	-0.097	0.000	0.	1.000	-0.	0.000	-90.
99.377	4.490	89.829	0	-0.570	0.003	0.	1.000	-0.	0.010	-90.
61.567	4.440	89.585	0	-0.868	0.007	0.	1.000	-0.	0.000	90.
39.554	4.390	89.386	0	-1.026	0.011	-0.	1.000	0.	0.010	90.
14.292	4.290	19.382	0	-0.484	0.366	0.	0.129	0.	1.000	90.
28.923	4.540	28.972	0	-0.147	0.650	0.	0.360	0.	1.000	90.
25.357	4.490	27.769	0	-0.273	0.682	0.	0.359	0.	1.000	90.
20.484	4.440	23.835	0	-0.337	0.694	0.	0.306	-0.	1.000	90.
18.295	4.390	20.170	0	-0.394	0.685	-0.	0.252	0.	1.000	90.
12.299	4.290	89.581	0	-0.756	0.007	-0.	1.000	180.	0.004	-90.
19.751	4.540	88.474	0	-0.513	0.027	0.	1.000	180.	0.040	90.
16.913	4.490	88.855	0	-1.105	0.020	0.	1.000	180.	0.033	90.
14.798	4.440	89.445	0	-1.390	0.010	0.	1.000	180.	0.023	90.
12.871	4.390	89.471	0	-1.683	0.009	-0.	1.000	-0.	0.016	-90.
11.085	4.290	8.509	0	-0.184	1.000	-0.	0.150	0.	0.033	90.

S3X110-60-90.0 FG 2G 3G 4G

PERIOD	PHVEL	XYANG		GPANG	UX	PHIX	UY	PHIY	UZ	PHIZ
201.000	4.140	1.593	0	0.000	0.716	-0.	0.020	90.	1.000	90.
122.586	4.090	5.019	0	0.000	0.710	-0.	0.062	90.	1.000	90.
92.502	4.040	7.898	0	0.000	0.717	0.	0.099	90.	1.000	90.
72.412	3.990	10.665	0	0.000	0.734	0.	0.138	90.	1.000	90.
52.378	3.940	14.447	0	0.000	0.771	-0.	0.199	90.	1.000	90.
18.070	3.840	25.646	0	0.000	0.812	-0.	0.393	90.	1.000	90.
309.821	4.540	83.186	0	0.000	0.032	0.	1.000	-90.	0.005	90.
97.297	4.490	84.215	0	0.000	0.101	0.	1.000	-90.	0.046	90.
53.943	4.440	79.787	0	0.000	0.180	-0.	1.000	-90.	0.119	90.
25.246	4.390	67.185	0	0.000	0.421	-0.	1.000	-90.	0.383	90.
18.582	4.330	52.756	0	0.000	0.760	0.	1.000	-90.	0.814	90.
15.252	4.280	49.114	0	0.000	0.729	0.	0.842	-90.	1.000	90.
12.581	4.230	69.767	0	0.000	0.369	-0.	1.000	90.	0.532	-90.
11.221	4.180	37.793	0	0.000	1.000	0.	0.775	90.	0.005	-90.
10.750	4.130	33.166	0	0.000	1.000	-0.	0.654	90.	0.074	90.
10.327	4.080	31.241	0	0.000	1.000	-0.	0.607	90.	0.107	90.
9.883	4.030	30.751	0	0.000	1.000	0.	0.594	90.	0.115	90.
27.235	4.540	39.424	0	0.000	0.656	0.	0.540	90.	1.000	90.
21.991	4.490	53.742	0	0.000	0.648	0.	0.883	90.	1.000	90.
19.057	4.440	61.159	0	0.000	0.551	0.	1.000	90.	0.883	90.
16.136	4.380	68.407	0	0.000	0.396	-0.	1.000	90.	0.748	90.
13.831	4.330	82.531	0	0.000	0.161	0.	1.000	90.	0.912	90.
11.706	4.280	36.677	0	0.000	1.000	-0.	0.745	90.	0.161	-90.
10.842	4.230	33.414	0	0.000	1.000	0.	0.660	90.	0.070	90.
8.793	4.180	67.195	0	0.000	0.420	0.	1.000	-90.	0.021	90.
8.706	4.130	66.932	0	0.000	0.426	0.	1.000	-90.	0.018	90.
8.632	4.080	65.799	0	0.000	0.449	-0.	1.000	-90.	0.016	90.
15.616	4.540	76.372	0	0.000	0.242	0.	1.000	-90.	0.226	90.
13.689	4.490	82.431	0	0.000	0.133	-0.	1.000	-90.	0.227	90.
12.685	4.440	85.368	0	0.000	0.081	0.	1.000	90.	0.211	-90.

S3X010-60-59.9 FG 2G 3G 4G

PERIOD	PHVEL	XYANG		GPANG	UX	PHIX	UY	PHIY	UZ	PHIZ
175.630	4.140	6.293	0	-0.767	0.694	-0.	0.077	0.	1.000	90.
117.249	4.090	5.327	0	-0.960	0.686	-0.	0.064	0.	1.000	90.
91.340	4.040	3.588	0	-1.213	0.690	-0.	0.043	0.	1.000	90.
73.533	3.990	1.613	0	-1.586	0.703	-0.	0.020	0.	1.000	90.
57.360	3.940	0.738	0	-2.179	0.725	-0.	0.009	-180.	1.000	90.
18.621	3.840	9.834	0	-4.430	0.840	-0.	0.146	180.	1.000	90.
162.269	4.540	89.689	0	0.065	0.005	0.	1.000	-0.	0.076	-90.
51.014	4.490	89.163	0	0.442	0.015	0.	1.000	-0.	0.140	-90.
31.440	4.440	88.850	0	0.574	0.020	-0.	1.000	-180.	0.194	90.
23.188	4.390	84.252	0	0.515	0.101	-0.	1.000	-180.	0.296	90.
18.465	4.340	78.320	0	0.306	0.207	-0.	1.000	-180.	0.442	90.
14.971	4.290	79.523	0	-0.030	0.185	-0.	1.000	-180.	0.553	90.
11.831	4.240	25.632	0	-0.391	1.000	0.	0.450	0.	0.212	-90.
10.823	4.190	8.922	0	-3.836	1.000	-0.	0.157	-180.	0.097	90.
10.555	4.140	9.929	0	-4.166	1.000	-0.	0.175	-180.	0.095	90.
10.268	4.090	10.514	0	-4.095	1.000	0.	0.186	180.	0.113	90.
9.945	4.040	11.139	0	-3.987	1.000	-0.	0.197	180.	0.116	90.
9.660	3.990	11.964	0	-3.864	1.000	-0.	0.212	180.	0.111	90.
9.270	3.940	13.158	0	-3.723	1.000	-0.	0.234	180.	0.096	90.
27.936	4.540	3.666	0	-0.212	0.655	0.	0.042	180.	1.000	90.
22.617	4.490	7.600	0	-0.586	0.679	0.	0.091	180.	1.000	90.
19.700	4.440	8.844	0	-0.763	0.685	0.	0.107	180.	1.000	90.
17.308	4.390	8.523	0	-0.812	0.658	-0.	0.099	180.	1.000	90.
15.021	4.340	9.230	0	-0.751	0.582	-0.	0.082	180.	1.000	90.
12.692	4.290	8.669	0	-0.623	0.763	-0.	0.089	-180.	1.000	-90.
10.970	4.240	12.654	0	-0.624	1.000	0.	0.225	180.	0.051	90.
8.800	4.190	82.841	0	0.373	0.126	0.	1.000	-0.	0.004	90.
8.715	4.140	81.762	0	0.606	0.145	-0.	1.000	-0.	0.004	90.
8.649	4.090	81.057	0	0.502	0.157	0.	1.000	-0.	0.004	90.
8.595	4.040	80.217	0	0.369	0.172	-0.	1.000	-0.	0.004	90.
8.548	3.990	79.146	0	0.197	0.192	-0.	1.000	-0.	0.004	90.
13.314	4.540	82.362	0	-0.239	0.134	0.	1.000	-0.	0.177	-90.
11.920	4.490	27.634	0	-2.119	1.000	0.	0.524	-0.	0.218	-90.
11.627	4.440	2.259	0	-3.595	1.000	0.	0.039	180.	0.102	-90.
11.449	4.390	7.746	0	-3.813	1.000	0.	0.136	-180.	0.047	-90.
11.220	4.340	9.506	0	-3.536	1.000	0.	0.167	180.	0.005	-90.
11.073	4.290	10.634	0	-2.419	1.000	0.	0.188	-180.	0.035	90.
10.088	4.240	19.136	0	-0.466	1.000	0.	0.347	180.	0.126	90.
8.448	4.190	45.791	0	-0.120	0.973	0.	1.000	-0.	0.025	90.
7.428	4.140	7.374	0	-4.020	1.000	0.	0.129	180.	0.166	-90.
7.283	4.090	7.846	0	-3.933	1.000	0.	0.138	-180.	0.202	-90.
7.085	4.040	8.341	0	-3.325	1.000	-0.	0.147	-180.	0.256	-90.
6.818	3.990	8.844	0	-3.699	1.000	0.	0.156	-180.	0.341	-90.

S3XT110-120-59.9 FU 26 36 46

PERIOD	PHVEL	XYANG		GPANG	UX	PHIX	UY	PHIY	UZ	PHIZ
154.968	4.140	5.095	0	-0.543	0.703	0.	0.063	100.	1.000	90.
99.544	4.090	8.386	0	-1.026	0.706	0.	0.104	101.	1.000	90.
72.740	4.040	9.603	0	-1.373	0.729	0.	0.124	102.	1.000	90.
16.466	3.940	9.213	0	-1.152	0.852	0.	0.138	107.	1.000	90.
235.451	4.540	28.134	0	-0.078	0.033	0.	1.000	-89.	0.013	102.
66.302	4.490	83.743	0	-0.599	0.110	0.	1.000	-89.	0.108	94.
34.456	4.440	78.394	0	-0.906	0.206	0.	1.000	-92.	0.228	93.
23.174	4.390	69.315	0	-0.719	0.368	0.	1.000	-97.	0.417	92.
18.685	4.340	62.252	0	-0.520	0.526	0.	1.000	-100.	0.617	92.
15.580	4.290	63.248	0	-0.509	0.504	0.	1.000	-100.	0.690	92.
12.897	4.240	83.207	0	-0.587	0.119	-0.	1.000	74.	0.407	-97.
10.350	4.190	22.295	0	-0.894	1.000	0.	0.410	97.	0.107	90.
9.734	4.140	16.248	0	-0.934	1.000	0.	0.291	105.	0.114	90.
9.378	4.090	16.543	0	-0.919	1.000	0.	0.297	106.	0.100	90.
9.078	4.040	16.373	0	-0.885	1.000	0.	0.332	107.	0.081	90.
8.685	3.940	38.874	0	-0.731	1.000	-0.	0.598	108.	0.046	90.
23.799	4.540	71.089	0	-0.573	0.327	-0.	1.000	73.	0.473	88.
17.040	4.490	85.988	0	-2.037	0.072	-0.	1.000	59.	0.127	72.
12.379	4.440	88.132	0	-2.073	0.033	0.	1.000	153.	0.036	-68.
11.241	4.390	50.747	0	-0.461	0.817	0.	1.000	104.	0.001	-90.
10.975	4.340	31.016	0	-0.728	1.000	-0.	0.601	103.	0.055	90.
10.699	4.290	22.564	0	-0.854	1.000	-0.	0.416	104.	0.087	90.
10.396	4.240	18.543	0	-0.892	1.000	0.	0.332	105.	0.107	90.
9.954	4.190	16.913	0	-0.705	1.000	0.	0.250	112.	0.117	90.
8.830	4.140	77.468	0	-0.277	0.222	0.	1.000	-74.	0.012	91.
8.735	4.090	76.032	0	-0.283	0.249	0.	1.000	-73.	0.012	91.
8.658	4.040	73.486	0	-0.316	0.296	0.	1.000	-73.	0.012	91.
8.536	3.940	68.172	0	-0.562	0.573	-0.	1.000	-72.	0.016	91.
14.777	4.540	25.142	0	-0.659	0.085	-0.	1.000	-83.	0.109	98.
12.666	4.490	58.981	0	-1.639	-0.053	0.	1.000	70.	0.088	-105.
11.358	4.440	33.090	0	-3.667	1.000	0.	0.652	-11.	0.016	-91.
10.275	4.390	78.426	0	-0.880	0.298	0.	1.000	-77.	0.032	91.
9.761	4.340	77.212	0	-0.449	0.227	0.	1.000	-77.	0.024	91.
9.350	4.290	78.399	0	-0.355	0.205	0.	1.000	-76.	0.019	91.
9.117	4.240	78.670	0	-0.312	0.200	0.	1.000	-75.	0.016	91.
8.952	4.190	78.438	0	-0.292	0.205	0.	1.000	-74.	0.014	91.

S3XT010-120-59.9 FG 26 36 46

PERIOD	PHVEL	XYANG		GPANG	UX	PHIX	UY	PHIY	UZ	PHIZ
180.408	4.140	1.717	0	-0.357	0.691	-0.	0.021	0.	1.000	90.
119.393	4.090	0.119	0	-0.535	0.684	-0.	0.001	180.	1.000	90.
92.228	4.040	1.459	0	-0.777	0.694	-0.	0.018	180.	1.000	90.
72.615	3.990	2.342	0	-1.057	0.715	-0.	0.029	180.	1.000	90.
46.240	3.940	2.813	0	-1.359	0.779	0.	0.038	180.	1.000	90.
15.201	3.840	4.402	0	-1.103	0.755	0.	0.058	180.	1.000	90.
94.135	4.548	89.882	0	-0.118	0.002	0.	1.000	-0.	0.075	-90.
60.113	4.547	89.368	0	-0.389	0.011	-0.	1.000	-180.	0.100	90.
37.875	4.540	85.613	0	-0.731	0.077	-0.	1.000	-180.	0.185	90.
35.116	4.537	84.172	0	-0.716	0.102	-0.	1.000	-180.	0.218	90.
30.077	4.527	79.385	0	-0.572	0.187	0.	1.000	-180.	0.327	90.
27.383	4.517	74.478	0	-0.454	0.278	0.	1.000	-180.	0.443	90.
25.584	4.507	69.481	0	-0.398	0.374	0.	1.000	-180.	0.567	90.
24.243	4.497	64.507	0	-0.392	0.477	0.	1.000	-180.	0.698	90.
23.473	4.490	61.110	0	-0.410	0.552	-0.	1.000	-180.	0.794	90.
23.174	4.487	59.689	0	-0.422	0.585	0.	1.000	-180.	0.836	90.
19.818	4.440	41.843	0	-0.745	0.733	0.	0.656	180.	1.000	90.
17.399	4.390	32.980	0	-1.092	0.718	0.	0.466	-180.	1.000	90.
15.304	4.340	34.783	0	-1.336	0.599	0.	0.416	180.	1.000	90.
13.218	4.290	79.003	0	-1.492	0.094	-0.	0.485	-0.	1.000	-90.
11.108	4.240	8.321	0	-1.567	1.000	-0.	0.006	0.	0.024	90.
10.336	4.190	4.383	0	-1.095	1.000	0.	0.077	-180.	0.109	90.
8.766	4.140	86.050	0	-0.996	0.069	-0.	1.000	-0.	0.003	90.
8.631	4.040	84.762	0	-0.913	0.092	-0.	1.000	0.	0.003	90.
21.806	4.548	76.517	0	-0.449	0.240	0.	1.000	-0.	0.274	90.
20.625	4.547	77.380	0	-1.135	0.224	0.	1.000	-0.	0.254	90.
17.577	4.540	79.478	0	-2.284	0.186	0.	1.000	-0.	0.216	90.
16.789	4.537	80.096	0	-2.429	0.175	0.	1.000	-0.	0.210	90.
14.900	4.527	82.503	0	-2.503	0.132	0.	1.000	-0.	0.203	90.
13.640	4.517	87.107	0	-2.307	0.051	-0.	1.000	0.	0.206	90.
12.762	4.507	82.319	0	-2.009	0.135	-0.	1.000	180.	0.220	-90.
12.190	4.497	60.256	0	-1.677	0.571	0.	1.000	180.	0.251	-90.
11.947	4.490	41.512	0	-1.455	1.000	-0.	0.885	180.	0.251	-90.
11.872	4.487	34.796	0	-1.371	1.000	0.	0.695	180.	0.208	-90.
11.434	4.440	7.976	0	-1.000	1.000	-0.	0.140	-180.	0.037	-90.
11.222	4.390	5.799	0	-1.073	1.000	-0.	0.102	180.	0.013	90.
11.020	4.340	5.243	0	-1.101	1.000	-0.	0.092	-180.	0.048	90.
10.792	4.290	5.119	0	-1.138	1.000	-0.	0.090	180.	0.077	90.
10.439	4.240	6.048	0	-1.472	1.000	0.	0.106	-180.	0.106	90.
8.858	4.190	86.732	0	-1.078	0.057	0.	1.000	0.	0.002	90.
7.105	4.140	3.184	0	-0.956	1.000	0.	0.056	180.	0.250	-90.
6.537	4.040	3.599	0	-0.903	1.000	0.	0.063	180.	0.448	-90.
12.573	4.548	85.707	0	-0.629	0.075	-0.	1.000	-0.	0.040	-90.
12.485	4.547	85.475	0	-1.197	0.079	0.	1.000	-0.	0.037	-90.
12.150	4.540	83.982	0	-1.731	0.105	0.	1.000	-0.	0.029	-90.
12.038	4.537	83.191	0	-1.817	0.119	-0.	1.000	-0.	0.027	-90.
11.727	4.527	79.045	0	-2.143	0.194	0.	1.000	0.	0.022	-90.
11.493	4.517	74.313	0	-2.686	0.338	-0.	1.000	-0.	0.015	-90.
11.294	4.507	69.883	0	-2.828	0.469	0.	1.000	-0.	0.002	90.
11.048	4.497	65.825	0	-2.514	0.387	0.	1.000	-0.	0.019	90.
10.848	4.490	77.539	0	-2.353	0.221	0.	1.000	-0.	0.016	90.
10.580	4.487	58.261	0	-1.188	0.619	-0.	1.000	180.	0.070	90.
10.072	4.440	87.599	0	-1.504	0.042	-0.	1.000	-0.	0.002	90.
9.628	4.390	87.402	0	-1.363	0.045	-0.	1.000	0.	0.003	90.
9.333	4.340	87.172	0	-1.267	0.049	0.	1.000	-0.	0.003	90.
9.126	4.290	86.942	0	-1.188	0.053	0.	1.000	-0.	0.003	90.
8.974	4.240	86.672	0	-1.120	0.058	0.	1.000	0.	0.003	90.
8.633	4.190	31.377	0	-1.665	1.000	-0.	0.610	-0.	0.045	90.
6.257	4.140	5.677	0	-1.687	1.000	0.	0.099	-180.	0.554	-90.

S3T110-60--0.1 FG 26 36 46

PERIOD	PHVEL	XYANG		GRANG	UX	PHIX	UY	PHIY	UZ	PHIZ
91.486	4.140	0.045	0	0.000	0.716	0.	0.001	-73.	1.000	91.
85.283	4.090	0.046	0	0.008	0.724	-0.	0.001	-69.	1.000	91.
49.677	4.040	0.037	0	0.008	0.746	-0.	0.000	-68.	1.000	90.
36.408	3.990	0.023	0	0.005	0.781	0.	0.000	-67.	1.000	90.
19.909	3.890	0.003	0	0.001	0.849	-0.	0.000	-66.	1.000	90.
365.097	4.340	89.996	0	-0.000	0.000	-0.	1.000	91.	0.000	136.
122.821	4.490	89.986	0	-0.002	0.000	-0.	1.000	96.	0.000	103.
78.467	4.440	89.977	0	-0.005	0.000	0.	1.000	99.	0.000	96.
53.812	4.390	89.970	0	-0.006	0.001	0.	1.000	101.	0.001	93.
35.609	4.340	89.968	0	-0.006	0.001	0.	1.000	101.	0.001	91.
12.956	4.240	89.995	0	0.000	0.000	0.	1.000	-89.	0.000	-90.
10.454	4.140	0.003	0	0.000	1.000	0.	0.000	-81.	0.101	90.
10.146	4.090	0.001	0	0.000	1.000	0.	0.000	-77.	0.114	90.
9.800	4.040	0.000	0	0.000	1.000	0.	0.000	-73.	0.115	90.
9.445	3.990	0.000	0	0.000	1.000	0.	0.000	-70.	0.104	90.
8.867	3.890	0.000	0	0.000	1.000	0.	0.000	-66.	0.065	90.
21.182	4.540	89.977	0	0.004	0.000	-0.	1.000	-123.	0.001	89.
18.540	4.490	89.987	0	0.003	0.000	-0.	1.000	-115.	0.000	90.
16.440	4.440	89.992	0	0.002	0.000	-0.	1.000	-111.	0.000	90.
14.494	4.390	89.997	0	0.002	0.000	-0.	1.000	-110.	0.000	90.
12.647	4.340	89.997	0	0.001	0.000	0.	1.000	70.	0.000	-90.
10.945	4.240	0.059	0	-0.001	1.000	-0.	0.001	85.	0.054	90.
9.261	4.140	90.000	0	-0.000	0.000	0.	1.000	98.	0.000	90.
9.032	4.090	90.000	0	-0.000	0.000	0.	1.000	103.	0.000	90.
8.876	4.040	90.000	0	-0.000	0.000	0.	1.000	107.	0.000	90.
8.763	3.990	90.000	0	-0.000	0.000	0.	1.000	110.	0.000	90.
8.610	3.890	90.000	0	-0.000	0.000	-0.	1.000	94.	0.000	95.
12.309	4.540	0.042	0	0.002	0.781	-0.	0.013	-174.	1.000	-90.
11.913	4.490	0.066	0	0.002	1.000	0.	0.001	178.	0.224	-90.
11.674	4.440	0.027	0	0.000	1.000	0.	0.000	-169.	0.119	-90.
11.493	4.390	0.020	0	-0.000	1.000	-0.	0.000	-149.	0.060	-90.
11.322	4.340	0.029	0	-0.001	1.000	-0.	0.001	-126.	0.015	-90.
10.103	4.240	89.993	0	0.001	0.000	0.	1.000	-100.	0.000	90.
7.309	4.140	0.000	0	0.000	1.000	0.	0.000	-85.	0.175	-90.
7.225	4.090	0.000	0	0.000	1.000	0.	0.000	-78.	0.217	-90.
7.080	4.040	0.000	0	0.000	1.000	0.	0.000	-74.	0.281	-90.
6.784	3.990	0.000	0	0.000	1.000	0.	0.000	-71.	0.382	-90.
5.982	3.890	0.000	0	0.000	1.000	0.	0.000	-87.	0.747	-90.

S3T010-60-00.1 FG 26 36 46

PERIOD	PHVEL	XYANG		GRANG	UX	PHIX	UY	PHIY	UZ	PHIZ
153.664	4.140	0.006	0	-0.001	0.626	180.	0.000	-180.	1.000	-90.
105.290	4.090	0.014	0	-0.002	0.696	180.	0.000	-0.	1.000	-90.
77.906	4.040	0.027	0	-0.004	0.713	180.	0.000	-0.	1.000	-90.
55.750	3.990	0.032	0	-0.006	0.742	180.	0.000	0.	1.000	-90.
30.708	3.940	0.016	0	-0.005	0.809	180.	0.000	-0.	1.000	-90.
20.356	3.890	0.004	0	-0.001	0.859	180.	0.000	0.	1.000	-90.
328.736	4.540	90.000	0	0.002	0.000	180.	1.000	0.	0.000	-90.
109.041	4.490	89.998	0	0.004	0.000	180.	1.000	180.	0.000	90.
68.925	4.440	89.993	0	0.012	0.000	180.	1.000	180.	0.000	90.
45.766	4.390	89.987	0	0.014	0.000	180.	1.000	-180.	0.000	-90.
14.667	4.290	89.992	0	0.017	0.000	180.	1.000	180.	0.000	-90.
10.463	4.140	0.002	0	-0.000	1.000	180.	0.000	0.	0.101	-90.
10.150	4.090	0.001	0	-0.000	1.000	180.	0.000	-0.	0.113	-90.
9.802	4.040	0.000	0	-0.000	1.000	180.	0.000	-0.	0.115	-90.
9.445	3.990	0.000	0	-0.000	1.000	180.	0.000	0.	0.104	-90.
9.123	3.940	0.000	0	-0.000	1.000	180.	0.000	-0.	0.086	-90.
8.867	3.890	0.000	0	-0.000	1.000	180.	0.000	0.	0.065	-90.
23.644	4.540	0.767	0	-0.003	0.677	180.	0.000	-180.	1.000	-90.
19.886	4.490	0.698	0	-0.004	0.678	180.	0.000	180.	1.000	-90.
17.377	4.440	0.503	0	-0.004	0.646	180.	0.000	-180.	1.000	-90.
15.042	4.390	0.038	0	-0.005	0.482	180.	0.000	-180.	1.000	-90.
11.307	4.290	0.288	0	-0.004	1.000	180.	0.005	180.	0.016	90.
9.259	4.140	90.000	0	0.000	0.000	180.	1.000	180.	0.000	-90.
9.031	4.090	90.000	0	0.000	0.000	180.	1.000	180.	0.000	-90.
8.876	4.040	90.000	0	0.000	0.000	180.	1.000	180.	0.000	-90.
8.763	3.990	90.000	0	0.000	0.000	180.	1.000	179.	0.000	-90.
8.677	3.940	90.000	0	0.000	0.000	180.	1.000	180.	0.000	-90.
8.610	3.890	90.000	0	0.000	0.000	180.	1.000	180.	0.000	-90.
20.540	4.540	89.963	0	0.007	0.001	180.	1.000	-0.	0.001	-90.
17.733	4.490	89.977	0	0.012	0.000	180.	1.000	-0.	0.001	-90.
15.639	4.440	89.991	0	0.012	0.000	180.	1.000	-0.	0.000	-90.
13.740	4.390	90.000	0	0.014	0.000	180.	1.000	-0.	0.000	-90.
10.466	4.290	89.928	0	0.027	0.001	180.	1.000	0.	0.000	-90.

S3T110-60-29.9 FG 2G 3G 4G

PERIOD	PHVEL	XYANG		GPANG	UX	PHIX	UY	PHIY	UZ	PHIZ
113.340	4.140	8.059	0	-0.341	0.709	-0.	0.100	106.	1.000	91.
78.526	4.090	9.635	0	-1.313	0.711	-0.	0.121	109.	1.000	91.
59.295	4.040	8.216	0	-1.468	0.728	-0.	0.113	110.	1.000	90.
44.252	3.990	8.414	0	-1.301	0.759	-0.	0.085	111.	1.000	90.
20.212	3.890	8.842	0	-0.121	0.850	0.	0.010	112.	1.000	90.
335.874	4.540	89.998	0	0.340	0.012	-0.	1.000	-88.	0.008	124.
109.642	4.490	84.672	0	0.301	0.058	0.	1.000	-84.	0.058	98.
67.289	4.440	84.891	0	0.543	0.091	0.	1.000	-82.	0.115	94.
44.569	4.390	85.735	0	0.676	0.110	0.	1.000	-81.	0.149	92.
29.336	4.340	85.436	0	0.614	0.115	0.	1.000	-82.	0.156	91.
15.235	4.240	89.405	0	-0.205	0.009	0.	1.000	90.	0.077	-90.
10.469	4.140	0.082	0	-0.054	1.000	0.	0.012	97.	0.101	90.
10.140	4.090	0.184	0	-0.019	1.000	0.	0.003	102.	0.113	90.
9.822	4.040	0.061	0	-0.008	1.000	0.	0.001	105.	0.115	90.
9.445	3.990	0.025	0	-0.003	1.000	-0.	0.000	107.	0.104	90.
8.867	3.890	0.005	0	-0.001	1.000	-0.	0.000	111.	0.065	90.
23.827	4.540	89.763	0	-0.519	0.127	-0.	1.000	64.	0.194	90.
19.235	4.490	86.085	0	-0.648	0.070	0.	1.000	69.	0.106	90.
16.932	4.440	87.603	0	-0.529	0.042	-0.	1.000	71.	0.067	90.
14.428	4.390	89.076	0	-0.363	0.016	0.	1.000	72.	0.036	90.
12.632	4.340	89.584	0	-0.229	0.009	-0.	1.000	-109.	0.014	-90.
10.928	4.240	11.189	0	0.020	1.000	0.	0.198	-97.	0.056	90.
9.261	4.140	89.838	0	-0.001	0.003	0.	1.000	-84.	0.000	90.
9.032	4.090	89.954	0	0.001	0.001	0.	1.000	-79.	0.000	90.
8.876	4.040	89.982	0	0.000	0.000	0.	1.000	-75.	0.000	90.
8.763	3.990	89.991	0	0.000	0.000	0.	1.000	-73.	0.000	90.
8.610	3.890	89.997	0	0.000	0.000	0.	1.000	-69.	0.000	90.
13.887	4.540	88.066	0	-0.565	0.034	-0.	1.000	-153.	0.307	89.
11.996	4.490	2.033	0	-0.069	1.000	0.	0.365	6.	0.272	-90.
11.691	4.440	6.730	0	-0.308	1.000	-0.	0.118	15.	0.126	-90.
11.495	4.390	4.554	0	-0.111	1.000	0.	0.030	34.	0.060	-90.
11.317	4.340	2.060	0	-0.006	1.000	0.	0.106	54.	0.014	-90.
10.148	4.240	88.705	0	-0.114	0.023	0.	1.000	79.	0.003	90.
7.389	4.140	0.026	0	-0.008	1.000	0.	0.000	92.	0.175	-90.
7.225	4.090	0.004	0	-0.001	1.000	-0.	0.000	100.	0.217	-90.
7.090	4.040	0.001	0	-0.000	1.000	0.	0.000	104.	0.281	-90.
6.784	3.990	0.000	0	-0.000	1.000	0.	0.000	107.	0.382	-90.
5.982	3.890	0.000	0	-0.000	1.000	0.	0.000	112.	0.747	-90.

S3T010-60-30.1 FG 2G 3G 4G

PERIOD	PHVEL	XYANG		GPANG	UX	PHIX	UY	PHIY	UZ	PHIZ
161.399	4.140	1.205	0	-0.220	0.690	180.	0.315	-180.	1.000	-90.
110.133	4.090	2.399	0	-0.330	0.690	180.	0.324	0.	1.000	-90.
84.419	4.040	4.746	0	-0.608	0.700	180.	0.358	0.	1.000	-90.
65.270	3.990	5.779	0	-0.937	0.721	180.	0.373	-0.	1.000	-90.
44.347	3.940	4.849	0	-1.373	0.764	180.	0.365	-0.	1.000	-90.
17.303	3.840	9.238	0	-0.085	0.829	180.	0.303	0.	1.000	-90.
184.212	4.540	89.952	0	0.374	0.201	180.	1.000	180.	0.062	90.
67.553	4.490	89.060	0	1.627	0.016	180.	1.000	180.	0.031	90.
41.080	4.440	88.347	0	1.993	0.024	180.	1.000	180.	0.017	-90.
24.889	4.390	88.268	0	1.762	0.030	180.	1.000	180.	0.036	-90.
11.773	4.290	43.224	0	-1.123	1.000	180.	0.940	-0.	0.182	90.
10.470	4.140	0.305	0	-0.045	1.000	180.	0.295	-0.	0.139	-90.
10.154	4.090	0.116	0	-0.019	1.000	180.	0.202	-0.	0.113	-90.
9.804	4.040	0.047	0	-0.008	1.000	180.	0.101	0.	0.115	-90.
9.446	3.990	0.020	0	-0.003	1.000	180.	0.050	0.	0.105	-90.
9.124	3.940	0.009	0	-0.001	1.000	180.	0.025	0.	0.087	-90.
8.679	3.840	0.003	0	-0.000	1.000	180.	0.006	-0.	0.047	-90.
25.164	4.540	67.392	0	-0.414	0.416	180.	1.000	-180.	0.617	-90.
21.019	4.490	63.197	0	-0.764	0.505	180.	1.000	-180.	0.769	-90.
18.397	4.440	58.220	0	-0.923	0.620	180.	1.000	-180.	0.921	-90.
16.150	4.390	54.852	0	-1.079	0.601	180.	0.353	180.	1.000	-90.
11.575	4.290	83.881	0	0.176	0.329	180.	1.000	-180.	0.982	90.
9.257	4.140	89.938	0	0.007	0.001	180.	1.000	-180.	0.000	-90.
9.031	4.090	89.972	0	0.003	0.000	180.	1.000	-180.	0.000	-90.
8.876	4.040	89.986	0	0.001	0.000	180.	1.000	180.	0.000	-90.
8.763	3.990	89.992	0	0.000	0.000	180.	1.000	180.	0.000	-90.
8.677	3.940	89.996	0	0.000	0.000	180.	1.000	180.	0.000	-90.
8.554	3.840	89.998	0	0.000	0.000	180.	1.000	180.	0.000	-90.
17.595	4.540	82.719	0	1.357	0.128	180.	1.000	-0.	0.235	-90.
14.734	4.490	86.719	0	2.583	0.057	180.	1.000	-0.	0.147	-90.
12.399	4.440	79.258	0	2.626	0.190	180.	1.000	-180.	0.129	90.
11.447	4.390	19.525	0	0.326	1.000	180.	0.355	-180.	0.048	90.
10.657	4.290	11.462	0	-1.419	1.000	180.	0.203	-180.	0.094	-90.

S3T110-60-59.9 FG 2G 3G 4G

PERIOD	PHVEL	XYANG		GPANG	UX	PHIX	UY	PHIY	UZ	PHIZ
152.075	4.140	5.190	0	-0.452	0.703	0.	0.064	106.	1.000	90.
100.766	4.090	7.393	0	-0.335	0.696	-0.	0.096	106.	1.000	90.
77.562	4.040	8.450	0	-1.062	0.704	-0.	0.105	106.	1.000	90.
60.381	3.990	7.684	0	-1.130	0.725	-0.	0.098	105.	1.000	90.
41.206	3.940	5.102	0	-0.888	0.771	-0.	0.069	105.	1.000	90.
17.302	3.840	0.252	0	-0.061	0.829	-0.	0.004	105.	1.000	90.
335.584	4.540	89.154	0	-0.039	0.015	-0.	1.000	-87.	0.005	84.
109.017	4.490	87.392	0	-0.277	0.046	-0.	1.000	-84.	0.043	89.
67.402	4.440	86.123	0	-0.485	0.064	0.	1.000	-83.	0.084	90.
44.328	4.390	85.156	0	-0.581	0.035	0.	1.000	-84.	0.115	90.
28.639	4.340	84.365	0	-0.498	0.104	0.	1.000	-86.	0.141	90.
19.061	4.290	82.767	0	-0.321	0.127	0.	1.000	-89.	0.173	90.
14.259	4.240	86.432	0	-0.397	0.062	0.	1.000	-91.	0.167	90.
11.859	4.190	35.712	0	-0.543	1.000	0.	0.719	89.	0.030	90.
10.475	4.140	1.157	0	-0.378	1.000	0.	0.020	93.	0.100	90.
10.154	4.090	0.249	0	-0.022	1.000	0.	0.004	96.	0.113	90.
9.804	4.040	0.076	0	-0.008	1.000	0.	0.001	99.	0.115	90.
9.446	3.990	0.027	0	-0.003	1.000	-0.	0.000	101.	0.105	90.
9.124	3.940	0.011	0	-0.001	1.000	-0.	0.000	103.	0.086	90.
8.678	3.840	0.003	0	-0.000	1.000	-0.	0.000	105.	0.047	90.
26.218	4.540	66.384	0	-0.344	0.437	0.	1.000	80.	0.668	90.
21.156	4.490	77.436	0	-0.853	0.223	-0.	1.000	80.	0.329	90.
18.329	4.440	82.618	0	-0.936	0.130	0.	1.000	80.	0.194	90.
15.837	4.390	86.760	0	-0.807	0.057	0.	1.000	79.	0.099	90.
13.355	4.340	89.849	0	-0.478	0.003	-0.	1.000	-102.	0.033	-90.
11.372	4.290	85.012	0	-0.199	0.123	-0.	1.000	-103.	0.004	-90.
10.934	4.240	10.129	0	-0.141	1.000	0.	0.179	-98.	0.056	90.
10.548	4.190	24.242	0	-0.492	1.000	0.	0.450	-92.	0.097	90.
9.263	4.140	89.642	0	-0.023	0.006	0.	1.000	-89.	0.001	90.
9.032	4.090	89.935	0	-0.001	0.001	-0.	1.000	-84.	0.000	90.
8.876	4.040	89.977	0	-0.000	0.000	0.	1.000	-81.	0.000	90.
8.763	3.990	89.990	0	-0.000	0.000	0.	1.000	-79.	0.000	90.
8.677	3.940	89.995	0	-0.000	0.000	0.	1.000	-77.	0.000	90.
8.554	3.840	89.997	0	-0.000	0.000	0.	1.000	-75.	0.000	90.
18.587	4.540	85.233	0	-0.617	0.083	-0.	1.000	-99.	0.131	-91.
15.375	4.490	85.306	0	-2.362	0.082	0.	1.000	-105.	0.169	90.
12.897	4.440	84.107	0	-3.169	0.105	0.	1.000	70.	0.177	-90.
11.620	4.390	72.830	0	-2.060	1.000	0.	0.421	66.	0.104	-90.
11.347	4.340	12.438	0	-0.599	1.000	-0.	0.221	69.	0.022	-90.
11.125	4.290	40.565	0	-0.100	1.000	-0.	0.856	75.	0.026	90.
10.264	4.240	86.731	0	-0.068	0.022	0.	1.000	79.	0.003	90.
9.589	4.190	89.004	0	-0.111	0.017	-0.	1.000	85.	0.002	90.
7.846	4.140	22.076	0	-0.693	1.000	0.	0.406	88.	0.072	-90.
7.225	4.090	0.007	0	-0.002	1.000	0.	0.000	94.	0.217	-90.
7.000	4.040	0.001	0	-0.000	1.000	-0.	0.000	98.	0.281	-90.
6.784	3.990	0.000	0	-0.000	1.000	-0.	0.000	101.	0.332	-90.
6.351	3.940	0.000	0	-0.000	1.000	-0.	0.000	103.	0.533	-90.
5.636	3.840	0.000	0	-0.000	0.963	0.	0.000	95.	1.000	-90.

S3T010-60-60.1 FG 2G 3G 4G

PERIOD	PHVEL	XYANG		GPANG	UX	PHIX	UY	PHIY	UZ	PHIZ
176.838	4.140	0.149	0	-0.153	0.695	180.	0.002	-180.	1.000	-90.
118.261	4.090	1.720	0	-0.272	0.683	180.	0.021	-0.	1.000	-90.
92.723	4.040	2.363	0	-0.427	0.686	180.	0.034	-0.	1.000	-90.
75.173	3.990	3.411	0	-0.589	0.700	180.	0.042	-0.	1.000	-90.
59.201	3.940	3.372	0	-0.709	0.725	180.	0.043	0.	1.000	-90.
17.422	3.840	0.147	0	-0.055	0.832	180.	0.002	-0.	1.000	-90.
175.366	4.540	89.930	0	-0.320	0.001	180.	1.000	180.	0.029	90.
58.536	4.490	89.455	0	-1.552	0.010	180.	1.000	180.	0.012	90.
34.742	4.440	89.290	0	-1.694	0.012	180.	1.000	180.	0.004	-90.
21.494	4.390	89.641	0	-1.155	0.006	180.	1.000	-180.	0.007	-90.
16.145	4.340	28.902	0	-1.114	0.618	180.	0.341	0.	1.000	-90.
11.507	4.290	88.716	0	-0.120	0.022	180.	1.000	0.	0.002	90.
10.812	4.190	0.521	0	-0.489	1.000	180.	0.009	0.	0.369	-90.
10.483	4.140	0.183	0	-0.084	1.000	180.	0.003	-0.	0.099	-90.
10.159	4.090	0.071	0	-0.022	1.000	180.	0.001	-0.	0.113	-90.
9.806	4.040	0.028	0	-0.007	1.000	180.	0.000	0.	0.115	-90.
9.447	3.990	0.012	0	-0.003	1.000	180.	0.000	0.	0.105	-90.
9.124	3.940	0.005	0	-0.001	1.000	180.	0.000	0.	0.086	-90.
8.678	3.840	0.002	0	-0.000	1.000	180.	0.000	0.	0.047	-90.
28.429	4.540	56.877	0	-0.417	0.652	180.	1.000	180.	0.996	-90.
23.161	4.490	52.419	0	-0.704	0.683	180.	0.923	-180.	1.000	-90.
20.326	4.440	49.426	0	-0.878	0.694	180.	0.810	-180.	1.000	-90.
18.119	4.390	57.900	0	-1.051	0.627	180.	1.000	-180.	0.919	-90.
14.424	4.340	89.704	0	-0.449	0.005	180.	1.000	180.	0.013	-90.
11.077	4.290	11.623	0	-0.488	1.000	180.	0.206	180.	0.035	-90.
9.615	4.190	89.965	0	-0.012	0.001	180.	1.000	-180.	0.000	-90.
9.257	4.140	89.965	0	-0.004	0.001	180.	1.000	-180.	0.000	-90.
9.031	4.090	89.983	0	-0.002	0.000	180.	1.000	-180.	0.000	-90.
8.876	4.040	89.992	0	-0.001	0.000	180.	1.000	180.	0.000	-90.
8.763	3.990	89.995	0	-0.000	0.000	180.	1.000	180.	0.000	-90.
8.677	3.940	89.997	0	-0.000	0.000	180.	1.000	180.	0.000	-90.
8.554	3.840	89.999	0	-0.000	0.000	180.	1.000	180.	0.000	-90.
15.673	4.540	84.140	0	-0.914	0.103	180.	1.000	-0.	0.203	-90.
12.749	4.490	78.775	0	-1.031	0.190	180.	1.000	180.	0.237	90.
11.748	4.440	19.985	0	-0.359	1.000	180.	0.364	-180.	0.150	90.
11.482	4.390	7.829	0	-0.278	1.000	180.	0.139	180.	0.056	90.
11.284	4.340	5.722	0	-0.323	1.000	180.	0.100	-180.	0.006	90.

S3T110-60-89.9 FG 2G 3G 4G

PERIOD	PHVEL	XYANG		GPANG	UX	PHIX	UY	PHIY	UZ	PHIZ
169.910	4.140	2.644	0	-0.001	0.700	0.	0.032	90.	1.000	90.
110.952	4.090	4.986	0	-0.003	0.690	0.	0.060	90.	1.000	90.
85.569	4.040	5.918	0	-0.004	0.695	-0.	0.072	90.	1.000	90.
67.721	3.990	5.391	0	-0.004	0.712	0.	0.073	90.	1.000	90.
50.066	3.940	4.789	0	-0.004	0.747	0.	0.063	90.	1.000	90.
17.356	3.840	0.206	0	-0.000	0.830	0.	0.003	90.	1.000	90.
364.432	4.540	89.570	0	-0.000	0.000	0.	1.000	-90.	0.002	90.
121.114	4.490	88.623	0	-0.002	0.023	-0.	1.000	-90.	0.018	90.
76.237	4.440	87.902	0	-0.003	0.035	0.	1.000	-90.	0.039	90.
51.552	4.390	87.347	0	-0.004	0.046	0.	1.000	-90.	0.060	90.
33.870	4.340	86.576	0	-0.005	0.060	0.	1.000	-90.	0.081	90.
15.098	4.240	84.653	0	-0.003	0.093	0.	1.000	-90.	0.171	90.
10.487	4.140	1.471	0	-0.000	1.000	0.	0.026	90.	0.099	90.
10.157	4.090	0.238	0	-0.000	1.000	-0.	0.004	90.	0.113	90.
9.805	4.040	0.065	0	-0.000	1.000	-0.	0.001	90.	0.115	90.
9.446	3.990	0.022	0	-0.000	1.000	-0.	0.000	90.	0.105	90.
9.124	3.940	0.009	0	-0.000	1.000	0.	0.000	90.	0.086	90.
8.678	3.840	0.003	0	-0.000	1.000	-0.	0.000	90.	0.047	90.
27.573	4.540	58.752	0	-0.001	0.656	0.	0.803	90.	1.000	90.
22.507	4.490	62.661	0	-0.004	0.517	0.	1.000	90.	0.758	90.
19.667	4.440	70.657	0	-0.005	0.351	0.	1.000	90.	0.511	90.
17.251	4.390	78.159	0	-0.007	0.210	0.	1.000	90.	0.320	90.
14.691	4.340	86.211	0	-0.009	0.066	0.	1.000	90.	0.151	90.
10.970	4.240	15.725	0	-0.003	1.000	-0.	0.244	-90.	0.050	90.
9.271	4.140	89.208	0	-0.001	0.014	-0.	1.000	-90.	0.001	90.
9.032	4.090	89.034	0	-0.000	0.001	0.	1.000	-90.	0.000	90.
8.876	4.040	89.920	0	-0.000	0.000	0.	1.000	-90.	0.000	90.
8.763	3.990	89.991	0	-0.000	0.000	0.	1.000	-90.	0.000	90.
8.677	3.940	89.996	0	-0.000	0.000	0.	1.000	-90.	0.000	90.
8.554	3.840	89.998	0	-0.000	0.000	0.	1.000	-90.	0.000	90.
19.994	4.540	86.434	0	-0.003	0.062	-0.	1.000	-90.	0.004	90.
17.518	4.490	86.551	0	-0.006	0.060	0.	1.000	-90.	0.005	90.
15.547	4.440	87.467	0	-0.008	0.044	-0.	1.000	-90.	0.084	90.
13.692	4.390	89.638	0	-0.010	0.006	-0.	1.000	-90.	0.065	90.
11.971	4.340	81.178	0	-0.012	0.155	0.	1.000	90.	0.044	-90.
10.239	4.240	87.867	0	-0.001	0.037	0.	1.000	90.	0.004	90.
8.626	4.140	58.737	0	-0.003	0.607	-0.	1.000	90.	0.052	90.
7.228	4.090	0.009	0	-0.000	1.000	-0.	0.000	90.	0.216	-90.
7.061	4.040	0.001	0	-0.000	1.000	-0.	0.000	90.	0.281	-90.
6.704	3.990	0.000	0	-0.000	1.000	0.	0.000	90.	0.382	-90.
6.351	3.940	0.000	0	-0.000	1.000	0.	0.000	91.	0.533	-90.
5.636	3.340	0.000	0	-0.000	0.963	0.	0.000	92.	1.000	-90.

S3T010-60-90.1 FG 2G 3G 4G

PERIOD	PHVEL	XYANG		GPANG	UX	PHIX	UY	PHIY	UZ	PHIZ
183.397	4.140	0.003	0	0.000	0.696	180.	0.000	180.	1.000	-90.
121.913	4.090	0.007	0	0.001	0.680	180.	0.000	180.	1.000	-90.
96.021	4.040	0.010	0	0.002	0.682	180.	0.000	180.	1.000	-90.
78.617	3.990	0.010	0	0.002	0.693	180.	0.000	180.	1.000	-90.
63.417	3.940	0.010	0	0.002	0.715	180.	0.000	180.	1.000	-90.
17.470	3.840	0.000	0	0.000	0.833	180.	0.000	180.	1.000	-90.
328.576	4.540	90.000	0	0.002	0.000	180.	1.000	-0.	0.000	90.
109.155	4.490	89.999	0	0.011	0.000	180.	1.000	-0.	0.000	90.
68.371	4.440	89.996	0	0.018	0.000	180.	1.000	-0.	0.000	-90.
45.240	4.390	89.997	0	0.022	0.000	180.	1.000	0.	0.000	-90.
27.657	4.340	89.996	0	0.025	0.000	180.	1.000	-0.	0.000	-90.
13.127	4.240	0.486	0	0.005	0.206	180.	0.002	180.	1.000	90.
10.499	4.140	0.081	0	0.001	1.000	180.	0.000	-180.	0.092	-90.
10.167	4.090	0.000	0	0.000	1.000	180.	0.000	180.	0.113	-90.
9.807	4.040	0.000	0	0.000	1.000	180.	0.000	180.	0.115	-90.
9.447	3.990	0.000	0	0.000	1.000	180.	0.000	180.	0.105	-90.
9.124	3.940	0.000	0	0.000	1.000	180.	0.000	180.	0.086	-90.
8.678	3.840	0.000	0	0.000	1.000	180.	0.000	180.	0.047	-90.
29.970	4.540	0.130	0	0.001	0.643	180.	0.001	0.	1.000	-90.
24.132	4.490	0.125	0	0.002	0.680	180.	0.001	0.	1.000	-90.
21.184	4.440	0.101	0	0.003	0.696	180.	0.001	0.	1.000	-90.
18.988	4.390	0.072	0	0.004	0.697	180.	0.001	0.	1.000	-90.
17.058	4.340	0.027	0	0.004	0.667	180.	0.000	0.	1.000	-90.
10.832	4.240	0.016	0	0.002	1.000	180.	0.000	-180.	0.063	-90.
9.259	4.140	90.000	0	0.000	0.000	180.	1.000	0.	0.000	-90.
9.031	4.090	90.000	0	0.000	0.000	180.	1.000	0.	0.000	91.
8.876	4.040	90.000	0	0.000	0.000	180.	1.000	0.	0.000	-90.
8.763	3.990	90.000	0	0.000	0.000	180.	1.000	-0.	0.000	-90.
8.677	3.940	90.000	0	0.000	0.000	180.	1.000	-0.	0.000	-90.
8.554	3.840	90.000	0	0.000	0.000	180.	1.000	-0.	0.000	-90.
20.267	4.540	89.995	0	0.010	0.000	180.	1.000	180.	0.000	-90.
17.553	4.490	89.996	0	0.022	0.000	180.	1.000	180.	0.000	-90.
15.504	4.440	89.998	0	0.026	0.000	180.	1.000	180.	0.000	-90.
13.639	4.390	90.000	0	0.028	0.000	180.	1.000	180.	0.000	-90.
11.936	4.340	89.994	0	0.032	0.000	180.	1.000	-0.	0.000	90.
10.380	4.240	89.997	0	0.011	0.000	180.	1.000	0.	0.000	-90.

S4X110-60--90.0 FG 2G 3G 4G

PERIOD	PHVEL	XYANG		GPANG	UX	PHIX	UY	PHIY	UZ	PHIZ
156.683	4.140	0.608	0	0.000	0.681	0.	0.007	-90.	1.000	90.
107.397	4.090	1.337	0	0.000	0.685	-0.	0.016	-90.	1.000	90.
81.767	4.040	1.995	0	0.000	0.704	-0.	0.025	-90.	1.000	90.
59.080	3.990	2.842	0	0.000	0.745	0.	0.037	-90.	1.000	90.
15.354	3.890	7.212	0	0.000	0.731	0.	0.099	-90.	1.000	90.
0000000000000000000000000000000000000000000000000000000000000000000000000000000000000000000000000000000000										
272.256	4.540	89.637	0	0.000	0.006	0.	1.000	90.	0.001	90.
84.569	4.490	88.833	0	0.000	0.020	-0.	1.000	90.	0.011	90.
47.900	4.440	87.934	0	0.000	0.036	0.	1.000	90.	0.027	90.
28.793	4.390	86.296	0	0.000	0.065	-0.	1.000	90.	0.059	90.
19.529	4.340	83.792	0	0.000	0.109	-0.	1.000	90.	0.110	90.
14.732	4.290	84.253	0	0.000	0.101	-0.	1.000	90.	0.143	90.
11.316	4.240	65.300	0	0.000	0.460	0.	1.000	-90.	0.011	-90.
8.958	4.190	31.756	0	0.000	0.145	-0.	1.000	90.	0.010	90.
8.738	4.090	80.039	0	0.000	0.176	-0.	1.000	90.	0.008	90.
000000000000000000000000000000000000000000000000000000000000000000000000000000000000000000000000000000000										
26.289	4.540	14.969	0	-0.000	0.744	0.	0.199	-90.	1.000	90.
21.127	4.490	21.226	0	0.000	0.773	0.	0.300	-90.	1.000	90.
18.445	4.440	25.008	0	0.000	0.770	0.	0.359	-90.	1.000	90.
16.235	4.390	29.739	0	0.000	0.711	0.	0.406	-90.	1.000	90.
14.142	4.340	47.491	0	0.000	0.414	-0.	0.452	-90.	1.000	90.
11.997	4.290	4.469	0	0.000	1.000	-0.	0.078	90.	0.321	-90.
10.477	4.240	10.847	0	0.000	1.000	0.	0.192	-90.	0.102	90.
8.227	4.190	67.306	0	0.000	0.418	-0.	1.000	-90.	0.003	-90.
6.622	4.090	5.752	0	0.000	1.000	0.	0.101	-90.	0.412	-90.
000000000000000000000000000000000000000000000000000000000000000000000000000000000000000000000000000000000										
15.913	4.540	87.269	0	0.000	0.048	0.	1.000	90.	0.042	90.
13.327	4.490	88.986	0	0.000	0.013	0.	1.000	90.	0.038	90.
11.673	4.440	78.704	0	0.000	0.200	0.	1.000	-90.	0.026	-90.
11.153	4.390	38.587	0	-0.000	1.000	0.	0.798	-90.	0.026	90.
000000000000000000000000000000000000000000000000000000000000000000000000000000000000000000000000000000000										
000000000000000000000000000000000000000000000000000000000000000000000000000000000000000000000000000000000										

SoT110-60--90.0 FG 2G 3G 4G

PERIOD	PHVEL	XYANG		GPANG	UX	PHIX	UY	PHIY	UZ	PHIZ
176.740	4.140	4.831	0	0.000	0.690	0.	0.058	-90.	1.000	90.
119.907	4.090	7.921	0	0.000	0.682	0.	0.095	-90.	1.000	90.
93.665	4.040	9.200	0	0.000	0.687	0.	0.111	-90.	1.000	90.
75.279	3.990	9.266	0	0.000	0.702	0.	0.114	-90.	1.000	90.
58.233	3.940	8.145	0	0.000	0.729	-0.	0.104	-90.	1.000	90.
17.410	3.840	0.354	0	0.000	0.831	-0.	0.005	-90.	1.000	90.
392.164	4.540	89.214	0	0.000	0.014	0.	1.000	90.	0.004	90.
130.545	4.490	87.039	0	0.000	0.041	-0.	1.000	90.	0.034	90.
82.518	4.440	86.455	0	0.000	0.062	-0.	1.000	90.	0.071	90.
56.464	4.390	85.403	0	0.000	0.080	-0.	1.000	90.	0.105	90.
38.573	4.340	84.082	0	0.000	0.104	-0.	1.000	90.	0.140	90.
26.369	4.290	81.193	0	0.000	0.155	-0.	1.000	90.	0.206	90.
20.340	4.240	76.092	0	0.000	0.248	-0.	1.000	90.	0.327	90.
16.604	4.190	72.799	0	-0.000	0.310	0.	1.000	90.	0.443	90.
13.950	4.140	82.043	0	-0.000	0.140	0.	1.000	90.	0.434	90.
11.459	4.090	43.130	0	-0.000	1.000	-0.	0.937	-90.	0.082	-90.
9.813	4.040	0.501	0	-0.000	1.000	-0.	0.009	-90.	0.115	90.
28.387	4.540	59.294	0	0.000	0.594	-0.	1.000	-90.	0.903	90.
23.600	4.490	69.365	0	0.000	0.377	0.	1.000	-90.	0.551	90.
20.771	4.440	75.361	0	0.000	0.261	0.	1.000	-90.	0.376	90.
18.120	4.390	80.832	0	0.000	0.160	0.	1.000	-90.	0.235	90.
15.145	4.340	86.866	0	0.000	0.055	0.	1.000	-90.	0.106	90.
11.240	4.290	85.576	0	0.000	0.077	-0.	1.000	90.	0.017	-90.
10.974	4.240	7.111	0	0.000	1.000	-0.	0.125	90.	0.049	90.
10.727	4.190	1.546	0	0.000	1.000	0.	0.027	90.	0.080	90.
10.453	4.140	0.756	0	0.000	1.000	0.	0.013	90.	0.101	90.
10.133	4.090	0.774	0	-0.000	1.000	0.	0.014	90.	0.114	90.
8.949	4.040	76.796	0	-0.000	0.235	0.	1.000	90.	0.018	90.
20.042	4.540	85.328	0	0.000	0.082	0.	1.000	90.	0.123	90.
17.465	4.490	85.369	0	0.000	0.081	0.	1.000	90.	0.128	90.
15.465	4.440	86.624	0	0.000	0.059	0.	1.000	90.	0.114	90.
13.562	4.390	89.358	0	0.000	0.002	0.	1.000	90.	0.089	90.
11.928	4.340	72.520	0	0.000	0.315	0.	1.000	-90.	0.064	-90.
11.191	4.290	39.989	0	0.000	1.000	-0.	0.839	-90.	0.012	90.
10.270	4.240	88.975	0	0.000	0.018	0.	1.000	-90.	0.002	90.
9.613	4.190	89.333	0	0.000	0.003	-0.	1.000	-90.	0.000	90.
9.257	4.140	89.922	0	0.000	0.001	0.	1.000	-90.	0.000	90.
9.031	4.090	89.931	0	0.000	0.001	0.	1.000	-90.	0.000	90.
8.868	4.040	83.642	0	-0.000	0.024	0.	1.000	-90.	0.002	90.

A P P E N D I X II

The significance of isotropic inversion of anisotropic surface-wave dispersion

Paper to be published in Geophysical Journal of the Royal astronomical Society (in press)

Geophys. J. R. astr. Soc. (1978) 55,

PROOF

The significance of isotropic inversion of anisotropic surface-wave dispersion

S. C. Kirkwood *Department of Geophysics, University of Edinburgh, Edinburgh EH9 3JZ*

Received 1978 February 28

Summary. The limitations of isotropic modelling in the inversion of anisotropic surface-wave phase velocities are examined. Inversion of synthetic dispersion data for some model ocean-basin structures is used to demonstrate that isotropic inversions can give inaccurate and misleading estimates of upper-mantle properties when anisotropy is present.

1 Introduction

The dispersion of fundamental-mode Rayleigh and Love waves has been widely used to determine average seismic velocities in the Earth's crust and upper mantle. The observed dispersion, either phase or group velocity, is compared with that predicted by models using curve-fitting or, more recently, linear-inversion techniques (e.g. McEvilly 1964; Forsyth 1975). It is not yet practicable to use anisotropic models with these techniques as calculations would require very large amounts of computer time. In several studies (e.g. Schule & Knopoff 1977; Forsyth 1975; McEvilly 1964), anisotropic structures have been inferred from inversions using isotropic modelling. Schlue & Knopoff studied waves crossing the Pacific Basin and found that different velocity profiles were required to satisfy Rayleigh-wave and Love-wave data, but no azimuthal variation of velocity was resolved. Forsyth found, in waves crossing the Nazca plate, both a 2 per cent azimuthal variation of Rayleigh-wave phase velocity and a discrepancy between the models required to fit the Rayleigh and Love data.

The use of isotropic models in inversion of observations from an anisotropic earth is inappropriate (Crampin 1976). This paper discusses the limitations of isotropic models. An inversion of synthetic dispersion data, simulating observations of mixed oceanic paths is presented, and the accuracies of the results are examined.

2 Limitations of isotropic models

In an isotropic earth the dispersion of Rayleigh waves depends on the distribution of velocities of longitudinal waves, α, and vertically-polarized shear waves, β_{SV}, and on density, within the Earth. The dispersion of Love waves is most sensitive to the velocities of

horizontally-polarized shear waves, β_{SH}. However, in an anisotropic material, energy is distributed among three, independent body waves with mutually orthogonal polarizations: a quasi-longitudinal wave, qP, and two quasi-shear waves, qSH and qSV, according to the isotropic polarization which they most resemble. These three waves have velocities which vary with direction of propagation and have polarizations which are intermediate between P, SH and SV, but which, for each direction of propagation, are fixed relative to the symmetry directions of the anisotropic medium (Crampin 1977). Except for propagation in isolated symmetry directions, these body waves do not have pure P, SH or SV polarization. In a layered structure with an anisotropic layer, boundary conditions at interfaces require that P, SH and SV waves must all coexist in the isotropic layers. Correspondingly, any surface-wave mode in an anisotropic structure generally has coupled sagittal and transverse particle-motion. These generalized modes may have polarizations which resemble isotropic Rayleigh or Love modes and, for convenience of notation, are termed Rayleigh-type or Love-type. Numerical examination of reasonable models of ocean-basin structure indicates that the dispersion and near-surface particle-motion of the first and second generalized modes, FG and 2G, respectively, are similar to those of the isotropic fundamental-Rayleigh and fundamental-Love modes respectively (Kirkwood 1977). At depth, however, in both FG and 2G, the polarization of particle motion is intermediate between Love-type and Rayleigh-type. A significant fraction of the energy carried by the FG wave, for example, is associated with transverse particle motion. In the same way, a Love-type mode, 2G, which samples mainly β_{SH} in layers near the surface, is sensitive to α, β_{SH}, and β_{SV} (or α_{qP}, β_{qSH}, β_{qSV}, where appropriate) in all the layers, to a degree which depends on the nature of the anisotropy, the distribution of velocities with depth and on the period of the wave. It is, therefore, difficult to make detailed general statements about the effects of anisotropy on dispersion and a numerical approach is required.

3 Anisotropic phase velocity data

The calculated phase-velocity dispersions of FG and 2G (and in one case fundamental Rayleigh and Love), for five models of ocean-basin structure, form the synthetic data used in the inversions. Model parameters are given in Table 1. These are simple, six-layer models

Table 1. Parameters for five models of ocean-basin structure. Miller indices are referred to a cubic lattic whose axes are parallel to those of the true orthorhombic lattices.

		THICKNESS km	P-WAVE VELOCITY km/s	S-WAVE VELOCITY km/s	DENSITY kg/m^{3}x10^3
CRUSTAL MODEL :		4.5	1.500	0.000	1.0
		0.5	2.016	0.251	1.9
		6.0	6.600	3.800	2.9
UPPER MANTLE :	IS103	60.0	8.100	4.400	3.3
		60.0	7.172	4.098	3.4
	S1X010	60.0	(010)-cut TOL2080		
		60.0	7.172	4.098	3.4
	S1X101	60.0	(101)-cut TOL2080		
		60.0	7.172	4.098	3.4
	S1Y011	60.0	8.100	4.400	3.3
		60.0	(011)-cut SSOL2080		
	S3T010	60.0	8.100	4.400	3.3
		60.0	(010)-cut ELOWVTOL		
MANTLE BELOW 131km :			8.251	4.548	3.5

Table 2. Elastic constants of anisotropic layers used in ocean-basin models.

	TOL2080	ELOWVTOL	SSOL2080
CONSTITUENTS	20 transversely-isotropic OLIVINE 80 α=7.80 β=4.57	50 transversely-isotropic OLIVINE 50 α=5.67 β=3.75	20 OLIVINE 80 α=7.47 β=4.10
DENSITY	3.324	3.324	3.385
C(1111)	225.487	215.175	217.120
C(2222)	205.237	164.925	191.120
C(3333)	205.237	164.925	202.120
C(1122)	66.526	52.225	57.480
C(2233)	71.025	56.725	61.280
C(3311)	66.526	52.225	61.480
C(1212)	70.805	57.800	61.540
C(2323)	67.105	54.100	59.320
C(1313)	70.805	57.800	61.880

based on Forsyth (1975). One model has only isotropic layers (IS103), two have an anisotropic low-velocity channel at 71–131 km depth (S3T010 and S1Y011), and two have an anisotropic lid at 11–71 km depth, overlying an isotropic channel (S1X010 and S1X101). The anisotropic layers are formed by mixing orthorhombic olivine with isotropic materials in order to derive materials with seismic velocities similar to those found by Forsyth (1975), and with shear-wave velocity anisotropy of 4–8 per cent. The elastic constants of these materials are shown in Table 2 and the velocities of body waves through them are illustrated by Fig. 1.

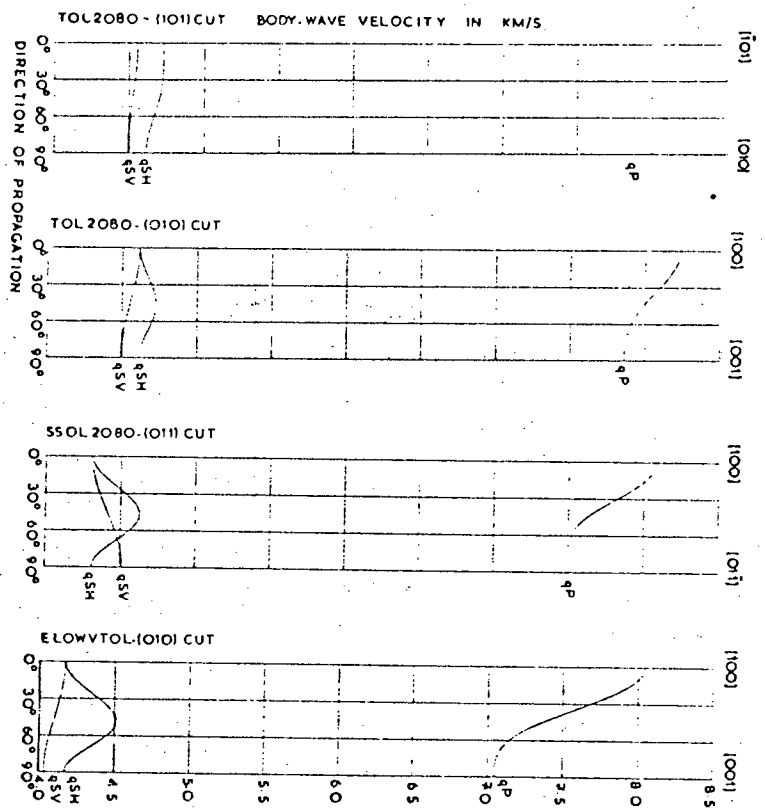

Figure 1. Body-wave velocities in anisotropic media.

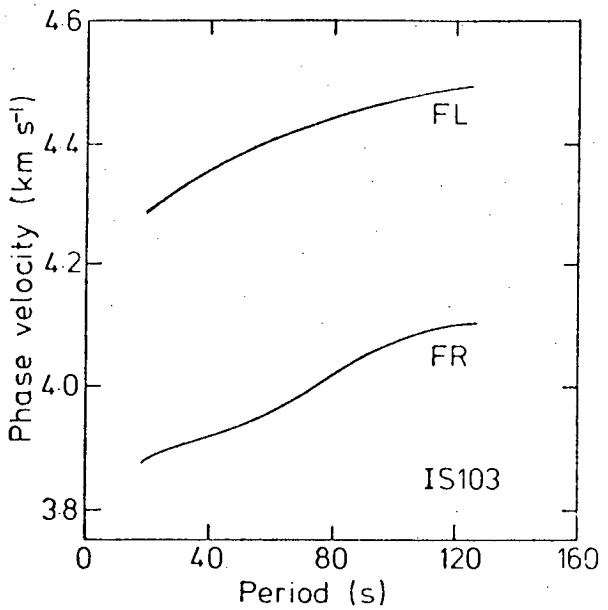

Figure 2. Model IS1O3 phase-velocity dispersion.

It has been suggested by several authors (e.g. Francis 1969) that a transversely isotropic alignment, with a horizontal symmetry axis, due to preferred orientation of orthorhombic olivine, is a likely configuration for anisotropy in the upper mantle. This is modelled by S1X010 and S2T010. The possibility of other configurations cannot be excluded and models S1X101 and S1Y011, having only one (vertical) plane of symmetry, represent other possible alignments of olivine or pyroxene. Phase velocities for anisotropic models are

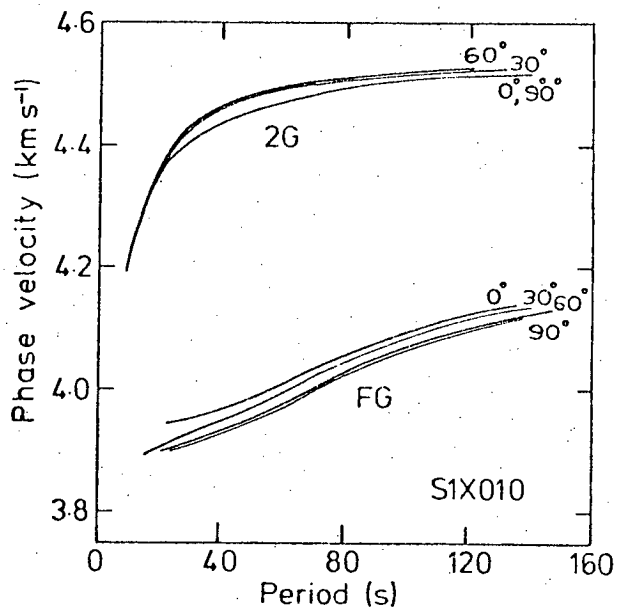

Figure 3. Model S1X010 phase-velocity dispersion for azimuths at 30° intervals between [100] and [011].

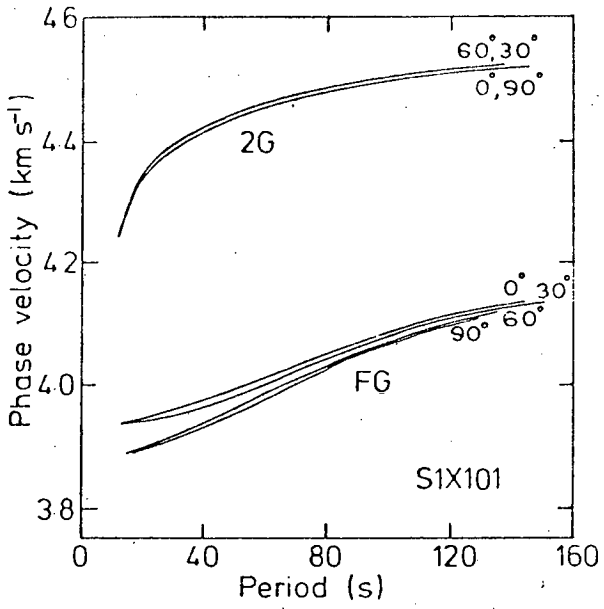

Figure 4. Model S1X101 phase-velocity dispersion for azimuths at 30° intervals between [$\bar{1}$01] and [010].

calculated using the program of Crampin & King (1977), modified to admit a liquid layer at the surface. Isotropic dispersions are found using the PV7 program of Dorman (1959, 1962). The anisotropic phase-velocities are for plane-layered models as no corrections for earth-curvature have been developed. Isotropic dispersions have also been calculated for a flat earth. Both procedures give compatible results for isotropic structures. Dispersion curves, for four different directions of propagation, are shown in Figs 2–6.

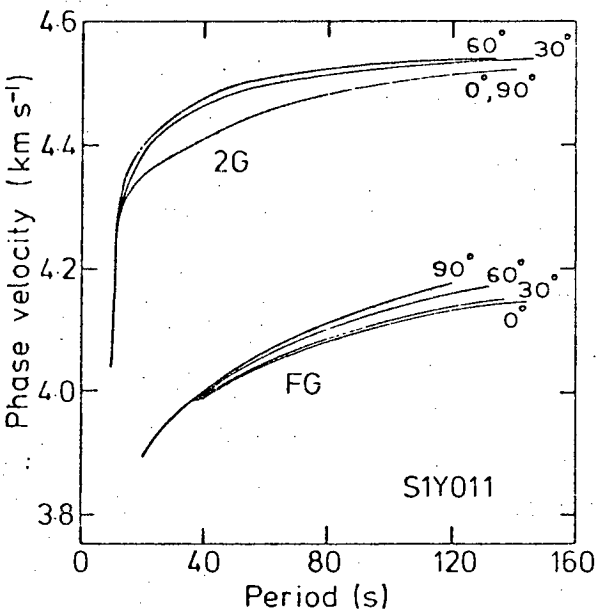

Figure 5. Model S1Y011 phase-velocity dispersion for azimuths at 30° intervals between [100] and [01$\bar{1}$].

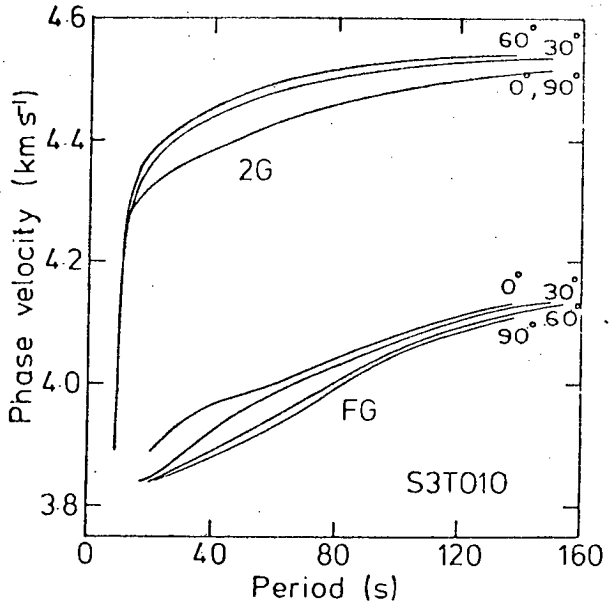

Figure 6. Model S3T010 phase-velocity dispersion for azimuths at 30° intervals between [100] and [001].

In the anisotropic models, the azimuthal variation of phase velocity varies with period, is never more than 0.1 km/s (about 2 per cent) and is usually much less. It is difficult to resolve such a small velocity variation in surface waves which have travelled long distances over the real Earth. Surface waves travelling long oceanic paths will cross many isochrons and so areas of possibly differing anisotropic alignments. When no azimuthal dependance of velocity can be resolved, observations will indicate some average over several directions of propagation (as in Schlue & Knopoff 1977). In this paper azimuthal averages are estimated for each anisotropic model.

The variation of velocity with azimuth at a given period can be expressed as a Fourier series which, for orthorhombic symmetry, has the form:

$$C(\theta, T) = C(T) + \sum_{n=1}^{\infty} A_n(T) \cos 2n\theta \qquad (1)$$

where

T = period
θ = angle between direction of propagation and a direction of sagittal symmetry
$C(T)$ = average phase velocity over all θ for period T
$A_n(T)$ = are constants for period (T)

Smith & Dahlen (1973) showed that, for weakly anisotropic media, only the constant term and terms in 2θ and 4θ are required to describe the Rayleigh or Love-type phase velocities. In this study, dispersions for four values of θ were calculated (θ = 0, 30, 60, 90°) so that the fourth coefficient in equation (1), the term in 6θ, could be resolved. For all models, and all periods, $|A_3(T)|$ is an order of magnitude less than $|A_1(T)| + |A_2(T)|$ and higher-order terms were assumed negligible. The value for $C(T)$ found from the four values of $C(\theta, T)$ can then be taken as an estimate of the azimuthal average. The value of $C(T)$ for the models used are shown in Table 3.

Fundamental Mode (Rayleigh-Type)

MODEL	PHASE VELOCITY (kms^{-1})					
	120s	100s	80s	60s	40s	20s
IS1O3	4.10	4.07	4.02	3.96	3.92	3.88
S1X1O1	4.11	4.08	4.04	3.99	3.96	3.92
S1XO1O	4.11	4.08	4.04	3.99	3.95	3.91
S1YO11	4.15	4.12	4.10	4.06	3.99	3.89
S3TO1O	4.10	4.06	4.02	3.96	3.92	3.86

Second Generalised Mode (Love-Type)

MODEL	PHASE VELOCITY (kms^{-1})					
	120s	1COs	80s	60s	40s	20s
IS1O3	4.49	4.47	4.44	4.40	4.35	4.29
S1X1O1	4.51	4.50	4.49	4.46	4.42	4.34
S1XO1O	4.52	4.51	4.50	4.48	4.45	4.36
S1YO11	4.53	4.52	4.50	4.48	4.45	4.38
S3TO1O	4.52	4.50	4.48	4.46	4.42	4.35

Table 3. Dispersion data: azimuthal averages for anisotropic models, values calculated by program based on Dorman PV7 for IS1O3.

4 Inversion method

A grid of isotropic models is set up for comparison with the four anisotropic models and IS1O3. Since the structures of the anisotropic models and IS1O3 are known, only a small number of isotropic models with similar structures need be considered. It is well known that Rayleigh phase velocities are an order of magnitude less sensitive to variations in P-wave velocity than to variations in shear-wave velocity so α is held constant across the grid. Although Rayleigh phase-velocities are also sensitive to density this parameter is not usually determined by inversion. If an attempt is made to resolve both shear velocities and densities, large uncertainties in densities result (Schlue & Knopoff 1977). Therefore, as in the surface-wave studies cited above, density is here held constant. The only parameters which vary across the grid are the shear velocities in the lid and low-velocity zone which are incremented in steps of 0.05 km/s. The isotropic models are otherwise identical to IS1O3.

The dispersion of an anisotropic mode (or IS1O3 mode) is compared with that calculated for the corresponding mode in each model of the grid. Anisotropic FG modes are compared with isotropic fundamental Rayleigh, 2G with fundamental Love. The closeness of fit is calculated for each point:

$$R^2 = \sum_{n=1}^{6} (C_{en} - C_{on})^2 \times 10^4 \qquad (2)$$

where

C_{en} = phase velocity in km/s, at period 20 n s, for the isotropic mode
C_{on} = phase velocity in km/s, at period 20 n s, for the anisotropic (or IS1O3) mode.

The variation of R^2 over the grid is illustrated by contour plots, as shown in Figs 7(a) to (e), where the lowest values of R^2 occur for the isotropic models which best fit the anisotropic (or IS1O3) data. Additional isotropic models were interpolated between those of the basic grid, where necessary, to determine whether contours form separate closed loops or merely pinch together.

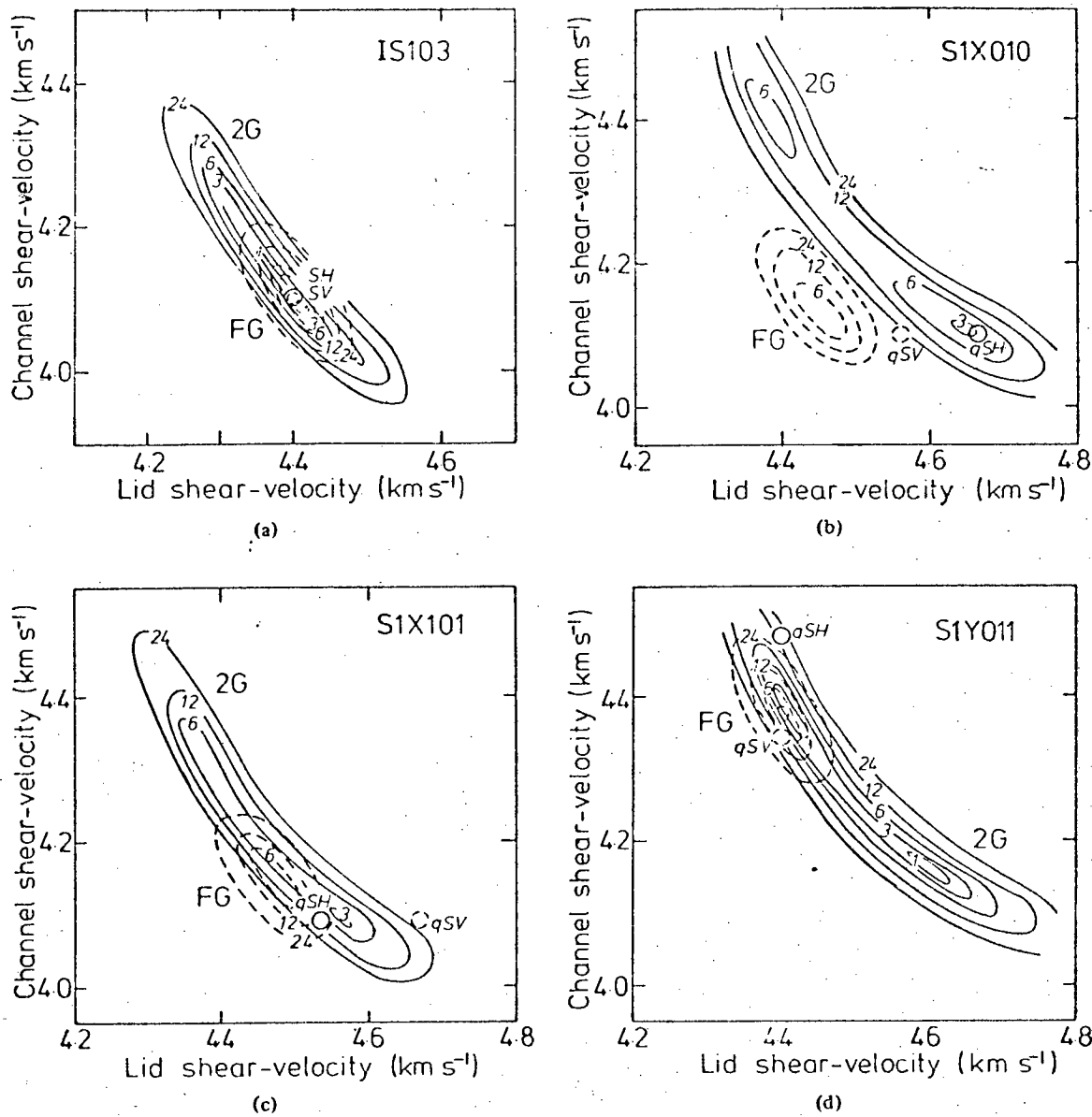

Figure 7. R^2 contour plots: dashed lines for Rayleigh-type mode, solid lines for Love-type mode. Minima of R^2 correspond to parameters which give the closest fit to surface-wave dispersion. (a) model IS103, (b) model S1X010, (c) model S1X101, (d) model S1Y011, (e) model S3T010.

5 Interpretation of contour plots

The isotropic models which give the lowest values of R^2, separately for each mode, are the best solutions, but any model which yields R^2 less than the error in the anisotropic data is an acceptable solution. The anisotropic dispersion curves (Figs 2–6) are derived from computations of period for a discrete series of fixed phase velocities, generally at intervals of 0.05 km/s. These periods can be computed to only three decimal places because of rounding errors in the computations. Interpolation to particular periods must be made by curve

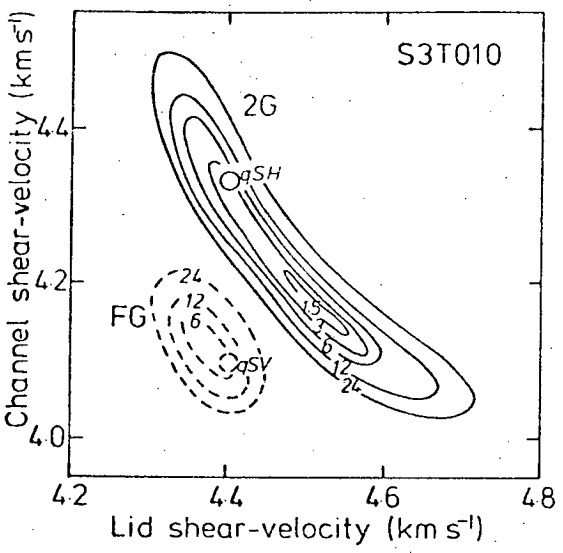

Figure 7(e)

fitting and the phase velocities so found are then averaged according to equation (1). The azimuthal-average phase-velocities are then accurate to about ± 0.005 km/s. A further source of error is the discrepancy in *P*-wave velocities and densities between anisotropic and isotropic models.

In the isotropic models, *P*-wave velocities and densities were fixed at 8.10 km/s and 3.3×10^3 kg m^{-3} in the lid and at 7.18 km/s and 3.4×10^3 kg m^{-3} in the low-velocity channel. The densities and average *qP* velocities in the anisotropic models differ slightly from these values. For example, in model S3T010 the average values of *qP* velocity and density in the low-velocity channel are 7.55 km/s and 3.324×10^3 kg m^{-3}. It would be unreasonable to expect a close fit to the S3T010 dispersion even for an isotropic model with shear velocities close to the average values for S3T010. By comparing, with IS1O3, similar models with a *P*-velocity of 7.5 km/s or a density of 3.325×10^3 kg m^{-3} in the low-velocity channel, the effect of these parameters on phase velocity can be estimated. In the period range of interest, the increase in *P* velocity of 0.32 km/s leads to an increase in Rayleigh phase-velocity of just less than 0.005 km/s. The decrease in density of 75 kg m^{-3} gives a decrease in Rayleigh phase-velocities of, on average, 0.012 km/s and a decrease in Love phase velocities of about 0.004 km/s. Combining this with the possible error in the estimates of anisotropic phase-velocities of ± 0.005 km/s, it can be seen that any isotropic model whose Rayleigh phase-velocities lie between 0.002 and 0.012 km/s less than those for S3T010 should be considered as fitting that data. The inversion method is such that any isotropic model with phase velocities within ± 0.012 km/s of those for S3T010 is considered to satisfy the data. The conclusions drawn from this study are not affected by this approximation.

The parameter R^2, defined by equation (2), is simply the sum of squares of the differences between isotropic and anisotropic phase velocities. A maximum difference at each period of 0.012 km/s corresponds to a maximum value for R^2 of 9. A fit to S3T010 for Rayleigh waves is therefore defined by $R^2 < 9$, and for Love waves by $R^2 < 5$. For all the other anisotropic models, densities are closer to the fixed values and, for Love waves, $R^2 < 2$ is required. Consideration of the appropriate *qP* velocities and densities gives the

requirement for Rayleigh waves of $R^2 \leq 9$, for S1Y011, $R^2 \leq 2$ for S1X101 and $R^2 \leq 7$ for S1X010.

6 Results of inversions

Given the above conditions, all inversions have found isotropic models with dispersions which fit the Rayleigh-type models. For two of the models, S1X010 and S1X101, there are apparently no models to fit the Love-type modes, as the lowest contour is $R^2 = 3$. A discrepancy between isotropic and anisotropic dispersion, which is larger than the errors in the data, must be allowed for acceptable isotropic models to be found. In the inversion of the isotropic model IS1O3, Fig. 7(a), the best fit to the Love mode is found for models in the middle of a diagonal zone of almost-acceptable models. For all the anisotropic models, 7(a) to (e), that diagonal zone is longer and the closest fit is found for isotropic models at one or both ends of the zone. This means that, although the solutions require the presence of anisotropy, in that different isotropic models are required to fit FG and 2G modes, it is not possible to determine whether anisotropy is confined to the low-velocity channel or to the lid. Where it is possible to make some distinction, the result may be misleading, for example, for model S3T010, Fig. 7(e), the data are best satisfied by models with an isotropic channel, $\beta = 4.15$ km/s and an anisotropic lid, $\beta_{qSH} = 4.50$ km/s and $\beta_{qSV} = 4.35$ km/s. In fact, in S3T010 it is the channel which is anisotropic. Even if larger values of R^2 are admitted such misinterpretation could still occur.

Consider model S1X010, which has an anisotropic lid, and the contours for R^2 shown in Fig. 7(b). Acceptable models might be defined as those for which R^2 is less than 6, and which are closest to a starting model with an isotropic lid in which $\beta = 4.4$ km/s and an anisotropic channel in which $\beta_{qSH} = 4.4$ km/s and $\beta_{qSV} = 4.1$ km/s. There are closed areas of acceptable models close to this starting model, so an anisotropic channel would be erraneously confirmed.

7 Discussion of solutions

It is frequently assumed that models found by isotropic inversion indicate the true body-wave velocities in any isotropic layers and some average of body-wave velocities in the anisotropic layer, allowing for different values for β_{SH} and β_{SV}. This might be expected to be particularly true at long periods, where the wavelength of surface waves is much greater than any likely layer thickness and the associated body-wave decompositions in the anisotropic layer will be travelling nearly horizontally. Inversion of FG and 2G would then indicate the average velocities in an anisotropic layer of β_{qSV} and β_{qSH} waves, respectively, travelling in a horizontal plane, provided the polarizations of these waves are close to pure SV or SH. The quasi-shear velocities for the models used in this study can be found from Fig. 1 and Table 1 and their locations in parameter-space are marked on Fig. 7(a) to (e).

The acceptable models found by the inversion procedure discussed in Section 6 do not indicate the same quasi-shear velocities. If a less exact fit is allowed, say $R^2 \leq 12$, then the true values of β in the isotropic layers can occur in an acceptable isotropic model, as can the average value for β_{qSH} in the anisotropic layer. This is true for all the data inverted. However, even if one admits yet larger values of R^2, say $R^2 \leq 24$, then the expected values for β_{qSV} in the models with an anisotropic lid (Fig. 7(b) and (c)) are not found in any acceptable isotropic model.

It seems, then, that isotropic inversion can indicate the true velocities in the isotropic layers adjoining anisotropic layers, only if low resolution is accepted, no matter how good the data. It cannot always give a useful estimate of velocity in any anisotropic layer.

Forsyth (1975) was able to resolve azimuthal anisotropy so that his data do not correspond to azimuthal averages. However, an average FG dispersion is nearly the same as the dispersion for $\theta = 45^\circ$ and an average 2G dispersion resembles the 2G dispersion for $\theta = 30$ or 60° (equation (1)). The body-wave averages are similarly related to body-wave velocities in particular directions. So remarks in this section, although derived from inversion of azimuthal averages, are equally applicable to inversion of dispersion for those particular directions for FG and 2G modes.

8 Conclusions

When inverting data from an anisotropic earth, isotropic inversion can indicate a higher resolution than is really valid. This has to important consequences:

(a) isotropic layers may be labelled as anisotropic and vice-versa,
(b) in restricted inversions, the result is likely to depend heavily on the choice of starting model.

This means that upper-mantle shear velocities found for Forsyth (1975) and Schlue & Knopoff (1977) cannot be considered an accurate guide to the elastic constants in that zone. In addition, it will not be possible to determine whether anisotropy is confined to one depth range, using only isotropic modelling.

Forsyth (1975) recognized such ambiguity in his inversion but Schlue & Knopoff's (1977) results suggested anisotropy confined to the low-velocity zone. However, in neither work has allowance been made for the possibly large, possibly systematic error inherent in isotropic inversion so that the uncertainty in the resultant upper-mantle models has been under estimated. Inversions will be more useful if a wider range of models, either isotropic or anisotropic, is considered. Monte Carlo methods may, therefore, be more appropriate than linear inversion techniques. If isotropic models are used, even those giving only a poor fit to the data should not be rejected. It is likely that the ambiguity mentioned above will not be resolved by the use of anisotropic modelling in phase or group-velocity inversions, so information must be sought in other ways. For example, studies of surface-wave particle motion, such as Crampin & King 1977, may indicate the type of alignment present and this may place constraints on temperature and pressure conditions in any anisotropic layer (Ave'Lallemant & Carter 1970).

Acknowledgment

This research was conducted while the author was in receipt of a studentship from the NERC.

References

Ave'Lallemant, H. G. & Carter, N. L., 1970. Syntectonic recrystallization of olivine and modes of flow in the upper mantle, *Geol. Soc. Am. Bull.*, 81, 2203–2220.

Crampin, S., 1970. The dispersion of surface waves in multilayered anisotropic media, *Geophys. J. R. astr. Soc.*, 21, 387–402.

Crampin, S., 1976. A comment on 'The early structural evolution and anisotropy of the oceanic upper mantle', *Geophys. J. R. astr. Soc.*, 46, 193–197.

Crampin, S., 1977. A review of the effects of anisotropic layering on the propagation of seismic waves, *Geophys. J. R. astr. Soc.*, 49, 9–27.

Crampin, S. & King, D. W., 1977. Evidence for anisotropy in the upper mantle beneath Eurasia from the Polarization of higher mode seismic surface waves, *Geophys. J. R. astr. Soc.*, 49, 59–85.

Forsyth (1975) was able to resolve azimuthal anisotropy so that his data do not correspond to azimuthal averages. However, an average FG dispersion is nearly the same as the dispersion for $\theta = 45°$ and an average 2G dispersion resembles the 2G dispersion for $\theta = 30$ or $60°$ (equation (1)). The body-wave averages are similarly related to body-wave velocities in particular directions. So remarks in this section, although derived from inversion of azimuthal averages, are equally applicable to inversion of dispersion for those particular directions for FG and 2G modes.

8 Conclusions

When inverting data from an anisotropic earth, isotropic inversion can indicate a higher resolution than is really valid. This has two important consequences:

(a) isotropic layers may be labelled as anisotropic and vice-versa,
(b) in restricted inversions, the result is likely to depend heavily on the choice of starting model.

This means that upper-mantle shear velocities found for Forsyth (1975) and Schlue & Knopoff (1977) cannot be considered an accurate guide to the elastic constants in that zone. In addition, it will not be possible to determine whether anisotropy is confined to one depth range, using only isotropic modelling.

Forsyth (1975) recognized such ambiguity in his inversion but Schlue & Knopoff's (1977) results suggested anisotropy confined to the low-velocity zone. However, in neither work has allowance been made for the possibly large, possibly systematic error inherent in isotropic inversion so that the uncertainty in the resultant upper-mantle models has been under estimated. Inversions will be more useful if a wider range of models, either isotropic or anisotropic, is considered. Monte Carlo methods may, therefore, be more appropriate than linear inversion techniques. If isotropic models are used, even those giving only a poor fit to the data should not be rejected. It is likely that the ambiguity mentioned above will not be resolved by the use of anisotropic modelling in phase or group-velocity inversions, so information must be sought in other ways. For example, studies of surface-wave particle motion, such as Crampin & King 1977, may indicate the type of alignment present and this may place constraints on temperature and pressure conditions in any anisotropic layer (Ave'Lallemant & Carter 1970).

Acknowledgment

This research was conducted while the author was in receipt of a studentship from the NERC.

References

Ave'Lallemant, H. G. & Carter, N. L., 1970. Syntectonic recrystallization of olivine and modes of flow in the upper mantle, *Geol. Soc. Am. Bull.*, 81, 2203–2220.

Crampin, S., 1970. The dispersion of surface waves in multilayered anisotropic media, *Geophys. J. R. astr. Soc.*, 21, 387–402.

Crampin, S., 1976. A comment on 'The early structural evolution and anisotropy of the oceanic upper mantle', *Geophys. J. R. astr. Soc.*, 46, 193–197.

Crampin, S., 1977. A review of the effects of anisotropic layering on the propagation of seismic waves, *Geophys. J. R. astr. Soc.*, 49, 9–27.

Crampin, S. & King, D. W., 1977. Evidence for anisotropy in the upper mantle beneath Eurasia from the polarization of higher mode seismic surface waves, *Geophys. J. R. astr. Soc.*, 49, 59–85.

Dorman, J., 1959. Numerical solutions for Love wave disperions on a half-space with double surface layer, *Geophysics*, **24**, 12–29.

Dorman, J., 1962. Period equation for waves of Rayleigh type on a layered liquid–solid half-space, *Bull. seism. Soc. Am.*, **52**, 289–397.

Forsyth, D. W., 1975. The early structural evolution and anisotropy of the oceanic upper mantle, *Geophys. J. R. astr. Soc.*, **43**, 103–162.

Francis, T. J., 1969. Generation of seismic anisotropy in the upper mantle along the mid-oceanic ridges, *Nature*, **221**, 162–165.

Kirkwood, S. C., 1977. Computed characteristics of seismic surface-waves for anisotropic models of oceanic structure (abstract), *Geophys. J. R. astr. Soc.*, **49**, 304.

McEvilly, T. V., 1964. Central U.S. crust – upper mantle structure from Love and Rayleigh wave phase velocity inversion, *Bull. seism. Soc. Am.*, **54**, 1997–2016.

Schlue, J. W. & Knopoff, L., 1977. Shear wave polarization anisotropy in the Pacific Basin, *Geophys. J. R. astr. Soc.*, **49**, 145–165.

Smith, M. L. & Dahlen, F. A., 1973. The azimuthal dependance of Love and Rayleigh wave propagation in a slightly anisotropic medium, *J. geophys. Res.*, **78**, 3321–3333.